2016

An experimental study on solvent liquefaction

Martin Robert Haverly
Iowa State University

An experimental study on solvent liquefaction

by

Martin Robert Haverly

A dissertation submitted to the graduate faculty

in partial fulfillment of the requirements for the degree of

DOCTOR OF PHILOSOPHY

Co-Majors: Mechanical Engineering and Biorenewable Resources and Technology

Program of Study Committee:
Robert C. Brown, Major Professor
Mark Mba Wright
Theodore J. Heindel
Steven J. Hoff
Max D. Morris

Iowa State University
Ames, Iowa
2016

TABLE OF CONTENTS

NOMENCLATURE

AF – ash-free

ANOVA – analysis of variance

DI – de-ionized

EDS – Exxon Donor Solvent

ESP – electrostatic precipitator

FTIR – Fourier Transform Infrared spectroscopy

GC-MS/FID – gas chromatography – mass spectroscopy/flame ionization detector

GPC – gel permeation chromatography

HDS – hydrogen donor solvent

HPLC – high performance liquid chromatography

HPTT – high pressure thermal treatment

HSP – Hildebrand solubility parameter

IC – ion chromatography

LCO – light cycle oil

mGC – micro gas chromatograph

MF – moisture-free

NCG – non-condensable gas

PDU – process development unit

PERC – Pittsburgh Energy Research Center

PM – phenolic monomers

PDU – process development unit

RMSE – root mean square error

RMW – relative molecular weight

SEM – scanning electron microscopy

SF# – stage fraction #

SL – solvent liquefaction

TAN – total acid number

THF – tetrahydrofuran

THW – thin hot wire

TGA – thermogravimetric analyzer

WPI – Worcester Polytechnic Institute

WSS – water soluble sugars

2-FEBM –2-furanethanol-beta-methoxy-(S)

5-HMF – 5-hydroxymethylfurfural

5-MF – 5-methylfurfural

ACKNOWLEDGMENTS

I would like to express my deepest gratitude to Dr. Robert Brown for giving me the opportunity to pursue this degree. His financial support, guidance, and expertise enabled me to be successful in my endeavors and to produce significant results. He fostered a research environment of exceptional quality.

I am also indebted to my committee members, Dr. Mark Mba Wright, Dr. Ted Heindel, Dr. Steve Hoff, and Dr. Max Morris for their support and guidance. Their constructive feedback encouraged me to pursue the highest standards.

I must also express my sincere gratitude to the BioEconomy Institute (BEI) staff. Specifically, I would like to thank Patrick Johnston, Patrick Hall and Marge Rover for their assistance with analytical techniques and method development. Thank you also to Ryan Smith for always providing a fresh outlook on any given situation. My time spent with Lysle Whitmer, Andrew Friend, Jordan Funkhouser, Taylor Shultz, and Andy Suby at the BioCentury Research Farm was also very valuable to me, and I appreciate all the memories we shared.

I was very fortunate to meet and work alongside extremely talented colleagues in my time at the BEI. I am grateful for the discussion and assistance offered by so many. I would especially like to thank Tannon Daugaard for his expertise, conversation, and friendship.

I was able to accomplish unbelievably more over the past few years through the help of an incredible number of undergraduate assistants, including Cameron Knights, Dan Hunting, Dustin Monat, Josh Piske, Jesse Moellers, Sam Johnson, Hannes Reinot, Cody

Christianson, and Kelley Okoren, just to name a few. I am truly grateful for all of their hard work and dedication.

Finally, I would like to thank my family for their unwavering support throughout my graduate studies and beyond. My parents, Steve and Twila, who taught me to be responsible, to work hard, and to honor the Lord. I am forever grateful to them for who they raised me to be. My wife, Julie, who was an infinite source of love, encouragement, and optimism. I could not have done this alone.

Above all, I thank my Lord and Creator for instilling in me a sense of curiosity and a desire to work. Soli Deo Gloria!

ABSTRACT

Solvent liquefaction (SL) is a promising technology for converting biomass to renewable fuels and chemicals. However, many technical barriers currently prevent the technology from commercial advancement. This research focused on the technical challenges that were confronted during the development of a continuous SL process development unit (PDU).

A 1 kg hr^{-1} pilot plant was designed to evaluate the technical feasibility of a continuous hydrocarbon-based SL process. The process was demonstrated to convert Loblolly pine to liquid products at a yield of 51.2 wt%. The liquid products were low in oxygen content (23.2 wt%) and moisture (13.4 wt%). In addition to validating product yields and quality, several unit operations were also evaluated. Online solids filtration continuously separated over 99% of the solid residue from the product stream. Acetone, injected into the process to aid in solids filtration, was continuously recovered with only 3 wt% loss to the process. Bio-oil fractionation via a distillation column was also demonstrated. A medium oil cut, suitable for use as a recycle solvent, was recovered using this system. This cut accounted for approximately 93 wt% of the initial solvent.

The effect of moisture on SL of biomass in a hydrocarbon solvent (tetralin) was evaluated to help determine the extent to which the feedstock should be dried for the SL PDU. These experiments were conducted in a quasi-batch reactor with independent pressure control and external vapor recovery. It was found that increasing the feedstock moisture from 1 to 50 wt% resulted in a reduction in liquid yield of 25, 21, and 35 wt%, for pine, cellulose, and lignin, respectively. Analysis of the solid residue, which increased proportionally to the

decrease in liquid yield, indicated acid-catalyzed polymerization of liquid products was the likely mechanism for solids-formation. The measured reduction of monomeric content in the liquid products supported this hypothesis. This behavior was attributed to the ionic dissociation of water at the reaction conditions, which resulted in increased acidic behavior. Although water was less than 20 wt% of the solvent loading in these experiments, it strongly influenced SL of biomass.

A response surface methodology statistical model was constructed to evaluate the influence of process conditions on the SL of lignin in a phenolic solvent. The goal of this work was to develop a process capable of producing high liquid yields from lignin with a high selectivity for phenolic monomers suitable for use as a recycle solvent. The effects of hydrogen donor solvent blend ratio, reaction temperature, solids loading, and residence time were studied. Hydrogen donor solvent and reaction temperature were found to be the most significant factors. Maximum liquid yield (58.6 wt%) was achieved at temperatures as low as 260 °C and hydrogen donor solvent blend ratios of less than 30 wt%. As much as 40 wt% of the liquid products were volatile below 340 °C, which indicated a significant production of distillable phenolic monomers suitable for use as a recycle solvent. Thus, the use of a phenolic solvent at moderate reaction temperatures was demonstrated to be suitable for the design basis of a continuous SL process.

The thermal stability of fractionated fast pyrolysis bio-oil was evaluated to determine the effect of rapid heating on bio-oil quality. The goal of this work was to develop a method with which to simulate rapid heating similar to the heating required for conventional refining processes, and to investigate the factors that most impacted thermal stability. Bio-oil

fractions were produced from fast pyrolysis of Loblolly pine at 500 °C. Each fraction was heated to 100, 200, and 300 °C in under 120s. Bio-oil acidity, as measured by total acid number (TAN), was found to be the most significant indicator of thermal instability. Samples with higher TAN values exhibited increased tendency to undergo polymerization reactions upon rapid heating. These findings were later extended to determine the thermal stability of bio-oil produced from the SL PDU. The goal of this was to evaluate the impact of thermal fractionation on bio-oil quality.

In order to design and build the SL PDU, alternative methods were developed to determine selected thermophysical properties of bio-oil. The goal of this work was to utilize readily available laboratory equipment, instead of costly ASTM test methods and specialty apparatus. Specific heat, thermal conductivity, viscosity, surface tension, and enthalpy of vaporization were measured for six unique stage fractions and a mixture of these fractions from the fast pyrolysis of Loblolly pine. The results and methods obtained from this work were then used as the design basis for the SL PDU.

CHAPTER 1

INTRODUCTION

Biomass as a Renewable Source of Carbon

A fundamental aspect of the present-day economy is the sale of goods manufactured from carbon. This includes the production of fuels, chemicals and fibers. To date, the most convenient and reliable source of the carbon needed to sustain the growth of the developed world has been fossil fuels (e.g. coal, natural gas, crude petroleum, etc.). In 2014 alone, the most recent year for which data is available, the U.S. produced 542.8 million tons of coal, 31.3 trillion ft^3 of natural gas, and 3.2 billion barrels of crude oil [1-3]. Whether these fossil fuels were used to produce energy or consumer goods, they were all harvested and utilized primarily because they are a cheap source of carbon.

Crude petroleum is possibly the most valuable source of carbon due to its liquid phase which allows for easier storage, transport, and upgrading than either solid or gaseous carbon feedstocks. An immense amount of infrastructure around the world has been built for processing crude petroleum into value-added products such that none of it goes to waste.

Related to the increasing demand for and consumption of fossil fuels is the concern over the release of carbon dioxide, a known greenhouse gas. In 2014 the U.S. released approximately 5960 tons of carbon dioxide [4] into the atmosphere, most of which originated from fossil fuels. This unchecked release of greenhouse gases has been linked to concerning trends in global weather patterns, and has been the primary impetus for recent development of alternative energy.

Biorenewable resources present a unique opportunity to serve as a renewable source of carbon while also reducing the overall anthropogenic carbon footprint. Biomass can be broadly defined as organic materials of recent biological origin. Throughout the life cycle of autotrophic organisms, inorganic carbon in the form of carbon dioxide is removed from the atmosphere through a process called the Calvin Cycle [5]. This is one of the integral processes of photosynthesis wherein sunlight is harnessed to convert carbon dioxide and water to oxygen and glucose. Eventually the glucose is then modified by the organism to form a variety of plant materials [5]. By taking advantage of the ability of biomass to capture gaseous carbon dioxide, bio-based products are able to effectively close the carbon cycle.

Throughout the cradle-to-grave evaluation of bio-based products there are points at which the carbon cycle can be significantly impacted. The use of fossil fuels in the production of bio-based products is one way that the carbon footprint of these products can be negatively impacted. For example, substantial release of carbon dioxide into the atmosphere while harvesting and transporting biomass can result in a net positive release of carbon into the atmosphere. Conversely, there are also ways to a net negative carbon footprint from the production of bio-based products. An example of this is to sequester some of the bio-based carbon in the earth. A primary goal for biorenewable production is to design processes and products that result in the lowest possible net release of carbon and are also sustainable so that the process or product does not pose a threat in some other facet (e.g. water consumption).

Bio-based products are generally classified into four main categories: food, fuels, chemicals, and fibers. In 2016 the U.S. Department of Energy released an update to the

original *Billion Ton Study* from 2005 in which they evaluated multiple scenarios in which the U.S. could feasibly produce approximately one billion tons of biomass per year for use as biofuel and bioenergy [6]. Only biomass that would otherwise not be utilized as food was eligible for inclusion in this study. The primary message of this study is that a sufficient source of biomass already exists such that the U.S. could displace up to 30% of the fossil fuel demands in the energy sector by properly utilizing this natural resource.

Though biomass is a promising source of carbon for fuels and energy, the molecular oxygen present in the biomass structure presents a number of challenges to its use. This is most palpable by examining a general correlation for the higher heating value of lignocellulosic biomass based on its elemental analysis shown below [7]:

$$\text{HHV [MJ/kg]} = 0.335\ \text{C} + 1.423\ \text{H} - 0.154\ \text{O} - 0.145\ \text{N}.$$

Here it can be seen that the presence of molecular oxygen detracts from the heating value of lignocellulosic biomass, thus rendering it a less energy-dense fuel than a corresponding hydrocarbon feedstock. Many pathways have been developed to try to improve the overall energy density of biomass as a fuel. The most common of these methods attempt to deconstruct biomass into molecules that exist as liquids and gases. The two foremost means of accomplishing this goal are biochemical and thermochemical conversion [8]. Biochemical conversion uses microorganisms to convert feed material. The most common example of biochemical conversion is fermentation of monosaccharides to ethanol. Biochemical processes are generally very selective, but they are also relatively slow processes that tend to be easily upset by foreign debris and changes in operating conditions.

Thermochemical conversion uses heat and pressure to convert feed material. There are four main classifications of thermochemical conversion: combustion, gasification, pyrolysis, and direct liquefaction. The primary difference between each of these four classifications is the temperature at which they occur, though pressure also varies widely. Another key parameter is control over the stoichiometric ratio of feed to oxygen. Limiting the amount of oxygen allowed into the system has a profound impact on the temperature of the process due to exothermic combustion reactions that tend to occur in the presence of oxygen. Generally speaking, combustion occurs in the presence of excess oxygen, gasification in sub-stoichiometric amounts, while pyrolysis and direct liquefaction are typically in the complete absence of oxygen.

Due to the absence of oxygen and the moderate temperatures employed by both pyrolysis and direct liquefaction, the products of these processes are the result of incomplete decomposition of the feed material. Thus, they are predominantly in the liquid phase, though some permanent gases and solid byproducts are also formed. To better understand the nature of the products formed from these processes, it is helpful to understand the molecular composition of most biomass feed material.

Biomass Composition

Biomass is generally made up of five primary building blocks: lignin, carbohydrates, lipids, proteins, and chitin. Two main classifications of biomass arise depending upon which of these building blocks are most prevalent in a given material: these are lignocellulosic and oleaginous. Lignocellulosic biomass is the structural component of most plants, including

stalks and branches. Lignin, cellulose and hemicellulose are the three main building blocks of lignocellulose. Oleaginous biomass is generally the energy storage portion of a plant, containing primarily carbohydrates, lipids, and proteins. Thermochemical conversion is often regarded as the most favorable means of processing lignocellulosic feedstocks due to their recalcitrant nature, although oleaginous feedstocks can also be processed thermochemically.

Cellulose is a structural homogeneous polysaccharide composed of repeating glucose units linked by β (1-4) glycosidic bonds in long chains of approximately 10,000 units [9]. Approximately 70% of the native cellulose in most plants has a crystalline structure due to hydrogen bonding between hydroxyl groups demonstrated in Figure 1, while small regions have an amorphous structure [10].

Hemicellulose is a heterogeneous polysaccharide comprised of a variety of 5- and 6-ring sugars connected by myriad linkages. It is an amorphous polymer consisting of approximately 50-300 repeating units which makes it much easier to decompose than cellulose [11].

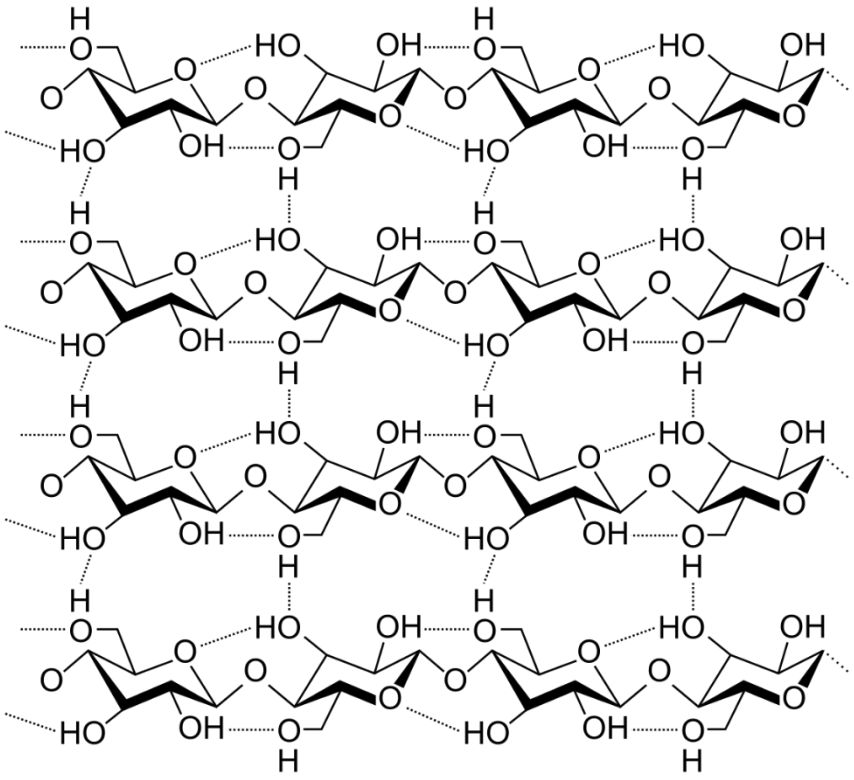

Figure 1. Structure of crystalline cellulose showing the β (1-4) glycosidic bonds between monomers and the hydrogen bonding between strands. Image was created by Luca Laghi, and distributed for use under a CC-BY-SA ver. 2.5 license.

Lignin serves to provide rigidity to the plant by binding polysaccharides together, making lignin the most complicated biomass building block. It is predominantly composed of the three phenylpropane alcohols shown in Figure 2. These monolignols are often known as paracoumaryl alcohol, coniferyl alcohol and sinapyl alcohol, but are sometimes referred to as H-, G-, or S-lignin, respectively. The actual structure and composition of the lignin polymer varies greatly by the source [10, 12, 13]. A proposed structure for softwood lignin is shown in Figure 3. Here the cross-linking between the monomers is palpable, and result in an amorphous and complicated macrostructure.

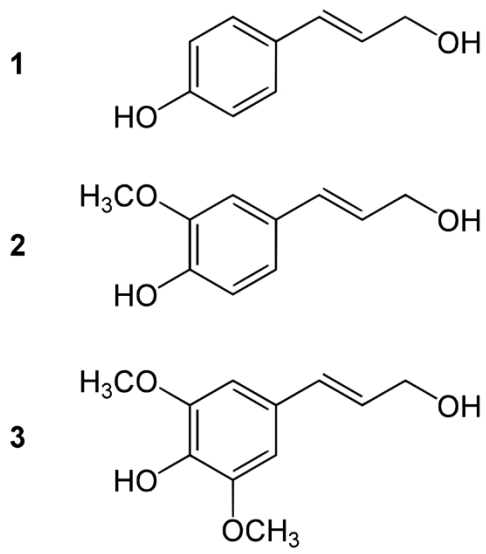

Figure 2. Three most common phenylpropane monomers found in lignin. The occurrence and placement of methoxy substitutions differentiate them as 1) paracoumaryl alcohol, 2) coniferyl alcohol, and 3) sinapyl alcohol.

Lignin has a much lower oxygen content than either cellulose or hemicellulose, and the presence of aromatic rings make it a promising feedstock for conversion to fuels and chemicals. However, lignin is particularly recalcitrant to most methods of conversion. It is essentially impervious to chemical and biological attack [14, 15], and thermally decomposes across a wide temperature range [11]. Thermal decomposition of lignin begins at approximately 200°C, but temperatures in excess of 400°C are often necessary to achieve complete thermal decomposition [13]. It is generally considered to be the most thermally stable of the three bio-polymers [16]. Feeding lignin into many reactor types has proven to be challenging due a softening of lignin that results in the formation of a lignin-plastic that tends to plug feeders and reactors [17].

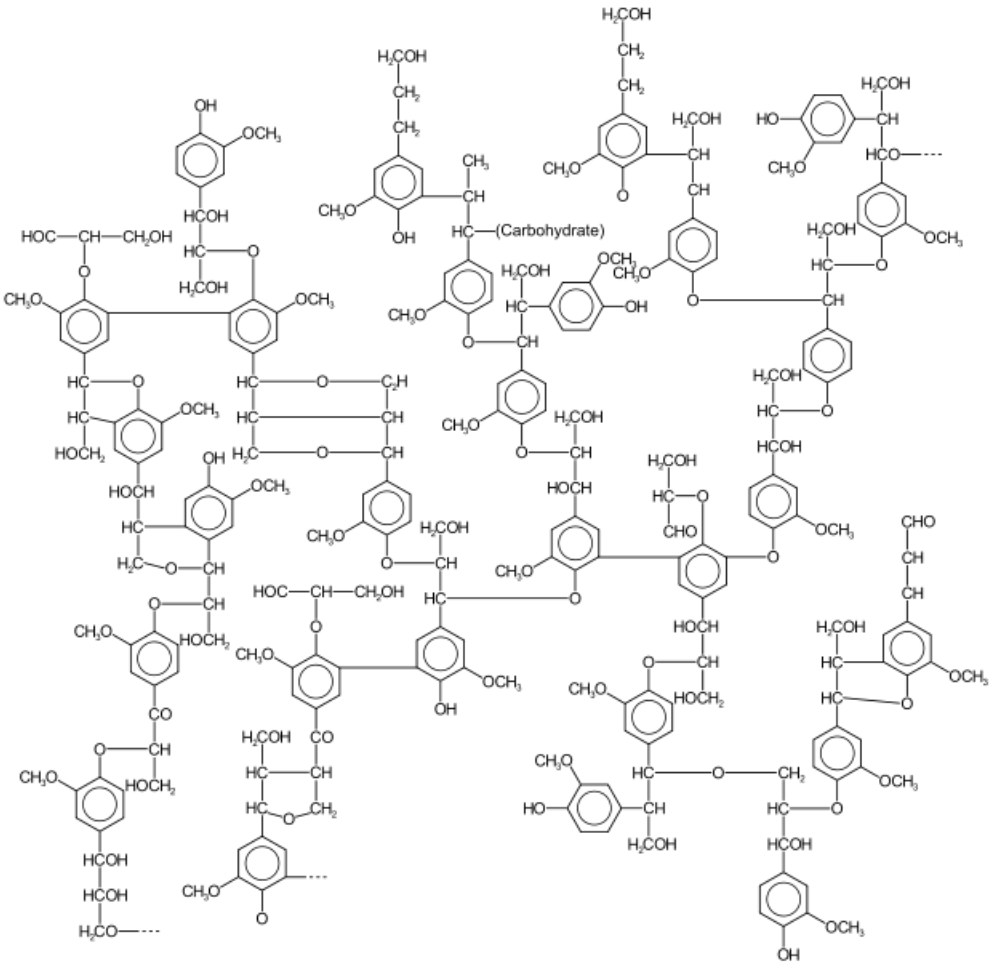

Figure 3. Proposed structure of native lignin showing the extent of cross-linking between phenylpropane monomers and the resultant amorphous structure. Image was created by Karol Głąb, and distributed for use under a CC-BY-SA ver. 2.5 license

Overview of Direct Liquefaction

Direct liquefaction is a process by which carbonaceous feedstocks are converted to predominantly liquid products in the presence of a liquid solvent at moderate temperatures (200-400°C) and pressures (20-200 bar). The moderate temperature range and the production of liquids make it tempting to think of direct liquefaction as merely “pyrolysis in a solvent”

though this is overly simplistic. Most solvents fundamentally alter the chemistry of feedstock decomposition, and therefore the process deviates from conventional pyrolysis reactions.

Solvent selection is a key parameter for optimal liquefaction performance. Solvents must be selected that are reasonably stable at the process conditions, are miscible with the product stream, and satisfy the intended reaction chemistry. The process must also then be configured so that a given solvent remains in the liquid phase, though in some instances it is preferred to operate in the supercritical regime. Often it is also desirable to select a solvent that is easily recovered from the product stream. This is most often achieved by selecting a low-boiling point solvent than can be flashed out of solution. Figure 4 shows the pressure-temperature curve for six common direct liquefaction solvents. Ethanol, water and butanol all reach a critical point below 400°C and require a substantial amount of pressure to remain in the liquid phase. Conversely, phenol, tetralin and γ-valerolactone can be considered to be high boiling point solvents and require only mild pressure to remain a liquid.

The presence of a liquid solvent offers several advantages compared to “dry” processing such as pyrolysis. The most palpable advantage is dilution of potentially reactive species. Biomass degradation products are notoriously reactive. Fast pyrolysis bio-oils for instance, are well documented to continue to undergo reactions for extended periods of time after collection [18, 19]. This reactive behavior is partially due to the fact that fast pyrolysis vapors are intentionally condensed prior to reaching thermodynamic equilibrium [20]. Another contributing factor is that most bio-oils are mixtures of hundreds of different compounds all in solution, so additional reactions between these compounds are likely to occur. Dilution of fast pyrolysis bio-oil with various solvents has been shown to reduce the

extent of undesired reactions in the condensed phase [21, 22]. Similar dilution benefits are also realized from most solvents used in direct liquefaction. For certain processing schemes wherein the solvent is not removed from the product stream, the benefits of dilution would thus continue even throughout storage of these products.

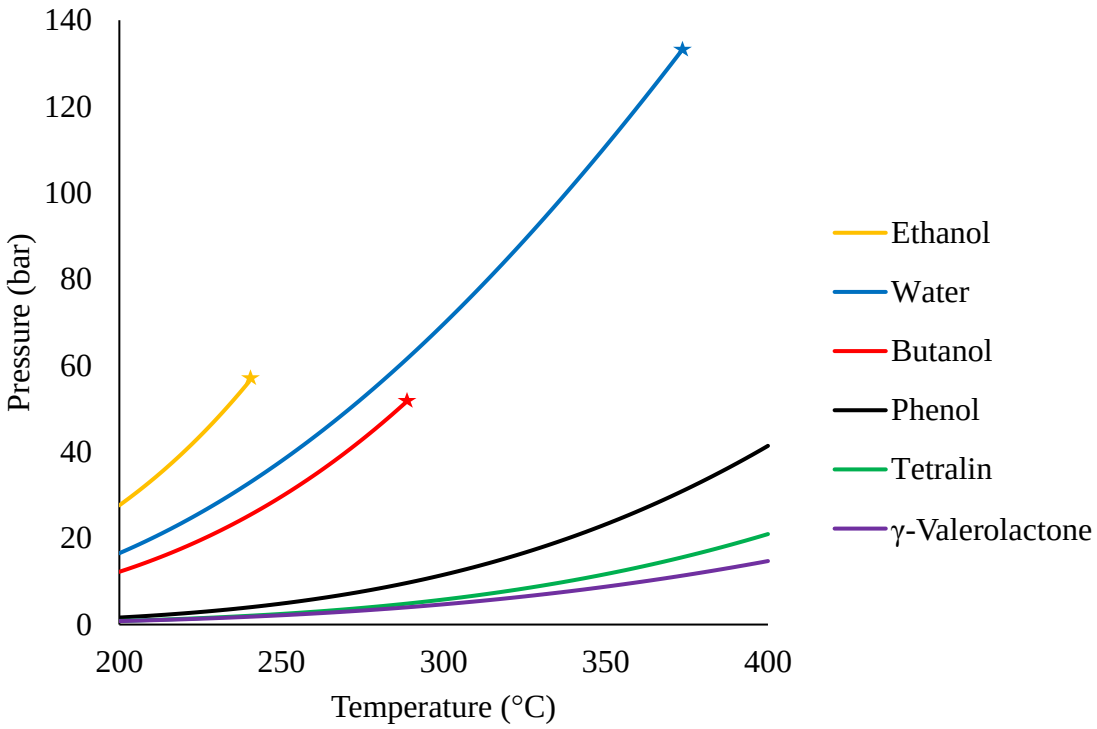

Figure 4. Pressure-temperature curves for several common direct liquefaction solvents as determined by the Antoine equation for each pure species. The star at the end of the ethanol, water, and butanol curves denote their critical point.

Liquid phase processing also provides the opportunity for the recovery of solubilized non-volatile products. Recovery of these products is typically not possible in gas-phase processing like pyrolysis because these molecules do not volatilize at even moderate reaction temperatures. Therefore, they are either entrained in the exiting gas stream or broken down

until they reach a molecular size that is volatile. To be sure, simply because these high-boiling point products can be retained in the solvent stream does not mean that they are trivial to recover. Due to the inherent difficulty of using a thermal process to recover them suggests that more extensive separation processes are necessary; usually this results in implementation of potentially costly solvent extraction methods.

Some solvent interactions advance beyond merely physical, wherein the solvent participates in the reaction chemistry. One manner in which solvents interact chemically with the feedstock is through solvolysis reactions. This interaction often gives rise to the use of the term solvolysis interchangeably with direct liquefaction. However, given that not all direct liquefaction processes undergo solvolysis reactions and that solvolysis reactions are not the exclusive (or even the dominant) reaction type in these processes, the use of the word in this manner is imprecise.

Solvolysis reactions are a type of nucleophilic substitution or elimination reaction wherein the nucleophile is a solvent molecule. Thus, the presence of a liquid solvent in direct liquefaction allows for these reactions to occur. Hydrolysis of polysaccharides in water to form monosaccharides and alcoholysis of triglycerides in methanol to form fatty acid methyl esters are two common examples of solvolysis reactions. Similar to these solvolysis reactions are hydrogenation or alkylation reactions wherein the solvent contributes a hydrogen atom or alkane group to a solute molecule, respectively. These reactions are often desirable in many biomass applications due to the opportunity for decreasing the oxygen content of biomass degradation products. The addition of a hydrogen donor solvent (HDS) is the most prevalent means of promoting this behavior [23]. Though this often promotes the formation of products

with a favorable C/O and C/H ratios, consumption of the solvent in this manner can be a limiting factor for process economics. In most instances, the utilization of a solvent intended to participate in solvolysis reactions should be limited to yield only the optimal benefit for the cost.

Solvents need not be consumed in a liquefaction system for their chemical benefits to be realized. In some schemes the solvent can simply behave as a catalyst to promote desired reactions. Ionic liquids are perhaps the most impressive catalytic solvents. They have been demonstrated to be effective at decomposing biomass at very low temperatures [24]. The cost of producing these solvents and the need for complete recovery challenges their utilization at any significant scale. Acid and base solvents exhibit similar catalytic behavior to more exotic ionic liquids, but without the same high cost of production. However, the corrosivity and process handling concerns of using these solvents undoubtedly limit their adoption. Polar aprotic solvents are a potentially more cost effective and benign alternative to the other catalytic solvents mentioned above. Tetrahydrofuran, γ-valerolactone, and other similar solvents have been shown to significantly reduce the activation energy for cellulose decomposition without being consumed during the reaction [25, 26].

Water is a particularly desirable solvent for many liquefaction applications. This is primarily due to its wide availability, low cost, and potentially favorable reaction chemistry. Extensive research has been conducted on a variety of processing conditions using water as a solvent, and has led to a secondary classification for aqueous versus non-aqueous direct liquefaction systems [27-29]. Hydrothermal liquefaction encompasses all systems where

water is the primary solvent, and solvent liquefaction (SL) is then reserved for all non-aqueous systems. This body of work will focus on SL (i.e. non-aqueous solvent) processes.

Continuous Processing

As previously mentioned, the United States processes over 3.1 billion barrels of crude oil annually [3]. If biomass is to compete with this extensive amount of production in any arena it is essential that biomass utilization technologies be continuous and scalable. Continuous SL processes can be traced back to the early 20th century and development of the Bergius process. In 1914 Friedrich Bergius, who later won the Nobel Prize in Chemistry for his efforts in high pressure chemistry, developed a process for the liquefaction of coal mixed with heavy oil in the presence of hydrogen [30]. His initial process was carried out in a 400L batch reactor capable of treating 150 kg of coal at 400 °C and 203 bar, but was converted to continuous mode of operation by the mid-1920s [31].

Synthetic fuels from coal eventually fell out of favor as the global supply of crude oil increased. The energy crisis of the 1970s, when much of the world experienced escalating prices for crude oil as the global supply could not meet the apparent demand, brought renewed interest to continuous SL processes. The most notable effort was developed by Appell et al. [32] at the Pittsburgh Energy Research Center (PERC) of the U.S. Bureau of Mines. The PERC process, as it was known, reacted finely ground Douglas fir wood in recycled wood oil at 350-370 °C and 270 bar. Presumably spurred on by increasing petroleum prices and promising initial results, the process was eventually scaled up to a 3 ton day^{-1} continuous demonstration unit in Albany, Oregon [33].

The Albany project was met with numerous technical difficulties that ultimately proved the process to be too expensive to continue to operate, and the Albany facility was shut down. Perhaps the foremost challenge faced by the PERC process was an inability to feed slurries with a solids loading greater than 8% [32]. Researchers at the University of Arizona sought to remedy this challenge by adopting a modified single-screw extruder as the feed mechanism. This method was able to feed up to 60 wt% wood flour into a reactor operating at up to 250 bar and 400 °C [34]. Wood oil taken from the Albany facility was used as the solvent, while carbon monoxide and steam were used as the pressurizing gas [35]. This process was able to achieve bio-oil yields of approximately 48-58 wt%, which the researchers determined to be within 80-100% of the maximum theoretical yields. The bio-oil had an oxygen content of approximately 6-10 wt% [36].

While the Biomass Liquefaction Experimental Facility was underway in Albany, OR a separate process was being developed at the Worcester Polytechnic Institute (WPI) in Worcester, MA. The researchers at WPI sought to make a continuous process that could produce fuel oil from powdered newspaper in a mineral oil solvent. A mixture of 20 wt% newspaper and 0.2 wt% nickel hydroxide catalyst was slurried in mineral oil and then pumped into a 1 L CSTR reactor at a solids feed rate of approximately 1 kg h^{-1} [32]. A typical run was conducted at 400-455 °C, 34-102 bar of hydrogen, and a residence time of approximately 15-38 min [37]. This facility was intended to provide the necessary data for a 1000 ton day^{-1} commercial-scale facility, but the process was not pursued beyond the pilot scale. The technology required to feed larger particles at the next phase of the process development was a known issue for scale-up [37].

Researchers at the Université de Sherbrooke in Québec, Canada sought to address the problem of feeding slurries with a high solids loading through use of a pretreatment reactor. According to the work of Overend and Chornet [32] direct liquefaction can be divided into 4 distinct processes that occur somewhat sequentially. In order, these are structural disintegration, defibrillation of individual polymer chains, chain depolymerization sufficient to enable polymer solubility, and solvolytic hydrogenation/deoxygenation [32]. Based on this understanding, the researchers developed a pretreatment wherein 4 kg hr^{-1} of debarked poplar wood was reacted in a solvent at 200-240 °C. A pump circulated the mixture across a mixing valve that forced the wood to experience a 6-35 bar pressure drop. The heat and pressure gradient caused the wood to undergo structural disintegration and defibrillation, resulting in a slurry that was pump-able with a solids loading of 20-32 wt%, though the researchers note that slurries of 14-18 wt% solids were explored most often. Ethylene glycol or creosote oil were used separately as the solvent. The reactor was simply a tube submerged in a molten salt bath held at approximately 320-350 °C. The pretreated slurry was mixed with a stream of either nitrogen or hydrogen gas and then pumped through the tubular reactor. Oil yields of 40-55 wt% and 51-61 wt% were obtained from the process when using ethylene glycol and creosote oil, respectively [38].

Academic research groups were not the only entities to develop continuous SL processes. Most notable among the industrial involvement in solvent liquefaction was the Exxon Donor Solvent (EDS) liquefaction system developed in the late 1970s. Due to the apparent lack of global oil supply at this time there were multiple entities working to develop a method of coal liquefaction. However, the EDS system was unique in that it utilized a

hydrocarbon solvent that was not derived from the process itself (i.e. it was not a product of coal liquefaction). The process was modelled after the Bergius process, and was designed to liquefy coal in the presence of a hydrogen donor solvent (HDS) at approximately 400-450 °C and 3-21 bar [39]. In order to maintain a sufficient amount of available hydrogen for upgrading the coal, the EDS system separated the hydrocarbon solvent from the product stream and hydrotreated it prior to recycling it back into the reactor. This approach was what set the EDS system apart from most other efforts. Furthermore, the EDS process was largely successful, and in 1980 it was scaled up to a pilot plant capable of processing 250 ton day^{-1} of dry feed [40]. This process was also considered for the SL of biomass, but no significant progress was made.

In addition to the continuous SL development units mentioned above, considerable work has also been done on the development of continuous hydrothermal liquefaction [41-43], though this work will not be explored in detail here.

Dissertation Organization

SL is a promising technology to deconstruct solid carbonaceous feedstocks, particularly biomass, to more readily usable forms. It is capable of not only achieving high liquid yields from biomass, but many SL processes can be tailored to directly produce desirable molecules, such as phenolic monomers and fermentable sugars. However, for these benefits to be realized, a considerable amount of research must still be conducted to advance the technology. The foremost hurdle is the development of robust processes that are

continuous and scalable. The work presented in this dissertation is all aimed at addressing core technological hurdles towards this goal.

In addition to the introduction and conclusions section, this dissertation is organized into five chapters. *Chapter 2* outlines the design and operation of a 1 kg hr^{-1} continuous SL unit. This system was designed to be a process development unit (PDU) with which to develop a hydrocarbon solvent liquefaction technology in conjunction with Chevron, USA, the industrial sponsor. Dry Loblolly pine was converted to liquid products with low viscosity and low moisture content at yields greater than 50 wt%. The use of a hydrocarbon solvent promoted hydrogenation and hydro-deoxygenation of the biomass degradation products, which resulted in liquid products with reduced oxygen content. In addition to developing the core technology, several unit operations were also developed on the SL PDU. Continuous online solids filtration, acetone injection and recovery, and bio-oil fractionation were key components to the success of the project. Given that many of the aspects of this project were unique, many additional research studies were conducted to support its development. The development and execution of these additional projects account for the remaining chapters of this dissertation. In some situations, these projects focused on the evaluation of fast pyrolysis bio-oils as a surrogate for solvent liquefaction bio-oils because they were conducted prior to the SL PDU.

Throughout the process of developing the SL PDU numerous questions arose regarding the fundamental chemistry of the process. One of the initial questions that arose was on the impact of water on a hydrocarbon SL. It was fairly well understood that SL were not as significantly impacted by moisture as fast pyrolysis, but a clearer understanding of the

effects of water were desired. *Chapter 3* seeks to address this quandary. Unfortunately, due to the scale of the SL PDU, it was not possible to efficiently conduct experiments of this nature on this system. Therefore, a quasi-batch bench-scale reactor system was developed to closely simulate the SL PDU reactor. This reactor was used extensively throughout these studies to examine the influence of moisture on loblolly pine as well as the primary constituents: cellulose and lignin.

In addition to the influence of feed moisture, many of the questions that arose from development of the SL PDU centered around the optimal processing conditions for the production of phenolic monomers (PM). *Chapter 4* seeks to answer these questions through the use of a four-factor design of experiments and response surface methodology. This study explored the concentration of HDS, reaction temperature, residence time, and solids loading for the optimal production of liquids and phenolic monomers from extracted lignin.

Chapter 5 outlines a set of experiments that were conducted to evaluate the thermal stability of bio-oil when exposed to conditions required for thermal processing. This was specifically designed to address concerns over the operating conditions employed in the bio-oil fractionation system of the SL PDU. Of principal concern was the issue over whether the bio-oil quality would be significantly impacted by short exposures to elevated temperatures.

Chapter 6 details the development of alternative methods for determining selected thermophysical properties of bio-oil. These methods were developed as a cost-effective means of acquiring the engineering data necessary for accurate design of the SL PDU and related subsystems. Many of the properties evaluated in this study were not easily assumed from pure compound data nor directly transferable from studies of similar processes.

Chapter 7 provides a summary of several key findings from the preceding chapters. Recommendations for future work and general comments on the future state of the industry are also provided.

References

1. Administration, U.S.E.I. *Annual Coal Report*. 2014 22 April 2016].

2. Administration, U.S.E.I. *Natural Gas Annual*. 2014 22 April 2016].

3. Administration, U.S.E.I. *Crude Oil Production*. 2014 22 April 2016].

4. Administration, U.S.E.I. *U.S. Energy-Related Carbon Dioxide Emissions*. 2014 23 May 2016].

5. Campbell, N.A., *Biology / Neil A. Campbell, Jane B. Reece*. 6th ed.. ed, ed. J.B. Reece. 2002, San Francisco: San Francisco : Benjamin Cummings.

6. Energy, U.S.D.o., *US billion-ton report: advancing domestic resources for a thriving bioeconomy.* M.H. Langholtz, B.J. Stokes, L.M. Eaton. Oak Ridge, Tennessee USA: Oak Ridge National Laboratory, 2016.

7. Demirbaş, A., *Calculation of higher heating values of biomass fuels.* Fuel, 1997. **76**(5): p. 431-434.

8. Brown, R.C. and T.R. Brown, *Biorenewable resources: engineering new products from agriculture*. 2013: John Wiley & Sons.

9. Sjöström, E., *Wood chemistry : fundamentals and applications / Eero Sjöström*.

10. Browning, B.L., *The chemistry of wood.* 1963.

11. Kalia, S., B. Kaith, and I. Kaur, *Cellulose fibers: bio-and nano-polymer composites: green chemistry and technology*. 2011: Springer Science & Business Media.

12. Sarkanen, K.V. and C.H. Ludwig, *Lignins: occurrence, formation, structure and reactions.* Lignins: occurrence, formation, structure and reactions., 1971.

13. Joffres, B., et al., *Thermochemical Conversion of Lignin for Fuels and Chemicals: A Review.* Oil & Gas Science and Technology–Rev. IFP Energies nouvelles, 2013. **68**(4): p. 753-763.

14. Guillén, F., et al., *Biodegradation of lignocellulosics: microbial, chemical, and enzymatic aspects of the fungal attack of lignin.* Int Microbiol, 2005. **8**(195204): p. 187204Minami.

15. Bobleter, O., *Hydrothermal degradation of polymers derived from plants.* Progress in Polymer Science, 1994. **19**(5): p. 797-841.

16. Borrega, M. and P. Kärenlampi, *Effect of relative humidity on thermal degradation of Norway spruce (Picea abies) wood.* Journal of Wood Science, 2008. **54**(4): p. 323-328.

17. Kaminsky, W. and H. Schwesinger, *Properties and Decomposition of Lignins Isolated by Means of an Alcoholic-Water-Mixture. Part 3: Decomposition by Pyrolysis in a Fluid-Bed.* Holzforschung-International Journal of the Biology, Chemistry, Physics and Technology of Wood, 1980. **34**(3): p. 73-75.

18. Czernik, S., D.K. Johnson, and S. Black, *Stability of wood fast pyrolysis oil.* Biomass and Bioenergy, 1994. **7**(1): p. 187-192.

19. Adjaye, J.D., R.K. Sharma, and N.N. Bakhshi, *Characterization and stability analysis of wood-derived bio-oil.* Fuel Processing Technology, 1992. **31**(3): p. 241-256.

20. Chen, D., et al., *Evaluation methods and research progresses in bio-oil storage stability.* Renewable and Sustainable Energy Reviews, 2014. **40**: p. 69-79.

21. Diebold, J. and S. Czernik, *Additives To Lower and Stabilize the Viscosity of Pyrolysis Oils during Storage.* Energy & fuels, 1997. **11**(5): p. 1081-1091.

22. Boucher, M., et al., *Bio-oils obtained by vacuum pyrolysis of softwood bark as a liquid fuel for gas turbines. Part II: Stability and ageing of bio-oil and its blends with methanol and a pyrolytic aqueous phase.* Biomass and Bioenergy, 2000. **19**(5): p. 351-361.

23. Vasilakos, N.P. and D.M. Austgen, *Hydrogen-donor solvents in biomass liquefaction.* Industrial & Engineering Chemistry Process Design and Development, 1985. **24**(2): p. 304-311.

24. Honglu, X. and S. Tiejun, *Wood liquefaction by ionic liquids.* Holzforschung, 2006. **60**(5): p. 509-512.

25. Mellmer, M.A., et al., *Effects of γ-valerolactone in hydrolysis of lignocellulosic biomass to monosaccharides.* Green Chemistry, 2014. **16**(11): p. 4659-4662.

26. Ghosh, A., R.C. Brown, and X. Bai, *Production of solubilized carbohydrate from cellulose using non-catalytic, supercritical depolymerization in polar aprotic solvents.* Green Chemistry, 2016. **18**(4): p. 1023-1031.

27. Akhtar, J. and N.A.S. Amin, *A review on process conditions for optimum bio-oil yield in hydrothermal liquefaction of biomass.* Renewable and Sustainable Energy Reviews, 2011. **15**(3): p. 1615-1624.

28. Peterson, A.A., et al., *Thermochemical biofuel production in hydrothermal media: A review of sub-and supercritical water technologies.*

29. Toor, S.S., L. Rosendahl, and A. Rudolf, *Hydrothermal liquefaction of biomass: a review of subcritical water technologies.* Energy, 2011. **36**(5): p. 2328-2342.

30. Stranges, A.N., *Friedrich Bergius and the Rise of the German Synthetic Fuel Industry.* Isis, 1984. **75**(4): p. 643-667.

31. Stranges, A. and A.N. Stranges, *Synthetic petroleum from coal hydrogenation: its history and present state of development in the United States.* Journal of Chemical Education, 1983. **60**(8): p. 617.

32. Chornet, E. and R.P. Overend, *Biomass liquefaction: an overview*, in *Fundamentals of thermochemical biomass conversion*. 1985, Springer. p. 967-1002.

33. Ergun, S., *Biomass liquefaction efforts in the United States*. 1980, Lawrence Berkeley Laboratory.

34. White, D., N. Schott, and D. Wolf, *Experimental study of an extruder-feeder for biomass direct liquefaction.* The Canadian Journal of Chemical Engineering, 1989. **67**(6): p. 969-977.

35. White, D.H., D. Wolf, and Y. Zhao, *Biomass liquefaction utilizing extruder-feeder reactor system.* Amer. Chem. Soc., Div. Fuel Chem. Prprts., 1987. **32**(2): p. 106.

36. Elliott, D.C., et al., *Developments in direct thermochemical liquefaction of biomass: 1983-1990.* Energy & Fuels, 1991. **5**(3): p. 399-410.

37. Kaufman, J.A., et al., *Catalytic hydrogenation of solid waste carbohydrates to fuel oil.* Chemie Ingenieur Technik, 1974. **46**(14): p. 609-609.

38. Vanasse, C., E. Chornet, and R.P. Overend, *Liquefaction of lignocellulosics in model solvents: Creosote oil and ethylene glycol.* The Canadian Journal of Chemical Engineering, 1988. **66**(1): p. 112-120.

39. Neavel, R.C., *Liquefaction of coal in hydrogen-donor and non-donor vehicles.* Fuel, 1976. **55**(3): p. 237-242.

40. Neavel, R.C., C.F. Knights, and H. Schulz, *Exxon Donor Solvent Liquefaction Process [and Discussion]*. Philosophical Transactions of the Royal Society of London A: Mathematical, Physical and Engineering Sciences, 1981. **300**(1453): p. 141-156.

41. Elliott, D.C., et al., *Process development for hydrothermal liquefaction of algae feedstocks in a continuous-flow reactor.* Algal Research, 2013. **2**(4): p. 445-454.

42. Elliott, D.C., et al., *Hydrothermal liquefaction of biomass: Developments from batch to continuous process.* Bioresource Technology, 2015. **178**(0): p. 147-156.

43. Jazrawi, C., et al., *Pilot plant testing of continuous hydrothermal liquefaction of microalgae.* Algal Research, 2013. **2**(3): p. 268-277.

CHAPTER 2

CONTINUOUS SOLVENT LIQUEFACTION OF BIOMASS IN A HYDROCARBON SOLVENT

A paper to be submitted to Energy & Fuels.

Martin R. Haverly, Taylor Schulz, Lysle Whitmer, Andrew Friend, Jordan Funkhouser, Ryan G. Smith, Robert C. Brown

Abstract

Solvent liquefaction (SL) of biomass is a promising technology for the conversion of biomass to renewable fuels and chemicals. Liquid-phase thermal deconstruction of biomass in the presence of hydrocarbon-based hydrogen-donating solvents can result in bio-oils with low moisture and low oxygen content. These oils are thermally stable and highly miscible with hydrocarbon streams, which make them a promising biorenewable blendstock for petroleum refineries. We have developed a 1 kg hr^{-1} continuous SL pilot plant to evaluate the performance of SL of southern yellow pine in a hydrocarbon solvent. The process development unit (PDU) was also designed to evaluate several unit operations critical to large-scale operations. Online solids removal was conducted with inline wire mesh barrier filters with separation efficiency of over 99%. Acetone injection was used to aid in solids removal, and an online recovery system was demonstrated with greater than 97% acetone recovery. Continuous online bio-oil fractionation was also demonstrated using a distillation

column to separate approximately 93 wt% of the initial solvent from the biomass-derived products.

Introduction

Direct liquefaction thermally decomposes solid carbonaceous feedstocks into predominantly liquid products using a liquid solvent. It is generally carried out at moderate temperatures and pressures, typically ranging from 200-400 °C and 20-200 bar, respectively. The operating pressure of a given direct liquefaction system is largely dictated by the vapor pressure of the solvent, but it can be impacted by the vapor pressures of the products, as well. Direct liquefaction is a broad category that includes several subcategories delineated by the primary solvent employed. Hydrothermal liquefaction, in which water is the primary solvent, and solvent liquefaction (SL), which employs non-aqueous solvents, are the most common.

The products of SL vary widely based on the reaction conditions and the solvent employed. The mixture of solubilized products are generally referred to as bio-oil, although they have historically also been termed proto-oil [1]. Bio-oils produced from SL closely resemble the products of fast pyrolysis.

The choice of solvent can have a strong impact on product distribution and yield [2, 3]. For example, recent studies suggest that certain solvents can lower the apparent activation energy for cellulose depolymerization [4, 5].

There are several key attributes of SL bio-oils that are advantageous for use as renewable chemical and fuel precursors. For instance, SL bio-oils tend to have lower oxygen content than fast pyrolysis bio-oils due mild deoxygenation of the product molecules.

Deoxygenation can be promoted several ways, but one of the most common is through the use of a hydrogen-donor solvent (HDS) which provides hydrogen to the process [6]. Formic acid, light alcohols such as 2-propanol, and hydrocarbons such as tetralin are among the most common HDSs studied in the literature [6-8]. HDSs are also effective at stabilizing thermal decomposition products. This has a net effect of reducing repolymerization of products [6, 8]. In addition to HDS capabilities, the solvent dilutes the products improving their thermal stability [9].

Thermal stability of bio-oil is defined as resiliency against changes in chemical and physical properties upon exposure to elevated temperatures. Bio-oils are generally regarded as having poor thermal stability due to the presence of reactive oxygenated compounds [19]. As a result, attempts to fractionate bio-oil through distillation have largely been unsuccessful [20-22].

Although these solvent effects are beneficial, the addition of solvent represents a considerable operating cost in commercial operations [3]. For this reason, the development of solvent recycle is very important for the economic viability of SL.

The origins of continuous SL can be traced back to the Bergius process, which was developed early in the 20th century to convert bituminous coal to synthetic fuels. However, it was not until the latter half of the century that continuous SL of biomass was investigated in earnest, largely due to the energy crisis of the 1970s. At that time several processes were developed to produce a bio-based product that resembled crude petroleum. The foremost effort originated with the Pittsburgh Energy Research Center (PERC) of the Bureau of Mines. Researchers developed a process that reacted Douglas fir in recycled wood oil at 350-

370 °C and 270 bar [10]. It became known as the PERC Process. This effort culminated with the construction of a 3 ton day^{-1} demonstration unit located in Albany, Oregon [11]. Unfortunately, the facility was plagued with technical difficulties, and was ultimately abandoned due to poor economics. A principle problem was the inability to feed biomass slurries greater than 8 wt% dry solids [10]. Despite this setback, research related to the PERC Process was continued at both the Lawrence Berkeley Laboratory and the University of Arizona.

Researchers at the University of Arizona employed a modified single-screw extruder feeder instead of more conventional positive displacement pumps to convey slurries up to 60 wt% wood flour [12]. They demonstrated continuous wood flour liquefaction at pressures up to 25 MPa and temperatures up to 400 °C in the presence of wood oil vacuum bottoms taken from the Albany facility, mixed with steam and carbon monoxide [13]. This work produced bio-oil with an oxygen content of approximately 6-10 wt%, with relative yields at 80-100% of the maximum theoretical yields, or absolute yields of 48-58% [14].

Liquefaction of carbonaceous materials has also been explored in industry. The Exxon donor-solvent coal liquefaction process was developed in the 1970s by the Exxon Research and Engineering Company. This technology was modeled after the Bergius process, and was scaled up to a 1 ton day^{-1} plant. Over the nearly 10 year span of the project, research efforts explored the impact of HDSs, solvent recycle, and product separation techniques [15]. Similar coal liquefaction processes were subsequently explored and patented by Chevron Research Company [16] and Mobil Oil Corporation [17]. Comprehensive review

articles on continuous SL have been published by Chornet & Overend [10], Elliott et al., [14], and van Rossum et al. [3].

Despite the long history of SL, the technology faces many practical technology barriers. Thus, the goal of this study was to evaluate several technical barriers pertaining to continuous SL of biomass in a hydrocarbon solvent. In order to study continuous SL at a scale relevant to industrial development, a 1 kg hr^{-1} SL process development unit (PDU) was constructed at Iowa State University. Three separate experiments, each more than twelve hours long, were conducted using the SL PDU. The product yields and quality were determined for each experiment. Furthermore, three unit operations were explored in this study. These were continuous solids separation using barrier filters, continuous acetone injection and recycle, and continuous online bio-oil fractionation. To our knowledge, research on continuous solids separation and acetone recycle for SL of biomass has not yet been published.

The studies on bio-oil fractionation have two goals. The first is to demonstrate a bio-oil fractionation system that can continuously separate and recover a stream suitable for use as a recycle solvent. This should be achieved without significantly impacting the product quality and composition. Thus the thermal stability of the product stream entering the bio-oil fractionation system was extensively evaluated.

The second goal is to investigate the thermal stability of the resulting bio-oil. It was hypothesized the bio-oil would have improved thermal stability due to its reduced oxygen

content and the presence of the thermally stable hydrocarbon solvent. Improvement on the thermal stability of pyrolysis oils by the presence of a co-solvent has been well documented [23, 24].

Materials and Methods

Biomass feedstock

Southern yellow pine sawmill residue was acquired from Weyerhaeuser and shipped to Iowa State University in polymer drums. The material consisted primarily of heartwood, but did contain trace amounts of bark. No pine needles were included. The biomass was dried in Fisher Scientific Isotemp ovens from the as-received moisture content of approximately 55 wt% down to 4 wt% or less. Moisture content was periodically measured with an Ohaus MB 25 moisture analyzer to monitor progress. After drying, the material was sieved with a 6.4 mm (0.25 in) square weave screen. Only the material that passed through the screen was kept as feedstock. The combined results of proximate and ultimate analysis of the dried and sized biomass are shown in Table 1.

Table 1. Southern yellow pine feedstock proximate and ultimate analyses (uncertainty reflects 95% confidence interval).

Proximate Analysis (wt%)	
Moisture	4.10 ± 0.26
Volatiles (MF)	82.56 ± 0.41
Fixed Carbon (MF)	13.3 ± 0.55
Ash (MF)	0.55 ± 0.14
Ultimate Analysis (wt% AF/MF)	
C	52.77 ± 0.37
H	5.33 ± 0.12
N	0.19 ± 0.04
S	0.01 ± 0.01
O (by difference)	41.70 ± 0.32

Solvent feedstock

The solvent was a blend of two hydrocarbon liquids. The majority of the solvent was comprised of commercially available naphthalene-depleted heavy aromatic solvent (CAS # 64742-94-5). The hydrogen donor solvent was a proprietary cut of light cycle oil (LCO) (CAS # 64741-59-9) that was specially hydrotreated. As much as 25 wt% of the solvent mixture was comprised of the hydrotreated LCO. Higher blend ratios were limited by the economics of providing hydrogen to the process in this manner.

Feed system

An illustration of the feed system and reactor are shown in Figure 1. Biomass feeding was done in a two-stage process to feed the solids into a pressurized reactor. The first stage (FDR-1) was an Acrison Weight-Loss-Differential Weigh Feeder model 406 operating at

atmospheric pressure. This feeder consisted of a 15 L hopper atop a single screw auger capable of metering up to 12.7 L hr^{-1} of solids. A biomass feed rate of 0.7 kg hr^{-1} was held constant across all tests.

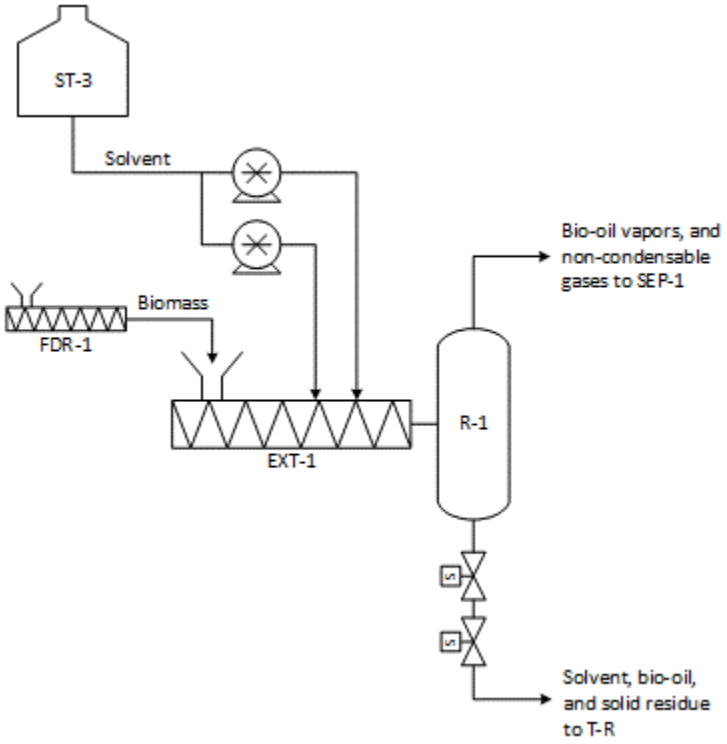

Figure 1. Process flow schematic of the biomass and solvent feed system and reaction vessel.

The second stage (EXT-1) was a Coperion ZSK-26 custom twin-screw compounding extruder. The extruder consisted of two co-rotating intermeshed screws that extended through the middle of 14 stainless steel blocks that collectively make up the extruder barrel. Each screw was comprised of 126 individual elements each measuring about 19 mm in length. Ten separate types of elements were used, dictated by the specific function of different sections of the extruder screw. In order to create a dynamic pressure seal, two sections of reverse flight

elements were used. These sections essentially compacted the biomass such that the biomass formed a seal capable of withstanding the pressures required for SL.

Biomass was metered out of FDR-1 and gravity-fed into the feed port of EXT-1. Upon entering EXT-1 the biomass was conveyed and gradually heated to 121 °C. Once at this temperature, the biomass passed through the two seal sections described above. Prior to start-up, a sufficient amount of solvent to conduct a given experiment was premixed and loaded into the primary solvent storage tank, ST-3. The solvent mixture was then injected into the feed stream by two Teledyne Isco 260D tandem syringe pumps such that the solvent to biomass ratio was approximately 4:1. Two separate injection ports were used so as to not overwhelm the biomass with the incoming solvent. The solvent and biomass were continually mixed as the material advanced through the remainder of the barrel. The last 4 barrel blocks were held near the final temperature of 400 °C. Due to the small available volume for expansion, pressures in EXT-1 ranged from 42 to 53 bar. It is assumed that a substantial amount of the reaction had already occurred by the time biomass exited EXT-1.

Reactor

Initial work suggested that although much of the reaction had already occurred in EXT-1, additional residence time was necessary. This was achieved in reaction vessel R-1 operated at 400 °C and 43 bar. The vessel was constructed from a 108.1 cm long section of 8.9 cm I.D. pipe with an internal volume of 7.1 L. Unless otherwise specified, all materials of construction were 316 series stainless steel to minimize corrosion. Grayloc flanges, rather than ASME flanges, were used as the primary flange type on R-1 and other high-pressure

vessels. This helped to reduce the weight and physical size of the vessels as well as the maintenance requirements due to the use of only 4 bolts per flange. R-1 was configured such that the biomass slurry could be fed into one of three different locations: the bottom 1/3, the middle, and the top 1/3.

In addition to providing residence time for the reaction to proceed, R-1 served as a gas/liquid separator. As depicted in Figure 1, the top of R-1 was open to allow vapors and non-condensable gases to exit the reactor while the bottom was configured to handle solid residue and the bulk of the reaction liquid. The bottom tap of R-1 was connected to a product filtration tank by way of two MOGAS RSVP 2.5 cm ball valves with a 1.6 cm diameter bore. The valves were programmed to cycle opposite one another, so that material could be safely batched out of the system.

Overhead products handling

Compounds that were volatile at the reaction conditions (400°C and 43 bar) passed through R-1 and were carried into the overhead products handling system depicted in Figure 2. The transfer tubing was controlled to a temperature of 302 °C. SEP-1 and SEP-2 were of identical construction. Each was made from 4.5 cm I.D. pipe 86.4 cm in length, with an internal volume of approximately 1.4 L. SEP-1 was configured with 2 separate heating zones. The bottom zone was designed to maintain a liquid temperature of 260 °C while the top zone maintained a vapor temperature of 302 °C. These temperatures were intended to maintain water and light oxygenates in the vapor phase, but condense any hydrocarbons or phenolic monomers produced from the biomass. The vapor stream that exited SEP-1 passed through a

custom-built tube-in-tube heat exchanger chilled with propylene-glycol to approximately 27 °C. SEP-2 was uninsulated and allowed to operate at ambient temperature. Any remaining condensable vapors were collected in SEP-2. All overhead non-condensable gases passed through in SEP-2. The gas was then filtered through a 10 μm barrier filter prior to a Fisher Baumann 51000 pressure control valve that reduced the pressure from 43 bar to atmospheric pressure. All soft-seat materials and polymer gaskets were composed of polytetrafluorethylene (PTFE) due to its well demonstrated resistance to degradation when exposed to bio-oils for extended durations [18]. SEP-3 was as a knockout vessel to trap any liquid carryover in the gas stream prior to gas monitoring and analysis.

A bank of nitrogen cylinders was connected to the overhead line of SEP-2 to pressurize the overheads product system and R-1 reaction vessel. An Alicat Scientific PCH pressure control valve was used to electronically control the pressure. An external pressure source was not needed after the process reached steady state as the 43 bar of pressure was easily maintained by the production of non-condensable gases.

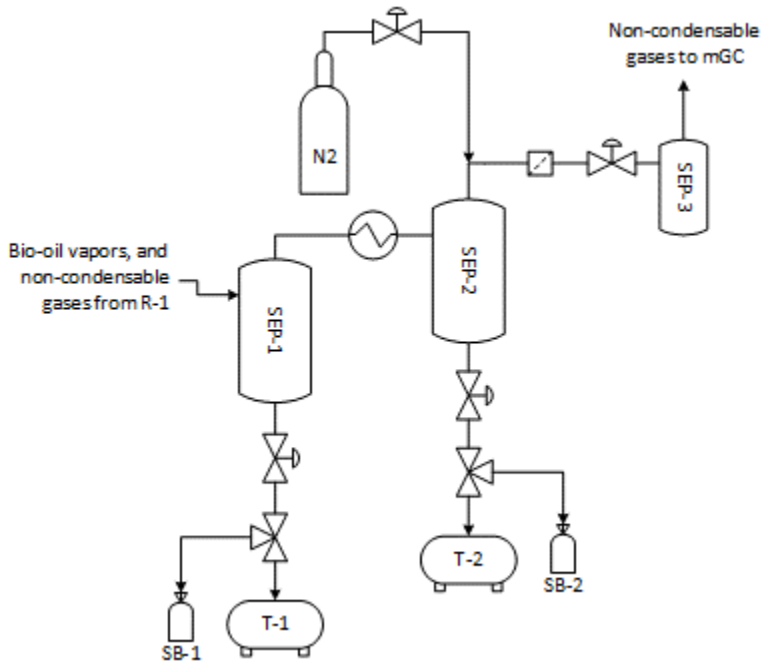

Figure 2. Process flow schematic of the overheads product handling system.

Solids filtration

As previously described, the system was designed such that any solid residue would settle to the bottom of R-1 for removal by batch-wise operation of severe-service ball valves. The heavy bio-oil and solid residue that passed through these valves were released into the solids removal vessel (T-R) shown in Figure 3. T-R was a 30 L elliptical-bottom tank operated at ambient temperature and pressure. To agitate the fluid mixture and prevent the solid residue from trapping bio-oil, a 10 cm mixer was inserted below the liquid level. A 50 µm stainless steel pleated mesh filter was submerged into the liquid a short distance from the bottom of T-R. This filter prevented large solid particles from being carried along with the free liquid that was pumped out of T-R through a Teledyne-Isco 500HP high-viscosity pump. Another stainless steel mesh filter with a nominal pore size of 5 µm was placed after the

pump to remove any fine particles remaining in the liquid stream. The solids-free liquid was then pumped into SEP-4 where the liquid was held at ambient conditions prior to being pumped to the bio-oil fractionation unit.

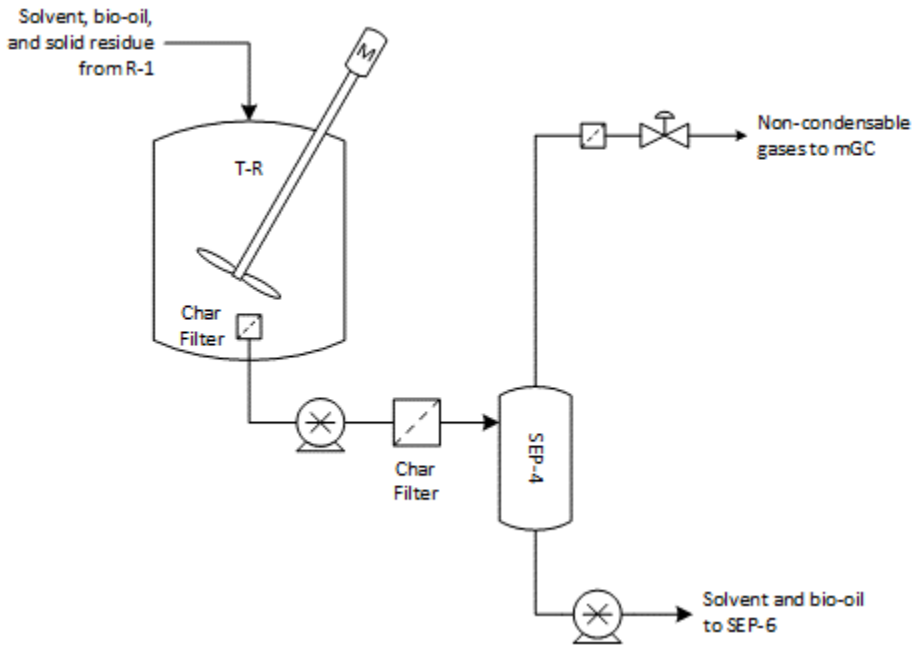

Figure 3. Process flow schematic of the solids filtration system.

The solids removal system was also designed to operate with an optional acetone stream injected into T-R, as shown in Figure 4. Lab-work suggested that acetone was able to solubilize tarry compounds that otherwise inhibited the filtration of bio-oil and could help disengage char from the liquid stream. Continuous consumption of acetone would be prohibitively expensive at an industrially relevant scale, so a system was devised to recover and recycle acetone. SEP-4 was built from tubing with an I.D. of 9.8 cm and a length of 40.6 cm for an internal volume of approximately 4.0 L. The liquid stream entered SEP-4 at approximately 120 °C, while the vessel itself was controlled to 93 °C and 1.1 bar. The

operating conditions were established such that acetone would flash from the liquid phase and carry overhead from SEP-4 into SEP-5. Acetone vapor was then condensed in HX-5, a 55-tube shell-and-tube heat exchanger purchased from Exergy LLC that was chilled to 10 °C with propylene-glycol. Condensed acetone was collected in SEP-5, which was of identical construction to SEP-4 and was held at ambient temperature. ST-5 was added as a storage tank for fresh acetone that was added to SEP-5 as necessary so that acetone was always available to be pumped into T-R.

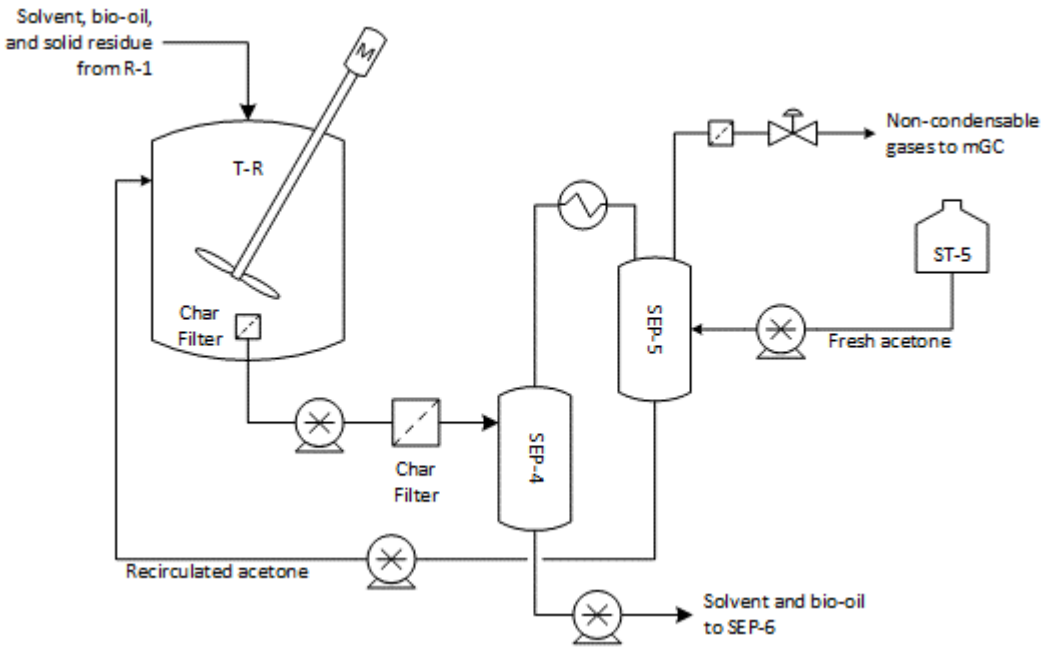

Figure 4. Process flow diagram of the acetone-assisted solids filtration system and subsequent acetone recovery.

Bio-oil fractionation

After solids and acetone were removed from the liquid stream, bio-oil was transferred from the bottom of SEP-4 to the bio-oil fractionation system depicted in Figure 5. The

primary goal of the fractionation system was to separate a cut of the bio-oil for use as a potential recycle solvent. This cut was targeted to contain molecules near the boiling point range of the hydrocarbon solvent. SEP-6 was designed as a randomly packed distillation column with an inner diameter of 4.7 cm. The total packing height in the stripping and rectifying sections was 15.8 and 41.7 cm, respectively. Each section was dump-packed with Cannon Pro-Pak distillation packing.

Hot nitrogen gas was used as the stripping agent. Flow was precisely controlled with an Alicat mass flow controller, and the gas was injected into the column at the bottom of the stripping section. The column was divided into 4 individual heat zones, which ranged in temperature from 149 to 316 °C, though the column was often operated isothermally. The internal column pressure was controlled to approximately 1.1 bar.

The overheads stream passed through an Exergy 55 tube heat exchanger (HX-7) that condensed products at 5 °C and collected in SEP-7, which was of identical construction to SEP-5. SEP-7 was also uninsulated and therefore held at ambient temperature.

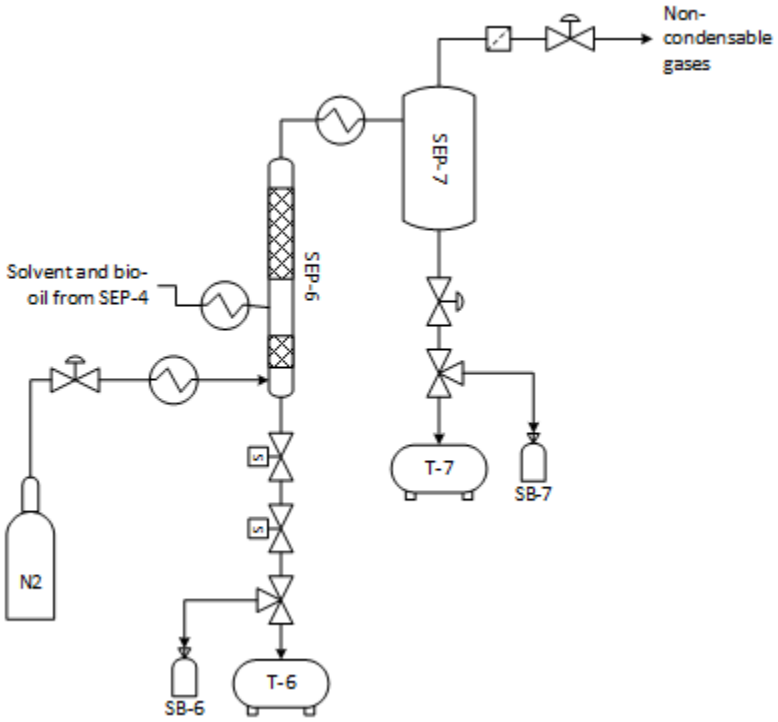

Figure 5. Schematic of the bio-oil fractionation system.

Product sampling

An automated protocol was developed to ensure consistent product sampling. Three-way valves were placed prior to the product tanks (T-#) at each sampling location. When actuated, the 3-way valves diverted flow from the product tanks into sample bottles (SB-#). The sample bottles were all sized such that they could contain the normal accumulation of product over the desired sample period, usually 20 minutes. After the sample period expired, flow was diverted back to the product tanks. Sample bottles were then collected, and their masses were recorded for the steady-state mass balance. All liquid samples were stored in HDPE bottles and placed in a cooler held at 5 °C for subsequent analysis.

Alicat Scientific M-series mass flow meters were used to quantify the flow rate of non-condensable gas streams that exited the system. After the flow meters, a slipstream was passed through a desiccate canister to remove residual moisture. Characterization of the dry slipstream was conducted with a Varian CP-4900 micro gas chromatograph (mGC). The mGC was calibrated to measure N_2, H_2, O_2, CO, CO_2, methane (CH_4), ethane (C_2H_6), ethylene (C_2H_4), and acetylene (C_2H_2). It was assumed that N_2 and O_2 were not products of the solvent liquefaction process. Thus, N_2 and O_2 weight fractions were subtracted from the gas stream data to complete the mass balance of biomass degradation products.

Analytical Methods

Total acid number (TAN) is the standard metric used by the petroleum industry to quantify the total acidity of a liquid sample. Following standard ASTM D664, this method accounts for the presence of strong acids (mineral acids), weak acids (carboxylic acids), and very weak acids (phenolic acids). A 798 MPT Titrino autotitrator was used, with 0.1 N potassium hydroxide in 2-propanol as the titrant. The solvent mixture was composed of 50 wt% reagent grade toluene, 49.5 wt% reagent grade 2-propanol, and 0.5 wt% 18.2 MΩ de-ionized water. A TAN standard was purchased from Fisher Scientific and was used to verify calibration of the instrument. A minimum of two tests were performed for each sample.

Ultimate analysis was conducted on a Elementar vario MICRO cube elemental analyzer. Samples were weighed out to be approximately 5 mg. Mass fractions of C, H, N, and S were calculated directly by the instrument, while O was calculated by difference. A minimum of three trials were performed for each analysis. Values are reported on a moisture-

free basis. HHV was calculated from the results of ultimate analysis according to the correlation published by Channiwala and Parikh [19].

Proximate analysis was conducted using a Mettler Toledo TGA/DSC 1 Thermo-Gravimetric Analyzer to determine the volatile content, fixed carbon, and ash content of a sample. A minimum of two samples were analyzed.

Moisture content was measured with a MKS 500 Karl Fischer Moisture Titrator according to ASTM E203. The titrant was Hydranal Composite 5K and the solvent was Hydranal Working Medium K. Samples were analyzed a minimum of four times.

Results & Discussion

Liquefaction performance

Three tests were conducted to evaluate the overall liquefaction performance and repeatability of the SL PDU. The average mass distribution of each product stream (including the solvent) is shown in Table 2. At least three steady-state samples were collected for each run to determine the reported averages. mGC analysis of overhead product gas streams was done continuously throughout the first several hours of each run, after which the mGC was switched over to analyze bottoms product gas. Most of the product gas was accounted for in the overhead products system, however some degassing did occur in the solids filtration and acetone recovery system due to the pressure letdown in T-R. The gas values reported in Table 2 are the sum of these sample locations.

As previously described, the process was operated at conditions to minimize product carryover into SEP-1. Thus, no mass was collected in SEP-1 for either of the three runs

reported here. The bio-oil collected in SB-2 existed as a two-phase mixture, with an oil phase on top and an aqueous phase on bottom. SEP-2 collected the majority of the water present in the system. Water was either fed into the system as biomass moisture or produced as a result of dehydration reactions. The white opaque aqueous phase in SEP-2 accounted for 88.9 wt% of the mass collected from SEP-2, and only 7.2 wt% of the total mass exiting the SL PDU. The oil phase collected in SB-2 was light brown in color and translucent. SB-4 accounted for approximately 85.5 wt% of the mass output by the SL PDU. This was unsurprising given that the operating conditions were such that solvent and most of the bio-oil would remain in the liquid phase. This bio-oil was black in appearance and was recovered as a single phase. The bio-oil collected in SB-4 was the same material that is pumped into the bio-oil fractionation system (see Figure 5). Further details on the performance of the fractionation system will be discussed later.

Table 2. Mass distribution (wt%) of product streams collected from the SL PDU.

Sample ID	**3-20160712A**	**3-20160726A**	**3-20160802A**	**Average**
Acetone Insolubles	3.5 ± 0.1	3.8 ± 0.1	5.1 ± 0.1	4.1 ± 0.4
SB-1	-	-	-	-
SB-2	8.1 ± 0.5	6.7 ± 0.3	4.3 ± 0.1	6.4 ± 0.9
Top	0.9 ± 0.1	0.9 ± 0.3	1.0 ± 0.1	1.0 ± 0.1
Bottom	7.2 ± 0.7	5.8 ± 0.4	3.3 ± 0.1	5.4 ± 0.9
SB-4	84.1 ± 0.6	85.0 ± 0.4	87.4 ± 0.2	85.5 ± 0.8
SB-6	25.4 ± 0.7	20.9 ± 0.3	18.4 ± 0.3	21.6 ± 1.7
SB-7	58.7 ± 0.6	64.1 ± 0.7	69.0 ± 0.2	63.9 ± 2.4
Gas	2.4 ± 0.3	2.0 ± 0.1	3.1 ± 0.3	2.5 ± 0.3

Uncertainty reflects the standard error of the mean for a minimum of 3 samples.

Table 3 summarizes the composition of the gas stream. Primary gases produced during liquefaction were deoxygenation products CO_2 and CO. Minor gaseous products were light hydrocarbons (CH_4, C_2H_4, and C_2H_6).

Table 3. Gas composition (wt%) during steady-state SL PDU operation.

Compound	3-20160712A	3-20160726A	3-20160802A	Average
H_2	0.1 ± 0.1	0.1 ± 0.1	0.1 ± 0.1	0.1 ± 0.1
CH_4	2.1 ± 0.1	1.4 ± 0.1	1.7 ± 0.1	1.7 ± 0.3
C_2H_4	0.3 ± 0.1	0.3 ± 0.1	0.3 ± 0.1	0.3 ± 0.1
C_2H_6	0.7 ± 0.1	0.516 ± 0.1	0.6 ± 0.1	0.6 ± 0.1
CO	27.4 ± 0.2	26.2 ± 1.0	27.9 ± 0.2	27.2 ± 0.9
CO_2	69.5 ± 0.2	71.5 ± 1.0	69.5 ± 0.1	70.2 ± 1.2

Uncertainty reflects the standard error of the mean for a minimum of 3 samples.

The data shown in Table 2 was further analyzed to determine the yield of biomass derived products on an ash-free (AF) and moisture (MF) biomass basis. This was conducted by subtracting the mass of solvent injected into the system from the total liquid mass output from the system. Assuming that all aqueous, solid, and gaseous products were generated solely from the biomass, the solvent-free liquid mass represented all biomass-derived liquid products. Unfortunately, complete quantification of the concentration of hydrocarbon solvent in each fraction was not possible and this analysis can only be reported on a total system basis, as illustrated in Figure 6. The bio-oil yield for the system ranged from 47.2 wt% to 54.1 wt%, with an average of 51.2 wt% across the three runs. On average, the mass fraction of remaining products was essentially equal: aqueous (13.4 wt%), gas (17.7 wt%), and char (18.8 wt%) products.

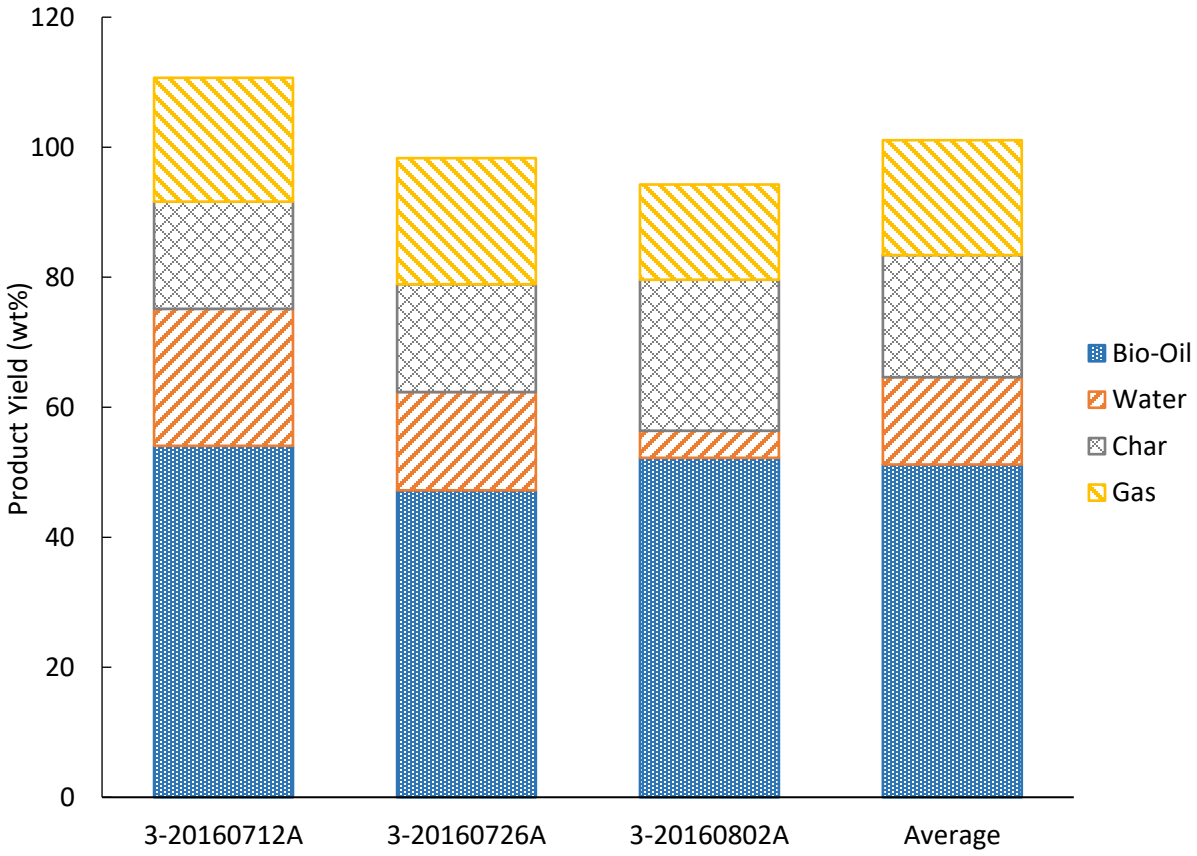

Figure 6. Total biomass-derived product yields generated during pine liquefaction in hydrocarbon solvent on an ash-free, moisture-free biomass basis.

Due to the tendency of the bio-oils collected from the SL PDU to separate into organic and aqueous phases, bio-oils had very low moisture content, as shown in Table 4. This behavior is attributed to the use of a hydrocarbon solvent and the mild hydro-deoxygenation of biomass degradation products. Given that the average mass fraction of water was 13.4 wt%, the SL process explored in this study produced less water than is typically found in fast pyrolysis, which is known to produce bio-oils with 15-30 wt% water

content [20]. Total acid number (TAN) and viscosity were also substantially lower and the higher heating value (HHV) was higher than for bio-oil from fast pyrolysis [21, 22].

Table 4. Selected physical properties of liquid products collected from the SL PDU.

Sample ID	**Moisture (wt%)**	**TAN (mg_{KOH} g^{-1})**	**Dynamic Viscosity[a] (cP)**	**Calculated HHV (MJ kg^{-1})[b]**
SB-1	-	-	-	-
SB-2	-	-	-	-
Top	0.8 ± 0.3	10.7 ± 0.1	2.1 ± 0.1	38.8 ± 0.6
Bottom	82.3 ± 0.4	83.0 ± 0.4	2.8 ± 0.1	10.2 ± 0.1
SB-4	-	-	-	-
SB-6	0.9 ± 0.1	50.9 ± 0.1	17.7 ± 0.6	38.1 ± 0.2
SB-7	0.8 ± 0.1	3.1 ± 0.2	2.05 ± 0.1	37.4 ± 0.2

[a] Measured at 40 °C
[b] Determined on an ash-free, moisture-free basis
Uncertainty reflects the standard error of the mean for a minimum of 3 samples.

Given that the hydrocarbon solvent did not contain any elemental oxygen, it was possible to conduct an oxygen balance on the entire system. This was useful to determine the fate of oxygen and evaluate the effectiveness of deoxygenating the feedstock. The average balance across the three runs is shown in Figure 7. Approximately 17.6 wt% of the initial oxygen in the feedstock was recovered as water produced from dehydration and hydrodeoxygenation. Hydrodeoxygenation of organic compounds can occur if sufficient hydrogen is available in the system.

Decarbonylation and decarboxylation are also prominent means for deoxygenation [23]. Over 23.4 wt% oxygen was rejected from the biomass through these reactions. This resulted in approximately 55.6 and 3.4 wt% of the oxygen remaining in the bio-oil and solid

residue, respectively. Considering the initial oxygen content of the southern yellow pine was 41.7 wt% (Table 1) this results in a total oxygen content of 23.2 wt% in the bio-oil as a whole.

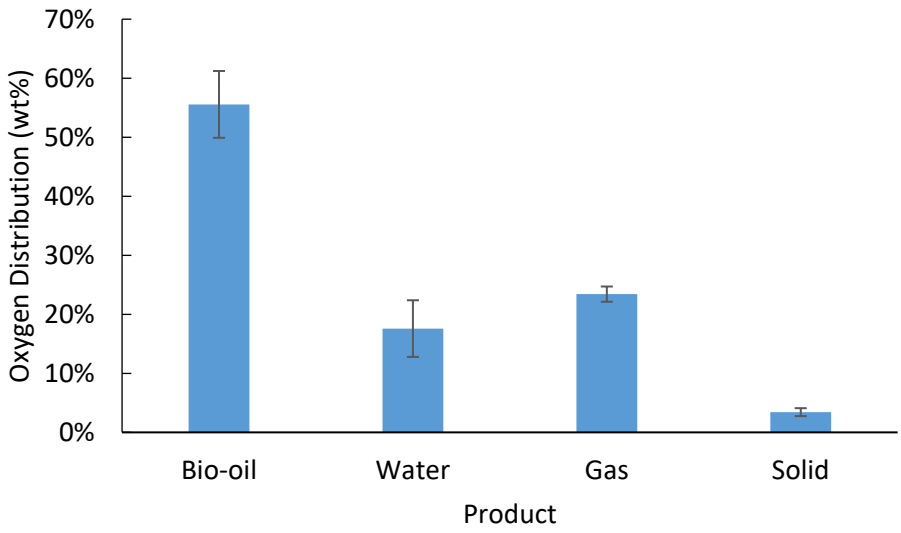

Figure 7. Oxygen balance across the whole system on an ash-free, moisture-free biomass basis. Error bars represent the standard error of the mean for the three runs.

Char separation

Char was removed with the acetone-free on-line filtration system (depicted in Figure 3) for at least 6 h of continuous operation without clogging the 50 µm particulate filter or the in-line 5 µm finishing filter. Off-line acetone-assisted filtration of the SEP-4 product stream through 0.45 µm PTFE filters demonstrated that the tandem filtration system (50 µm filter in T-R and in-line 5 µm finishing filter) was able to remove a significant portion of solids in the stream leaving R-1. The bio-oil/solids mixture entering T-R was comprised of approximately

5 wt% solids, while the bio-oil collected in SEP-4 contained an average of 0.01 wt% solids. This resulted in a total calculated filtration efficiency of 99.8%.

It was apparent that some potentially recoverable liquid remained in T-R at the end of each experiment. We hypothesized two possible explanations. First, the placement of the 50 μm off-take filter made it difficult to pump all the free liquid from the tank. Second, solid residue in T-R trapped some liquid, making it difficult to pump out this liquid regardless of filter placement. For one experiment, as much as 9.2 kg of solids-laden liquid was remaining in T-R. To determine the amount of free (theoretically pumpable) liquid remaining, all of this material was vacuum-filtered without the use of acetone. Approximately 3.8 kg (41 wt% of the mixture) was recovered as free liquid. The remainder was assumed to consist of char and trapped liquid. The remaining material was then vacuum-filtered with acetone to determine the amount of trapped liquid and clean char. Approximately 88 wt% of this media was acetone-soluble material, resulting in a recovery of only 0.5 kg of clean solid residue from the initial 9.2 kg sample. This demonstrated the significant benefits of acetone-assisted filtration, and the need for efficient filtration methods to recover all available liquid from the solid residue stream.

Initial char filtration attempts were conducted without the use of the mixer shown in Figure 3. Operation of the system without the impeller resulted in even more significant loss of bio-oil to the char that described above. It was determined that without mechanical agitation, the char/bio-oil mixture created a sludge (shown in Figure 8) that trapped a substantial amount of liquid. In the picture, it can be seen that there are two distinct phases of material that developed after letting a char/bio-oil mixture settle for nearly 3 h. The top phase

was free liquid (solvent and bio-oil) and accounted for only a small fraction of the material initially placed in the beaker. The majority of the char/bio-oil mixture was contained in the sludge at the bottom of the beaker. We hypothesized that this sludge was formed when char particles were allowed to settle slowly to the bottom of a vessel. Due to a small density difference between the char and the heavy liquid, this mixture could set up and trap a substantial amount of free liquid within the interstitial space between char particles if given enough time.

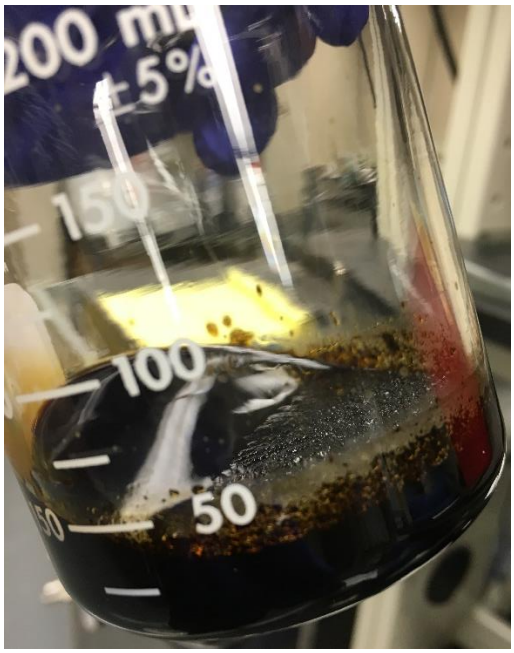

Figure 8. Char/bio-oil sludge formed after mixture was allowed to settle for 3 h.

Acetone separation and recovery

Acetone pumped into the stream entering the solids filtration vessel (T-R) was separated via the flash separation vessel (SEP-4) and subsequently recovered in SEP-5. It is

desirable to recover close to 100% of the acetone fed into the system for an economical process. Given the already low pressure of SEP-4 (1.1 bar) and the desire to avoid vacuum service, liquid temperature was the only parameter available to influence the separation of acetone from the liquid stream. A model was constructed in Aspen Plus to simulate flash separation at temperatures ranging from 93-149 °C. Several tests were then conducted on the SL PDU to validate the model and demonstrate continuous separation and recovery of acetone. The goal of the experiments was to minimize the loss of acetone to the stream exiting SEP-4 bottoms. Predicted and experimental data was plotted in Figure 9. Surprisingly, the acetone separation was more effective in the experiment than was predicted by the model. This was likely due to limitations in the chemical interactions of the mixture as predicted by the model.

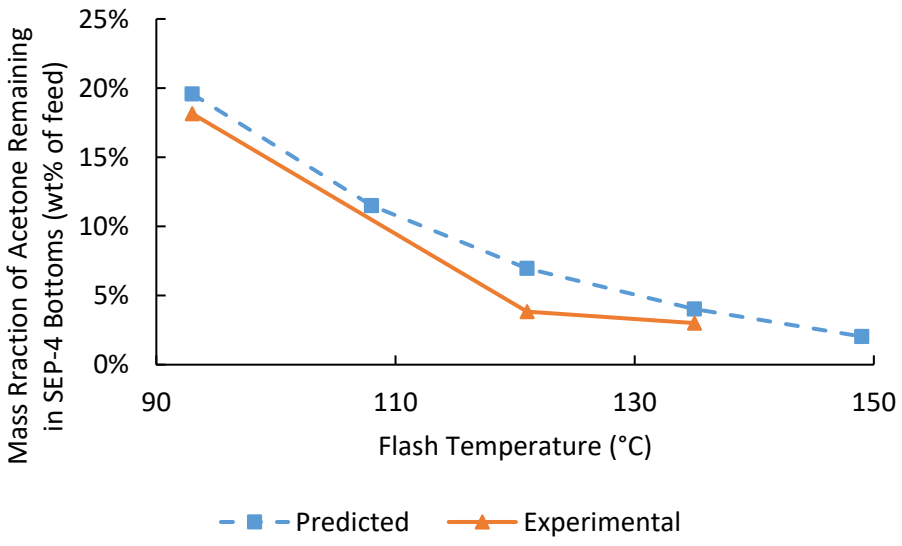

Figure 9. Predicted (Aspen Plus) and experimental data for acetone loss to SEP-4 bottoms. Data is presented as weight percent of acetone feed that remained in the liquid stream leaving SEP-4 bottoms.

Acetone separation achieved 97% efficiency (i.e. 3% acetone loss) at a flash temperature of 135 °C. Additional increases in the vessel temperature were expected to result in improved separation efficiency, but concerns over long-term thermal stability of the bio-oil also increased at elevated temperatures. Furthermore, given that the separation was 1% better than the model predicted, it was determined to be sufficient for the purposes of this study.

Acetone recovery was also experimentally determined by the amount of acetone collected in SEP-5 during the separation tests described above. The difference between the separation efficiency and the recovery efficiency indicated whether acetone was likely being consumed by the process. However, no indication for acetone consumption was observed. The acetone recovery was determined to be 83.5, 93.7 and 98.6 wt% at 93, 121 and 135 °C, respectively. Thus, there was no concern over the reactivity of acetone at these temperatures, indicating successful acetone recycle.

Bio-oil fractionation

Prior to implementation of the fractionation system, a series of tests were conducted to determine the thermal stability of the product stream. Several samples of acetone-free heavy bio-oil recovered from SEP-4 were placed in 13.5 mL stainless steel vessels and heated to 100, 200, or 300 °C for 60 or 120 seconds. A more thorough explanation of the experimental procedure and analytical methods can be found elsewhere [24]. The temperatures and duration were selected to closely approximate the thermal severity of the fractionation process used in the SL PDU. Change in relative molecular weight (RMW) of

the thermally processed samples compared to that of the starting sample is shown in Figure 10. Only modest changes of about 5% or less were found for this bio-oil, and increasing temperature up to 300 °C appeared to have insignificant influence compared to lower temperatures. The conclusion of this portion of the study was that the heavy oil product of the SL PDU exhibited sufficient thermal instability to remain unchanged following thermal fractionation up to 300 °C.

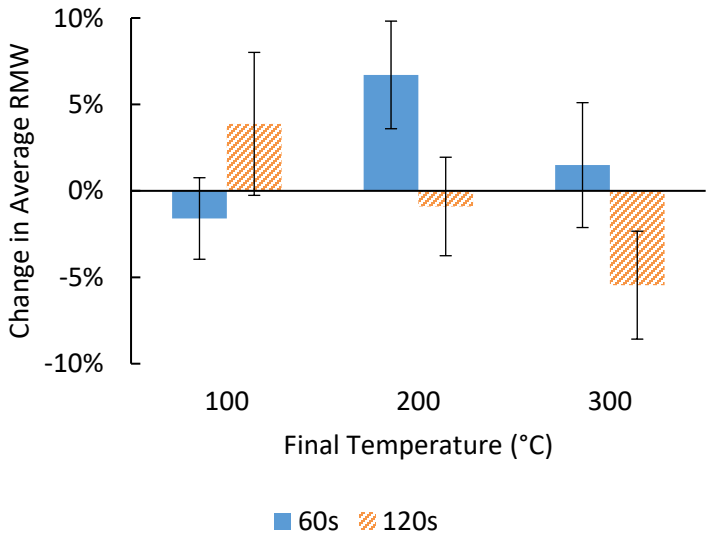

Figure 10. Change in average relative molecular weight (RMW), as determined by gel permeation chromatography, of acetone-free heavy bio-oil recovered from SEP-4 after thermal processing at elevated temperatures. Error bars reflect the standard error of the mean for a minimum of 3 samples.

The first several runs on the bio-oil fractionation system were used to explore the influence of column temperature on the distribution of the distillate and raffinate. The goal of these tests was to demonstrate separation and recovery of recycle solvent at the lowest column temperature possible. Preliminary modelling suggested that a column temperature approaching 200 °C would be necessary to achieve the desired split. Across two separate

runs all variables were held constant except for the column temperature, which was gradually increased from 149 to 204 °C. Recovery of the distillate and raffinate was compared as a mass fraction of the column feed, as shown in Figure 11. At 204 °C the mass of distillate recovered from the bio-oil fractionation system accounted for over 86% of the solvent fed to the reactor. This was determined to be a sufficient recycle rate for the purposes of this project, with the balance being made-up with fresh hydrogen donor solvent.

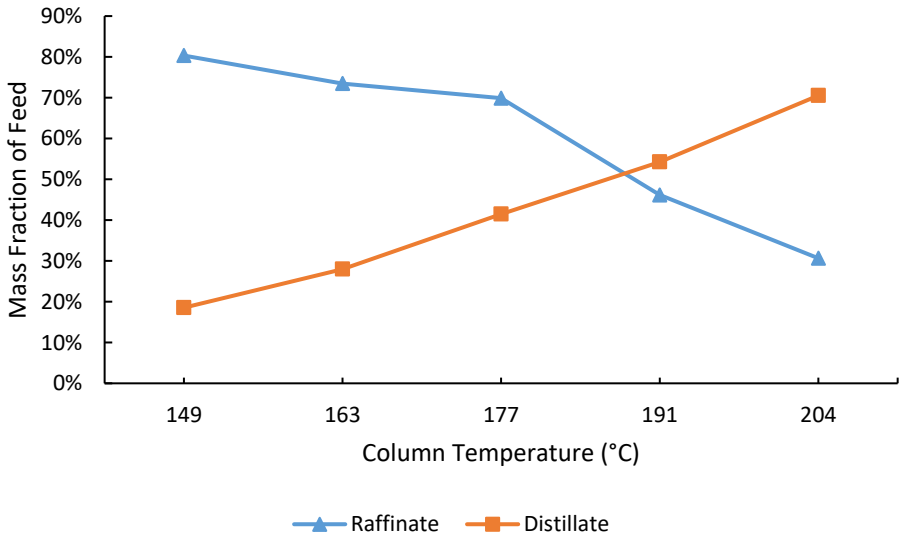

Figure 11. Influence of column temperature on the mass fraction of the feed recovered as distillate or raffinate. All other variables were held constant.

After the operating conditions of the bio-oil fractionation system were established, several extended-duration experiments were conducted to verify its operational consistency. For more than 25 h of run time the average split was 24% raffinate and 76% distillate, each with a 1% standard error of the mean. The distillate is predominantly recovered hydrocarbon solvent and wood-derived monomers with boiling points below 204 °C. This stream accounts for approximately 93 wt% of the initial solvent input. As shown in Figure 12, the distillate

was a low-viscosity clear liquid with an amber hue. It is suitable for use as recycle solvent. Conversely, the raffinate was black in color with a slightly higher viscosity, though still mobile at ambient conditions. This cut likely contained phenolic oligomers and anhydrosugars produced from lignin and carbohydrate, respectively, in the biomass.

Figure 12. Acetone-free bio-oil from SEP-4 (left) is fed into the bio-oil fractionation system which separates the feed into a raffinate (center) and distillate (right), otherwise referred to as heavy bio-oil and medium oil, respectively.

Conclusions

Loblolly pine was converted into liquid products at total average yield of 51.2 wt%, which compares favorably to the PERC process (40-50 wt%) [25] and similar continuous SL processes [14, 26]. The proprietary hydrocarbon solvent used in this study resulted in product streams with low viscosity, low oxygen content, and low moisture. The liquid products were collected in three separate cuts, according to boiling point. Continuous on-line bio-oil fractionation separated the hydrocarbon solvent and biomass-derived monomers from a heavy oil cut containing phenolic oligomers and anhydrosugars with a small amount of

residual hydrocarbon solvent to reduce the mixture viscosity. The mass split from the bio-oil fractionation system was demonstrated to be consistent and repeatable, and the liquid feed was shown to have sufficient thermal stability that the product quality was not jeopardized. Apart from an aqueous product stream that phase separated with the rest of the products, all organic streams were miscible in hydrocarbons, and therefore suitable for use as petroleum blendstock.

On-line char separation was explored with and without the use of acetone. Without acetone it was determined that mechanical agitation was necessary to reduce the amount of liquid retained in the char. In the presence of acetone, char readily separated from the liquid stream with minimal losses of residual liquid. Solids concentration downstream of the 5 μm polishing filter was less than 1 ppm, resulting in a solids separation efficiency of greater than 99.8%. Continuous recycle of acetone via a one-stage flash separation operated at just above ambient pressure was demonstrated with 97% recovery.

Acknowledgements

The authors would like to thank BEI staff scientists Patrick Hall, Patrick Johnston and Marge Rover for their assistance with analyzing the SL PDU product streams. We would also like to thank our crew of undergraduate research assistants who helped to construct, operate, and maintain the SL PDU. Lastly, a special thanks to personnel at Chevron, U.S.A for their expertise and guidance throughout the project.

Funding Sources

This work was supported by the U.S. Department of Energy and Chevron U.S.A, Inc. acting through its division Chevron Technology Ventures.

References

1. Moffatt, J.M. and R.P. Overend, *Direct liquefaction of wood through solvolysis and catalytic hydrodeoxygenation: an engineering assessment.* Biomass, 1985. **7**(2): p. 99-123.

2. Behrendt, F., et al., *Direct liquefaction of biomass.* Chemical engineering & technology, 2008. **31**(5): p. 667-677.

3. van Rossum, G., et al., *Liquefaction of Lignocellulosic Biomass: Solvent, Process Parameter, and Recycle Oil Screening.* ChemSusChem, 2014. **7**(1): p. 253-259.

4. Ghosh, A., R.C. Brown, and X. Bai, *Production of solubilized carbohydrate from cellulose using non-catalytic, supercritical depolymerization in polar aprotic solvents.* Green Chemistry, 2015.

5. Mellmer, M.A., et al., *Effects of γ-valerolactone in hydrolysis of lignocellulosic biomass to monosaccharides.* Green Chemistry, 2014. **16**(11): p. 4659-4662.

6. Vasilakos, N.P. and D.M. Austgen, *Hydrogen-donor solvents in biomass liquefaction.* Industrial & Engineering Chemistry Process Design and Development, 1985. **24**(2): p. 304-311.

7. Kleinert, M. and T. Barth, *Towards a lignincellulosic biorefinery: direct one-step conversion of lignin to hydrogen-enriched biofuel.* Energy & Fuels, 2008. **22**(2): p. 1371-1379.

8. Kim, K.H., et al., *Hydrogen-Donor-Assisted Solvent Liquefaction of Lignin to Short-Chain Alkylphenols Using a Micro Reactor/Gas Chromatography System.* Energy & Fuels, 2014. **28**(10): p. 6429-6437.

9. Liu, Z. and F.-S. Zhang, *Effects of various solvents on the liquefaction of biomass to produce fuels and chemical feedstocks.* Energy Conversion and Management, 2008. **49**(12): p. 3498-3504.

10. Chornet, E. and R.P. Overend, *Biomass liquefaction: an overview*, in *Fundamentals of thermochemical biomass conversion*. 1985, Springer. p. 967-1002.

11. Ergun, S., *Biomass liquefaction efforts in the United States*. 1980, Lawrence Berkeley Laboratory.

12. White, D., N. Schott, and D. Wolf, *Experimental study of an extruder-feeder for biomass direct liquefaction.* The Canadian Journal of Chemical Engineering, 1989. **67**(6): p. 969-977.

13. White, D.H., D. Wolf, and Y. Zhao, *Biomass liquefaction utilizing extruder-feeder reactor system.* Amer. Chem. Soc., Div. Fuel Chem. Prprts., 1987. **32**(2): p. 106.

14. Elliott, D.C., et al., *Developments in direct thermochemical liquefaction of biomass: 1983-1990.* Energy & Fuels, 1991. **5**(3): p. 399-410.

15. Furlong, L., et al., *Coal processing: the Exxon donor solvent process.* Chem. Eng. Prog.;(United States), 1976. **72**(8).

16. Chen, N.Y., et al., *Liquefaction of carbonaceous materials*. 1981, Google Patents.

17. Kuehler, C.W., *Three-stage coal liquefaction process*. 1981, Google Patents.

18. Haverly, M.R., L.E. Whitmer, and R.C. Brown, *Evaluation of Polymer Compatibility with Bio-oil Produced from Thermochemical Conversion of Biomass.* Energy & Fuels, 2015. **29**(12): p. 7993-7997.

19. Channiwala, S.A. and P.P. Parikh, *A unified correlation for estimating HHV of solid, liquid and gaseous fuels.* Fuel, 2002. **81**(8): p. 1051-1063.

20. Brown, R.C., *Thermochemical processing of biomass: conversion into fuels, chemicals and power*, ed. C. Stevens. Vol. 12. 2011: John Wiley & Sons.

21. Pollard, A., M. Rover, and R. Brown, *Characterization of bio-oil recovered as stage fractions with unique chemical and physical properties.* Journal of Analytical and Applied Pyrolysis, 2012. **93**: p. 129-138.

22. Oasmaa, A., E. Kuoppala, and Y. Solantausta, *Fast pyrolysis of forestry residue. 2. Physicochemical composition of product liquid.* Energy & fuels, 2003. **17**(2): p. 433-443.

23. Wang, K., K.H. Kim, and R.C. Brown, *Catalytic pyrolysis of individual components of lignocellulosic biomass.* Green Chemistry, 2014. **16**(2): p. 727-735.

24. Haverly, M.R., K.V. Okoren, and R.C. Brown, *Thermal stability of fractionated bio-oil from fast pyrolysis.* 2016.

25. Lindemuth, T. *Investigations of the PERC process for biomass liquefaction at the Depatment of Energy, Albany, Oregon Experimental Facility*. in *ACS Symp. Ser.;(United States)*. 1978. Bechtel National, Inc., San Francisco, CA.

26. Vanasse, C., E. Chornet, and R.P. Overend, *Liquefaction of lignocellulosics in model solvents: Creosote oil and ethylene glycol.* The Canadian Journal of Chemical Engineering, 1988. **66**(1): p. 112-120.

CHAPTER 3

THE EFFECT OF MOISTURE ON HYDROCARBON-BASED SOLVENT LIQUEFACTION OF BIOMASS

A paper to be submitted to *Green Chemistry*

Martin R. Haverly, Arpa Ghosh, Robert C. Brown

Abstract

In this paper, we examined the effect of moisture on the solvent liquefaction of loblolly pine, cellulose, and lignin in tetralin at 280 °C and pressures ranging from 15 to 70 bar. Solvent liquefaction experiments were conducted in a quasi-batch reactor capable of continuous pressure control and external vapor condensation. Moisture was varied by the controlled addition of de-ionized water. Control over the system pressure subsequently impacted the removal of water vapor from the reactor. Liquid yield decreased by 25, 21, and 35 wt%, for pine, cellulose, and lignin, respectively, when moisture content was increased from 1 to 50 wt% at 42 bar. Humins were observed in the solid residue from liquefaction of wet cellulose. Wet lignin yielded a substantial amount of solid residue compared to dry lignin with a corresponding decrease in total phenolic monomer production. It was concluded that the ionic dissociation of water was an important factor in loss of liquid yield in the presence of water. Although water was less than 20 wt% of the solvent loading in these experiments, it strongly influenced the liquefaction of biomass and biomass components.

Introduction

Direct liquefaction is a promising technology for converting biomass to liquid fuels and chemicals for a variety of reasons. Among these is the ability for direct liquefaction to process feedstocks with a relatively high moisture content. Alternative conversion pathways like fast pyrolysis and gasification are unable to accommodate high-moisture feedstocks due to the extremely high heating rates required to thermally fragment biomass into desirable compounds [1, 2]. Conversely, direct liquefaction processes such as hydrothermal liquefaction and solvent liquefaction (SL) are generally considered to be less affected by heating rates [3, 4]. This benefit is largely attributed to the interaction of liquid solvents with the biomass degradation products in two key ways. The first is simply dilution of reactive degradation compounds, preventing further recombination or repolymerization [5, 6]. The second is to solubilize, fragment, and even react with the products of pyrolytic degradation, as is the case with hydrogen donor solvents [7]. Some solvents have also been shown to enhance the rate of primary decomposition reactions [5, 8].

Although high moisture content is less of a barrier to direct liquefaction of biomass than it is for other thermochemical conversion processes [9], water clearly influences conversion of biomass and yields of products during solvent liquefaction. For example, water can promote both hydrolysis of biomass and dehydration of products [10, 11].

As defined in this study, SL processes employ solvents other than water. Thus, if water is introduced to the system, whether directly as a co-solvent or indirectly as biomass moisture, understanding its behavior has significant bearing on the design of a continuous solvent-mediated process. This is of particular interest for a hydrocarbon SL system because

of the extremely low solubility between water and hydrocarbons. Tetralin is a widely used solvent for SL of biorenewable feedstocks [12-16]. This is predominantly due to its ability to donate as many as four moles of hydrogen per mole of tetralin at relatively low temperatures and pressures [7]. It is also a promising solvent for use in continuous systems, such as the Exxon Donor Solvent process, due to its thermal stability for recovery and ease of hydrogenation for recycle [17, 18].

Li et al. has examined the impact of using water and tetralin as co-solvents in the liquefaction of bagasse [19] and eucalyptus woodchips [20] pretreated with NaOH. They found that at 300 °C, mixtures of 1:1 water and tetralin yielded the highest solids conversion and heavy-oil yield. This compared favorably to either solvent by itself. These results led the researchers to conclude that the presence of water caused the pressure of their closed-system reactor to increase and thereby enhanced the hydrogen shuttling capability of tetralin.

Water has been explored by several other researchers as a co-solvent for polar solvent systems, like phenol [21-23] and p-cresol [24]. Improved liquid yields are often achieved with the addition of water to these systems when in the supercritical regime [22], while the addition of a base catalyst is necessary to see improved yields in the subcritical regime [23].

van Rossum et al. [25] observed significant difference between the SL of dry and wet (50 wt% moisture) wood. They found that wet wood had decreased solid yields over dry wood when reacted in guaiacol, hexanoic acid, and n-undecane at 300 °C. The decrease in solids yield with water was found to be most significant for the polar solvents, guaiacol and hexanoic acid, than for non-polar n-undecane [25]. Another study from van Rossum was also conducted using pine with 0, 10 and 20 wt% moisture in guaiacol [4]. Here the authors noted

that water acted primarily as a catalyst to accelerate wood conversion, thereby reducing the necessary residence time. This resulted in a minor solid yield reduction when compared to dry feed at long residence times. The researchers did also note that the addition of moisture greatly increased the operating pressure of the closed system.

The majority of research on SL of biomass has been conducted in lab-scale batch reactors. These reactors are almost exclusively operated as closed systems, wherein the contents are not removed until the reactor has been brought back to ambient conditions at the end of the desired residence time. This approach has several inherent limitations when attempting to extrapolate these results to continuous liquefaction systems. The foremost of which is a lack of control over the system operating pressure. A small number of previous studies were able to explore this effect, and system pressure has been shown to impact the conversion of biomass in both aqueous and non-aqueous systems [3, 26, 27]. It should be noted that even among the studies mentioned, many do not control the pressure of the system directly, but rather by varying the initial charge pressure of the cold reactor.

The lack of pressure control is most consequential when examining SL systems that employ solvents with relatively high boiling points. These systems do not require immense pressures to maintain the solvent in the liquid phase, and therefore are very attractive for scale-up. However, since lab-scale units are typically operated in a closed system configuration, the pressure often greatly exceeds that which would be expected in a continuous system. This results in exaggerated system equilibria, and therefore has the potential to skew reaction results. This is perhaps most significant when examining the behavior of water during SL in non-aqueous solvents.

This study explores the influence of moisture on the SL of loblolly pine, cellulose and lignin in tetralin solvent. A quasi-batch stirred tank reactor with continuous pressure control and vapor condensation was employed to emulate the isobaric conditions of continuous processing. Using this apparatus, we first demonstrate the isolated effect of pressure on the product distribution of each feed material in the absence of moisture. We then explore the combined effects of moisture and pressure on product distribution and quality. The observed decrease in liquid yield and corresponding increase in solid yields for wet cellulose and lignin are thoroughly investigated. The ionic dissociation of water is found to be a primary driver in the deleterious influence of moisture on the SL of biomass in tetralin.

Experimental

Loblolly pine (pinus taeda) consisting of 39% cellulose, 32% hemicellulose, and 29% lignin on a mass basis served as whole biomass for this study. It was ground and sieved to a particle size of 6.4 mm (0.25 in) or less. Microcrystalline cellulose was purchased from Sigma Aldrich. Technical lignin came from the Renmatix, Inc., which extracts lignin from mixed hardwoods via supercritical hydrolysis. This lignin is thought to be less modified than many other technical lignins, making it a suitable proxy for behavior of native lignin. Elemental analysis and as-received moisture of each material is shown below in Table 1.

Table 1. Ultimate analysis and as-received moisture of loblolly pine, cellulose, and lignin used in experiments. All values are reported on a mass basis, the ultimate analysis values were adjusted for ash and moisture content.

	Loblolly Pine	**Cellulose**	**Lignin**
C	52.8%	42.1%	55.2%
H	5.3%	5.5%	5.2%
N	0.2%	0.0%	0.1%
S	0.0%	0.0%	0.0%
O (by difference)	41.7%	52.4%	39.4%
Initial Moisture	55%	4%	7%

All samples were dried in an electric convection oven at 105 °C for a minimum of 48 h to reach a moisture of less than 1 wt%, with the exception of partially-dried pine samples discussed later. Moisture was determined using an Ohaus MB 25 moisture analyzer.

Reagent grade (≥ 97%) 1,2,3,4-tetrahydronaphthalene (tetralin) was acquired from Advanced Aromatics as the primary solvent for these experiments. 18.2 MΩ de-ionized (DI) water produced on-site was used as a surrogate moisture. 5-hydoxymethylfurfural (5-HMF) and furfural model compounds were purchased from Fisher Scientific with a purity of greater than 99%. D-Glucose (purity > 99%) and D-mannose (purity > 99%) were purchased from Fisher Scientific and Acros Organics, respectively.

In an effort to gain continuous control over the operating pressure of the SL system and to emulate a continuous process, a high-pressure overheads handling system was employed in conjunction with a 500 mL Parker Autoclave Engineers EZE-Seal Stirred

Reactor. As shown in Figure 1, gases and vapors that left the reactor passed through Condenser 1 which reduced the process stream to 10 °C and collected any condensable products. Any remaining vapors and all non-condensable gases continued through Condenser 1 to a back pressure regulator set to ambient pressure. Condenser 2 was also chilled to 10 °C, and collected any additional condensate prior to ventilation.

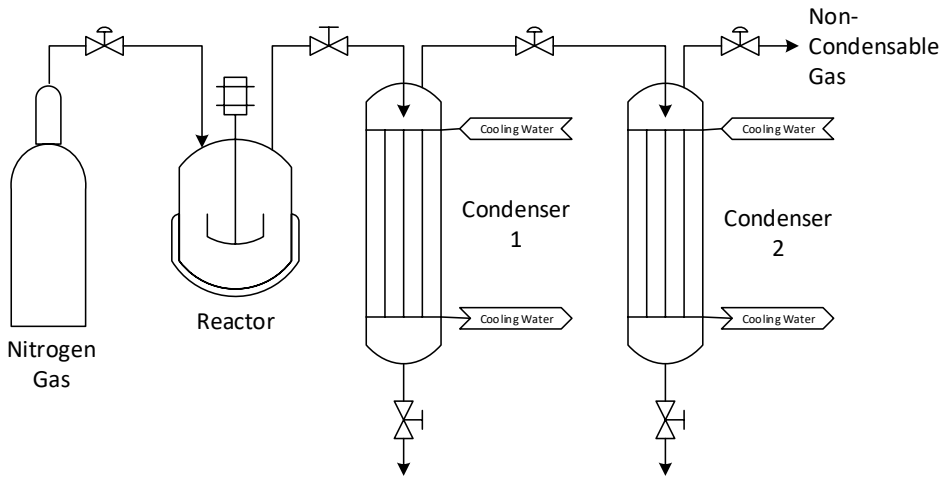

Figure 1. Block flow diagram for the continuous condensation and pressure relief system attached to the continuously stirred reactor.

In the present study, system pressure was controlled to 15, 29, 42 or 70 bar. These pressures were selected based on the vapor pressure of pure water at the reaction temperature of 280 °C. From the Antoine equation coefficients determined by Liu and Lindsay [28], the vapor pressure of pure water at 280 °C was calculated to be 55.7 bar. Thus, by manipulating the process pressure water was either predominantly in the vapor or liquid phase at the final reaction temperature as shown in Figure 2. Furthermore, water vapor was able to leave the reactor entirely, rendering the reaction mixture almost entirely moisture-free. Data from

preliminary experiments that explored the physical behavior of water at various pressures can be found in Appendix A.

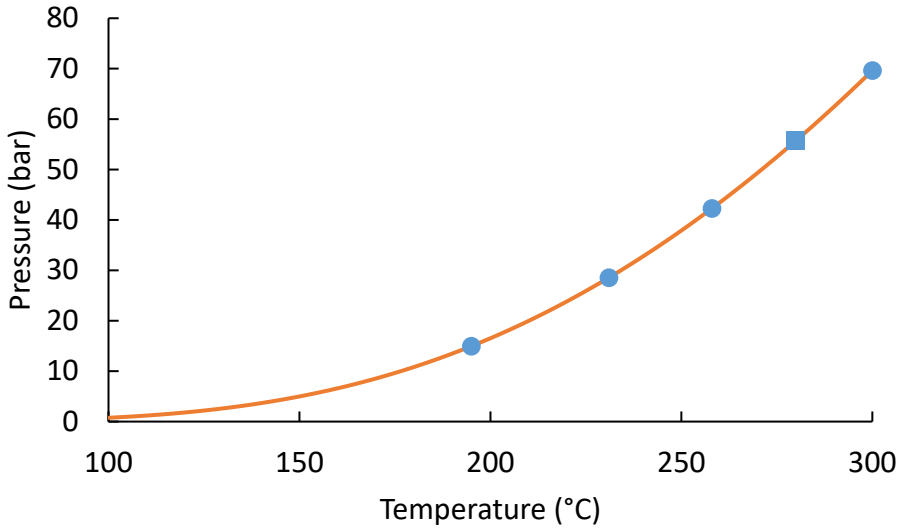

Figure 2. Boiling point curve for pure water as determined by the Antoine equation. The square (■) corresponds to the theoretical vapor pressure of pure water at the final reaction temperature of 280 °C. The circles (●) correspond to the theoretical boiling point of pure water at each of the operating pressures explored in this study.

SL experiments were conducted with 25 g of bone-dry samples. Specific quantities of 18.2 MΩ DI water were then added to wet the samples to prescribed moisture levels as indicated in Table 2 prior to adding 100 g of tetralin. This procedure allowed for precise control of starting moisture in the samples and in the reactor. Validation for the method of controlling moisture in this manner versus controlled drying of the feed materials can be found in Appendix B. Regardless of the moisture content of the sample, the dry biomass-to-solvent ratio was held at 1:4. The solvent and wetted biomass samples were manually mixed to ensure uniform distribution before sealing the reactor on the test stand. Nitrogen gas was used to purge and initially pressurize the reactor. The reactor was heated by a 1000 W

heating jacket controlled by the internal process temperature, resulting in heating rate of approximately 5 °C min^{-1}. The final temperature of 280 °C was held for 25 min, after which the heating jacket was removed and the reactor was fan-cooled until it reached approximately 120 °C at which point liquid coolant was allowed to flow through the reactor cooling coil to bring the contents to ambient temperature.

Table 2. Simulated moisture and mass loading data.

Mass of dry feed (g)	**Mass of water added (g)**	**Effective moisture content of biomass sample (wt%)**
25.0	0.0	1
25.0	1.2	5
25.0	12.5	33
25.0	25.0	50

Following the experiment, all products were collected from Condensers 1 and 2. These condensates are referred to as light oil. The reactor was removed from the test stand and weighed. Gas production was determined using the following equation:

$$gas\ production = (mass\ of\ reactor + mass\ of\ intial\ reactor\ contents) - (mass\ of\ reactor + mass\ of\ light\ oil + mass\ of\ final\ reactor\ contents)$$

Figure 3 depicts how the products were separated and analyzed. The oil remaining in the reactor after cooling, referred to as heavy oil, was a mixture of solvent and produced liquid. Several products of cellulose liquefaction were analyzed using high performance liquid chromatography (HPLC). Prior to analyzing these compounds on HPLC, a water wash

was necessary to extract the water-soluble compounds from the water-insoluble tetralin solvent. HPLC characterization was only done on the water-soluble fraction of the heavy oil.

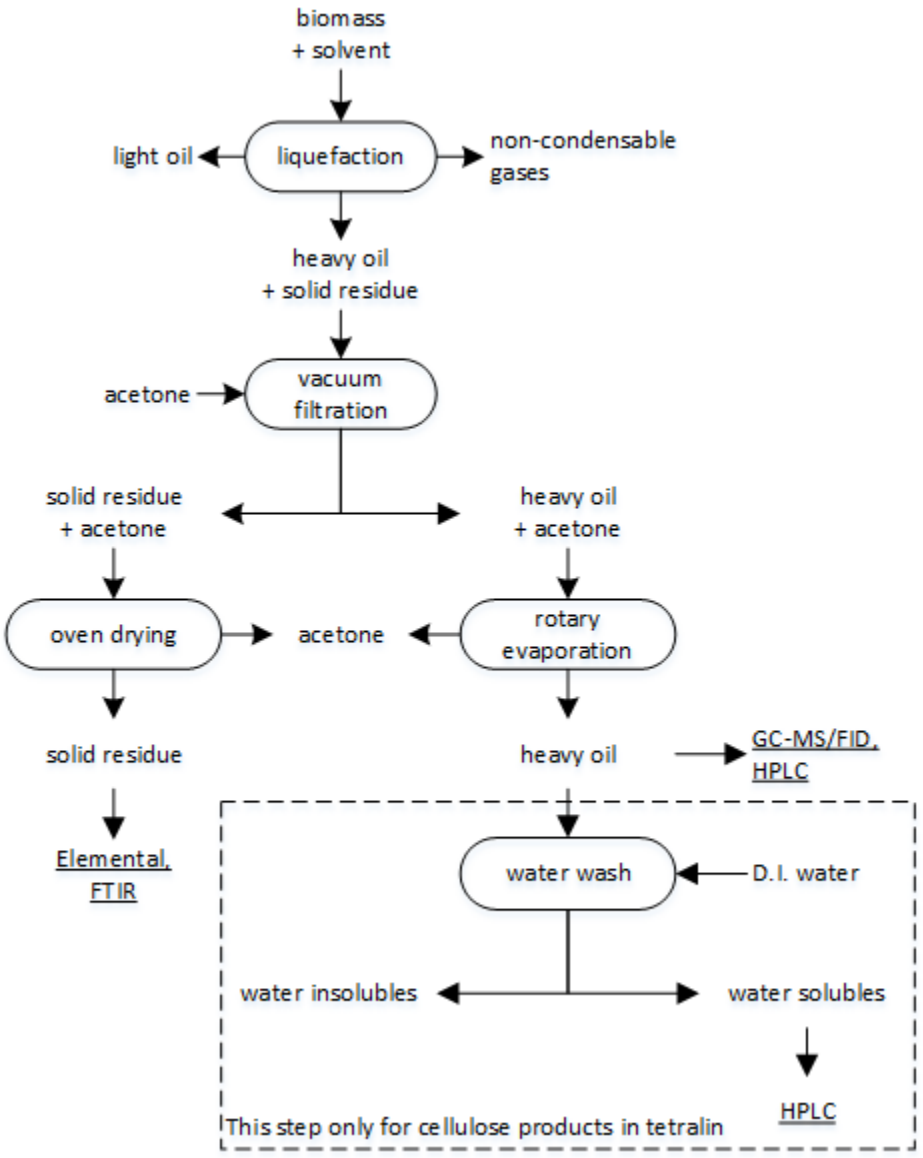

Figure 3. Procedure for separations and analysis of solvent liquefaction products.

Control tests were conducted with the pure tetralin to verify that they did not decompose to gas or solids at the reaction conditions. Based on these results, it was assumed

that tetralin was not significantly destroyed or consumed during reaction with biomass. Tetralin is capable of donating up to four moles of hydrogen per mole of tetralin [7]. However, any transfer of mass in this manner would be very small, and any mass balance effects were assumed to be negligible. The mass of liquid products was therefore determined by subtracting the mass of solvent and moisture inputs from the final combined mass of heavy oil and light oil. All solid and gas products were attributed to the biomass.

Analytical Methods

Ultimate analysis of the feed materials, liquid products, and solid residue was conducted using an Elementar vario MICRO cube. Approximately 5 mg of sample was used for each test, and samples were analyzed in triplicates.

Functional differences between solid and liquid samples were determined using a Thermo Scientific Nicolet iS10 Fourier transform infrared (FTIR) spectrometer. Analysis of each sample was preceded by background collection. Each sample was scanned 32 times with a resolution of 4 wavenumbers and attenuated reflectance correction. All spectra were analyzed and exported with the OMNIC Software operating system that accompanied the spectrometer.

Volatile cellulose products in the heavy oil were analyzed on a gas chromatograph (GC) with both a mass spectrometer (MS) and flame ionization detector (FID). The Agilent 7890B GC-MS/FID was equipped with two identical Phenomenex ZB 1701 capillary columns, one for each MS and FID. The injection port was held at a constant temperature of 250 °C while the FID detector was maintained at 300 °C. The GC oven was programmed to

start at 40 °C and ramp up to 240 °C at a rate of 3 °C min^{-1}. Helium was used as the carrier gas at a flow of 1 mL min^{-1}. Injection volume of the sample mixture was 1 µL.

Non-volatile products in the heavy oil from solvent liquefaction of cellulose were analyzed on two Dionex UltiMate 3000 HPLC systems, each equipped with a refractive index detector. Depending on the sugar analyzed, one of the HPLCs had a Bio-Rad Aminex HPX-87P column following a guard column of Micro-Guard de-ashing cartridge in a Bio-rad de-ashing holder while the other HPLC had a HyperRez XP Carbohydrate column following a guard column of Carbohydrate H^+ cartridge in a Thermo Fisher Scientific guard holder. The Aminex HPLC column was held at 80 °C throughout the duration of the analysis whereas HyperRez column temperature was fixed at 55 ºC. Ultrapure 18.2 MΩ deionized water was used as the effluent at a flow rate of 0.6 and 0.2 mL min^{-1} for Aminex and HyperRez column, respectively.

Lignin liquid products were analyzed on a Bruker 430-GC outfitted with a Phenomenex ZB 5-MS capillary column. The injection port and detector were both operated isothermally at 300 °C throughout the analysis. The GC oven was programmed to ramp from 35 to 300 °C at a rate of 5 °C min^{-1}. Sample injection volume was 1 µL with helium carrier gas injected at 1 mL min^{-1}.

Results and Discussion

Effect of system pressure on SL of dry pine, cellulose and lignin

Preliminary experiments examined the effect of system pressure on product distribution for SL of dry pine, cellulose and lignin in tetralin. The results demonstrate a

strong pressure dependence of liquid yield across the pressure range tested in this study for pine and cellulose (Figure 4a and Figure 4b, respectively). Liquid yield from both pine and cellulose was increased by approximately 10 wt% when the pressure was increased from 29 to 70 bar. Conversely, Figure 4c shows a relative lack of pressure dependence on the product yields for SL of lignin. At elevated pressures, solvents are able to penetrate the feed particle more readily thereby improving solubilization and interaction with decomposition products. Therefore, pressure effects are a compounding factor to the influence of moisture during SL.

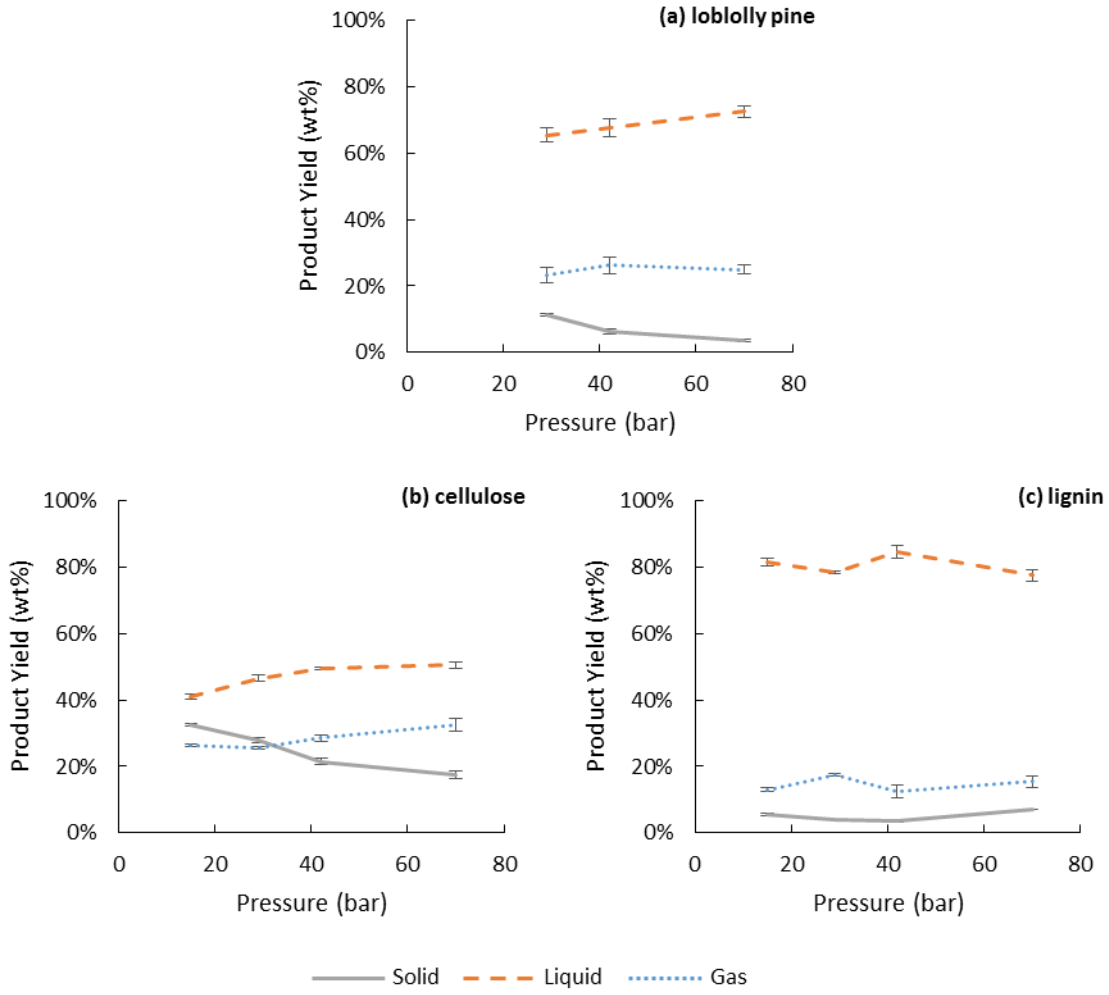

Figure 4. The effect of pressure in the absence of water on product yields for solvent liquefaction of (a) loblolly pine, (b) cellulose and (c) lignin in tetralin. Moisture content for all samples less than 1 wt%. Error bars represent the standard error of the mean for a minimum of two experiments.

Effect of moisture on SL of cellulose

Product yields from cellulose liquefaction are shown in Figure 5 as a function of cellulose moisture content. As shown in Figure 5a, solid yields increased substantially with increasing moisture at the expense of liquid yield at all pressures tested except at the lowest pressure (15 bar). Gas production remained relatively constant. These results suggest that

solid residue arose from secondary repolymerization reactions of the heavy oil. The absence of a moisture effect at 15 bar is likely due to vaporization of the water prior to reaching temperatures high enough for significant cellulose decomposition (> 220 °C).

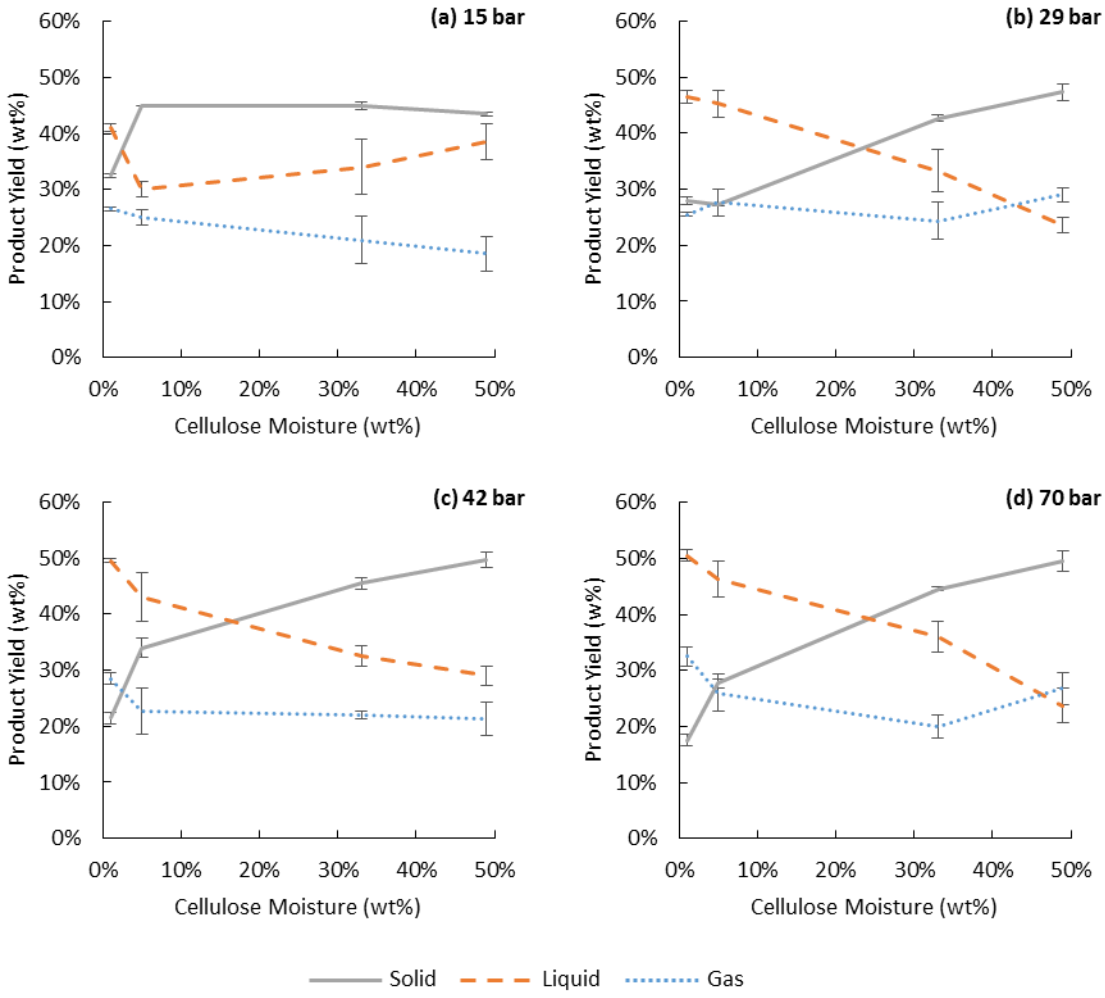

Figure 5. Product mass yields from the liquefaction of cellulose in tetralin at 280 °C as a function of cellulose moisture. Error bars represent the standard error of the mean for a minimum of two experiments.

Elemental analysis of the solid residue further supports the hypothesis that the solids were products of the SL process, rather than unreacted cellulose. This is demonstrated by the

van Krevelen diagram (Figure 6) comparing the O/C and H/C ratios of the cellulose solid residue from liquefaction at 42 and 70 bar. The O/C and H/C ratios for pure dry cellulose are 0.93 and 1.54, respectively. Here, it can be seen that significant reduction in the relative O and H content occurred between the cellulose and solid residue product; the solid residue was considerably more carbon-rich than cellulose. Furthermore, the elemental composition of the solid residue closely resembled that of humins, such as produced from cellulose by Sevilla and Fuertes [29]. The elemental composition of the cellulose solid residue generally approached that of humins as the moisture content of the feedstock increased. Solid residue produced from cellulose containing only 1 wt% moisture had lower H/C and O/C ratios than solid residue produced in the presence of higher moisture contents.

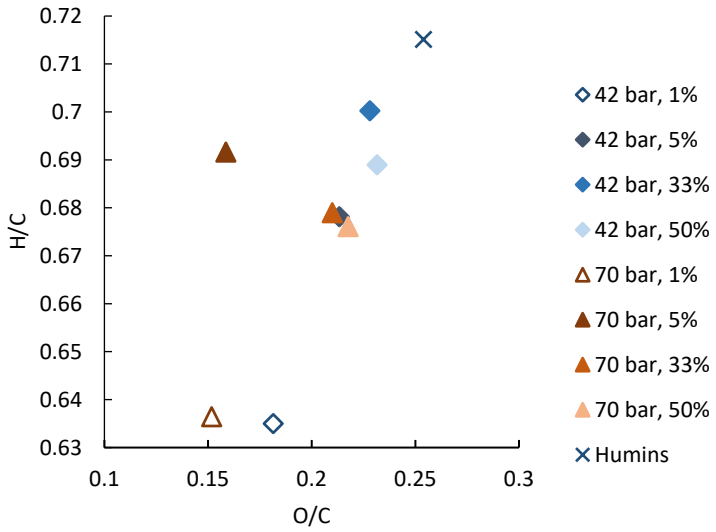

Figure 6. van Krevelen diagram comparing H/C and O/C ratios of cellulose solid residue and humins. Humin data taken from Sevilla et al. [29].

Humin formation is a phenomenon that often occurs in the hydrothermal liquefaction of cellulose and other saccharides [30]. The specific structure and formation mechanism of humins, however, is still fairly unclear [31, 32]. Generally speaking, humins are amorphous carbonaceous polymers formed from repolymerization of monosaccharides (glucose and fructose) and furans (5-hydroxymethylfurfural, furfural, and 5-methylfurfural) [29]. They tend to form most readily in a mildly acidic environment and at relatively low temperatures, typically in the range of 170-350 °C [30]. At these conditions, cellulose undergoes acid-catalyzed hydrolysis to monosaccharides, which can subsequently dehydrate to furans [10, 33, 34]. Polymerization of these products results in highly aromatized microspheres, which are readily identified via scanning electron microscopy (SEM) [29-32, 35, 36]. These aromatic polymers contain predominantly hydroxyl, carbonyl, and alkene functionality [31].

SEM analysis of the solid residue samples obtained from SL of cellulose resulted in clear evidence of humin microspheres. The images of solid residue produced from SL of cellulose containing 1 and 50 wt% moisture at 42 bar are shown in Figure 7a and Figure 7b, respectively. In addition to the presence of microspheres, it is clear that the particles were much larger and more amorphous when produced from cellulose containing 50 wt% moisture compared to cellulose containing only 1 wt% moisture. Possibly multiple microspheres coalesced to form the much larger globules seen in Figure 7b.

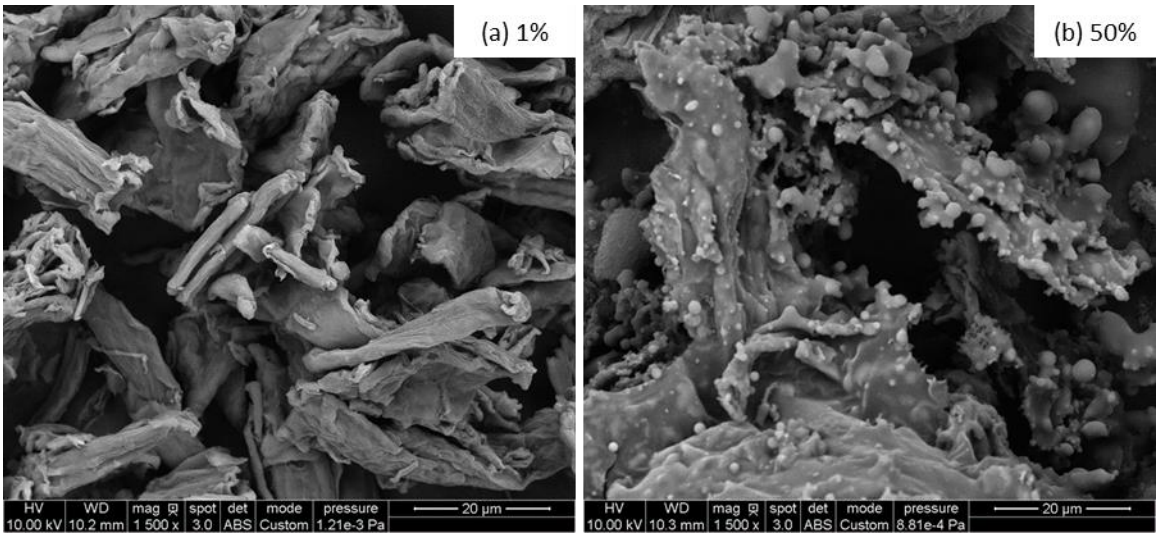

Figure 7. SEM analysis of the solid residue produced from cellulose liquefaction in tetralin at 280 °C and 42 bar, with a moisture of (a) 1 wt% and (b) 50 wt%.

Fourier transform infrared spectroscopy (FTIR) analysis of the solid residue samples produced at 70 bar, shown in Figure 8, further indicates the chemical structure of humins proposed by van Zandvoort et al. [31]. Aromatic alkene bond stretching (1445-1500 cm^{-1}) is indicative of an aromatic structure. The broad array of peaks caused by aromatic ether bond stretching (1205-1280 cm^{-1}) in conjunction with the aromatic signals suggest that furan rings are prevalent in the solid residue structure. These peaks are negligible for solid residue produced from cellulose with 1 wt% moisture content, but progressively increased in intensity with increasing moisture. Similarly, carbonyl bond stretching (1700 cm^{-1}) increases intensity with increasing moisture, as expected. Considering that both solid yield and FTIR peak intensities increased with only moderate change in elemental composition, it appears that increasing moisture content resulted in a selective increase in humins.

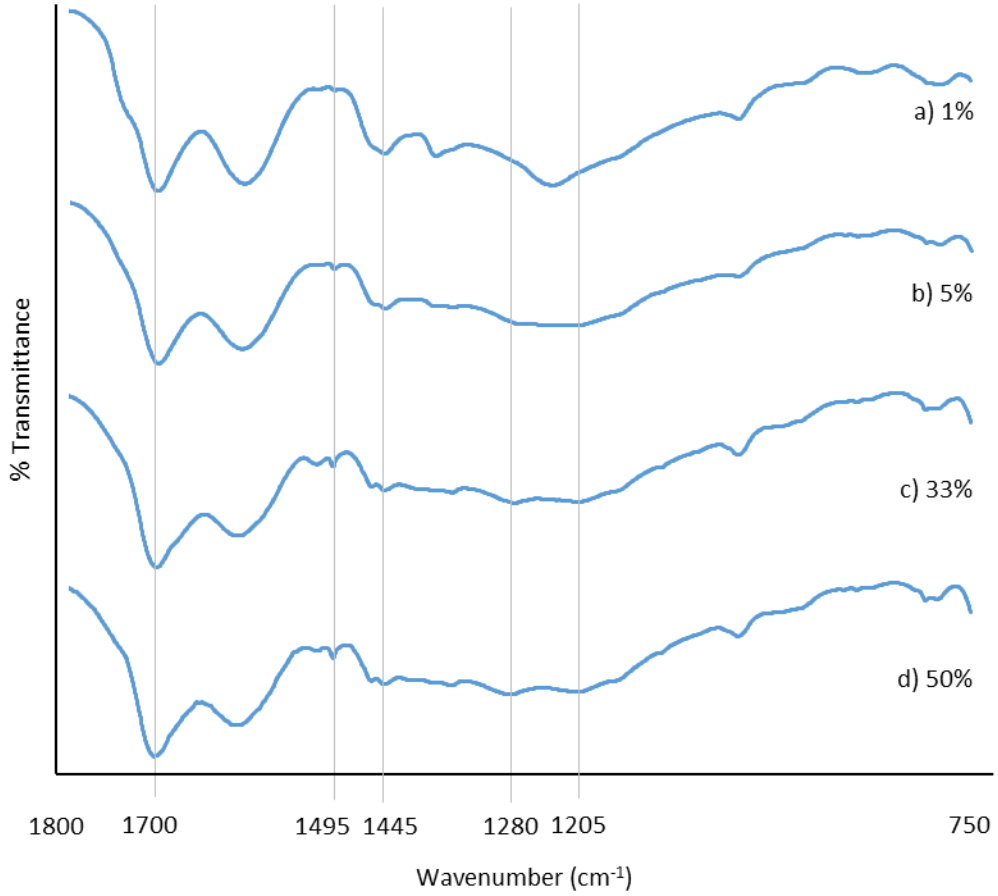

Figure 8. FTIR spectra of solid residue produced from SL of cellulose with (a) 1 wt%, (b) 5 wt%, (c) 33 wt% and (d) 50 wt% moisture in tetralin at 70 bar.

Mass balance data suggested that despite the profound effect of moisture on product distribution, water was not being consumed during the reaction. This supports the hypothesis that water behaved primarily as a catalyst to promote the formation of humins. It is well documented that production of humins and humin precursors from hydrothermal processing of saccharides is catalyzed by the presence of dilute acid [31, 33]. In the current liquefaction system, no acids were added to the system. Interestingly, the ionization constant of water reaches a maximum in the temperature range explored in this study. Figure 9 shows the

ionization constant of water determined by Bandura and Lvov [37] plotted against the boiling point curve of water. It is likely that hydronium ions formed during the dissociation of water promotes acid-catalyzed formation of humins.

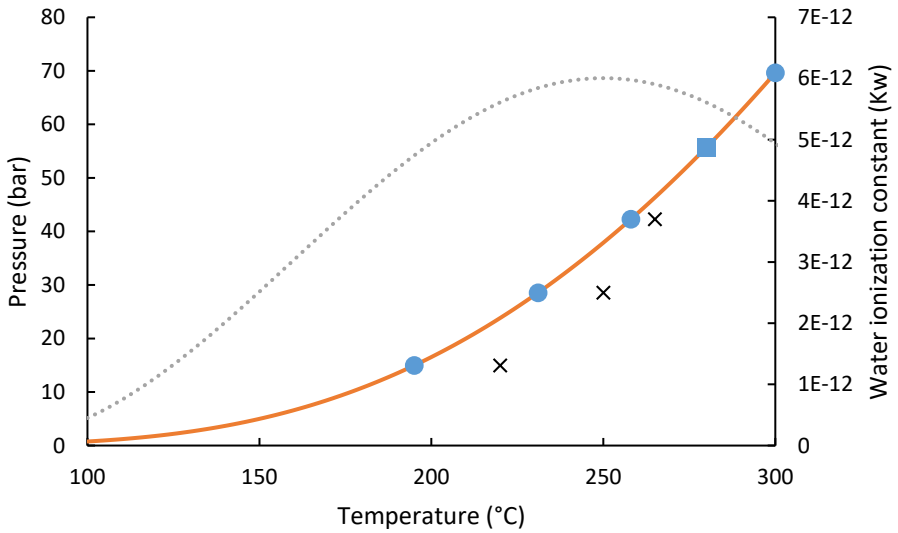

Figure 9. Boiling point curve for pure water, as shown previously in Figure 2, where (■) represents the theoretical vapor pressure of pure water at the final reaction temperature of 280 °C, and (●) represents the theoretical boiling point of pure water at each of the operating pressures. Experimentally determined boiling points for water in the reaction mixture are shown as (×). Plotted alongside these data is the self-ionization constant of water at its saturation pressure (taken from Bandura and Lvov [37]) (shown as a dotted line).

Quantitative analysis of liquid products is presented in Table 3. Unsurprisingly, no monosaccharides were detected at 1 wt% moisture due to the relative absence of water, which is necessary to hydrolyze glycosidic bonds [14]. On the other hand, the absence of levoglucosan was unexpected because it is the major product of thermal decomposition of cellulose in non-aqueous aprotic solvents [38, 39]. Very likely, the reaction temperature was not high enough to fully depolymerize the cellulose, resulting in solubilized anhydro oligosaccharides instead of the anhydro monosaccharide levoglucosan.

Table 3. Yield of the GC- and HPLC- quantifiable liquid products from cellulose. All yield values are in weight percent on a feed basis. Uncertainties reflect the standard error of the mean for a minimum of three samples.

Pressure (bar)	Moisture (wt%)	Mannose	Glucose	Cellobiosan	Levoglucosan	Furfural	5-HMF
15	1	0	0	0	0.11 ± 0.01	0.08 ± 0.01	0
	5	7.32 ± 0.02	0	0	0	0.15 ± 0.01	0
	33	7.56 ± 0.01	0	0	0	0.07 ± 0.01	0
	50	5.39 ± 0.05	0	0	0	0.06 ± 0.01	0
42	1	0	0	0	0	0	0
	5	6.42 ± 0.05	0	0	0	0.12 ± 0.01	0
	33	3.29 ± 0.01	0	0	0	0.23 ± 0.01	0
	50	3.40 ± 0.01	0	0	0	0.12 ± 0.01	0
70	1	0	0	0	0	0	0
	5	1.24 ± 0.01	0	0	0	0	0
	33	2.94 ± 0.01	0	0	0	0.11 ± 0.01	0
	50	2.61 ± 0.01	0	0	0	0.15 ± 0.01	0

Low-polarity solvents such as tetralin favor production of furanics [14]. We hypothesized that the low level of furanics detected in the heavy oil was the result of them being rapidly consumed by the formation of humins. Several low-temperature, short-residence time studies were conducted to further understand the evolution of liquid products. At 70 bar, cellulose with 50 wt% moisture content was heated to a final temperature in the range of 220 to 260 °C. Upon reaching the final temperature, the reactor was immediately cooled, which is characterized as a residence time of zero minutes at the reaction

temperature. Analysis of the products indicated increased furfural production (the only quantifiable furan detected) with increasing temperature. It was concluded that furfural was produced from cellulose in the presence of water, but was subsequently consumed during 25-minute residence at 280 °C.

To better understand how the catalytic behavior of water shifts the deconstruction of cellulose to production of humin precursors, a series of experiments were conducted using model compounds. Reagent grade glucose, mannose, furfural, and 5-hydroxymethylfurfural (5-HMF) were added to tetralin followed by addition of sufficient deionized water to simulate either 1 wt% or 50 wt% moisture content for the sugar or furanic preparations. These samples were placed in 2.5 mL capacity stainless steel reactors, as described elsewhere [38]. After reaction for 25 min at 280 °C the yield of solid was quantified and the liquid products characterized via GC-MS/FID and HPLC. In these experiments only glucose and mannose produced solid residue. When moisture was increased from 1 to 50 wt%, solid yield increased by 22 wt% and 17 wt% for glucose and mannose, respectively. No acetone-insoluble solid residue was collected from furfural or 5-HMF. The composition of the solid residue from glucose and mannose was different when water was present in higher amounts as shown in Figure 10. Similar to the shift that occurred for wet cellulose, the solid residue showed a reduction in both oxygen and hydrogen relative to carbon.

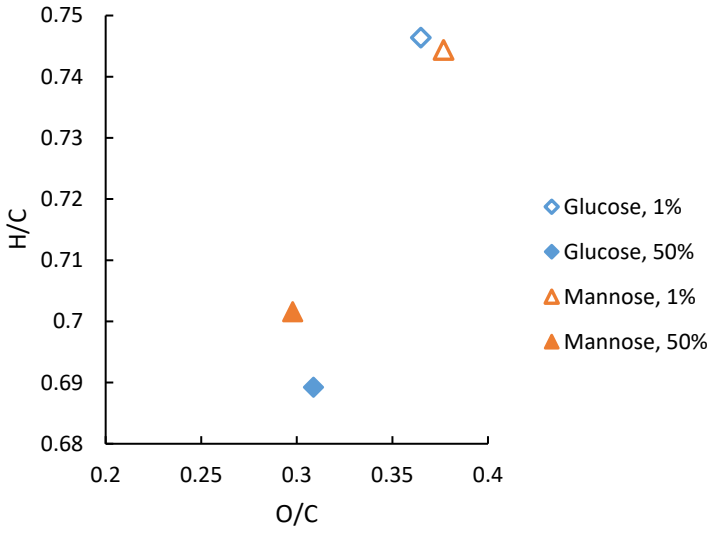

Figure 10. van Krevelen diagram of solid residue from liquefaction of glucose and mannose in tetralin with moisture of 1 and 50 wt%.

No monosaccharides were detected in the product liquid from SL of model compounds if water was present, even when glucose and mannose were the reactants, these being entirely consumed during reaction. Only furfural was quantified as a product of the reaction of these model compounds. GC-MS analysis of the liquid products indicated additional trace amounts of various furans. Analysis of the heavy oil from SL of pure furfural found a large peak corresponding to 2-furanethanol-beta-methoxy-(S) (2-FEBM). Similarly, trace amounts of 5-methylfurfural (5-MF) were detected when pure 5-HMF was reacted. These peaks were also present in the products of the previously described SL tests on high-moisture cellulose. We were not able to quantify 2-FEBM as there are no standards available for it. However, given that 2-FEBM was found as a product from furfural, it is an indicator that furfural was also present during the reaction of cellulose. Similarly, the presence of 5-MF indicates that 5-HMF was produced during liquefaction of cellulose. This is important

because furans, such as furfural and 5-HMF, are essential precursors to the formation of humins. Therefore, evidence that furfural and 5-HMF are produced during SL of wet cellulose supports the hypothesis that humins are being formed by the same mechanism by which they are produced during hydrothermal processing. It is also possible that 2-FEBM or 5-MF participate in humin-forming reactions, although not as readily as do furfural and 5-HMF.

These results demonstrated the strong role of even small amounts of water on the SL of cellulose in a hydrocarbon solvent. At these moderate temperatures, the ion-dissociation of water catalyzes the production of insoluble humins that detract from the liquid bio-oil yield. Interestingly, at moisture content of 50 wt%, the solid yield from cellulose liquefaction in tetralin at 280 °C was greater than that for either tetralin or water alone as the solvent [40].

Effect of moisture on SL of lignin

The effect of moisture on SL of lignin was similar to that of cellulose. Figure 11 shows that solid yield increased significantly with moisture content of the lignin. Again, solid yield increased at the expense of liquid yield, with gas production essentially constant. At 50 wt% moisture content of the lignin, solid yield reached 47-50 wt%, depending on the reaction pressure. In comparison, hydrothermal liquefaction of lignin at 260-280 °C produces 50-60 wt% solid residue [36, 40]. Processing lignin containing 50 wt% moisture in pure hydrocarbon is equivalent to water making up only 20% of the solvent in the reactor. It is surprising that SL of the high moisture lignin yields almost as much solid residue as

hydrothermal processing of lignin considering the much smaller amount of water present during SL.

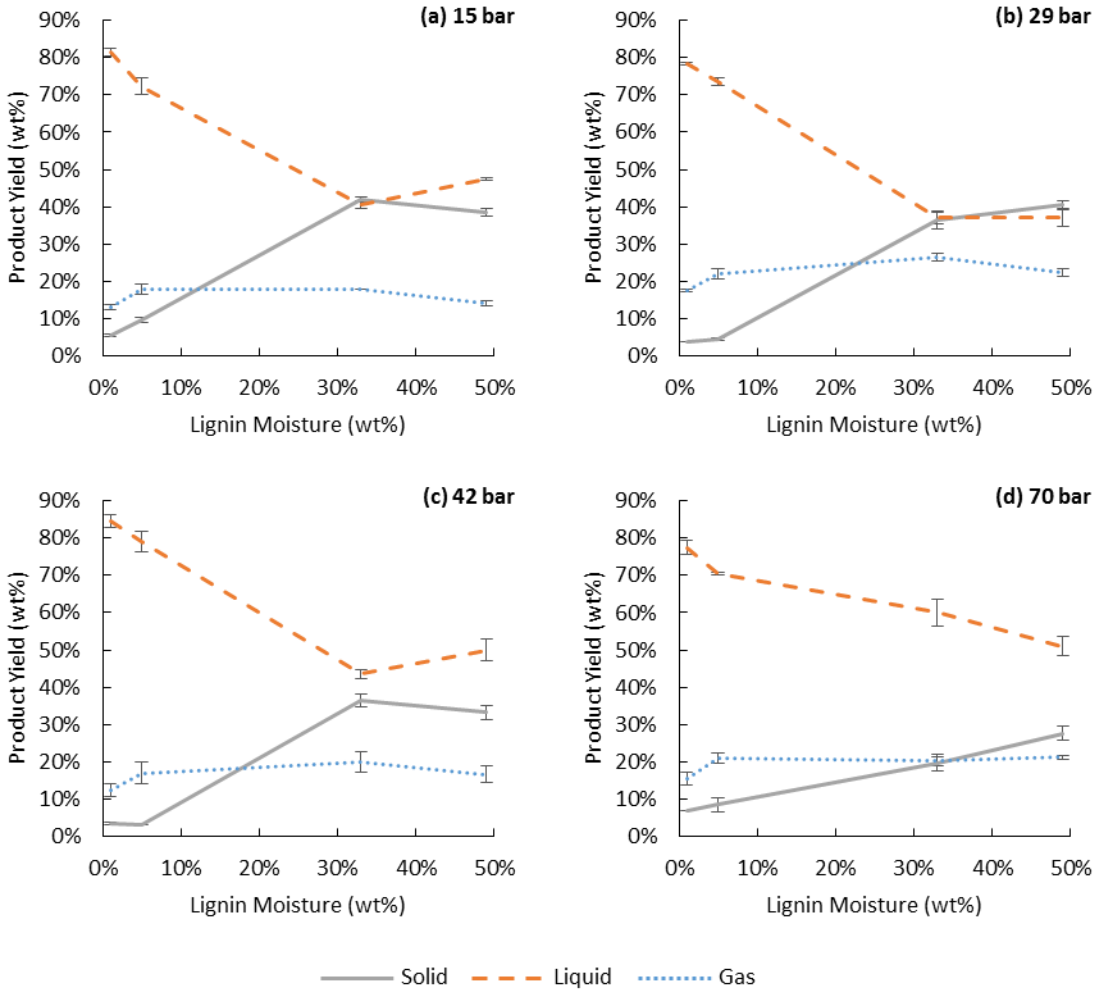

Figure 11. Product mass yields from the liquefaction of lignin in tetralin at 280 °C as a function of lignin moisture. Error bars represent the standard error of the mean for a minimum of two experiments.

The influence of moisture on the bio-oil quality was evaluated through GC-FID quantification of phenolic monomers (PM) as a proxy of bio-oil quality. Figure 12 shows the interaction effects of pressure and moisture on the yield of GC-FID detectable PM. As

discussed previously, increasing system pressure generally resulted in an increased production of PM. Conversely, increasing moisture in the lignin resulted in a substantial reduction in PM. Examining the isobaric portion of the data, it was determined that the relative reduction in PM in going from 1 to 50 wt% moisture was 74, 26, 71, and 80 wt% for the 15, 29, 42, and 70 bar experiments, respectively. From this it was concluded that the relative reduction in PM was caused by the presence of liquid water early in the reaction process. In other words, the deleterious effect of water was realized prior to it vaporizing.

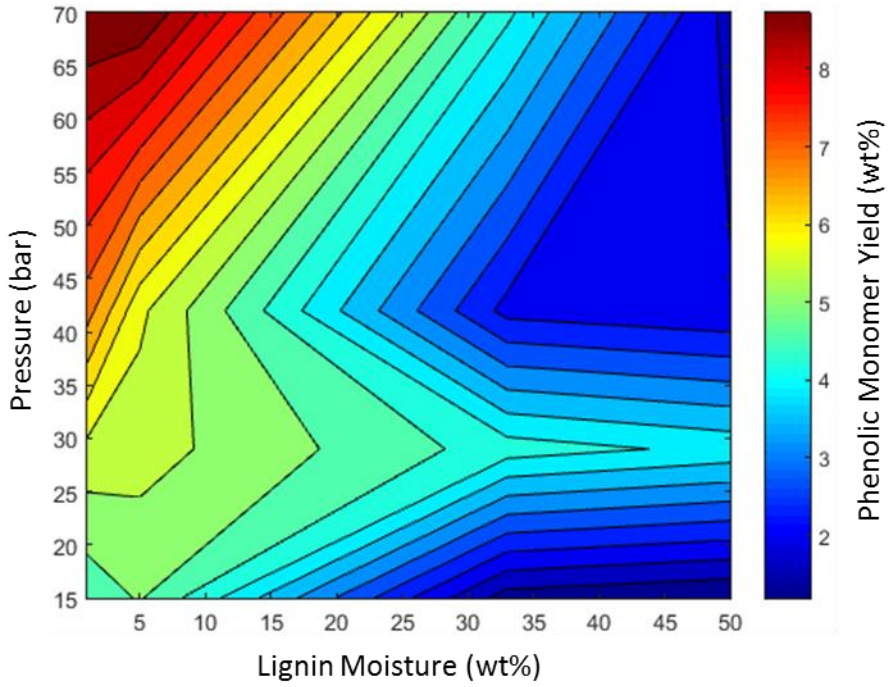

Figure 12. Interaction of pressure and moisture effects on the yield of phenolic monomers from the liquefaction of lignin in tetralin.

Figure 13 shows ten of the most prevalent PM compounds detected by GC-FID. Seven compounds exhibited a reduction of greater than 75 wt% when comparing the 1 wt% and 50 wt% moisture cases at 70 bar. Close examination of phenolic monomer yields further

indicate that the most significant reduction occurred for methoxyl-containing compounds: of the seven compounds that showed a significant reduction, six had at least one methoxyl group. Hydrothermal conditions have been shown to promote hydrolysis of methoxyl groups [41], which could explain the reduction in methoxyl-substituted products. However, this would suggest that other monomeric compounds would appear as methoxyl-substituted phenolic monomers disappeared, which was not the case. Thus, we hypothesized that deconstruction of lignin is altered in the presence of water to favor reactive intermediates that repolymerize to solid residue. To test this hypothesis, 25 g of water was added to a 100 g mixture of phenolic monomers containing phenol, o-cresol, m/p-cresol, 2-methoxyphenol, 2,6-dimethylphenol and 2-methoxy-4-methylphenol. The solution was then brought to 280 °C and held there for 25 minutes. Under these conditions, no solid residue was formed and GC-FID characterization of the liquid showed little change in the original composition.

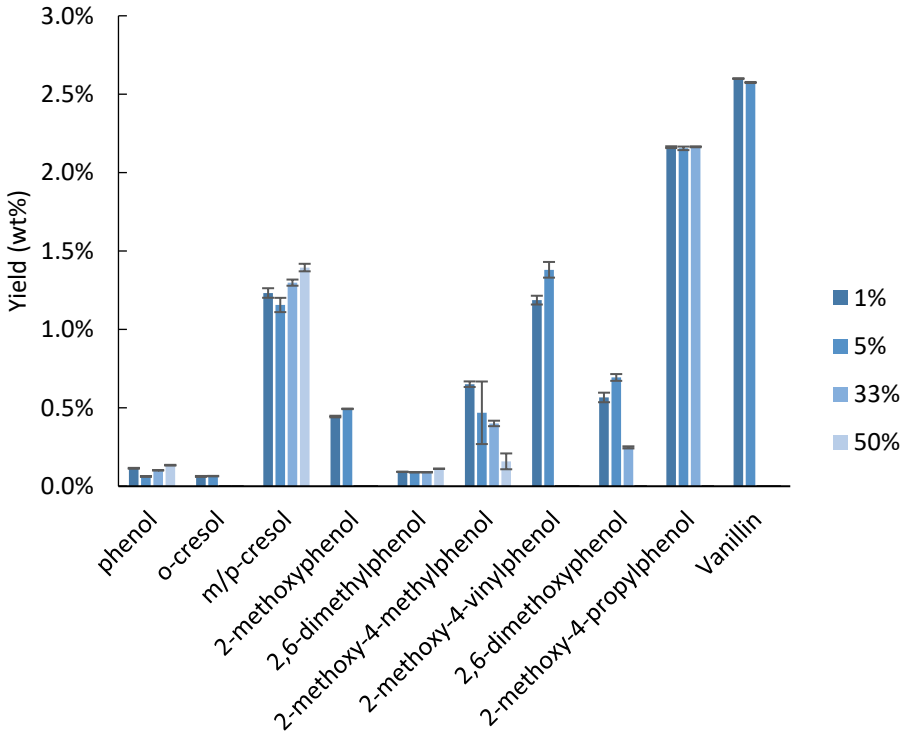

Figure 13. Yield of the most prevalent phenolic monomers produced from the liquefaction of lignin in tetralin at 70 bar for different moisture levels in the lignin. Error bars represent the standard error of the mean of triplicates.

This hypothesis was further supported by FTIR analysis of the solid residue. Within the 750-1800 cm^{-1} region shown in Figure 14, increasing moisture resulted in a noticeable reduction in the spectral transmittance at several wavelengths: 1685 cm^{-1} (aryl ketone), 1510-1430 cm^{-1} (aryl alkene), 1208 cm^{-1} (alkyl aryl ether), and 1110 cm^{-1} (aliphatic ether). When considered together, this suggests that there is an increase in the concentration of aromatic rings joined by ether linkages when water is present.

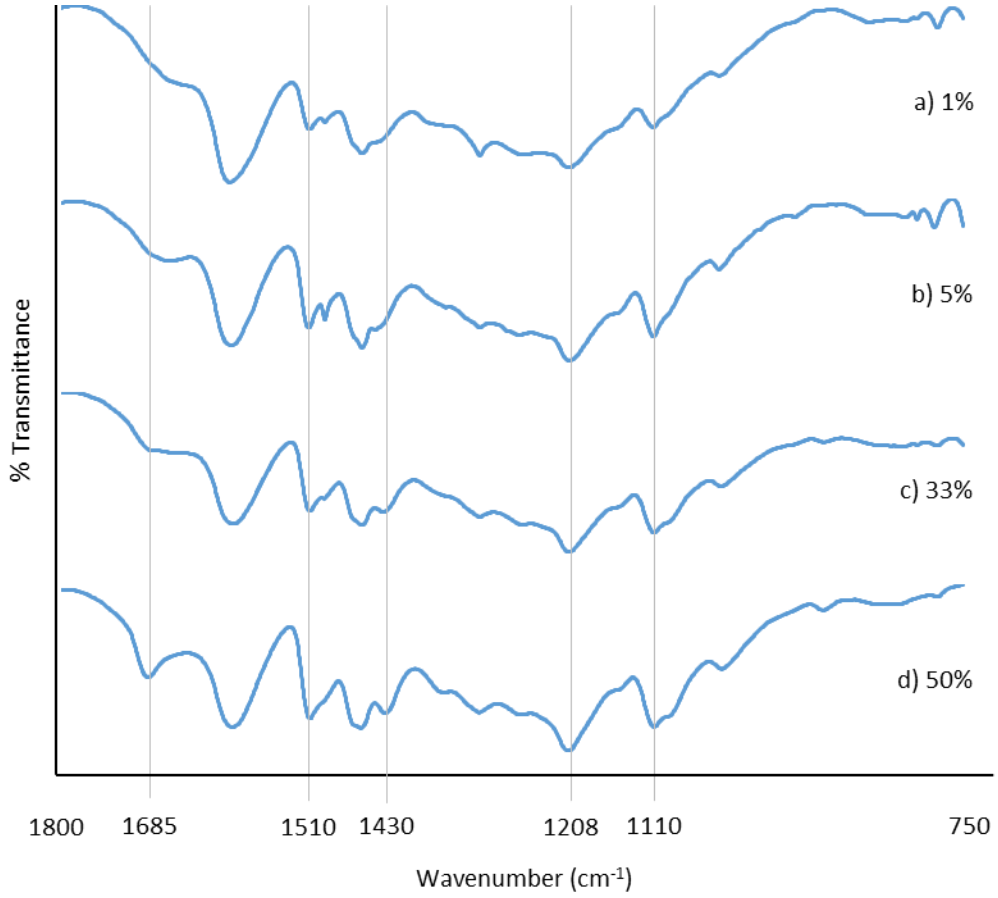

Figure 14. FTIR spectra of solid residue produced from SL of lignin with (a) 1 wt%, (b) 5 wt%, (c) 33 wt% and (d) 50 wt% moisture in tetralin at 70 bar.

A complete moisture balance was conducted for each of the reaction conditions explored in this study. The amount of water added to the system was compared to the moisture of the liquid product recovered in both the reactor and Condenser 1 according to the following equation:

$$Recovery\ (\%) = \frac{mass\ of\ water\ added - mass\ of\ water\ recovered}{mass\ of\ water\ added} \times 100$$

where positive values indicate a net production of water and negative values indicate water was consumed during the reaction. At 1 and 5 wt% moisture, water was found to be

generated by the process for a net gain of approximately 1-3 wt%. However, when the moisture was 33 or 50 wt% water was consistently consumed, resulting in a loss of about 5-20 wt%.

Hydrolysis of β-O-4 and α-O-4 ether bonds prevalent in lignin is the most likely explanation for the considerable consumption of water [42, 43]. The previously discussed ion dissociation of water is also understood to catalyze these reactions [42]. Hydrolysis of lignin would yield reactive phenolic oligomers that could then repolymerize to form polyaromatic molecules joined by thermally stable biphenyl C-C or C-O-C linkages [44].

Conclusions

The influence of moisture on solvent liquefaction of biomass at 280 °C in tetralin was investigated using a modified autoclave reactor. The reactor was operated as a quasi-batch system wherein volatile compounds (including water) and non-condensable gases were allowed to leave the reactor. Loblolly pine, cellulose, and lignin all demonstrated a decrease in liquid yield in the presence of moisture. At 42 bar, the liquid yield decreased by 25, 21 and 35 wt%, respectively, for these feedstocks when moisture was increased from 1 to 50 wt%. A subsequent increase in solid yield occurred at the expense of liquid. The solid produced from wet cellulose was determined to contain humins, a by-product of condensation reactions between monosaccharides and furanics. It was concluded that ionic dissociation of water was a contributing factor to production of humins. Similarly, the presence of moisture also influenced deconstruction of lignin, resulting in reactive intermediates that readily repolymerized to thermally stable solid residue. The concentrations of several phenolic

monomers, particularly methoxy-substituted monomers, also decreased in the presence of moisture. Increasing system pressure generally improved liquid yield for dry feedstocks, presumably due to increased solvent penetration into the feedstock pores. Conversely, when moisture was present, increasing pressure reduced liquid yield due to increased interaction between liquid water and feed material. These results illustrated the strong influence of moisture on solvent liquefaction of biomass in a hydrocarbon solvent.

References

1. Bridgwater, A.V., D. Meier, and D. Radlein, *An overview of fast pyrolysis of biomass.* Organic Geochemistry, 1999. **30**(12): p. 1479-1493.

2. Demirbas, A., *Effect of initial moisture content on the yields of oily products from pyrolysis of biomass.* Journal of Analytical and Applied Pyrolysis, 2004. **71**(2): p. 803-815.

3. Akhtar, J. and N.A.S. Amin, *A review on process conditions for optimum bio-oil yield in hydrothermal liquefaction of biomass.* Renewable and Sustainable Energy Reviews, 2011. **15**(3): p. 1615-1624.

4. Kumar, S., et al., *Liquefaction of Lignocellulose: Process Parameter Study To Minimize Heavy Ends.* Industrial & Engineering Chemistry Research, 2014. **53**(29): p. 11668-11676.

5. Ghosh, A., R.C. Brown, and X. Bai, *Production of solubilized carbohydrate from cellulose using non-catalytic, supercritical depolymerization in polar aprotic solvents.* Green Chemistry, 2016. **18**(4): p. 1023-1031.

6. Li, C.-Z., et al., *Comparison of thermal breakdown in coal pyrolysis and liquefaction.* Fuel, 1994. **73**(6): p. 851-865.

7. Vasilakos, N.P. and D.M. Austgen, *Hydrogen-donor solvents in biomass liquefaction.* Industrial & Engineering Chemistry Process Design and Development, 1985. **24**(2): p. 304-311.

8. Mellmer, M.A., et al., *Effects of γ-valerolactone in hydrolysis of lignocellulosic biomass to monosaccharides.* Green Chemistry, 2014. **16**(11): p. 4659-4662.

9. Gray, M.R., W.H. Corcoran, and G.R. Gavalas, *Pyrolysis of a wood-derived material. Effects of moisture and ash content.* Industrial & Engineering Chemistry Process Design and Development, 1985. **24**(3): p. 646-651.

10. Aida, T.M., et al., *Dehydration of d-glucose in high temperature water at pressures up to 80MPa.* The Journal of supercritical fluids, 2007. **40**(3): p. 381-388.

11. Sasaki, M., et al., *Dissolution and hydrolysis of cellulose in subcritical and supercritical water.* Industrial & Engineering Chemistry Research, 2000. **39**(8): p. 2883-2890.

12. Kim, K.H., et al., *Hydrogen-donor-assisted solvent liquefaction of lignin to short-chain alkylphenols using a micro reactor/gas chromatography system.* Energy & Fuels, 2014. **28**(10): p. 6429-6437.

13. Connors, W., et al., *Thermal degradation of kraft lignin in tetralin.* Holzforschung-International Journal of the Biology, Chemistry, Physics and Technology of Wood, 1980. **34**(1): p. 29-37.

14. Koriakin, A., et al., *Thermochemical Decomposition of Microcrystalline Cellulose Using Sub- and Supercritical Tetralin and Decalin with Fe3O4.* Industrial & Engineering Chemistry Research, 2015. **54**(18): p. 5184-5194.

15. Lalvani, S.B., et al., *Liquefaction of newsprint and cellulose in tetralin under moderate reaction conditions.* Fuel Processing Technology, 1993. **35**(3): p. 219-232.

16. Yan, Y., et al., *Liquefaction of sawdust for liquid fuel.* Fuel Processing Technology, 1999. **60**(2): p. 135-143.

17. Carlson, C.S., et al., *Thermal Hydrogenation. Transfer of Hydrogen from Tetralin to Cracked Residua.* Industrial & Engineering Chemistry, 1958. **50**(7): p. 1067-1070.

18. Neavel, R.C., C.F. Knights, and H. Schulz, *Exxon Donor Solvent Liquefaction Process [and Discussion].* Philosophical Transactions of the Royal Society of London A: Mathematical, Physical and Engineering Sciences, 1981. **300**(1453): p. 141-156.

19. Li, Z., et al., *Alkaline pretreatment and the synergic effect of water and tetralin enhances the liquefaction efficiency of bagasse.* Bioresource Technology, 2015. **177**(0): p. 159-168.

20. Li, Z., et al., *Effects of Mild Alkali Pretreatment and Hydrogen-Donating Solvent on Hydrothermal Liquefaction of Eucalyptus Woodchips.* Energy & Fuels, 2015. **29**(11): p. 7335-7342.

21. Saisu, M., et al., *Conversion of Lignin with Supercritical Water−Phenol Mixtures.* Energy & Fuels, 2003. **17**(4): p. 922-928.

22. Okuda, K., et al., *Disassembly of lignin and chemical recovery—rapid depolymerization of lignin without char formation in water–phenol mixtures.* Fuel Processing Technology, 2004. **85**(8–10): p. 803-813.

23. Maldas, D. and N. Shiraishi, *Liquefaction of biomass in the presence of phenol and H2O using alkalies and salts as the catalyst.* Biomass and Bioenergy, 1997. **12**(4): p. 273-279.

24. Okuda, K., et al., *Disassembly of lignin and chemical recovery in supercritical water and p-cresol mixture: Studies on lignin model compounds.* Bioresource Technology, 2008. **99**(6): p. 1846-1852.

25. van Rossum, G., et al., *Liquefaction of Lignocellulosic Biomass: Solvent, Process Parameter, and Recycle Oil Screening.* ChemSusChem, 2014. **7**(1): p. 253-259.

26. Behrendt, F., et al., *Direct liquefaction of biomass.* Chemical engineering & technology, 2008. **31**(5): p. 667-677.

27. Kruse, A. and A. Gawlik, *Biomass conversion in water at 330-410 C and 30-50 MPa. Identification of key compounds for indicating different chemical reaction pathways.* Industrial & Engineering Chemistry Research, 2003. **42**(2): p. 267-279.

28. Liu, C.-T. and W.T. Lindsay, *Vapor pressure of deuterated water from 106 to 300.deg.* Journal of Chemical & Engineering Data, 1970. **15**(4): p. 510-513.

29. Sevilla, M. and A.B. Fuertes, *The production of carbon materials by hydrothermal carbonization of cellulose.* Carbon, 2009. **47**(9): p. 2281-2289.

30. Sevilla, M. and A.B. Fuertes, *Chemical and structural properties of carbonaceous products obtained by hydrothermal carbonization of saccharides.* Chemistry–A European Journal, 2009. **15**(16): p. 4195-4203.

31. van Zandvoort, I., et al., *Formation, molecular structure, and morphology of humins in biomass conversion: influence of feedstock and processing conditions.* ChemSusChem, 2013. **6**(9): p. 1745-1758.

32. Patil, S.K. and C.R. Lund, *Formation and growth of humins via aldol addition and condensation during acid-catalyzed conversion of 5-hydroxymethylfurfural.* Energy & Fuels, 2011. **25**(10): p. 4745-4755.

33. Salak Asghari, F. and H. Yoshida, *Acid-Catalyzed Production of 5-Hydroxymethyl Furfural from d-Fructose in Subcritical Water.* Industrial & Engineering Chemistry Research, 2006. **45**(7): p. 2163-2173.

34. Sasaki, M., et al., *Cellulose hydrolysis in subcritical and supercritical water.* The Journal of Supercritical Fluids, 1998. **13**(1): p. 261-268.

35. Patil, S.K.R., J. Heltzel, and C.R.F. Lund, *Comparison of Structural Features of Humins Formed Catalytically from Glucose, Fructose, and 5-Hydroxymethylfurfuraldehyde.* Energy & Fuels, 2012. **26**(8): p. 5281-5293.

36. Kang, S., et al., *Characterization of Hydrochars Produced by Hydrothermal Carbonization of Lignin, Cellulose, d-Xylose, and Wood Meal.* Industrial & Engineering Chemistry Research, 2012. **51**(26): p. 9023-9031.

37. Bandura, A.V. and S.N. Lvov, *The Ionization Constant of Water over Wide Ranges of Temperature and Density.* Journal of Physical and Chemical Reference Data, 2006. **35**(1): p. 15-30.

38. Ghosh, A., R.C. Brown, and X. Bai, *Production of solubilized carbohydrate from cellulose using non-catalytic, supercritical depolymerization in polar aprotic solvents.* Green Chemistry, 2015.

39. Bao, G., S. Shiro, and H. Wang, *Cellulose decomposition behavior in hot-compressed aprotic solvents.* Science in China Series B: Chemistry, 2008. **51**(5): p. 479-486.

40. Karagöz, S., et al., *Comparative studies of oil compositions produced from sawdust, rice husk, lignin and cellulose by hydrothermal treatment.* Fuel, 2005. **84**(7–8): p. 875-884.

41. Toor, S.S., L. Rosendahl, and A. Rudolf, *Hydrothermal liquefaction of biomass: a review of subcritical water technologies.* Energy, 2011. **36**(5): p. 2328-2342.

42. Fang, Z., et al., *Reaction chemistry and phase behavior of lignin in high-temperature and supercritical water.* Bioresource Technology, 2008. **99**(9): p. 3424-3430.

43. Kang, S., et al., *Hydrothermal conversion of lignin: A review.* Renewable and Sustainable Energy Reviews, 2013. **27**: p. 546-558.

44. Vuori, A., *Liquefaction of Kraft Lignin: 1. Primary Reactions under Mild Thermolysis Conditions.* Holzforschung-International Journal of the Biology, Chemistry, Physics and Technology of Wood, 1988. **42**(3): p. 155-161.

CHAPTER 4

OPTIMIZATION OF PHENOLIC MONOMER PRODUCTION FROM SOLVENT LIQUEFACTION OF LIGIN

A paper to be submitted to *Energy & Fuels*

Martin R. Haverly, Kelley V. Okoren, Robert C. Brown

Abstract

Process conditions used for solvent liquefaction of technical lignin in mixtures of o-cresol and tetralin were explored for optimizing the yield of phenolic monomers (PM) and liquid products. The effects of solvent mixture, reaction temperature, solids loading, and residence time were evaluated using a central composite response surface statistical model. Six response variables were monitored to evaluate the influence of the four factors. Liquid and solid yield were tracked via mass balance. The yield of distillable products (distillate)was determined using a thermogravimetric analyzer (TGA). Gas chromatography (GC) was used to monitor the individual yields of phenol, guaiacol, and p-xylenol.

Tetralin, which served as a hydrogen donor, was most effective in enhancing liquid production, reducing solid products, and increasing selectivity towards PM when present at less than 30 wt% of the solvent mixture. The interaction of solids loading and solvent mixture further indicated o-cresol was more effective than tetralin at solubilizing lignin and stabilizing the liquid products. The hydrogen-donating capability of tetralin was most beneficial at temperatures near 340 °C. Residence time was not found to be a significant

factor for experiments lasting up to 30-minutes. Distillate yields as high as 40 wt% from lignin on a dry, ash-free basis indicated the ability of this process to generate low-boiling point PM suitable for recycle solvent. These results demonstrate this process to be robust and effective in converting technical lignin to valuable PM.

Introduction

Lignin is an essential component of vascular plant structure. The complex phenylpropane-based structure of lignin enables it to provide several functions essential to plant life. It is most commonly recognized as a binder, or glue, for cellulose and hemicellulose fibers, which makes the plant more rigid [1]. However, it also impacts the transport of nutrients by decreasing the permeation of water between cell walls, and it fortifies plant cells against the penetration of destructive enzymes from foreign microorganisms [2]. The structure and composition of lignin varies based on the plant source, though it is generally composed of three primary molecules: paracoumaryl, coniferyl, and sinapyl alcohol [2]. Given the aromatized structure of lignin it has long been desired to deconstruct the lignin polymer into valuable phenolic monomers (PM) [3]. A variety of C-C and C-O bonds must be cleaved in order for PM to be liberated from the lignin structure. An example of these bond types and proposed lignin structure is shown in Figure 1 [4]. β-O-4 ether linkages are the most prevalent, accounting for approximately 40-60 % of the bonds within lignin, with similar α-O-4 ether linkages accounting for another 6-8 % [5]. These ether

bonds have been shown to cleave at temperatures as low as 200 to 300 °C [6] while many of the remaining linkages have been shown to cleave below 430 °C without the use of catalysts [7].

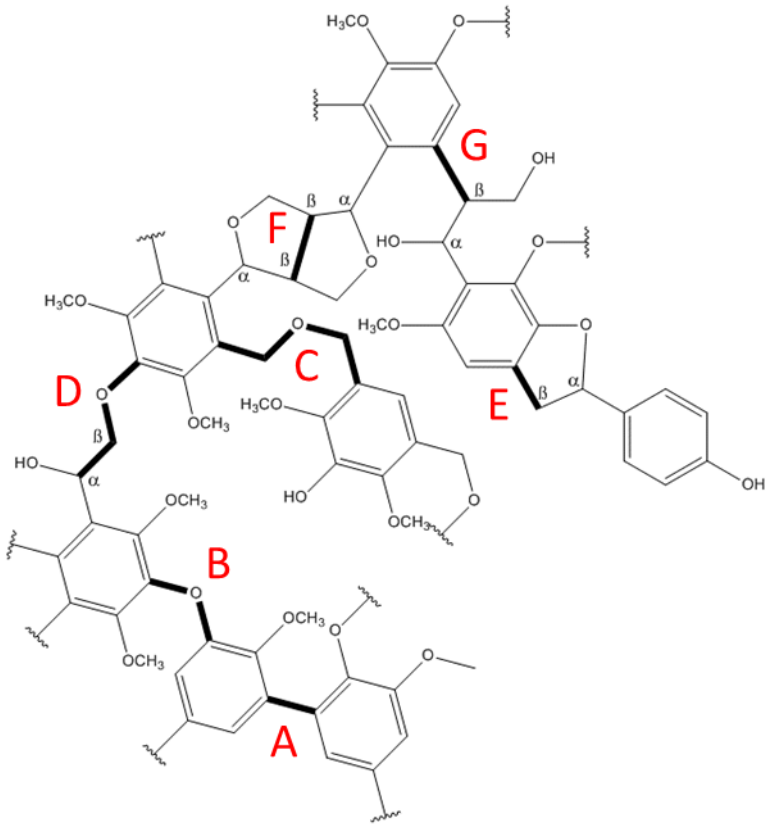

Figure 1. Lignin structure showing typical (A) biphenyl, (B) diphenyl ether, (C) dibenzyl ether, (D) β-O-4, (E) β-5, (F) β-β, and (G) β-1 linkages [adapted from Reichert et al. [4]].

Technical lignin is currently produced most widely from the pulp and paper industry via the Kraft process [3]. However, with the advent of cellulosic ethanol production, other forms of technical lignin are becoming more prevalent. To meet anticipated goals for biorenewable fuel production, the US Department of Energy predicts that as much as 225 million tons of lignin will be produced by the cellulosic ethanol industry by 2030 [8]. At

present, much of the lignin produced is burned as low-value fuel [9, 10]. However, the use of lignin as a renewable resource for the production of select industrial chemicals and products is already demonstrated in a few instances [9, 11]. PM are currently used in fuel and chemical markets, ranging in value from $1.21-$4.41 per kilogram [8]. Cost effective means of producing PM from lignin could improve the economics of cellulosic ethanol production, and could offer an improvement over current PM production methods. For example, producing phenol directly from lignin could be more cost-effective than petroleum-derived phenol, in which benzene is converted to cumene and then cumene hyperoxide followed by selective decomposition to phenol [12]. Phenol is the starting material for production of chemicals such as cyclohexanol, cyclohexanone, aminophenols, nitrophenols, and bisphenol A, among others [9]. Research and development in production of PM with various functionalities dates back to the early 1970s [13]. As with most biorenewable processes, development through the 1980s and 1990s was slow due to a boon in petroleum production. Several reviews have examined more recent technical progress in the development of the production of phenolic monomers from lignin [5, 14, 15].

The resistance of lignin to microbial attack is an important biological function, but also renders most biochemical processing of lignin ineffective [16]. Thermochemical conversion, on the other hand, has shown significant promise at depolymerizing lignin to lower-molecular-weight components, albeit with varying degrees of selectivity. Among thermochemical conversion options, solvent liquefaction is particularly well suited to produce valuable PM from lignin.

Most technical lignins can form relatively stable slurries in a variety of solvents at solids loadings of up to 30%. The presence of solvent has several benefits when thermally processing lignin. The most practical benefit is that it disperses the lignin particles and effectively prevents them from adhering into a plastic-like clump that can clog high-temperature dry feed mechanisms [17]. Similarly, solvents can dilute intermediates and reactive products, which reduces the likelihood for repolymerization [18]. Hydrogen donor solvents (HDS) are able to cap reactive species in addition to diluting them [19]. Lignin decomposition is generally understood to produce radical intermediates that readily undergo recombination to form thermally stable phenolic oligomers [20]. The use of HDS and radical-scavenger solvents, such as phenol, have been demonstrated as an effective means of reducing the formation of these oligomers [21-25].

Tetralin is one of the most widely used HDS for solvent liquefaction research. Initial work with tetralin began with coal liquefaction in the 1970s [26]. Given the compositional similarities between coal and lignin, the subsequent use of tetralin for lignin liquefaction is not surprising [6]. Several studies have demonstrated the ability of tetralin to donate hydrogen at moderate temperatures and pressures [7, 19]. The importance of hydrogen donation has been best demonstrated by comparing the products from the liquefaction of kraft lignin in tetralin and naphthalene (hydrogen-depleted) at 400 °C. Char yield was 9.7 and 38.5 wt% while ether-soluble phenols were 37.4 and 7.4 wt% between the tetralin and naphthalene experiments, respectively [7]. Other researchers have also found tetralin to promote favorable reaction chemistry [21, 25, 27-30].

Phenolic solvents have also been shown to promote thermal deconstruction and solubilization of lignin [22]. These solvents are unique because they could feasibly be produced from lignin itself. Most PM are thermally stable, allowing them to be distilled into pure components. For a solvent liquefaction process to be economically viable it is paramount that the primary solvent(s) be either very cheap or recyclable [31]. Using a PM-based solvent for lignin liquefaction is promising because the solvent is both produced during the process and recyclable. Solvent separation efficiency does not need to be 100% for such a process, given that the reaction produces a net increase in PM. This not only improves system reliability but also reduces the cost and complexity of the solvent recovery system.

The use of phenolic and hydrocarbon mixed solvents originated with the work of Pott et al. [32] in 1933 when phenolics were added to a coal liquefaction process to improve liquid yields. Although there are several hypotheses about the specific mechanism that increases liquid yields, researchers have concluded that phenolics (e.g. phenol, catechol, cresol, etc.) are able to improve ether bond cleavage [33]. The combined hydrogen donation capability of a HDS along with the catalytic activity of phenolic solvents provide a synergetic effect that has been shown to result in promising liquefaction performance [34].

The goal of this paper was to develop and demonstrate an economical and robust solvent liquefaction process with which to valorize lignin, obtained from the production of cellulosic ethanol, through the production of renewable chemicals. Our approach to this study was threefold. First was to evaluate key operating parameters for maximizing liquid yields from the solvent liquefaction of technical lignin in a PM-based solvent. Second was to

evaluate these parameters on the production of PM. Third was to demonstrate that the process yielded an excess of distillable liquid products suitable for use as recycle solvent.

Materials and Methods

Technical lignin was acquired from DuPont for this study. It was extracted from corn stover using a proprietary mild ammonia-based extraction method. The lignin was received as dry powder. Data from the ultimate and proximate analysis of the lignin is shown in Table 1.

Table 1. Proximate and ultimate analysis of ammonia-extracted corn stover lignin.

Proximate Analysis (wt%)	
Moisture	0.9
Volatiles (MF)	58.4
Fixed Carbon (MF)	25.1
Ash (MF)	16.4
Ultimate Analysis (wt% AF/MF)	
C	58.04
H	4.86
N	4.23
S	1.25
O (by difference)	31.63

O-cresol was selected as a model PM solvent. Kilogram quantities of reagent grade (<98% purity) were purchased from Fischer Scientific. Reagent grade tetralin (≤97% purity) acquired from Advanced Aromatics was utilized as HDS. Preliminary tests were conducted to verify the thermal stability of both o-cresol and tetralin at reaction conditions. One hundred grams of each solvent was heated to 340 °C for 30 minutes, after which the liquid mass and composition were recorded. Both solvents demonstrated satisfactory resistance to thermal degradation, with negligible reduction in liquid mass or to other GC-detectable liquid products.

Solvent Liquefaction Methodology

A 500 mL Parker Autoclave Engineers EZE-Seal Stirred Reactor was used for all solvent liquefaction experiments conducted in this study. The reactor system was modified, as shown in Figure 2, with a bolt-on high-pressure overheads handling system for the purpose of continuous pressure control and vapor recovery. The reactor and condenser were operated consistently at 70 bar. The condenser, chilled to 10 °C regardless of reaction temperature, collected all condensable vapors prior to ventilation. Quasi-batch operation in this manner emulates a continuous process more closely than does a closed system.

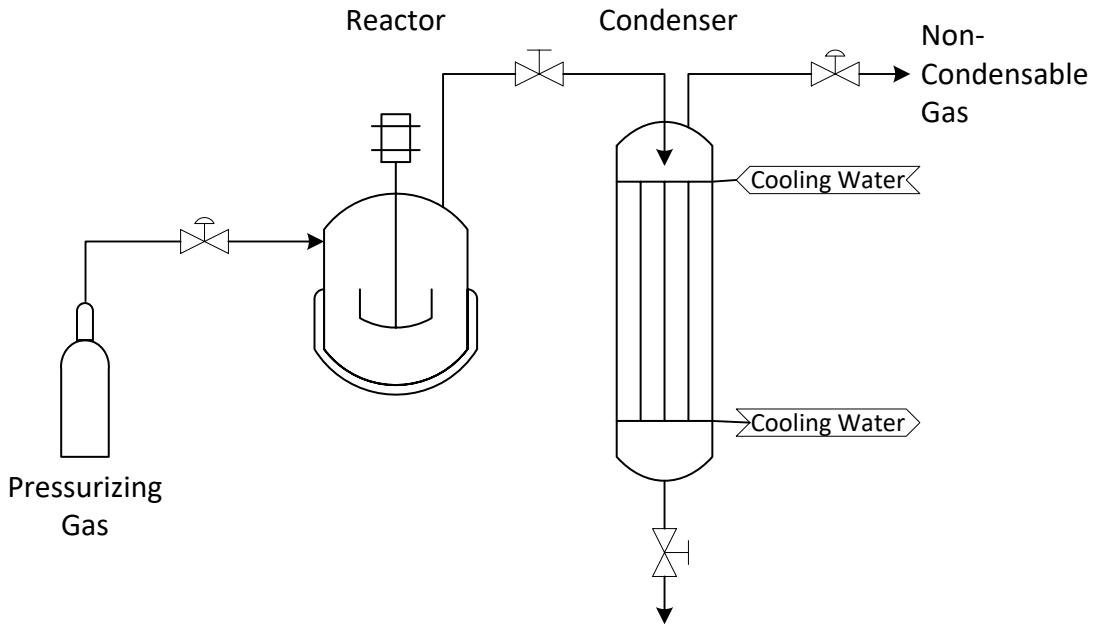

Figure 2. Block flow diagram of the autoclave reactor system with high-pressure overheads handling.

For each experiment, 100g of solvent mixture was loaded into the reactor vessel. A prescribed quantity of dry lignin was then added to the reactor. The loaded reactor was then sealed onto the test stand, purged with nitrogen gas, and pressurized to 70 bar. A 1000 W heater, controlled by the internal process temperature, provided heat to the system at a rate of approximately 5 °C min^{-1} until the desired set point was reached. Upon reaching the final temperature, the reaction timer was started and the temperature was maintained to ± 5 °C. After the desired residence time elapsed, the heater was removed and a fan was directed on the reactor body to cool it to approximately 120 °C. Water chilled to 10 °C was then pumped through an internal cooling coil until the reactor reached ambient temperature.

Following the reaction, any residual pressure was vented and the condenser drained of any liquid, which contains heavy oil and solid residue. Condensate is referred to as light

oil. Subsequent product separation and analysis is outlined in Figure 3. Gas production was calculated as the reactants minus the mass of products in the reactor and the mass of light oil.

The mass closure for all of the experiments in this data set was between 99 and 102 wt%. All product yields are with respect to lignin and reported on a moisture free, ash free basis.

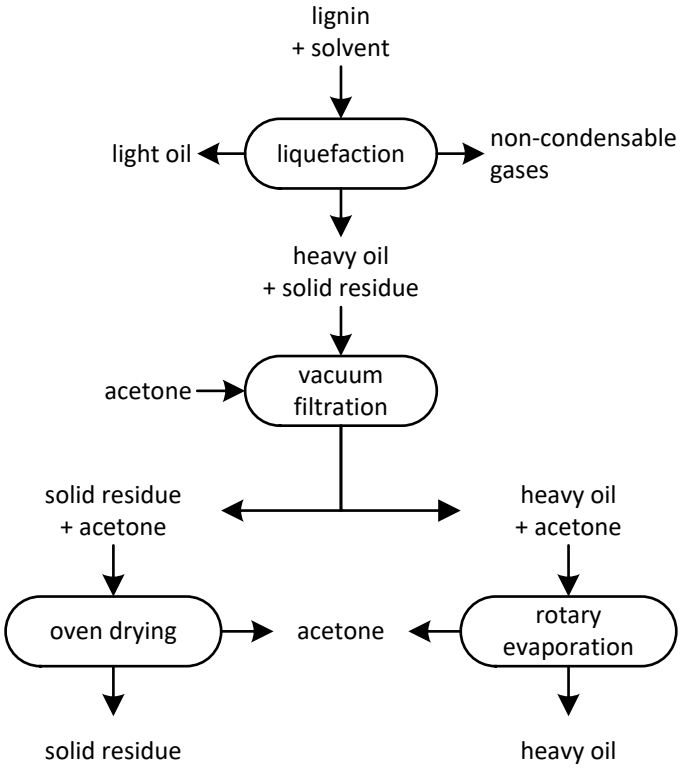

Figure 3. Procedure outline for separation and analysis of solvent liquefaction products.

Analytical Methods

PM in the liquid product were analyzed with a Bruker 430-GC gas chromatograph (GC) outfitted with a Phenomenex ZB 5-MS capillary column and flame ionization detector

(FID). Five-point calibrations were conducted for 15 different compounds expected to be found in the products. The injection port and detector were both operated isothermally at 300 °C throughout the analysis. The GC oven was programmed to ramp from 30 to 400 °C at a rate of 5 °C min^{-1}. Sample injection volume was 1 µL, and helium carrier gas was injected at 1 mL min^{-1}.

A Mettler-Toledo TGA/DSC 1 thermogravimetric analyzer (TGA) was used to determine the boiling point range of the heavy oil. A liquid sample weighing approximately 300 mg was dispensed into a ceramic crucible and loaded into the TGA. The oven was programmed to ramp from 35 to 400 °C at a rate of 20 °C min^{-1} under a flow of nitrogen gas. After reaching 400 °C, air was flushed into the oven while it continued to ramp to 900 °C to combust any residue. Mass loss prior to 400 °C was attributed to volatilization of liquid products. This data was then used to compile a boiling point curve for the sample. O-cresol and tetralin boiled within range of PM found in the heavy oil, as illustrated in Table 2. Given that the starting solvents were not extracted from the heavy oil, extra care was required when analyzing boiling point data. To avoid any analytical discrepancies, the mass of volatile PM was calculated as the product of the mass fraction of the material vaporized below 340 °C and the mass of the heavy oil minus the initial mass of the solvent.

In this manner the solvent was assumed to be preserved in the heavy oil, while the mass of volatile PM was that part that boiled below 340 °C after accounting for the solvent. The cut-off was set at 340 °C based on the assumption that above this temperature it was possible for dimers to volatilize; separation of phenolic oligomers was not desired.

Table 2. Pure compound boiling points for solvents (bold) and phenolic monomers often found in this study.

Compound Name	Pure Boiling Point (°C)
Phenol	182
o-Cresol	**191**
2-Ethylphenol	196
m/p-Cresol	203
Guaiacol	205
Tetralin	**207**
p-Xylenol	212
4-Ethylphenol	219
Creosol	222
2-Methoxy-4-vinylphenol	224
4-Ethyl-2-methoxyphenol	235

Experimental Design and Statistical Modelling

Response surface methodology was used to evaluate the optimal processing conditions using a limited number of experiments [35]. Given that only four factors were evaluated, a central composite design was selected as the statistical model. Central composite designs are constructed using 2^n factorial experiments, $2n$ axial experiments, and additional center-point experiments as necessary to determine the system variability, where n represents the number of factors. Each location of the factor-level is coded as shown in Figure 4, where center points are “0”, cube points are “-1/+1” and axial points are “-α/+α.”

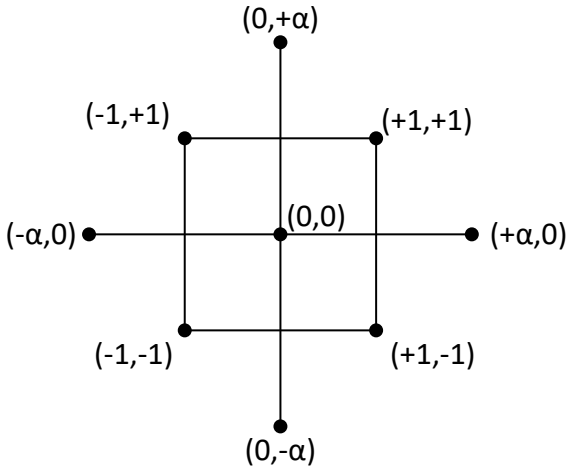

Figure 4. Example central composite design space for a 2-factor design. Each level is coded such that center points are "0", cube points are "-1/+1" and axial points are "-α/+α."

Seven factors were initially identified as variables of interest, and four of these were subsequently selected for full investigation after initial screening. Preliminary experiments also aided to establish the range over which these factors were explored. The factor-level combinations are shown in Table 3. The total number of experiments for this study was 31: 7 center points, 16 cube points, and 8 axial points.

Table 3. Factor-level combinations for central composite design of experiments.

Factor	**-α**	**-1**	**0**	**+1**	**+α**
HDS blend ratio (wt%)	0	25	50	75	100
Reaction temperature (°C)	260	280	300	320	340
Solids loading (wt%)	5	10	15	20	25
Residence time (min)	0	7.5	15	22.5	30

HDS blend ratio was explored across the full range (0 to 100 wt%) to examine the trade-off between the hydrogenation from tetralin and superior solvation of o-cresol. The reaction temperature range was balanced between promoting lignin thermal decomposition and reducing the extent to which PM were decomposed. Preliminary experiments indicated that phenolic monomers degraded at elevated temperatures, and therefore the study was centered on 300 °C. The range for solids loading was established based on the limits of forming a stable slurry of lignin and solvent. Beyond approximately 25 wt% solids loading, particles readily fell out of suspension when mixed in a glass beaker. Below 5 wt% solids loading it was thought that PM production from lignin would not be sufficient to displace any losses in a hypothetical solvent recovery system. Residence time was selected based on prior liquefaction experiments that suggested long durations were detrimental to overall liquid yield.

Six response variables were selected to evaluate the influence of each of the four factors on solvent liquefaction performance. Of the six variables, five were desired to be maximized: yields of liquid, distillate, phenol, guaiacol, and p-xylenol; while the yield of solid was to be minimized. Solid yield was included due to the practical implications of filtering a high concentration of solids from the product liquid. The order in which the experiments were conducted was completely random in an effort to avoid the introduction of systematic error.

All results were entered into JMP 12 Pro for regression fitting and statistical analysis. Each response variable was fitted with a regression curve that contained an intercept, linear term(s), interaction term(s), and quadratic term. The full model, containing all combinations

of factors and factor interactions, often did not fit the data well, so a reduced model was adopted. The reduced model was desired to have a high adjusted correlation value while the analysis of variance remained significant to the 95% confidence level. Some non-significant terms (p-value > 0.05) were often left in the reduced model to improve the overall fit of the regression. A lack-of-fit test was also conducted to the 95% confidence level to ensure that the model type was appropriate.

After the reduced models were generated, a plot showing the residuals versus the actual data was examined for each model. Random scatter indicated no systematic error was present, and the models could be trusted. Another plot, showing actual versus predicted data for each model, was then examined for outliers. The solids loading negative axial point ($-\alpha$, 0, 0, 0) was found to be a consistent outlier. This data point was ultimately excluded from the model after repeat experiments confirmed it as an outlier. The low solids loading (5%) in this case presumably resulted in lignin-derived products in concentrations too low for consistent and reliable quantification.

Results and Discussion

Thermal stability of phenolic monomers

Preliminary experiments were conducted to evaluate the thermal stability of beechwood creosote. Beechwood creosote was purchased from Sigma Aldrich as a surrogate mixture for lignin-derived PM. One hundred grams of creosote was processed for 25 minutes at 325, 350, and 375 °C. The residual liquid mass, composition, and boiling point distribution of the creosote was monitored. GC-FID analysis indicated a significant reduction in guaiacol,

1,2-dihydroxybenzene, and 2,6-dimethylphenol, as shown in Figure 5. The absence of a corresponding increase in other compounds suggested that the compounds were polymerizing rather than decomposing to smaller molecules. This was also supported by a substantial increase in the boiling point distribution of these samples illustrated in Figure 6. Gas production also increased with increasing temperature with 2, 7, and 11% gas yield at 325, 350, and 375 °C, respectively. Following these findings, an additional experiment was conducted at 300 °C. All metrics suggested that the PM were essentially unaffected at this temperature.

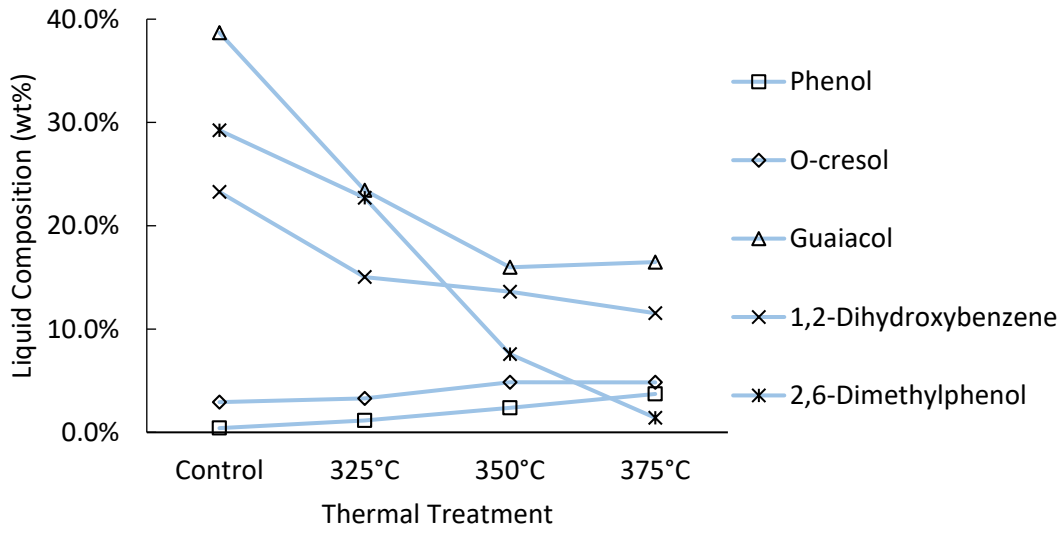

Figure 5. Compositional changes in beechwood creosote after processing at 325, 350, and 375 °C.

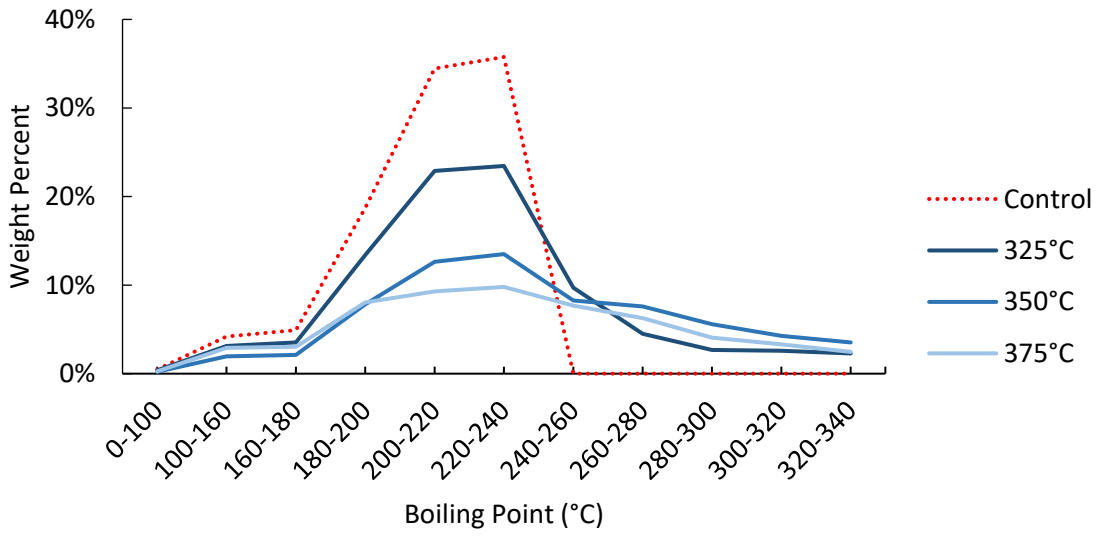

Figure 6. Boiling point distribution of the beechwood creosote control sample and samples processed at 325, 350, and 375°C for 25 minutes.

Product Yields and Composition

Solvent liquefaction performance was consistent and repeatable across the entire design space, with the exception of the solids loading negative axial point discussed previously. The mean yields, root mean square error (RMSE), R^2 correlation value, and analysis of variance (ANOVA) p-value taken across the entire design space for each response variable are shown in Table 4. The majority of the models had excellent fits with the experimental data. Distillate yield had the poorest fit, yet the model was still significant at the 95% confidence level. Distillate yield also correlated well with liquid yield (Figure 7), which supported the initial hypothesis that distillable phenolics would increase with liquid yield. The trend shows a quadratic relationship such that at high liquid yields (> 60 wt%) there is a rapid increase in the yield of distillable phenolics. This might be due to an increase in low

molecular weight compounds that are liberated only after the majority of lignin is depolymerized to soluble phenolic oligomers.

Table 4. Mean yields, summary of fit, and analysis of variance (ANOVA) statistical measures for the fit of the model with the actual data for each response variable.

	Summary of Fit			ANOVA	
Response	Mean (wt%)	RMSE	R^2	P-value	Significant?
Liquid Yield	52.8	3.9	0.91	<0.0001	YES
Solid Yield	15.6	1.9	0.92	<0.0001	YES
Distillate Yield	21.8	4.7	0.63	0.0187	YES
Phenol Yield	5.3	1.3	0.96	<0.0001	YES
Guaiacol Yield	1.4	0.4	0.79	<0.0001	YES
p-Xylenol Yield	3.4	0.6	0.96	<0.0001	YES

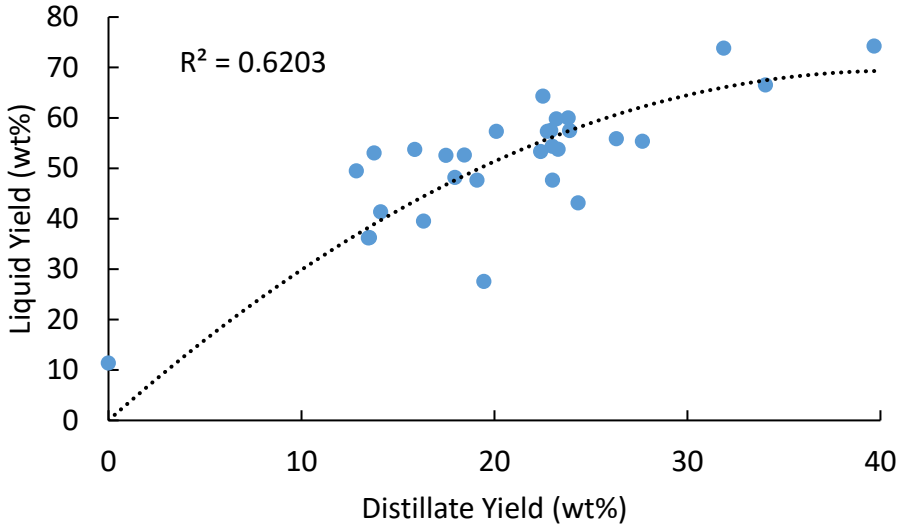

Figure 7. Liquid yield versus distillate yield demonstrated a quadratic relationship where beyond liquid yields of approximately 60 wt% a significant increase in distillate yield occurred.

Effect of HDS Blend Ratio

The initial concentration of HDS was found to be one of the most significant factors for every response variable. The modeled univariate effect of HDS blend ratio on each response is shown in Figure 8 while all other factors were held constant at their center points. Guaiacol and distillate yields were best modeled using linear regressions, while all other responses demonstrated quadratic relationships with HDS blend ratio.

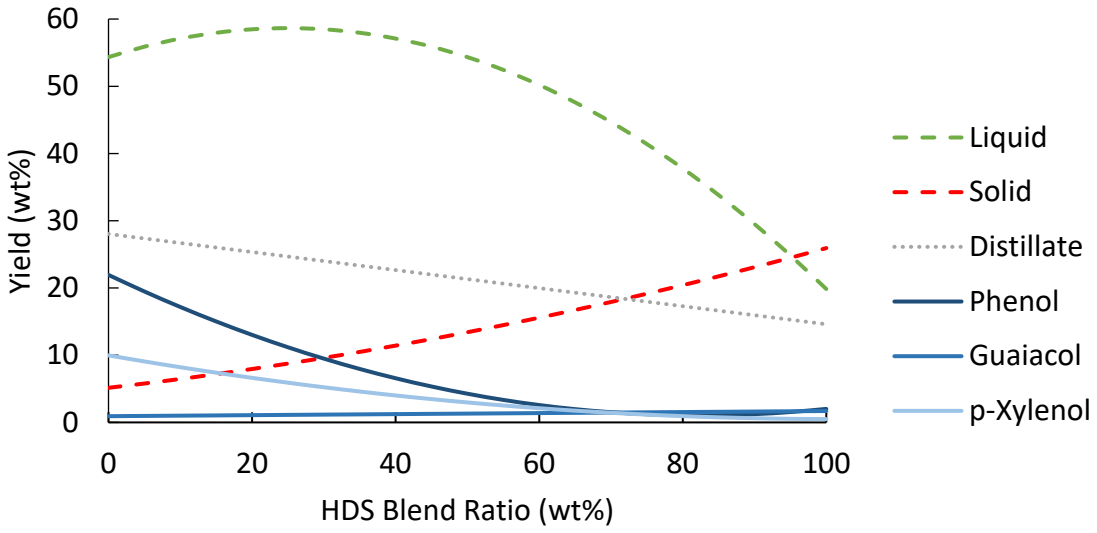

Figure 8. Modeled univariate effect of HDS blend ratio on each response variable while all other factors were held constant at their center points (300 °C reaction temperature, 15 wt% solids loading, 15 minute residence time).

Maximization of liquid yield was perhaps the most critical target for this study. We hypothesized that maximum liquid yield would correspond with maximum PM yield. It was also desirable to liquefy as much lignin as possible as liquid is more desirable in applications ranging from steam raising to hydrocracking to transportation fuels. Liquid yield was strongly dependent upon the HDS blend ratio. According to the model (Figure 8), liquid yields ranged from a maximum of 58.6 wt% to a minimum of 19.8 wt% at HDS blend ratios of 25 and 100 wt%, respectively, when all other variables were held constant. The strong quadratic behavior demonstrates the trade-off between a sufficient amount of available hydrogen and superior solvation from the PM solvent.

Solvation of lignin derived compounds is critical to discourage interaction between reactive species. One method of estimating the solubility of a compound is to compare the

Hildebrand solubility parameter (HSP). A good solvent is one where the difference between the HSP of the solvent and solute is less than 3 $MPa^{0.5}$ [36]. Table 5 shows HSP calculated at the mean reaction temperature (300 °C) for each solvent and several PM commonly found in this study. Of the two solvents, o-cresol is clearly the preferred solvent for solubilizing PMs. Tetralin is generally a good solvent, but as shown in Table 5 the difference in HSP between phenol and tetralin exceeds the recommended maximum difference of 3 $MPa^{0.5}$. This demonstrates the reduced effectiveness of tetralin at solubilizing the wide range of PM products generated from lignin.

Table 5. Hildebrand solubility parameter calculated at the mean reaction temperature (300 °C) for solvents (bold) and phenolic monomers often found in this study.

Compound	**Hildebrand Solubility Parameter ($MPa^{0.5}$)**
Phenol	20.99
o-Cresol	**19.54**
Guaiacol	19.17
Syringol	18.70
p-Xylenol	18.64
2-Ethylphenol	18.46
Creosol	18.26
Tetralin	**16.70**

Interestingly, the minimum solid yield did not correspond to maximum liquid yield. Rather, this minimum occurred when no HDS was present. Although the liquid yield at this point was also very high (54.3 wt%) the offset between these two optimums suggests that the

volatile content released from the feedstock between 0 and 25 wt% HDS was predominantly in the form of non-condensable gases. Similarly, it appears that gas production increased rapidly at high HDS blend ratios, reaching a maximum of 30 wt% gas yield at 100 wt% HDS blend ratio.

The yields of phenol and p-xylenol also demonstrated strong quadratic behaviors. Maximum phenol yield (21.9 wt%) and p-xylenol yield (10.0 wt%) occurred when the solvent was entirely composed of PM. Given that both of these compounds have very limited oxygenate functionality, it is not surprising that they did not require any HDS to remain at high concentrations in the product liquid. Furthermore, as previously discussed, it is likely that the increase in phenolic content in the solvent aided in the deconstruction of lignin to phenol and other PM.

Distillate yields had a negative linear correlation with the concentration of tetralin in the solvent. It is not surprising that this yield was less severely impacted by HDS blend ratio than either the liquid or phenol yields. Though 100% o-cresol appears to be a more effective solvent at deconstructing lignin to volatile PM (distillate yield of 28.0 wt%), the hydrogenation capability of tetralin is still valuable at producing stable molecules with relatively low boiling points. Comparing the liquid and distillate yields from pure tetralin (19.8 and 14.6 wt%, respectively) it is clear that the majority of the liquid products at this condition were volatile, which supports the notion that hydrogenation is a tangible benefit.

Despite a relatively low yield, guaiacol also exhibited a strong relationship with HDS blend ratio. The positive linear correlation predicted that guaiacol yield nearly doubled from

0.9 to 1.7 wt% when the solvent was shifted from pure o-cresol to pure tetralin. This behavior is likely due to the influence of readily available hydrogen on preserving methoxyl groups.

Effect of Reaction Temperature

Reaction temperature was a significant factor for many of the response models. Its univariate effect on each of the response variables is shown in Figure 9. Only phenol and guaiacol yields demonstrated quadratic relationships with temperature, although neither reached an optimum within the range tested. Liquid and solid yields were both negatively correlated with temperature, which suggests that increasing temperature results in an increase in gas production. This result was anticipated from the PM thermal stability study discussed earlier, where increasing temperature also resulted in an increase in gas production.

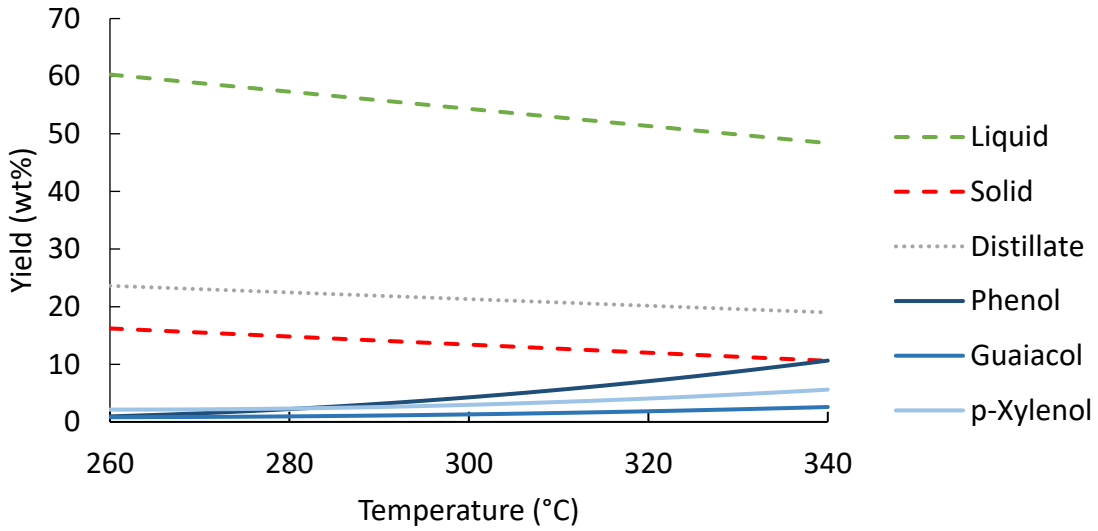

Figure 9. Modeled univariate effect of reaction temperature on each response variable while all other factors were held constant at their center points (50 wt% HDS blend ratio, 15 wt% solids loading, 15 minute residence time).

Liquid yield reached its maximum (60.3 wt%) at 260 °C and steadily decreased to 48.4 wt% at 340 °C. Interaction effects between reaction temperature and HDS blend ratio (Figure 10) demonstrate the importance of increasing the concentration of HDS as reaction temperature increases. This is likely due to an increase in thermal stability of hydrogenated products. As the HDS blend ratio increased the temperature curves are shown to converge, which suggests that elevated temperatures are preferred when tetralin is the primary solvent. Work conducted by Connors et al. [7] and Dorrestijn et al. [37] also found that elevated temperatures were preferred when pure tetralin was used.

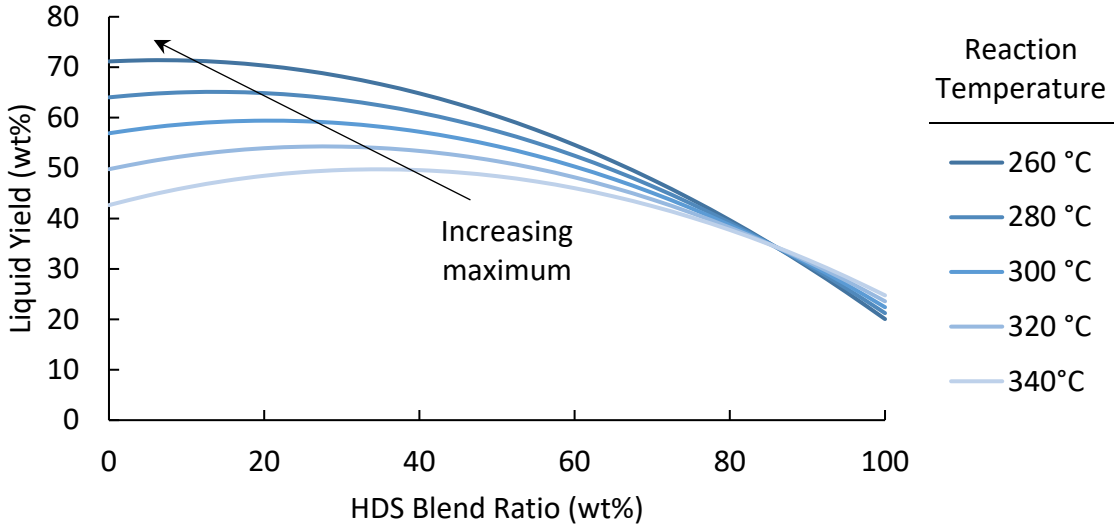

Figure 10. Interaction effects of reaction temperature and HDS blend ratio on liquid yield. Models were generated while holding all other factors constant at their center points (15 wt% solids loading and 15 minute residence time).

Also evident in Figure 10 is the bivariate shift in maximum liquid yield. The overall maximum liquid yield (71.4 wt%) for these two variables is achieved at a reaction temperature of 260 °C and HDS blend ratio of approximately 6.5%. As the temperature

increased, not only did the relative maxima decrease, but HDS blend ratio corresponding to the relative maximum increased. For example, the relative maximum for a reaction temperature of 340 °C was 49.7 wt% at blend ratio of 34.7 wt%. This trend further demonstrates the importance of HDS for achieving maximum liquid yields at elevated temperatures. However, it also indicates that low temperatures and low HDS blend ratios actually result in higher liquid yields. This has significant impact on the operating costs of a process given that lower temperatures and lower HDS inputs are both economically favored over their alternatives.

Phenol yield increased from 1.0 to 10.6 wt% when reaction temperature was raised from 260 to 340 °C. This was likely caused by an increase in extent of thermal decomposition of both lignin and high molecular weight phenolic products. Thring et al. [27] obtained similar results when exploring lignin liquefaction in tetralin. They found the yield of phenol and cresol increased with increasing reaction severity (a measure of the combined effects of temperature and residence time) [27].

Effect of Solids Loading

Solids loading was only statistically significant for the yields of phenol, guaiacol and p-xylenol, although the term was included in every model to improve overall fit with the experimental data. As previously discussed, the negative axial point of 5 wt% solids loading was excluded from the model due to a pervasive disagreement with the rest of the experimental data. For this reason, the univariate model of the effect of solids loading on the response variables has been shown in Figure 11 to begin at 10 wt%.

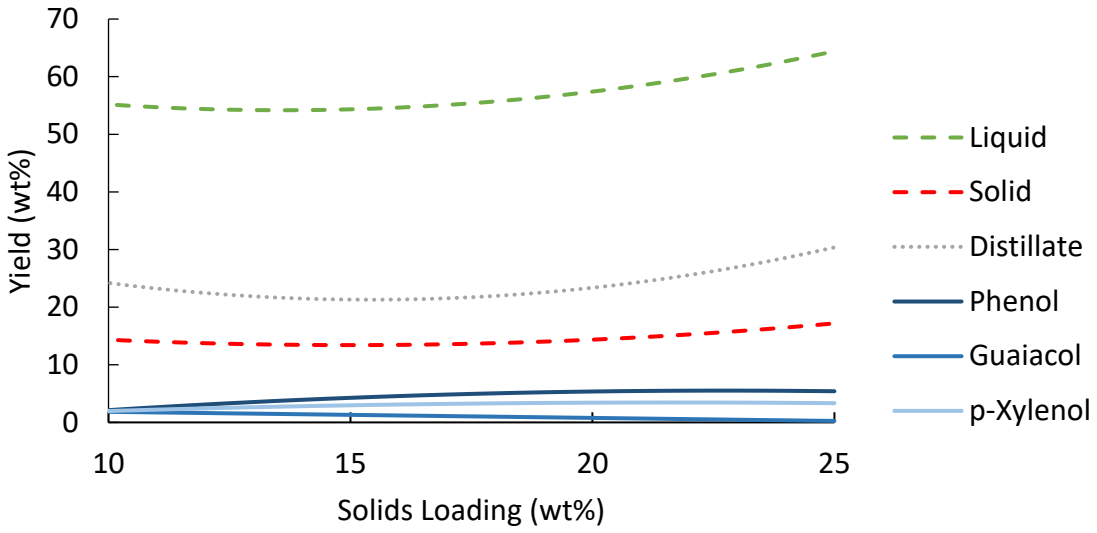

Figure 11. Modeled univariate effect of solids loading on each response variable while all other factors were held constant at their center points (50 wt% HDS blend ratio, 300 °C reaction temperature, 15 minute residence time). The negative axial point of 5 wt% solids loading was not included in the model, thus the design space has been shown to begin at 10 wt%.

In addition to the influence of solids loading on the ability to feed a slurry into a high pressure reaction, it also has bearing on the concentration of reactive species in the process. Higher solids loadings are preferred for process economics, but this must be balanced against effective solvation and dilution of the product stream. Interaction effects between solids loading and HDS blend ratio are an effective way to evaluate this behavior. For example, the interaction effect on guaiacol yields shown in Figure 12 demonstrate strong differences in solvation by o-cresol and tetralin. When the solvent was composed of pure o-cresol (0 wt% HDS blend ratio), guaiacol yields were essentially unaffected by an increase in solids loading. This suggests that guaiacol is effectively solvated and stabilized by o-cresol in all proportions. Conversely, when the solvent was composed of pure tetralin (100 wt% HDS

blend ratio), guaiacol yields were highly dependent upon solids loading, decreasing from 2.4 wt% at solids loading of 10 wt% to only 0.3 wt% for solids loading of 25 wt%.

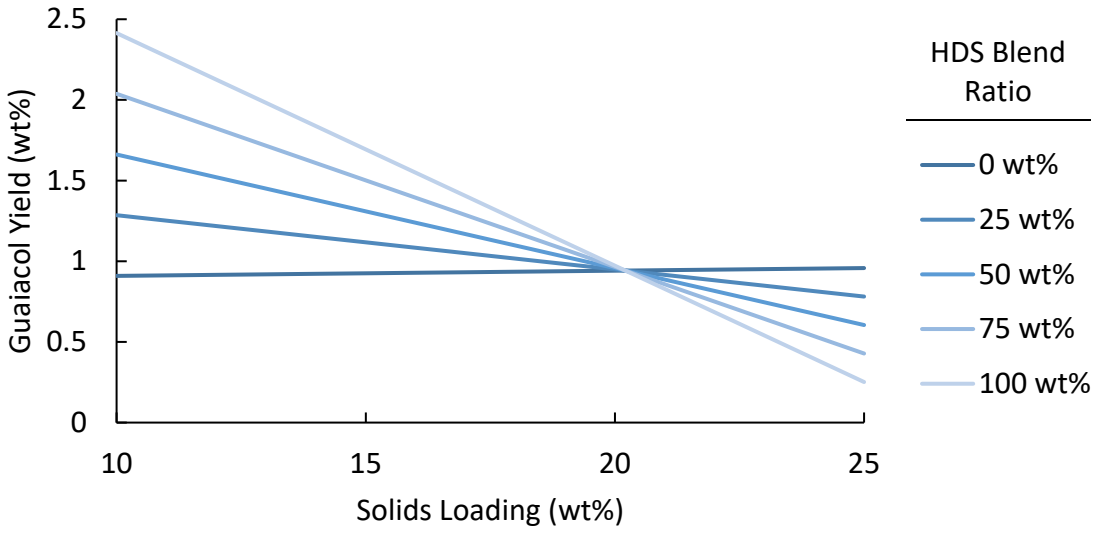

Figure 12. Interaction effects between solids loading and HDS blend ratio

Effect of Residence Time

Residence time was not a statistically significant factor for any of the response variables, although it was included in each model to improve the overall fit with the data. This is likely due to the relatively narrow residence time range explored in this study. At considerably longer residence times, on the order of several hours, work by Connors et al.[7] demonstrated that gas production increases at the expense of liquid yield [7]. Over the residence time range of 30 min, it shows minimal effect on yields (Figure 13). The lack of statistical foundation for the models means that conclusions cannot be confidently drawn from them. However, it can be concluded that short residence times do not appear to be

detrimental to yields. A continuous process would, therefore, not require excessive reactor volumes to maintain a high feed rate of lignin while still achieving the yields found in this study.

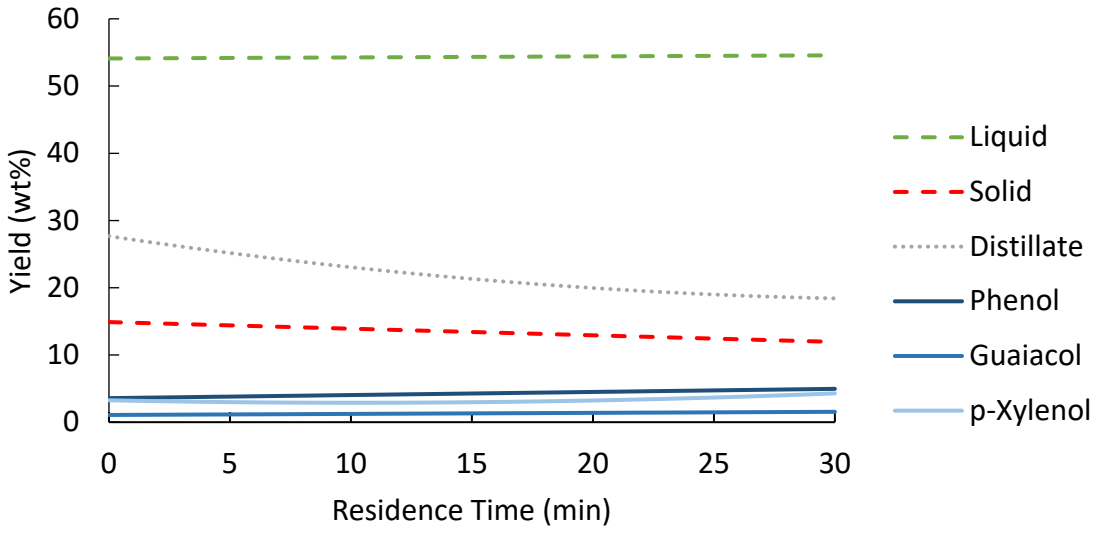

Figure 13. Modeled univariate effect of residence time on each response variable while all other factors were held constant at their center points (50 wt% HDS blend ratio, 300 °C reaction temperature, 15 wt% solids loading).

Conclusions

Solvent liquefaction of technical lignin in mixtures of o-cresol and tetralin was demonstrated to produce high liquid yields and a high selectivity towards PM. Utilizing response surface methodology, optimization of the processing conditions was demonstrated across a broad range of values for four factors: 1) HDS blend ratio, 2) reaction temperature, 3) solids loading, and 4) residence time. Low concentrations of HDS and low reaction temperatures were found to be the most significant factors for high liquid yields. The reduced statistical models indicated that residence time did not hold significant impact on liquefaction

performance or product selectivity. Characterization of the boiling point distribution of the liquid products indicated a high yield of molecules in the boiling point range of the solvent. Recovery of these products would allow for a sustainable recycle-solvent process, requiring only a modest input of HDS (if desired). A block flow diagram for a hypothetical integrated process based on this technology is shown in Figure 14.

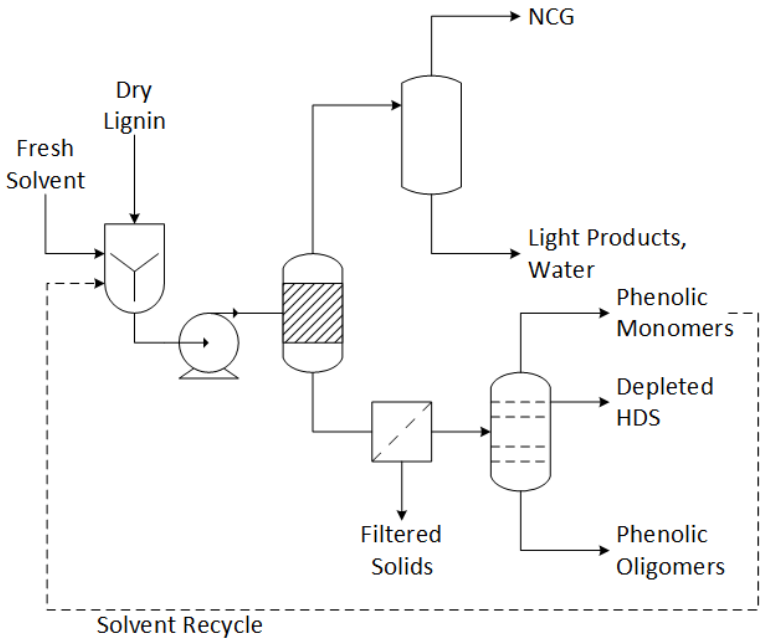

Figure 14. Block flow diagram for a proposed solvent liquefaction process to produce high yields of liquid products, with a high selectivity towards low-boiling point PM, from lignin in a PM recycle solvent.

Acknowledgements

The authors would like to thank Dr. Max Morris for his assistance with setting up the statistical model and preliminary analysis of the data. We would also like to thank Patrick Johnston for his assistance in TGA method development.

Funding for this research was provided by the Gary and Donna Hoover Endowment in Mechanical Engineering at Iowa State University and the U.S. Department of Energy under contract #EE0005974.

References

1. Browning, B.L., *The chemistry of wood.* 1963.

2. Sarkanen, K.V. and C.H. Ludwig, *Lignins: occurrence, formation, structure and reactions.* Lignins: occurrence, formation, structure and reactions., 1971.

3. Zakzeski, J., et al., *The catalytic valorization of lignin for the production of renewable chemicals.* Chemical reviews, 2010. **110**(6): p. 3552-3599.

4. Reichert, E., et al., *Electro-catalytic oxidative cleavage of lignin in a protic ionic liquid.* Physical Chemistry Chemical Physics, 2012. **14**(15): p. 5214-5221.

5. Azadi, P., et al., *Liquid fuels, hydrogen and chemicals from lignin: A critical review.* Renewable and Sustainable Energy Reviews, 2013. **21**: p. 506-523.

6. Dorrestijn, E., et al., *The occurrence and reactivity of phenoxyl linkages in lignin and low rank coal.* Journal of Analytical and Applied Pyrolysis, 2000. **54**(1): p. 153-192.

7. Connors, W., et al., *Thermal degradation of kraft lignin in tetralin.* Holzforschung-International Journal of the Biology, Chemistry, Physics and Technology of Wood, 1980. **34**(1): p. 29-37.

8. Holladay, J.E., et al., *Top Value-Added Chemicals from Biomass-Volume II—Results of Screening for Potential Candidates from Biorefinery Lignin*. 2007, Pacific Northwest National Laboratory (PNNL), Richland, WA (US).

9. Strassberger, Z., S. Tanase, and G. Rothenberg, *The pros and cons of lignin valorisation in an integrated biorefinery.* RSC Advances, 2014. **4**(48): p. 25310-25318.

10. Kleinert, M. and T. Barth, *Phenols from lignin.* Chemical Engineering & Technology, 2008. **31**(5): p. 736-745.

11. Calvo-Flores, F.G. and J.A. Dobado, *Lignin as renewable raw material.* ChemSusChem, 2010. **3**(11): p. 1227-1235.

12. Schmidt, R.J., *Industrial catalytic processes—phenol production.* Applied Catalysis A: General, 2005. **280**(1): p. 89-103.

13. Goldstein, I.S. *Perspectives on production of phenols and phenolic acids from lignin and bark*. in *Appl. Polym. Symp.* 1975. DTIC Document.

14. Amen-Chen, C., H. Pakdel, and C. Roy, *Production of monomeric phenols by thermochemical conversion of biomass: a review.* Bioresource Technology, 2001. **79**(3): p. 277-299.

15. Pandey, M.P. and C.S. Kim, *Lignin depolymerization and conversion: a review of thermochemical methods.* Chemical Engineering & Technology, 2011. **34**(1): p. 29-41.

16. Zeng, Y., et al., *Lignin plays a negative role in the biochemical process for producing lignocellulosic biofuels.* Current Opinion in Biotechnology, 2014. **27**: p. 38-45.

17. Kaminsky, W. and H. Schwesinger, *Properties and Decomposition of Lignins Isolated by Means of an Alcoholic-Water-Mixture. Part 3: Decomposition by Pyrolysis in a Fluid-Bed.* Holzforschung-International Journal of the Biology, Chemistry, Physics and Technology of Wood, 1980. **34**(3): p. 73-75.

18. Li, C.-Z., et al., *Comparison of thermal breakdown in coal pyrolysis and liquefaction.* Fuel, 1994. **73**(6): p. 851-865.

19. Vasilakos, N.P. and D.M. Austgen, *Hydrogen-donor solvents in biomass liquefaction.* Industrial & Engineering Chemistry Process Design and Development, 1985. **24**(2): p. 304-311.

20. Bai, X., et al., *Formation of phenolic oligomers during fast pyrolysis of lignin.* Fuel, 2014. **128**: p. 170-179.

21. Kim, K.H., et al., *Hydrogen-donor-assisted solvent liquefaction of lignin to short-chain alkylphenols using a micro reactor/gas chromatography system.* Energy & Fuels, 2014. **28**(10): p. 6429-6437.

22. Lin, L., et al., *Liquefaction mechanism of lignin in the presence of phenol at elevated temperature without catalysts. Studies on ß-O-4 lignin model compound. I. Structural characterization of the reaction products.* Holzforschung-International Journal of the Biology, Chemistry, Physics and Technology of Wood, 1997. **51**(4): p. 316-324.

23. Lin, L., et al., *Liquefaction mechanism of lignin in the presence of phenol at elevated temperature without catalysts. Studies on ß-0-4 lignin model compound. III. Multi-*

condensation. Holzforschung-International Journal of the Biology, Chemistry, Physics and Technology of Wood, 1997. **51**(4): p. 333-337.

24. Lin, L., et al., *Liquefaction mechanism of lignin in the presence of phenol at elevated temperature without catalysts. Studies on ß-O-4 lignin model compound. II. Reaction pathway.* Holzforschung-International Journal of the Biology, Chemistry, Physics and Technology of Wood, 1997. **51**(4): p. 325-332.

25. Jegers, H.E. and M.T. Klein, *Primary and secondary lignin pyrolysis reaction pathways.* Industrial & Engineering Chemistry Process Design and Development, 1985. **24**(1): p. 173-183.

26. Neavel, R.C., *Liquefaction of coal in hydrogen-donor and non-donor vehicles.* Fuel, 1976. **55**(3): p. 237-242.

27. Thring, R.W. and J. Breau, *Hydrocracking of solvolysis lignin in a batch reactor.* Fuel, 1996. **75**(7): p. 795-800.

28. Vuori, A., *Liquefaction of Kraft Lignin: 1. Primary Reactions under Mild Thermolysis Conditions.* Holzforschung-International Journal of the Biology, Chemistry, Physics and Technology of Wood, 1988. **42**(3): p. 155-161.

29. Vuori, A. and M. Niemelä, *Liquefaction of kraft lignin. 2. Reactions with a homogeneous Lewis acid catalyst under mild reaction conditions.* Holzforschung-International Journal of the Biology, Chemistry, Physics and Technology of Wood, 1988. **42**(5): p. 327-334.

30. Wang, G., et al., *Direct liquefaction of sawdust under syngas.* Fuel, 2007. **86**(10–11): p. 1587-1593.

31. van Rossum, G., et al., *Liquefaction of Lignocellulosic Biomass: Solvent, Process Parameter, and Recycle Oil Screening.* ChemSusChem, 2014. **7**(1): p. 253-259.

32. Pott, A., et al., *Die Auflösung von Kohle auf dem Wege der Druckextraktion unter besonderer Berücksichtigung der spaltenden Hydrierung der Extrakte.* Glückauf, 1933. **69**(39): p. 903-912.

33. King, H.-H. and L.M. Stock, *Aspects of the chemistry of donor solvent coal dissolution. The role of phenol in the reaction.* Fuel, 1982. **61**(11): p. 1172-1174.

34. Davoudzadeh, F., et al., *Depolymerization of lignin at low pressure using Lewis acid catalysts and under high pressure using hydrogen donor solvents.* Holzforschung-International Journal of the Biology, Chemistry, Physics and Technology of Wood, 1985. **39**(3): p. 159-166.

35. Kuehl, R.O., *Designs of experiments: statistical principles of research design and analysis*. 2000: Duxbury Press.

36. Vanasse, C., E. Chornet, and R.P. Overend, *Liquefaction of lignocellulosics in model solvents: Creosote oil and ethylene glycol.* The Canadian Journal of Chemical Engineering, 1988. **66**(1): p. 112-120.

37. Dorrestijn, E., et al., *Lignin depolymerization in hydrogen-donor solvents.* Holzforschung, 1999. **53**(6): p. 611-616.

CHAPTER 5

THERMAL STABILITY OF FRACTIONATED BIO-OIL FROM FAST PYROLYSIS

A paper published in *Energy & Fuels*

Martin R. Haverly, Kelley V. Okoren, Robert C. Brown

Abstract

A method was developed to simulate the rapid heating bio-oil fractions will undergo if upgraded using conventional petroleum refining processes. Bio-oil fractions were produced via fluidized bed fast pyrolysis of southern yellow pine sawmill residue. Thermal processing of the bio-oil fractions was evaluated at three temperatures (100, 200, and 300 °C) and two heating times (60 and 120 s). Thermal stability was defined as the increase in average relative molecular weight (RMW) of bio-oil samples after thermal treatment. The effect of moisture content and total acid number (TAN) on thermal stability was also investigated. Changes in chemical structures were observed via Fourier transform infrared spectroscopy (FTIR). Bio-oil fractions exhibited considerable instability at temperatures above 100 °C with substantial increases in average RMW for both 60 and 120 s heating times. The initial concentration of acids, as measured by TAN and ion chromatography (IC), was found to be the strongest predictor of thermal instability.

Introduction

Lignocellulosic biomass is comprised of lignin, cellulose and hemicellulose, which are complex biopolymers of carbon, oxygen, and hydrogen. Conversion of lignocellulosic biomass usually produces oxygenated organic compounds. In the case of biomass liquefaction, which includes pyrolysis and solvent liquefaction, oxygen takes the form of myriad functional groups such as aldehydes, ketones, hydroxyls, and esters in the liquid products [1-3]. The reactivity of these oxygenated functionalities is compounded by the fact that bio-oil is produced under conditions of non-equilibrium [1]. Rapid heating and quenching of reactants and products, respectively, yields significant quantities of bio-oil [4]. Even at room temperature, bio-oil is chemically reactive and unstable, often characterized by a gradual increase in bio-oil viscosity [5].

This change in viscosity is variously known as storage stability, bio-oil aging, and thermal stability, depending upon the context. Storage stability and bio-oil ageing are essentially the same phenomena, focusing on chemical and physical changes that occur in bio-oil after an extended period of time at ambient conditions, which determines the feasibility of storing or transporting bio-oil. Conversely, thermal stability mainly addresses the chemical and physical changes that occur in bio-oil after exposure to elevated temperatures, as often occurs during bio-oil upgrading. To be sure, there is considerable overlap between these two categories of instability, and the observed effects are often very similar.

Accelerated ageing is the practice of increasing bio-oil storage temperatures beyond ambient conditions, usually to 80-90 °C, to increase the rate of instability reactions thereby

decreasing the time needed to observe any changes that take place in the bio-oil [4]. In a 1994 study, Czernik et al. successfully fitted bio-oil ageing viscosity and molecular weight data to a first-order kinetic model, validating the use of accelerated ageing practices.[6] Since then, accelerated ageing of bio-oil at elevated temperatures has been widely adopted as an analytical methodology [3, 7-12].

Though extensive work has been done to evaluate the storage stability of various bio-oils, little has been done to evaluate high temperature thermal stability of bio-oils, which occurs very quickly compared to bio-oil aging at ambient conditions. The stability of bio-oils preheated prior to injection into Diesel or Brayton cycle engines has been previously studied. Boucher et al. [10] conducted thermal shock experiments to simulate preheating that would occur for bio-oil intended for use as gas turbine fuel. After heating samples to 80 °C for 135-285 s they found the solids content in the bio-oil increased from 0.38 to 0.49 wt% and the kinematic viscosity increased by 67% when measured at 40 °C [10], which explains why efforts to directly feed bio-oil into internal combustion engines has been largely unsuccessful [13].

Bio-oil distillation at elevated temperatures is notoriously difficult due to the high temperatures and long heating times required to evaporate high molecular weight components. Distillation tests with bio-oil are characterized by poor volatilization and the formation of solid residues [14-17]. Relatively high temperatures and long heating times are also detrimental to bio-oil upgrading, resulting in high yields of coke and tar at the expense of desired products [18].

High pressure thermal treatment (HPTT) [19], which operates at 300-340 °C at 140 bar for several minutes is likely to encounter thermal stability problems. The process produces separate oil and water phases, the former of which exhibits reduced oxygen content [20]. Though this process shows potential as a low-cost form of bio-oil upgrading, there is limited information available about the effect of rapid heating on bio-oil stability.

Pollard et al. [21] and Rover et al. [22] have demonstrated that bio-oil vapors can be selectively condensed/recovered according to boiling point. The net result is so-called stage fractions that concentrate anhydrosugars, phenolic monomers, light acids, and water. Fractionated bio-oils improve the prospects for producing value-added products from pyrolysis as well as present a unique opportunity to elucidate the impact of a given treatment on narrow groups of biomass degradation products.

The goal of the present study was to examine the effect of rapidly heating fractionated bio-oils to temperatures required for conventional thermal processes, such as distillation and hydrotreating. An experimental method was developed to explore the effect of both maximum temperature and short-term heating duration. Fractionated bio-oils from fast pyrolysis were tested to better understand bio-oil instability.

Materials and Methods

Fractionated bio-oil production

Bio-oil fractions were produced from southern yellow pine sawmill residue. As-received biomass was dried to approximately 4 wt% moisture and then passed through a 3.18

mm square weave sieve. Only the particles that passed through the sieve were retained for use.

Bio-oils used in this study were produced in a 15.4 cm diameter fluidized bed operated at 500 °C. The biomass feed rate into the reactor was approximately 6.2 kg hr^{-1}, with a N_2 gas fluidization rate of 114.4 SLPM. Char and biomass decomposition products that elutriated from the bed were collected with a staged bio-oil recovery system [21]. A pair of cyclones heated to 450 °C continuously removed char from the vapor stream. The liquid recovery system consisted of multiple pairs of a shell and tube heat exchanger and electrostatic precipitator (ESP) operated at consecutively lower temperatures. The heat exchangers were designed to lower the gas stream temperature to just below the dew point of target molecules to encourage their condensation. Similarly, the ESPs were operated at or slightly above the target dew point to avoid further condensation. The ESPs collected any liquid aerosols entrained in the gas stream by imparting a negative charge to the liquid droplets and then impinging them on the positively charged wall of the tube. The method of collection and operating parameters of each stage can be found in Table 1. Additional details about the pyrolysis reactor and collection system are found in Pollard et al. [21] and Rover et al. [22].

Table 1. Fractionated bio-oil collection parameters for the fast pyrolysis process development unit.

Collection Designation	Collection Type	Collection Temperature (°C)	Collection Pressure (bar)
SF-1	Condenser	102	1
SF-2	ESP	129	1
SF-3	Condenser	77	1
SF-4	ESP	77	1
SF-5	Condenser	18	1
SF-6	ESP	18	1

The bio-oil recovery system yielded bio-oil fractions with unique physical and chemical properties. A breakdown of the primary components of each stage fraction is depicted in Figure 1. The heavy fractions, SF-1 and SF-2, contained a large percentage of non-volatile compounds, which consist of pyrolytic lignin [23] and anhydro-monosaccharides [24]. These compounds, which are semi-solid at ambient temperatures, contribute to the high viscosity of the heavy fractions. Conversely, the remaining fractions have a significantly increased volatile content over SF-1 and SF-2 due to the presence of water, acids, furans, phenolic monomers and monosaccharides. Mass concentration of the eight most prevalent volatile organic compounds identified in the bio-oil fractions are outlined in Table 2. SF-3 and SF-4 have the highest proportion of furans and phenolic monomers. SF-5 and SF-6 each contain a substantial amount of acetic acid as shown in Table 2 and water as indicated by Figure 1.

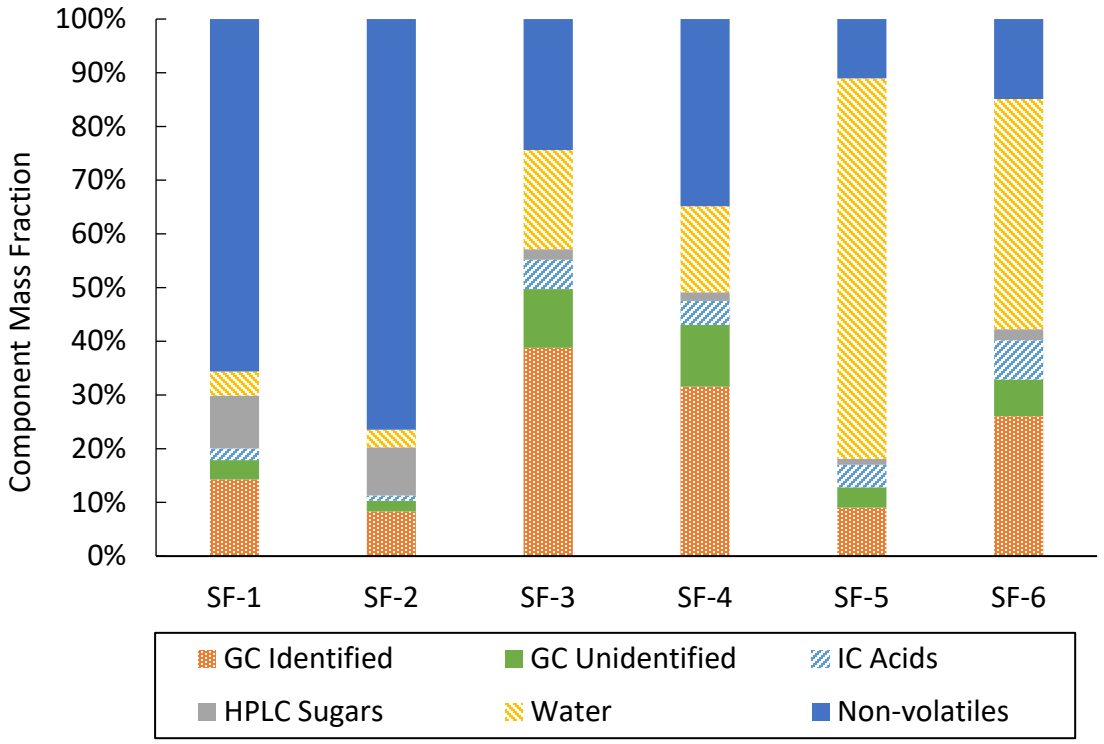

Figure 1. Mass fraction of the primary components of each bio-oil stage fraction recovered from the staged recovery system.

Table 2. Mass concentration of eight most prevalent volatile organic compounds found in fractionated bio-oil samples.

Compound	SF-1	SF-2	SF-3	SF-4	SF-5	SF-6
Levoglucosan	7.10±0.04	5.75±0.20	0.70±0.10	0.78±0.06	0.35±0.05	0.76±0.04
Acetic Acid	0.70±0.01	0.32±0.01	3.48±0.01	2.41±0.01	3.32±0.04	5.56±0.02
Glycolaldehyde	0.50±0.01	0.00±0.00	10.23±0.38	5.14±0.30	0.72±0.01	2.31±0.14
Acetol	0.64±0.01	0.39±0.01	2.73±0.05	2.24±0.07	2.63±0.01	4.47±0.02
Furfural	0.30±0.01	0.21±0.01	1.05±0.04	0.83±0.01	0.83±0.01	2.35±0.01
Guaiacol	0.50±0.01	0.28±0.01	1.36±0.02	1.22±0.01	0.22±0.01	1.11±0.01
Creosol	0.92±0.01	0.52±0.01	1.84±0.02	2.04±0.01	0.18±0.01	1.08±0.01
Isoeugenol	1.21±0.01	0.76±0.01	0.69±0.01	1.58±0.02	0.01±0.01	0.05±0.01

Fractionated bio-oil thermal processing

Thermal processing was conducted by placing 10 g of fractionated bio-oil in a small vessel made from a 15 cm long section of 1.3 cm diameter 316 stainless steel tubing. One end of the tubing was swaged with a solid metal cap while the other end was swaged with a union that allowed for a 3.2 mm diameter Type K thermocouple (KQIN-18U-12, Omega Engineering, Stamford, CT) to be inserted into the middle of the vessel, as depicted in Figure 2. The thermocouple was used to accurately monitor and record the temperature of the liquid sample during the heating process. When sealed, the total internal volume of the vessel was 13.5 mL. Although the densities of the fractionated bio-oil samples varied slightly, the liquid sample occupied 75% of the vessel volume at most, ensuring that any gas produced during thermal processing would have room for expansion.

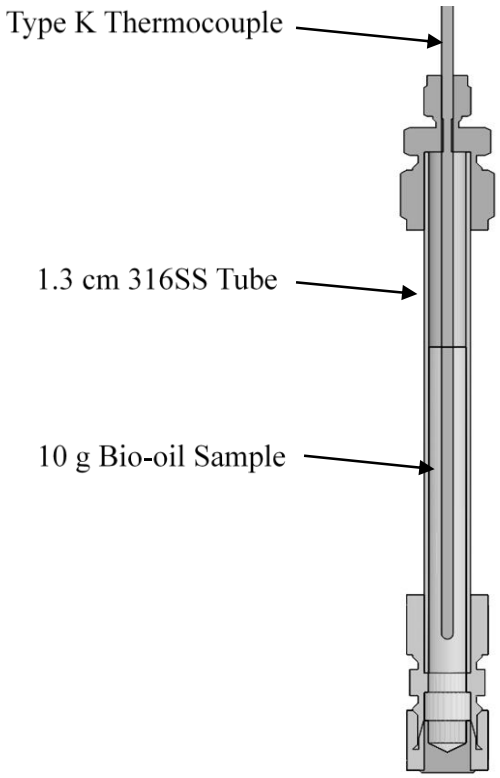

Figure 2. Vessel configuration used for fractionated bio-oil thermal processing.

After a sample was loaded into the thermal processing vessel, the whole assembly was submerged into a fluidized sand bath (Techne IFB51, Bibby Scientific Limited, Staffordshire, UK) which was preheated to a set temperature according to the desired heating rate and final sample temperature. The fluidization rate for the sand bath was determined according to the manufacturer's specifications. The bath temperature was determined by calculating the environmental temperature required to heat the sample vessel and its contents to the desired final sample temperature in the desired amount of time. The final sample temperatures were set to 100, 200, and 300 °C. Two separate heating times were established at 60 and 120 s as a close approximation to the expected heating rates for an industrial heat

exchanger. The internal sample temperature was closely monitored throughout the heating process, and upon reaching the desired final temperature, the sample vessel was quickly removed from the heating bath and immediately submerged in an ice bath. To illustrate the performance of the heating and quenching process, a sample thermal profile can be seen in Figure 3.

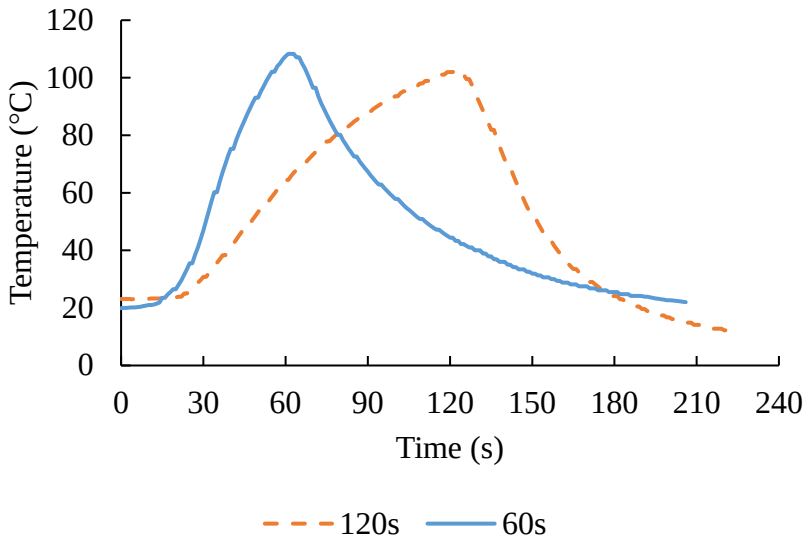

Figure 3. Sample thermal profiles recorded for thermal processing to 100 °C showing the rapid heating of the sample and subsequent ice bath quench after reaching the desired final sample temperature.

After a sample was heated and quenched, the outside of the vessel was blown with compressed air to remove any foreign debris and the top cap was loosened to relieve internal pressure. The whole assembly was weighed on an analytical balance (EOB120, Ohaus Corporation, Parsippany, NJ) to determine any change in mass attributed to the production of gaseous species due to thermal processing. Following this process, no significant mass loss was observed due to the production of gas for any of the samples tested. Finally, the bio-oil

samples were poured from the vessel into a polypropylene sample tube, and returned to a 5 °C cooler for subsequent analysis.

Analytical methods

Initial viscosity was measured with a Brookfield Viscometer DV-II+Pro rotational viscometer calibrated using Brookfield Viscosity standard 500 silicone (Brookfield Engineering Laboratories, Inc., Middleboro, MA). The bio-oils were analyzed using a constant temperature water bath at 60.0 ± 0.1 °C. SF-1 and SF-2 bio-oils were measured using a SC4-15 spindle, while all other bio-oils were measured using a YULA-15Z spindle in conjunction with the ULA chamber due to the low viscosities of these samples.

To determine the relative molecular weight (RMW) of the thermally processed bio-oil samples, gel permeation chromatography (GPC) was carried out using a Dionex Ultimate 3000 (Sunnyvale, CA) high performance liquid chromatography system equipped with a Shodex Refractive Index and Diode Array Detector. The eluent for the bio-oils was tetrahydrofuran (THF) with two Agilent PLgel 3 μm 100 Å 300 × 7.5 mm columns and one Mesopore 300 × 7.5 mm column. The column flow rate and temperature was 1.0 mL min^{-1} at 25 °C. The samples were prepared by diluting 0.02 g of bio-oil sample into 10 mL of THF. All samples were filtered with a Whatman 0.45 μm Glass Microfiber syringe filter prior to analysis. The GPC standards were purchased from Agilent (Agilent Technologies, Inc., Santa Clara, CA). Standards used for the bio-oil calibration curve ranged from 162 to 3790 g mol^{-1}. The polystyrene standards were diluted with JT Baker GPC grade Stabilized THF. Samples were analyzed in duplicates.

Analysis of the moisture content was conducted with a MKS 500 Karl Fischer Moisture Titrator (Kyoto Electronics Manufacturing Co., LTD, Kyoto, Japan) according to ASTM E203: Standard Test Method for Water Using Karl Fischer Reagent. The titrant was Hydranal Composite 5K and the solvent was Hydranal Working Medium K. Samples were analyzed a minimum of four times.

Total acid number (TAN) is a general indicator of the acidity of bio-oil, and is measured by the milligrams of potassium hydroxide required to neutralize the acids in a gram of oil. For bio-oils this includes the cumulative effect of mineral acids, carboxylic acids, and phenolics [21]. Tests were conducted on a 798 MPT Titrino (Metrohm AG, Herisau, Switzerland) autotitrator with 0.1 N potassium hydroxide in 2-propanol as the titrant (REATI91457, Metrohm AG, Herisau, Switzerland). The solvent was a mixture of 50 wt% reagent grade toluene, 49.5 wt% reagent grade 2-propanol, and 0.5 wt% 18.2 MΩ de-ionized water. A TAN standard was purchased from Fisher Scientific (Hanover Park, IL) and was used to verify calibration of the instrument. A minimum of three tests were performed for each sample.

Characterization of the organic acids was accomplished by Ion Chromatography (IC). This method was able to quantify the individual concentration of acetic acid, formic acid, glycolic acid, and propionic acid. Characterization was achieved by a Dionex® ICS3000 (Sunnyvale, CA) equipped with a conductivity detector and an Anion Micromembrane Suppressor AMMS-ICE300®. Tetrabutylammonium hydroxide in water at a 5 mM concentration was used as the suppressor regenerate at a flow rate of 4-5 mL min^{-1}. The mobile phase was a mixture of 1.0 mM heptaflourobutyric acid in water at a flow rate of

0.120 mL min^{-1} at 19 °C. The columns included a guard column in series with an IonPac® ICE-AS1 4x250 mm analytical column. A five-point linear calibration of acetate, propionate, formate, and glycolate standards with distilled water was conducted within a concentration range of 0-200 mg/L. Approximately 100 mg of a bio-oil sample was dissolved in 1.5 mL of methanol and 6 mL of distilled water. Each sample mixed thoroughly on a vortex mixer and then filtered through a Whatman® 0.45 μm glass microfiber filter before injection into the IC. Samples that resulted above the calibrated concentration range were diluted with up to 45 mL of distilled water to adjust the sample acid concentration to within the calibrated range.

Structural changes in the fractionated bio-oils were observed using a Thermo Scientific Nicolet iS10 Fourier transform infrared (FTIR) spectrometer (Thermo Fisher Scientific Inc., Waltham, MA). Analysis of each sample was preceded by background collection. Each sample was scanned 32 times with a resolution of 4 wavenumbers and attenuated reflectance correction. Sample spectra were analyzed and exported with the OMNIC Software operating system that accompanied the spectrometer.

Due to the relatively small sample size used in these experiments, viscosities of thermally treated samples were not explicitly measured. Furthermore, for the case of the high molecular weight bio-oil fractions (SF-1 and SF-2), the temperature of the sample must be raised to around 40-60 °C for several minutes to properly analyze the viscosity. This kind of additional thermal treatment would have been counterproductive for the purposes of this study. It is worth noting that upon pouring the bio-oil fractions out of the sample vessel an increase in fluid viscosity was palpable for the high molecular weight samples exposed to

either the 200 or 300 °C case, regardless of heating duration. For reference purposes, the initial viscosity of the bio-oil fractions was measured. This data can be seen in Table 3.

An increase in average molecular weight of bio-oil due to ageing has been shown to be directly correlated with an increase in the viscosity [4, 6]. Similar increases in molecular weight were also observed for the case of rapid thermal processing conducted in this study, as shown in Figure 4. This and all subsequent metrics are presented as percent change from the initial value, according to the following equation:

$$\% \, \Delta P = \frac{P_{final} - P_{initial}}{P_{initial}}$$

where P_{final} refers to the measured value of a particular sample property after thermal processing and $P_{initial}$ refers to the measured value of that property of the control sample. Thus, an increase in a given property over the value of the control sample results in a positive percent change, while a decrease results in a negative percent. Presentation of the data as relative change allows for the stability of the bio-oil fractions to be compared despite the wide range of initial properties, which varied considerably as seen in Table 3.

Table 3. Comparison of the initial elemental composition, moisture content, average relative molecular weight (RMW), and total acid number (TAN) of the selected bio-oil fractions.

Property	Unit	SF-1	SF-2	SF-3	SF-4	SF-5	SF-6
C (db)	wt%	61.7±0.1	64.5±0.1	55.4±0.1	60.0±0.1	41.5±0.1	52.9±0.3
H (db)	wt%	5.4±0.1	5.4±0.0	5.2±0.1	5.2±0.1	1.7±0.3	4.5±0.1
N (db)	wt%	0.2±0.0	0.2±0.0	0.7±0.1	0.6±0.0	1.6±0.1	0.9±0.1
S (db)	wt%	0.0±0.0	0.0±0.0	0.0±0.0	0.0±0.0	0.0±0.0	0.0±0.0
O* (db)	wt%	32.7±0.1	31.0±0.1	38.8±0.1	34.2±0.1	55.2±0.3	41.7±0.2
Moisture	wt%	4.5±0.2	3.3±0.3	18.5±0.3	16.0±0.4	70.8±0.9	42.9±0.5
Avg RMW	Da	455±1	435±1	136±2	232±1	113±1	104±1
TAN	$mg_{KOH}\ g^{-1}$	49.6±0.4	47.2±0.1	104±1	73.1±0.4	53.4±0.2	107±1
Viscosity	cP (60°C)	271±1	1610±10	4.65±0.01	6.66±0.01	0.98±0.01	1.51±0.01

* O determined by difference

db – dry basis; values are adjusted for moisture content

Uncertainties reflect the standard error of the mean.

Results and Discussion

All fractions of bio-oil demonstrated significant increases in average RMW across the heating ranges, as shown in Figure 4. SF-3 and SF-6 were the most unstable, with a maximum increase in average RMW of more than 200% for both heating times investigated. Interestingly, both of these samples also exhibited the highest initial TAN value, as seen in Table 3. This suggests that polymerization of the bio-oil is strongly acid-catalyzed. Organic acids such as acetic acid and formic acid have been found to be the most prominent in acid-catalyzed condensation reactions [12, 25, 26]. This is further evidenced by the relatively high initial concentration of organic acids in both SF-3 and SF-6, as shown in Table 4. Even in the

complete absence of organic acids, phenolics, which are weak acids, have been shown to auto-catalyze condensation reactions at temperatures in excess of 150 °C [26].

Table 4. Bio-oil fractions acid content (wt%) as identified by Ion Chromatography.

	SF-1	SF-2	SF-3	SF-4	SF-5	SF-6
Glycolic Acid	0.91±0.01	0.39±0.01	0.62±0.01	0.80±0.01	0.04±0.01	0.06±0.01
Formic Acid	0.46±0.01	0.21±0.01	0.98±0.01	0.93±0.01	0.49±0.01	0.99±0.01
Acetic Acid	0.70±0.01	0.32±0.01	3.48±0.01	2.41±0.01	3.32±0.04	5.56±0.02
Propanoic Acid	0.12±0.01	0.06±0.01	0.39±0.01	0.32±0.01	0.36±0.02	0.69±0.01
Total Acids	2.19±0.04	0.98±0.04	5.47±0.04	4.47±0.04	4.21±0.8	7.31±0.05

Uncertainties reflect the standard error of the mean

Figure 4 indicates a moderate dependence of polymerization on heating duration. For example, at 300 °C the change in RMW for SF-1 and SF-2 demonstrate a disparity of approximately 50% between the 60 and 120s heating duration. This suggests that very short durations are preferred when heating fractionated bio-oil to elevated temperatures. Similarly, Diebold et al. [27] demonstrated that the rate of ageing for hot-vapor-filtered bio-oil could be predicted as a function of storage temperature according to the following equation:

$$aging\ rate = 2.317 \cdot 10^{13} \cdot \exp\left(-\frac{9659}{T}\right)$$

where T represents the storage temperature in K, and the aging rate is defined as the increase in bio-oil viscosity in cP day^{-1}. This relationship, which was developed for whole bio-oil rather than fractionated bio-oil, predicts that bio-oil heat treated to 300 °C would age at a rate of approximately 768.6 cP min^{-1}, which for the bio-oil fractions SF-1 and SF-2 of the present

study would have resulted in semi-solid samples. These samples were readily removed as liquid from the heating vessel, indicating that the Diebold correlation over predicts the rate of aging for bio-oil fractions.

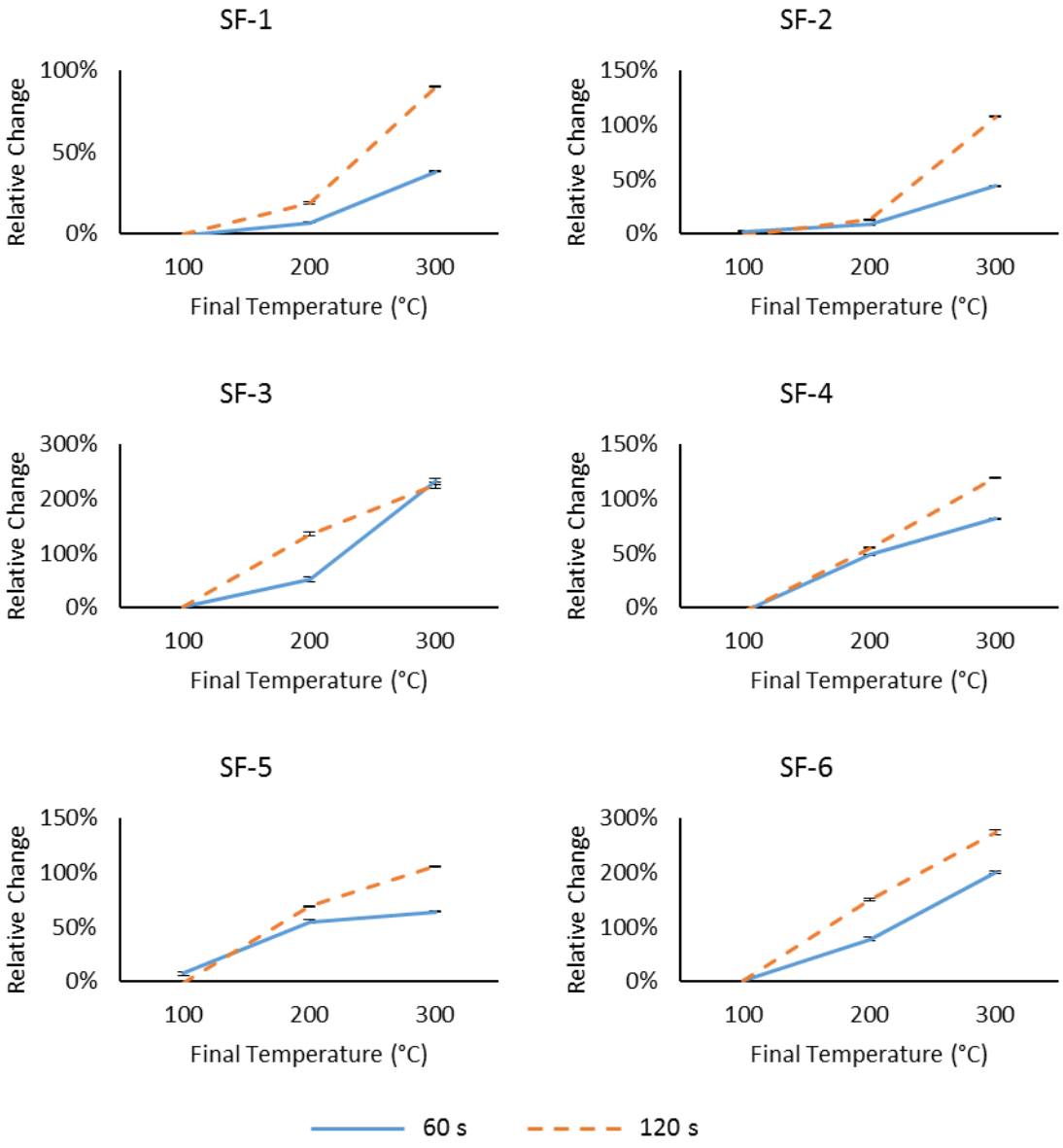

Figure 4. Relative change in the average RMW of pine bio-oil fractions produced from fast pyrolysis after thermal processing for 60 and 120 s. Error bars represent the standard error of the mean.

Despite SF-5 containing a relatively high concentration of organic acids, it should be less prone to polymerization since the high concentration of water in this fraction (70.8 wt%) is expected to dilute the light oxygenates that participate in polymerization reactions. A similar dilution effect for a variety of other solvents has been observed in the literature [10, 17, 27].

It should be noted that no phase separation was observed for any of the bio-oil fractions. At first this appears to be somewhat contradictory to the results obtained for the HPTT process where a single phase feed was converted to a viscous organic phase and a less viscous aqueous phase [19, 20]. However, this phenomenon can be explained by the nature of the fractionated bio-oil in this study versus the bulk phase bio-oil used for HPTT. In particular, the HPTT feed oil was reported to have an average moisture content of 23.0 wt%. In contrast, much of the moisture for bio-oil produced in the current study was isolated in SF-5, which had a moisture content of 70.8 wt%. Thus, the fractionated oil is less likely to phase separate after thermal processing due to its prior concentration into SF 5 [10].

Moisture content, as analyzed by Karl-Fisher titration, exhibited an unusual trend for the majority of the bio-oil samples. It can be seen in Figure 5 that many of the samples showed a slightly negative change in moisture after heating to 100 °C, but then trended towards increasing moisture content with increasing temperature. A possible explanation for this behavior is that water-consuming hydration and hydrolysis reactions dominate at lower temperatures but are then surpassed by condensation or esterification reactions that release water as temperature is increased. Hydration of aldehydes is known to readily occur at temperatures as low as 22 °C [28], so it is reasonable to expect this to occur through 100 °C.

Similarly, hydrolysis of levoglucosan and cellobiosan has been demonstrated at temperatures around 100 °C [29, 30], which would be further aided by the presence of the organic acids, as shown in Table 4.

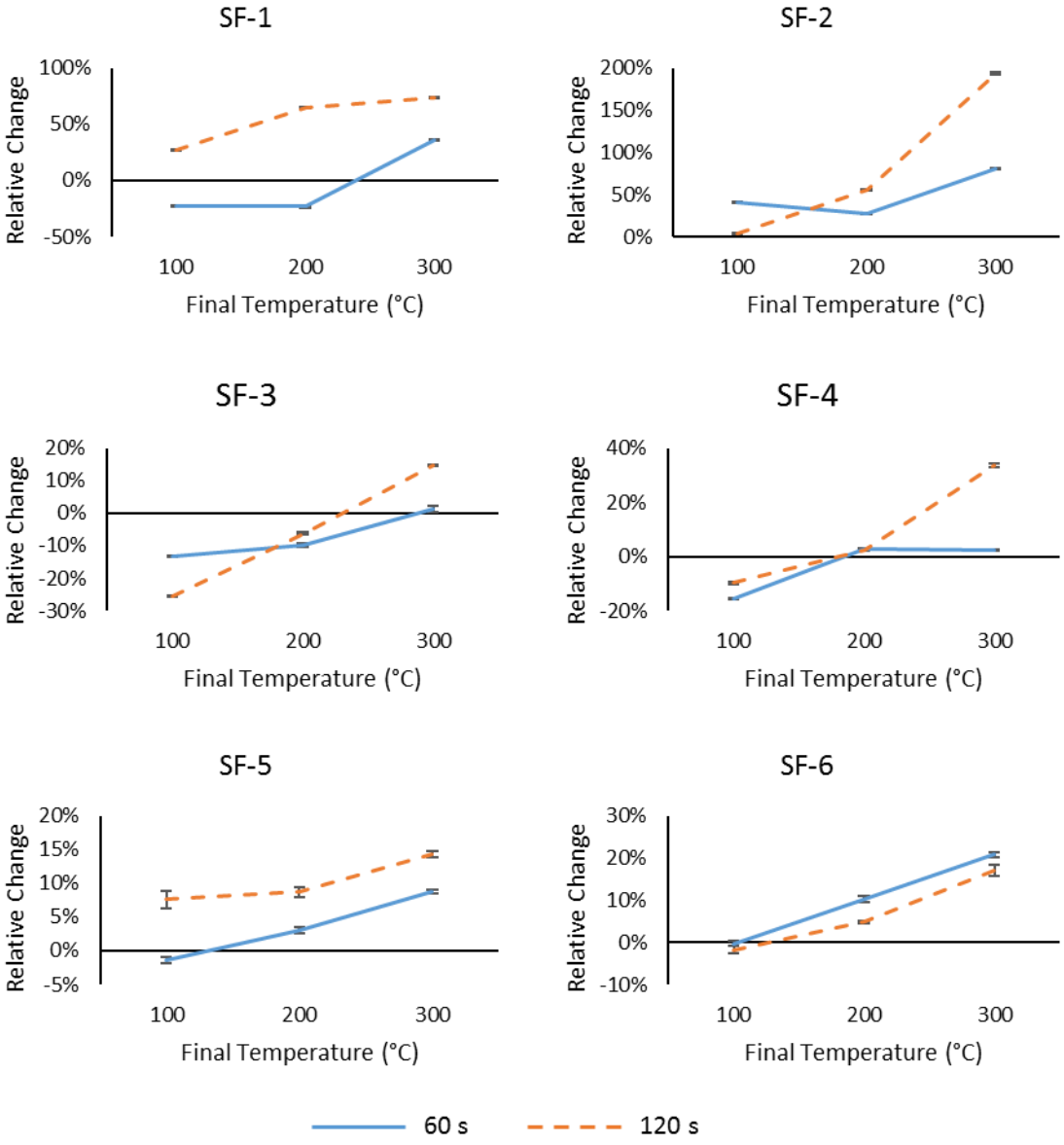

Figure 5. Relative change in the moisture content of pine bio-oil fractions produced from fast pyrolysis after thermal processing for 60 and 120 s. Error bars represent the standard error of the mean.

As previously indicated, TAN appears to be a strong predictor of condensation and polymerization reactions when bio-oil fractions are exposed to elevated temperatures. Figure 6 shows that the TAN of bio-oil fractions tends to increase as thermal processing temperature increases. This suggests that there is a net increase in the acidity of the samples, which could be due to a net increase in hydroxyls, aldehydes, and carboxylic acids. In a model compound study it has been shown that both acetic and formic acid increase in concentration with increasing temperature [26]. Such an increase in acidity would exacerbate their catalytic effect on polymerization and condensation reactions.

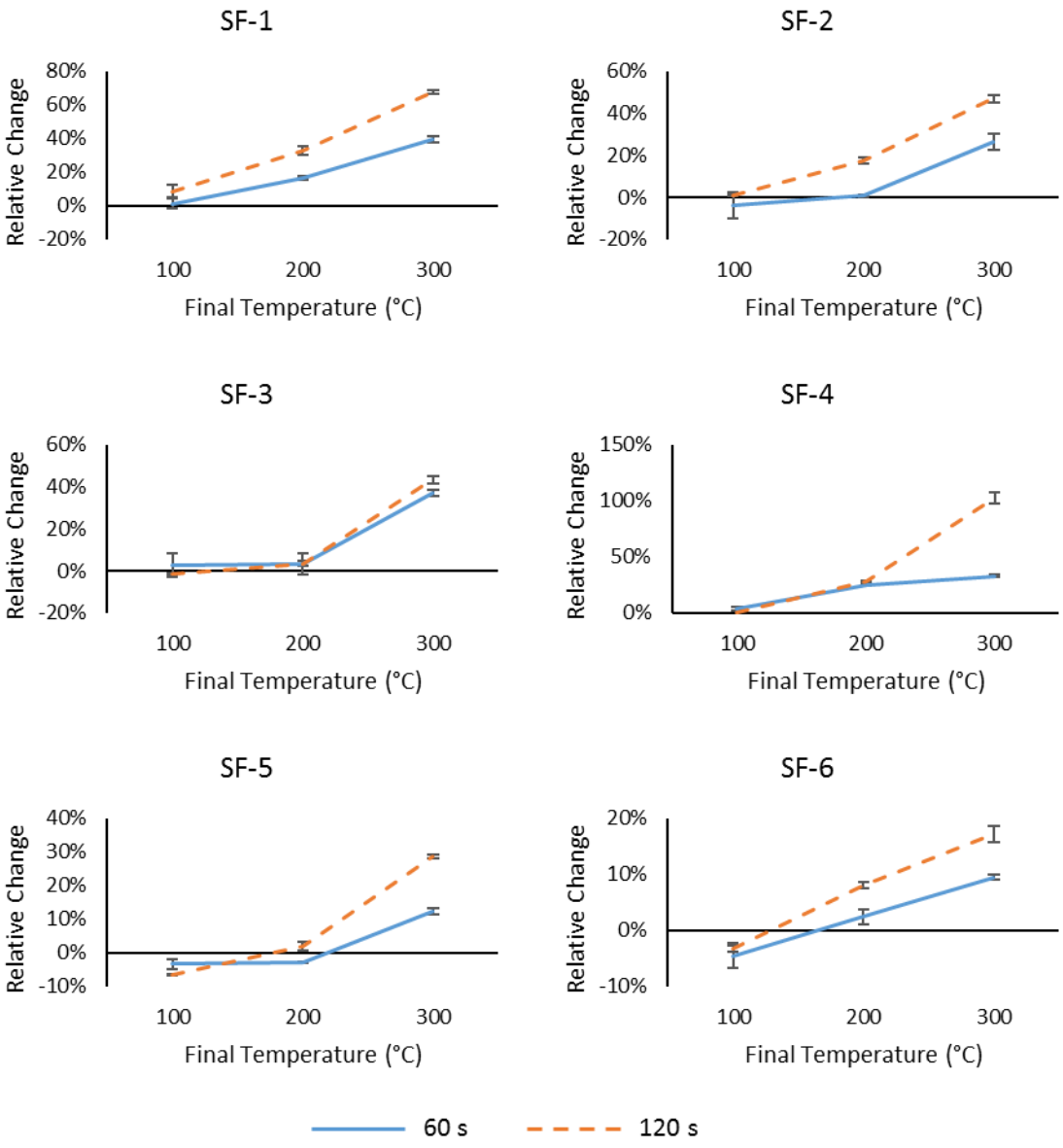

Figure 6. Relative change in the TAN of pine bio-oil fractions produced from fast pyrolysis after rapid thermal processing for 60 and 120 s. Error bars represent the standard error of the mean.

Changes in the chemical structure of the oil samples were examined via FTIR. The spectra for the SF-3 samples heated at the 120 s time scale are shown in Figure 7. Increases in –OH peak intensity (~3400 cm^{-1}) often associated with an increase in either hydroxyl

groups or moisture. Considering the observed increase in TAN and mixed results for moisture, it is most likely that the peak intensity is caused by an increased concentration of hydroxyl functionality. This combined with the sharp increase in the carbonyl peak (~1700 cm^{-1}) indicates the likely formation of carboxylic acids, which would again contribute to the observed increase in TAN. The substantial increase in the average RMW suggests that polymerization reactions could account for the increased alkane (~2930 cm^{-1}) peak intensity. However, the coincident increase in alkene (~1640 cm^{-1}) intensity indicates that polymerization was not entirely caused by unsaturated bonds. Instead, it is possible that polymerization occurred from condensation of furan derivatives, which is well understood to be acid-catalyzed [4]. Furan condensation reactions would also contribute to the significant reduction in ether stretching (~1030 cm^{-1}) [31].

Apart from the changes in peak intensities with increasing temperature discussed above, no significant functional changes occurred. This is in agreement with the literature, which indicates that instability reactions do not significantly alter bio-oil substituent functional groups.[32] Similar results were obtained for all of the bio-oil fractions analyzed.

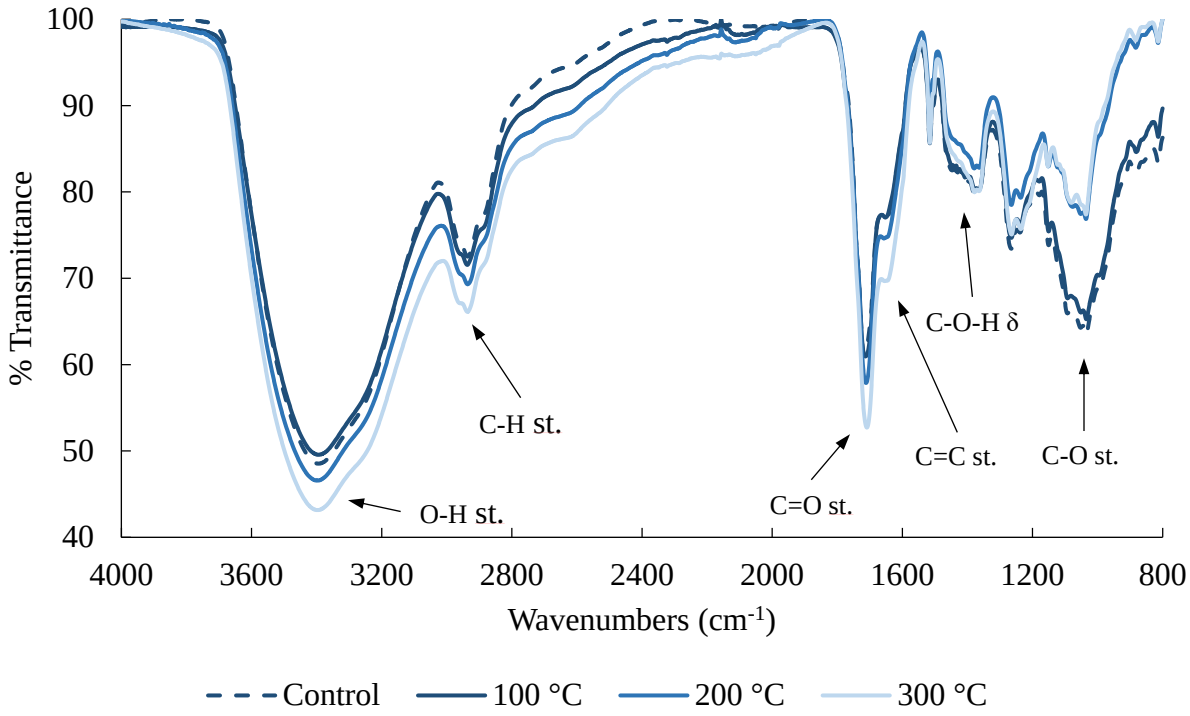

Figure 7. FTIR spectra for SF-3 control sample and samples thermally processed for 120 s.

Conclusions

This study demonstrated a method to simulate the rapid thermal treatment of bio-oil such as occurs during their upgrading to fuels and chemicals. Evaluation of the samples after thermal processing indicated a significant temperature dependence on instability reactions such as condensation and polymerization. A time-dependence was also observed for the heavy bio-oils that contain pyrolytic sugars and lignin-derived phenolic oligomers. These correlations were determined by comparison of the relative change in average RMW, moisture content, and TAN of the thermally processed bio-oil fractions.

Very little change was observed in any of the samples after thermal processing at 100 °C although higher temperatures increased both the average RMW and TAN significantly. These results suggest that thermal instability increases with increasing process temperature. Thus, development of low-temperature post-processing methods such as short path distillation [33, 34] and the recently proposed low-temperature low-pressure hydrogenation [35] will be important to successfully processing bio-oils.

Acknowledgements

Funding for this research was provided by the Gary and Donna Hoover Endowment in Mechanical Engineering at Iowa State University and the U.S. Department of Energy under contract #EE0005974. The authors would like to thank Tannon Daugaard for his expertise and assistance with IC determination of organic acids and Patrick Hall for his help with GPC.

References

1. Chen, D., et al., *Evaluation methods and research progresses in bio-oil storage stability.* Renewable and Sustainable Energy Reviews, 2014. **40**: p. 69-79.

2. Ortega, J.V., et al., *Physical and chemical characteristics of aging pyrolysis oils produced from hardwood and softwood feedstocks.* Journal of Analytical and Applied Pyrolysis, 2011. **91**(1): p. 190-198.

3. Oasmaa, A. and E. Kuoppala, *Fast Pyrolysis of Forestry Residue. 3. Storage Stability of Liquid Fuel.* Energy & Fuels, 2003. **17**(4): p. 1075-1084.

4. Diebold, J.P., *A review of the chemical and physical mechanisms of the storage stability of fast pyrolysis bio-oils.* 2000: Citeseer.

5. Elliott, D.C., et al., *Results of the IEA Round Robin on Viscosity and Aging of Fast Pyrolysis Bio-oils: Long-Term Tests and Repeatability.* Energy & Fuels, 2012. **26**(12): p. 7362-7366.

6. Czernik, S., D.K. Johnson, and S. Black, *Stability of wood fast pyrolysis oil.* Biomass and Bioenergy, 1994. **7**(1): p. 187-192.

7. Alsbou, E. and B. Helleur, *Accelerated Aging of Bio-oil from Fast Pyrolysis of Hardwood.* Energy & Fuels, 2014. **28**(5): p. 3224-3235.

8. Ba, T., et al., *Colloidal Properties of Bio-Oils Obtained by Vacuum Pyrolysis of Softwood Bark. Storage Stability.* Energy & Fuels, 2003. **18**(1): p. 188-201.

9. Ben, H. and A.J. Ragauskas, *In Situ NMR Characterization of Pyrolysis Oil during Accelerated Aging.* ChemSusChem, 2012. **5**(9): p. 1687-1693.

10. Boucher, M., et al., *Bio-oils obtained by vacuum pyrolysis of softwood bark as a liquid fuel for gas turbines. Part II: Stability and ageing of bio-oil and its blends with methanol and a pyrolytic aqueous phase.* Biomass and Bioenergy, 2000. **19**(5): p. 351-361.

11. Hilten, R.N. and K.C. Das, *Comparison of three accelerated aging procedures to assess bio-oil stability.* Fuel, 2010. **89**(10): p. 2741-2749.

12. Meng, J., et al., *Toward Understanding of Bio-Oil Aging: Accelerated Aging of Bio-Oil Fractions.* ACS Sustainable Chemistry & Engineering, 2014. **2**(8): p. 2011-2018.

13. Czernik, S. and A.V. Bridgwater, *Overview of Applications of Biomass Fast Pyrolysis Oil.* Energy & Fuels, 2004. **18**(2): p. 590-598.

14. Oasmaa, A. and S. Czernik, *Fuel Oil Quality of Biomass Pyrolysis OilsState of the Art for the End Users.* Energy & Fuels, 1999. **13**(4): p. 914-921.

15. Sharma, R.K. and N.N. Bakhshi, *Upgrading of wood-derived bio-oil over HZSM-5.* Bioresource Technology, 1991. **35**(1): p. 57-66.

16. Mohan, D., C.U. Pittman, and P.H. Steele, *Pyrolysis of wood/biomass for bio-oil: a critical review.* Energy & fuels, 2006. **20**(3): p. 848-889.

17. Adjaye, J.D., R.K. Sharma, and N.N. Bakhshi, *Characterization and stability analysis of wood-derived bio-oil.* Fuel Processing Technology, 1992. **31**(3): p. 241-256.

18. Elliott, D.C. and E.G. Baker, *Catalytic hydrotreating of biomass liquefaction products to produce hydrocarbon fuels: Interim report*, in *Other Information: Portions of this document are illegible in microfiche products. Original copy available until stock is exhausted*. 1986. p. Medium: ED.

19. Venderbosch, R.H., et al., *Stabilization of biomass-derived pyrolysis oils.* Journal of Chemical Technology & Biotechnology, 2010. **85**(5): p. 674-686.

20. Mercader, F.d.M., et al., *Pyrolysis oil upgrading by high pressure thermal treatment.* Fuel, 2010. **89**(10): p. 2829-2837.

21. Pollard, A.S., M.R. Rover, and R.C. Brown, *Characterization of bio-oil recovered as stage fractions with unique chemical and physical properties.* Journal of Analytical and Applied Pyrolysis, 2012. **93**(0): p. 129-138.

22. Rover, M.R., et al., *The effect of pyrolysis temperature on recovery of bio-oil as distinctive stage fractions.* Journal of Analytical and Applied Pyrolysis, 2014. **105**(0): p. 262-268.

23. Wang, Y., et al., *Separation and characterization of pyrolytic lignins from the heavy fraction of bio-oil by molecular distillation.* Separation and Purification Technology, 2015. **152**: p. 123-132.

24. Piskorz, J., et al., *Flash pyrolysis of cellulose for production of anhydro-oligomers.* Journal of Analytical and Applied Pyrolysis, 2000. **56**(2): p. 145-166.

25. Moens, L., et al., *Study of the Neutralization and Stabilization of a Mixed Hardwood Bio-Oil.* Energy & Fuels, 2009. **23**(5): p. 2695-2699.

26. Hu, X., et al., *Polymerization on heating up of bio-oil: A model compound study.* AIChE Journal, 2013. **59**(3): p. 888-900.

27. Diebold, J. and S. Czernik, *Additives To Lower and Stabilize the Viscosity of Pyrolysis Oils during Storage.* Energy & fuels, 1997. **11**(5): p. 1081-1091.

28. Sutton, H. and T. Downes, *Rate of hydration of formaldehyde in aqueous solution.* Journal of the Chemical Society, Chemical Communications, 1972(1): p. 1-2.

29. Helle, S., et al., *A kinetic model for production of glucose by hydrolysis of levoglucosan and cellobiosan from pyrolysis oil.* Carbohydrate Research, 2007. **342**(16): p. 2365-2370.

30. Bennett, N.M., S.S. Helle, and S.J.B. Duff, *Extraction and hydrolysis of levoglucosan from pyrolysis oil.* Bioresource Technology, 2009. **100**(23): p. 6059-6063.

31. Cheng, Y.-T. and G.W. Huber, *Production of targeted aromatics by using Diels-Alder classes of reactions with furans and olefins over ZSM-5.* Green Chemistry, 2012. **14**(11): p. 3114-3125.

32. Cordella, M., et al., *Yields and ageing of the liquids obtained by slow pyrolysis of sorghum, switchgrass and corn stalks.* Journal of Analytical and Applied Pyrolysis, 2013. **104**: p. 316-324.

33. Wang, S., et al., *Separation of bio-oil by molecular distillation.* Fuel Processing Technology, 2009. **90**(5): p. 738-745.

34. Guo, X., et al., *Properties of Bio-oil from Fast Pyrolysis of Rice Husk.* Chinese Journal of Chemical Engineering, 2011. **19**(1): p. 116-121.

35. Rover, M.R., et al., *Stabilization of bio-oils using low temperature, low pressure hydrogenation.* Fuel, 2015. **153**: p. 224-230.

CHAPTER 6

DEVELOPMENT AND APPLICATION OF ALTERNATIVE METHODS FOR DETERMINING THERMOPHYSICAL PROPERTIES OF PYROLYSIS LIQUIDS

A paper to be submitted to the Journal of Analytical and Applied Pyrolysis

Martin R. Haverly, Tannon J. Daugaard, Mark Mba Wright, Robert C. Brown*

Abstract

The purpose of this paper is to demonstrate the development of low-cost accessible methods of determining selected thermophysical properties of pyrolysis liquids for use in engineering design and process development. These methods are then demonstrated on, and data is reported for, pyrolysis liquids produced by a novel fractionating recovery system. Instead of consisting of a lignin-derived emulsion in an aqueous phase of carbohydrate-derived compounds, as exists for conventional bio-oil, these fractions are enriched in compounds according to boiling point, giving each fraction distinct thermophysical properties. Specific heat, thermal conductivity, viscosity, surface tension, and enthalpy of vaporization were measured for six unique stage fractions and a mixture of these fractions from the pyrolysis of southern yellow pine. In addition, detailed chemical characterization of each bio-oil fraction was conducted using high performance liquid chromatography (HPLC), ion chromatography (IC), Karl Fischer moisture titration, and gas chromatography (GC) with a Polyarc® reactor.

Introduction

Development of the biorenewable industry has grown substantially in recent years. Several fast pyrolysis demonstration facilities are now in operation, and the number of pilot scale units in operation continues to increase [1-4]. Similarly, development of bio-oil upgrading and processing technologies has also advanced [3, 5]. Design and development of downstream processing equipment such as condensers, electrostatic precipitators, heat exchangers, and pumps can be expensive in the absence of detailed thermophysical properties for the pyrolysis liquids.

To date, most efforts to determine the thermophysical and physicochemical properties of bio-oil have focused on using ASTM and ISO test methods to determine viscosity, thermal conductivity, specific heat and surface tension of bio-oil [6-9]. The most thorough of these investigations was conducted by Oasmaa and Peacocke [10]. Numerous attempts have been made to improve the quality of bio-oil for use as fuel by blending, upgrading, and other treatment methods [11-14]. Others have also evaluated the effect of processing conditions on selected chemical and physical properties of bio-oil [6, 15, 16].

There are numerous recognized standards for measuring important bio-oil properties for use as fuel oil [4]. However, many of these methods are costly, especially when certifications are unnecessary for engineering design purposes, and can take a considerable amount of time when analyzed at a certified testing facility. Accurate, cost effective, and convenient methods for evaluating bio-oil properties are sought for the design of safe and efficient processing plants.

This study examined fractionated bio-oil produced from the fast pyrolysis of southern yellow pine at 500 °C in a fluidized bed. The thermophysical properties selected for evaluation were isobaric heat capacity, thermal conductivity, viscosity, surface tension, and enthalpy of vaporization. These were selected because they are essential to specification of pumps, heat exchangers and other processing equipment commonly found in a pyrolysis plant. The primary goal of this study was to develop methods that can be economically configured in most laboratory environments to evaluate bio-oil properties for use in engineering design. A secondary goal of this project was then to demonstrate and report on the application of these methods for the evaluation of fractionated bio-oil.

Experimental Section

Bio-oil Production

Southern yellow pine was dried to a moisture content of approximately 4 wt% and ground to a maximum particle size of 3.18 mm (1/8 in). Data gathered from the proximate, ultimate and compositional analysis of the feedstock is shown in Table 1.

Table 1. Proximate, ultimate, and compositional analysis of southern yellow pine feedstock.

Proximate Analysis	**wt%**
Moisture	4.1
Volatile Matter (AF, MF)	86.6
Fixed Carbon (AF, MF)	13.4
Ash (MF)	0.6
Ultimate Analysis	**wt%**
C (AF, MF)	52.8
H (AF, MF)	5.3
N (AF, MF)	0.2
O * (AF, MF)	41.7
Compositional Analysis	**wt%**
Cellulose	39.4
Hemicellulose	31.8
Lignin	29.5

* O determined by difference

AF – ash free basis, MF – moisture free basis

The fluidized bed pyrolysis pilot plant shown in Figure 1 was used in this study to generate the bio-oil. Pine was fed at a rate of approximately 6.2 kg hr^{-1} into a 500 °C bubbling fluidized bed of silica sand. Nitrogen was used as the fluidizing gas. Following the reactor, char was separated from the process stream by two cyclones placed in series. The pilot plant also featured a novel bio-oil fractionation system that collected bio-oil according to dew points resulting in 6 individual stage fractions (SF). A more detailed explanation of

both the reactor and the bio-oil collection system can be found in studies by Pollard et al. [17] and Rover et al. [18].

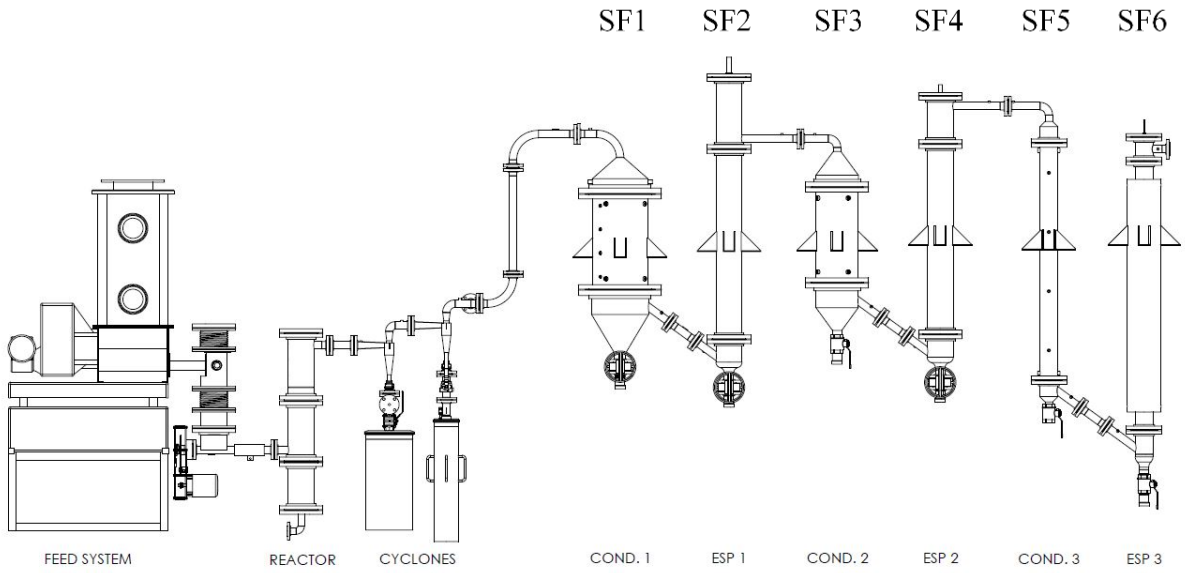

Figure 1. Schematic of the fluidized bed pyrolysis pilot plant feed system, reactor, cyclones, and bio-oil fractionation condensation system.

The yield of bio-oil on an ash-free (AF), moisture-free (MF) biomass basis was 64.5 wt%. Char and non-condensable gas (NCG) yields were 16.1 and 18.7 wt%, respectively. The distribution of bio-oil among the six stage fractions is shown in Figure 2. Mass closure for the system was 99.3%. To simulate unfractionated bio-oil produced from conventional bio-oil recovery systems, the six fractions were blended together to produce a “whole” bio-oil sample. The elemental composition, moisture content, and average molecular weight of the bio-oil fractions were also analyzed (Table 2).

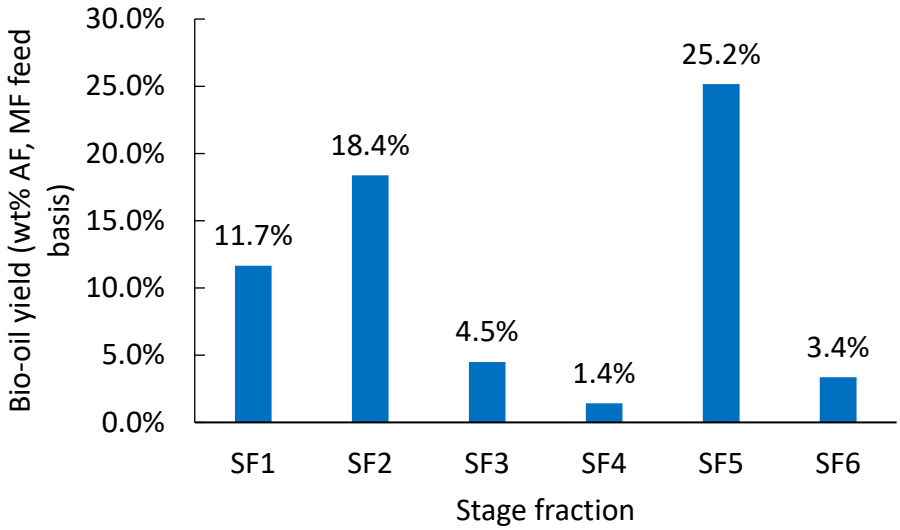

Figure 2. Yield of the six stage fractions of bio-oil on an ash-free moisture-free (AF, MF) biomass feed basis.

Table 2. Elemental composition, moisture content, and average molecular weight of the bio-oil fractions analyzed in this study.

	Elemental Analysis (wt% AF, MF)					Moisture Content	Average Molecular Weight
Bio-oil Fraction	**C**	**H**	**N**	**S**	**O***	**(wt%)**	**(Da)**
SF1	61.70	5.51	0.22	0.01	32.66	4.5	455.0
SF2	63.46	5.36	0.20	0.01	30.97	3.3	434.5
SF3	55.36	5.16	0.65	0.02	38.82	18.5	136
SF4	59.97	5.16	0.64	0.02	34.21	16.0	231.5
SF5	51.52	1.67	1.63	0.02	55.16	70.8	112.5
SF6	52.89	4.48	0.88	0.01	41.74	42.9	103.5
Whole	53.39	3.87	0.84	0.01	41.90	33.3	270.0

* O determined by difference

AF – ash-free, MF – moisture free

Analytical Methods

Like traditional (whole) bio-oil, the fractions produced for this study are mixtures prone to phase separation and settling [19]. To promote uniformity for all analyses conducted in this study, 1 L quantities of bio-oil were shaken vigorously prior to each test, and a sample was randomly taken from the mixture for analysis. The observed measurements indicate that the samples were representative of the overall mixture.

Isobaric Specific Heat

Isobaric specific heat was determined by monitoring the thermal equilibrium between known masses of bio-oil and a hot thermally-conductive material. A solid 99.99% copper rod with a diameter of 12.6 mm, length of 45.2 mm, and mass of 50.8 g was used as the hot mass for this experiment. Prior to each experiment, the copper rod was heated in a water bath held at precisely 90.0 °C. The copper rod was allowed to remain in the water bath until it reached a uniform temperature of 90.0 °C. Similarly, a known mass of bio-oil, usually about 75 g, was placed in an aluminum cup submerged in a water bath held at precisely 20.0 °C.

At the start of each test, an aluminum cup containing a pre-weighed bio-oil sample was quickly transferred to an insulated container such that there was an air gap surrounding the cup, as shown in Figure 3. The only contact the cup made with another surface was the minimal area at the top rim where the cup was supported by the insulated jacket. A 3.2 mm diameter platinum RTD probe was submerged in the bio-oil through a sealed hole in the insulated lid placed on top of the jacketed aluminum cup. Temperature measurements were recorded using a Measurement Computing USB-2404-UI data logger with 24-bit resolution

and a maximum sampling rate of 100 samples per second. Once the cup and RTD probe were in place, the copper rod was removed from the hot water bath, momentarily dried with a warm towel, and placed into the isolated bio-oil sample. The two bodies were then allowed to reach thermal equilibrium over the span of a few minutes while the temperature of the bio-oil was closely monitored with the data logger.

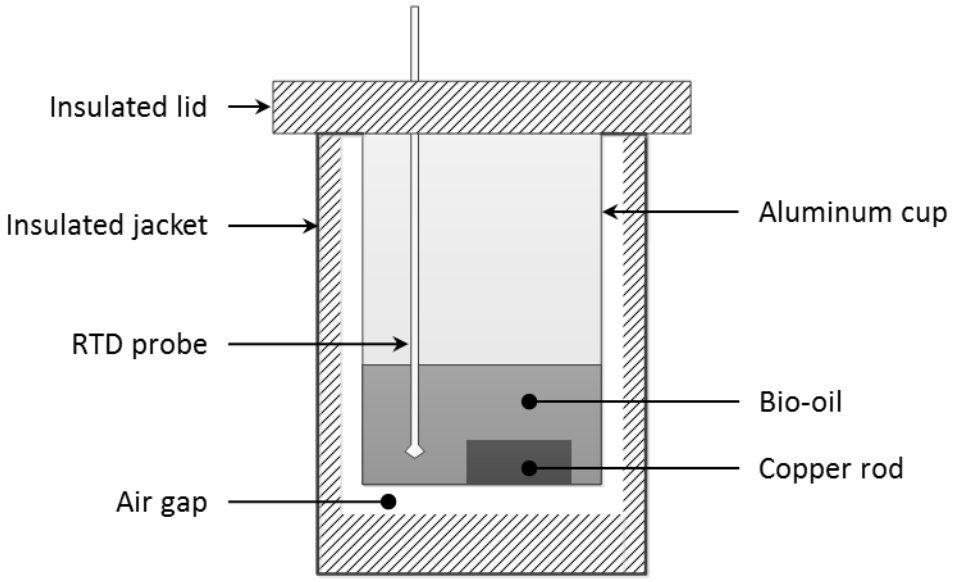

Figure 3. Depiction of the insulated test apparatus used to determine the isobaric specific heat of bio-oil fractions at standard pressure.

Thermal equilibrium was indicated by a plateau in the temperature rise of the bio-oil sample; typically less than 0.2% change in temperature after 2 minutes. After this point, the test was stopped. All wetted parts were then thoroughly washed with methanol and prepped for a repeat test with fresh bio-oil. A calibration procedure was conducted with de-ionized water before all bio-oil fractions were evaluated, each a minimum of 2 times.

The isobaric heat capacity of the bio-oil was determined according to the following equation:

$$C_{oil} = \frac{C_{copper} \cdot m_{rod} \cdot (T_H - T_{equil})}{m_{oil} \cdot (T_{equil} - T_C)}$$

where T_H = initial temperature of the copper rod (°C); T_C = initial temperature of the bio-oil sample (°C); T_{equil} = equilibrium temperature of the bio-oil and copper rod (°C); m_{oil} = mass of bio-oil sample (g); m_{rod} = mass of copper rod (g); C_{copper} = 0.385 J g^{-1} K^{-1} = isobaric heat capacity of copper at ambient temperature.

Thermal Conductivity

Thermal conductivity was determined via the transient hot wire (THW) method first proposed by Stalhane and Pyk [20]. The specific method employed in this study, however, was developed by Pittman [21]. This method is one of the most common experimental techniques to determine the thermal conductivity of a substance, particularly liquids [22]. The THW method relies on the principle of Joule heating, where heat is generated in a semiconductor from the application of a constant current. A thorough description of the operating principles and mathematical models for this method can be found elsewhere [21, 23, 24].

In the present study, a 99.99% copper wire with a diameter of 78.7x10^{-3} mm was used. Large copper wires were soldered to the ends of a known length (usually about 150.0 mm) of the thin wire such that the large wires did not impose significant resistance on the circuit. A four-wiring sensing technique was also used in this study to eliminate any influence of the resistance from the lead wires or contact points. Current was applied by a GW Laboratory GPS-3030D DC power supply capable of 0.02% load regulation. Voltage

drop across the THW corresponds to the change in temperature of the wire in the fluid being analyzed. This was monitored at a rate of 100 measurements per second with the Measurement Computing USB 2404-UI data logger described in the Specific Heat section above. Due to the resolution of this instrument, the voltage difference across the THW was measured directly without the use of a Wheatstone bridge, as is commonly used in these applications.

The THW was supported inside of a glass cylinder with a stainless steel arm so that it was held straight and taut. Approximately 200 mL of bio-oil was poured into the cylinder to submerge the wire as shown in Figure 4. The cylinder assembly was placed in a constant temperature water bath set to 60.0 °C and held there for a minimum of 15 minutes to allow the assembly to come up to temperature.

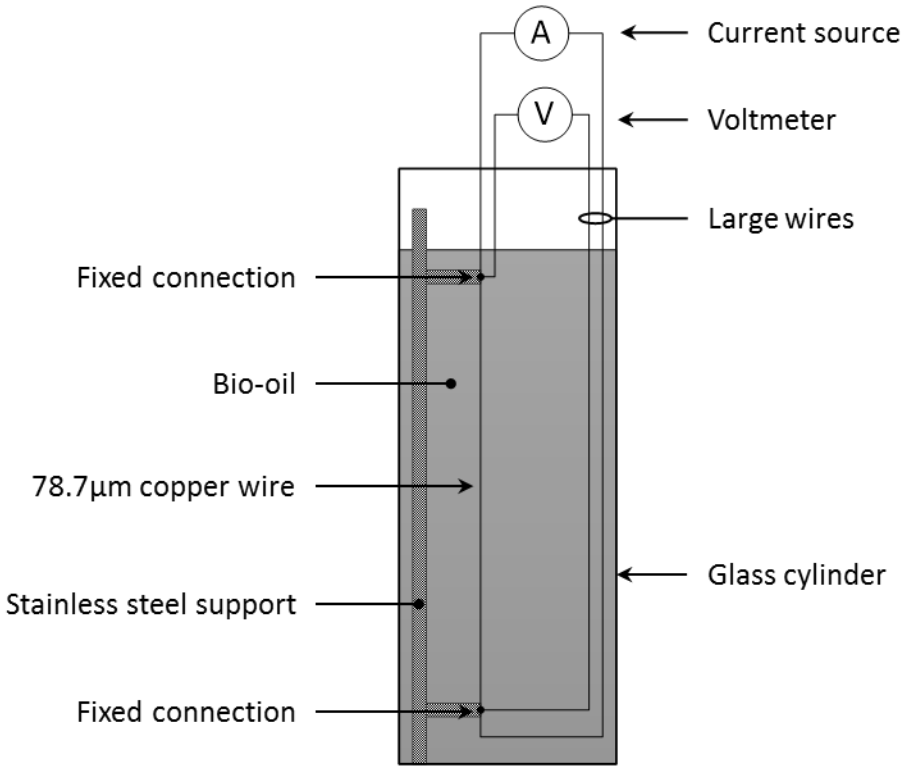

Figure 4. Thermal conductivity test apparatus that was placed in a hot water bath during analysis.

To determine thermal conductivity, a constant current load was applied to the THW. The voltage potential across the THW was monitored before the load was applied and until well after an equilibrium value was reached (usually about 8 seconds). After a test, the finite change in voltage with time, $\Delta V(t)$, is plotted against the natural log of time elapsed, $ln(t)$. The slope of this line can be used to determine the thermal conductivity coefficient, k, from the following equation [22]:

$$\frac{d(\Delta V(t))}{d(\ln(t))} = \frac{I^3 \cdot R_i^2 \cdot \sigma}{4 \cdot \pi \cdot L \cdot k}$$

where the first derivative on the left hand side of the equation is the slope, and the variables on the right hand side correspond to the following: I = constant supplied current (A); R_i = initial resistance of the THW (Ω); $\sigma = 0.003\ \Omega\ K^{-1}$ = resistance temperature coefficient of the THW; L = effective length of the THW (m). Reagent grade methanol was used to calibrate the apparatus. Each sample was analyzed at a minimum of four amperages, and the average of the thermal conductivity coefficient was reported.

Viscosity

Viscosity was determined using a Brookfield DV-II+ Pro rotational viscometer. A constant temperature water bath set to 60.0 °C was connected to pump through the heating jacket on the viscometer. All the bio-oil fractions were analyzed at this temperature. Due to the high initial viscosity of SF1 and SF2, these bio-oils were analyzed using a SC4-15 spindle. All other samples were analyzed using a YULA-15Z spindle with the ULA chamber.

For each test, bio-oil was placed in the chamber and the spindle was submerged. The viscometer was then turned on to the desired rotational velocity (approximately 20 rpm for the SC4-15 spindle, and 80 rpm for the YULA-15Z spindle). With the heating water flowing and the spindle turning, the sample was allowed to equilibrate for 10 minutes prior to taking any measurements. After 10 minutes the fluid viscosity was recorded every 30 seconds for a duration of 180 seconds. This procedure was done a minimum of two times for each sample.

Surface Tension

Surface tension was determined from measuring the capillary action of bio-oil in a very narrow glass tube. To conduct this test, a tensiometer was purchased from Cole-Parmer.

The capillary tube included in this apparatus was a 250 mm tall borosilicate glass cylinder with 1 mm graduations engraved up to 100 mm from the bottom and a 0.5 mm hole through the center. The apparatus also included an outer glass cylinder with a large opening at the top and a port on the side that could accommodate a pipette bulb. After a given amount of bio-oil was added to the outer tube (usually about 20 mL), the capillary tube was inserted into a rubber stopper that was then inserted into the outer glass cylinder, as depicted in Figure 5. Vacuum grease was applied to rubber-glass interfaces to ensure a tight seal.

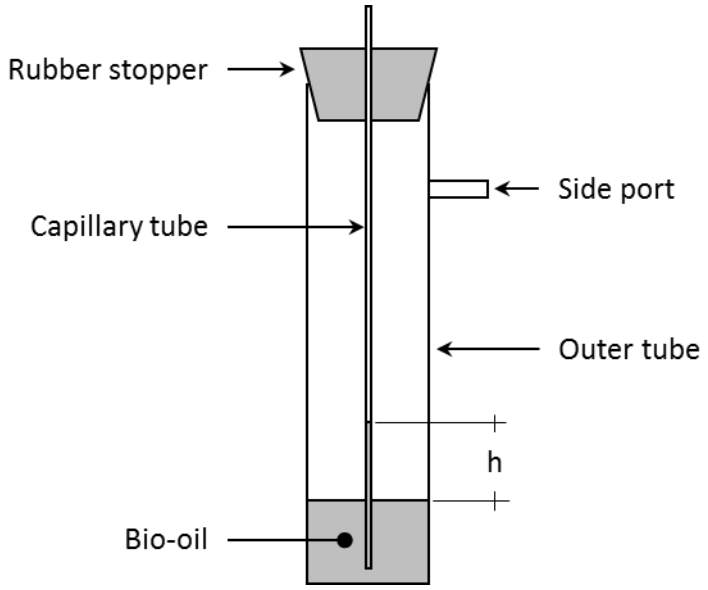

Figure 5. Test apparatus used to determine the surface tension of bio-oil. The height of capillary rise, h, was measured a minimum of four times for each sample.

The calculations to determine the surface tension of a substance using this method are relatively straightforward. However, the accuracy of the results is highly dependent upon the quality of the apparatus. Thus, several precautionary steps were taken to verify the quality of the apparatus used in this study. Firstly, all glass parts were sequentially rinsed with 5M

hydrochloric acid, 18.2 MΩ de-ionized water, reagent-grade methanol, and again with de-ionized water. This process was repeated prior to each individual test using this apparatus. Second, the diameter of the capillary tube was verified using pure benzene at 46 °C and ambient pressure. Using values for the surface tension and density of benzene provided by the apparatus manufacturer, the diameter was calculated to be 0.482 mm. This value was used in all subsequent calculations.

To determine the surface tension, approximately 20 mL of bio-oil was poured into the washed and dried outer tube. The capillary tube was then inserted into the rubber stopper, and placed so that the bottom of the capillary tube was below the liquid level. A pipette bulb was then used to expel air from the outer tube until the bio-oil sample rose out of the top of the capillary tube. The goal of this was to wet the tube with the sample. The bulb was then removed; the liquid inside the capillary was allowed to come to equilibrium, and the distance between the meniscus and the top of the liquid pool was measured. This was then repeated at least twice. Next, the pipette bulb was used to force air into the outer tube; the meniscus was allowed to return to equilibrium, and the distance between the liquid heights was measured. This was repeated a minimum of two times. The average of all of the readings was then used in the following equation to calculate the surface tension:

$$\gamma = \frac{1}{2} \cdot (h + \frac{r}{3}) \cdot r \cdot \rho \cdot G$$

where h = the distance between the meniscus and the top of the liquid pool (cm); r = inner radius of the capillary tube as determined experimentally using benzene (cm); ρ = density of the liquid sample (g mL^{-1}); G = 980.308 (m s^{-1} s^{-1}) = gravitational constant adjusted for

elevation. This equation assumes that the contact angle between the wall and the meniscus is 0°.

Enthalpy of Vaporization

The total enthalpy of vaporization of a mixture is equal to the sum of its parts as defined by the following equation:

$$H_{vap} = \sum x_i H_i$$

where x_i = mass fraction of pure species i in the mixture; H_i = enthalpy of vaporization of the pure species i (J kg^{-1}). Therefore, to accurately determine enthalpy of vaporization a thorough characterization of the chemical compounds present in the bio-oil was required. Enthalpy of vaporization values for the pure species were taken from RSC ChemSpider [25].

Quantification in this work was adapted from Choi et al. [26]. Water content was measured using Karl Fischer titration. Water soluble sugars and organic acids were quantified using High Performance Liquid Chromatography (HPLC) and Ion Chromatography (IC), respectively. Remaining volatile compounds were identified and quantified using gas chromatography (GC). Each bio-oil stage fraction was analyzed individually. Each of these chemical analyses is detailed below. The analyses for each bio-oil fraction were combined for reporting results for whole bio-oil.

Moisture Analysis

Water content in the bio-oil was measured using a Karl Fischer MKS-500® moisture titrator with Hydranal Composite 5K ® as the titrant. The solvent used was Hydranal Working Medium K®. Deionized water was used to calibrate the titrator before analysis. A minimum of 4 measurements were taken.

Water Soluble Sugars (WSS)

High Performance Liquid Chromatography was used to quantify cellobiosan, levoglucosan, galactose, maltose and xylose via a water wash method. Standards of levoglucosan, cellobiosan, and maltosan were obtained from Carbosynth. Xylose and galactose standards were purchased from Thermo Fisher Scientific. Complete WSS analysis procedure details are outlined by Choi et al. [26].

Ion Chromatography (IC Acids)

Ion Chromatography was used to analyze organic acids which included acetic acid, formic acid, glycolic acid and propanoic acid. Refer to Choi et al. for specific IC Acids methodology [26]. Approximately 100 mg of a bio-oil sample was dissolved in 1.5 mL of methanol and 6 mL of distilled water. Analyzed samples above the calibrated concentration range were diluted with up to 45 mL of distilled water, as opposed to the original 6 mL, to adjust the sample acid concentration into the calibrated range.

Gas Chromatography-Flame Ionization Detection (GC/FID)

Identification and quantification of volatile compounds in the bio-oil was done using gas chromatography as adapted from Choi et al [26]. Identification of compounds was first completed using an Agilent® 5977A GC/MSD coupled with an Agilent® 7890B GC. The mass spectrometer operated with electron impact ionization at a source temperature of 280 °C. Mass-to-charge ratio values (m/z) were recorded over a range of 35-650 m/z at a rate of 2 seconds per scan. Recorded peaks were identified using the 2008 NIST library. Identified peaks were confirmed through GC injection of commercially available pure compounds. GC-identifiable compound quantification was done using a Bruker® 430-GC equipped with a Varian® CP-8400 liquid autosampler and Galaxy® interface software. The capillary column used was a 60 m Phenomenex ZB-1701® with an inner diameter of 0.25 mm and a film thickness of 0.25 μm. The column is coated with 14% cyanopropylphenyl and 86% dimethylpolysiloxane. The GC injector operated isothermally at 280 °C with a split ratio of 20. A constant flow rate of 2 ml min^{-1} of ultra-high purity helium was used for the carrier gas. The oven temperature was programmed to hold at 35 °C for 3 minutes, followed by ramping at 5 °C min^{-1} to 300 °C and held there for 4 minutes.

Prior to quantification, a 4-point calibration of each identified compound was completed using pure compound diluted with methanol. Phenanthrene was also added as an internal standard. The calibration curves were produced using the relative areas from the integration of each compound and phenanthrene peaks. Correlations having R^2 values > 0.98 were obtained for the majority of the pure compounds. Commercially unavailable compounds were quantified using the FID relative response factor method. Each bio-oil

sample was quantified by mixing at approximately 15 wt% in a solution of methanol and phenanthrene. One µL of each diluted sample was injected on the GC following filtration through a Whatman® 0.45 micron glass microfiber filter.

Unidentifiable GC compounds were quantified using a Polyarc® reactor (Activated Research Company) coupled with a Bruker® 430-GC. The Polyarc® reactor is a catalytic microreactor that converts organic compounds leaving the GC column to methane molecules prior to detection in the FID. It is designed to quantify compounds using an internal standard with a response factor of one thus eliminating the need for calibrations. Conversion to methane is said to be greater than 99.9% from the manufacturer. More insight on the Polyarc® reactor can be found in a study by Beach et al [27].

The GC-FID with Polyarc® operating conditions and temperature programming was the same as outlined previously. Each bio-oil sample was filtered and injected into the GC at approximately 15 wt% in a solution of methanol and phenanthrene. Total GC volatiles were calculated using a response factor (RF = 1) and a ratio of the concentration and area of an internal standard (phenanthrene) with the total area of volatile compounds. The percent of GC unidentifiable compounds was then calculated from a balance of the total GC volatile compounds and the quantified GC identifiable compounds, which were commercially available as discussed previously.

Results and Discussion

Isobaric Specific Heat

The isobaric specific heat was determined from an initial fluid temperature of 25 °C at ambient pressure. A summary of the values calculated from the equilibrium temperature of the bio-oil and the copper rod is shown in Table 3.

Table 3. Summary of isobaric specific heat values at standard pressure. Uncertainty reflects the standard error of the mean.

Bio-oil Fraction	**C_p (J g^{-1} K^{-1})**
SF1	2.425 ± 0.138
SF2	2.180 ± 0.156
SF3	3.085 ± 0.018
SF4	2.875 ± 0.110
SF5	3.560 ± 0.014
SF6	3.400 ± 0.311
Whole	3.552 ± 0.046

A calibration test was conducted with de-ionized water prior to evaluation of the bio-oil samples. The value determined from these calibration tests was 4.211 ± 0.089 J g-1 K-1, which was deemed in an acceptable range of the accepted value of 4.18 J g^{-1} K^{-1} [28].

From the data, it is clear that the fractions with the highest moisture content, SF5 and SF6, had the highest isobaric specific heat, approaching that of pure water. As demonstrated by Figure 6, a linear correlation existed between the isobaric specific heat and the logarithm of the moisture content. The correlation held through pure water (100% moisture), and was

used to predict the isobaric specific heat of dry bio-oil (0% moisture) which was approximately 1.66 J g^{-1} K^{-1}.

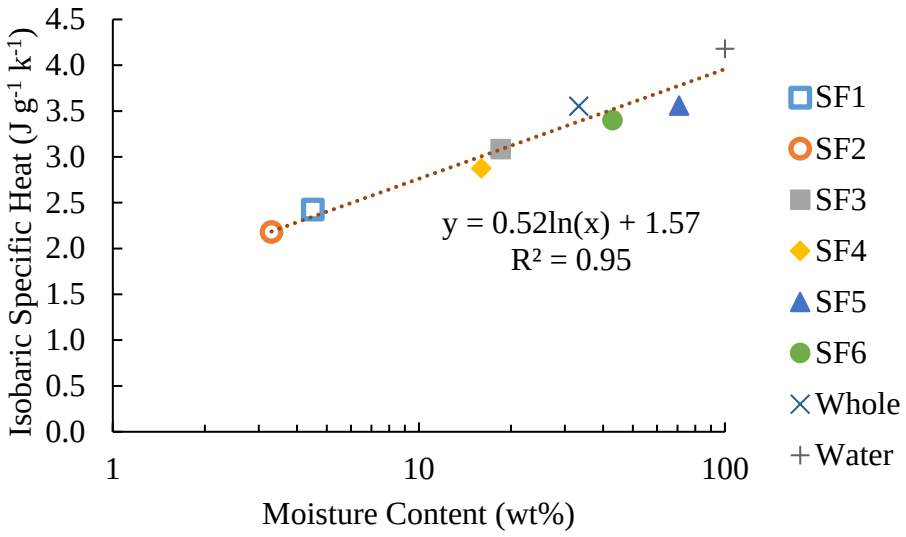

Figure 6. Comparison of the isobaric specific heat and logarithm of the moisture content of the bio-oil. A linear trend line closely fit the data, including that of pure water (4.18 J g^{-1} K^{-1}).

Thermal Conductivity

The thermal conductivity of methanol at 60 °C was evaluated prior to analyzing the bio-oils in an effort to calibrate the data collection. Data gathered from the methanol calibration runs at 0.3, 0.4, 0.5, and 0.6 A are shown in Figure 7. The change in voltage drop across the THW was monitored every 0.02 seconds, and plotted against the natural log of time elapsed to give a roughly linear trend. A trend line was then fitted to each of these curves across the most linear section of the data (usually about 0.2-2 s), and the slope of this line was used in the determination of the thermal conductivity at each constant current level.

The average of these values suggested that the thermal conductivity of methanol at 60 °C was 0.191 ± 0.009 W m^{-1} K^{-1}, which is within 5% of the accepted value of 0.202 W m^{-1} K^{-1} [29].

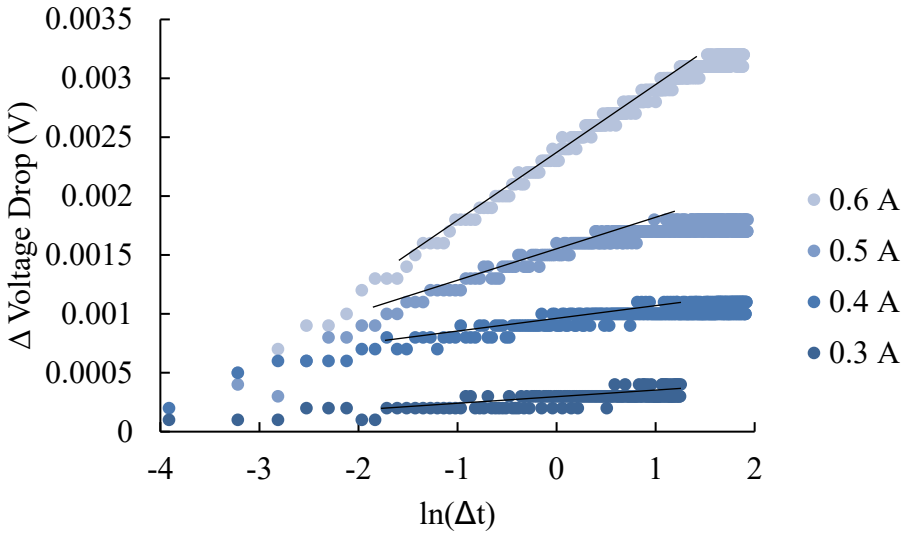

Figure 7. Plot of the change in voltage drop across the THW at each constant current level for methanol calibration experiments. The abscissa is plotted as the natural log of time elapsed in seconds. The slope of each trend line was used in the determination of the thermal conductivity of methanol at 60 °C.

Examination of Figure 8 reveals good agreement between the trend lines fitted to the data. Here, the slope of each trend line is plotted against the cube of the constant current value resulting in an R^2 correlation value of 0.992. This corroborates the low standard error uncertainty of the mean reported above. The values determined for each of the bio-oil fractions are reported in Table 4.

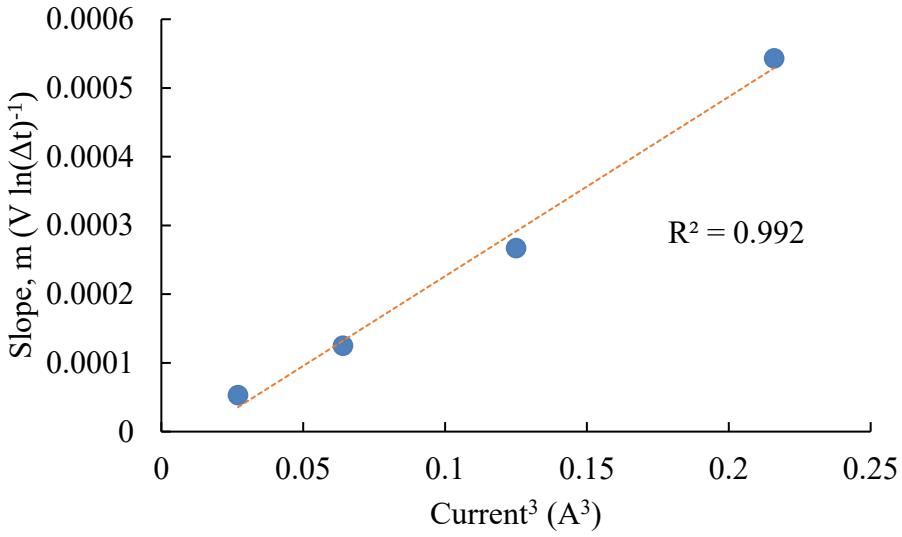

Figure 8. Plot comparing the slope values obtained from a linear fit of the experimental data (Figure 7), plotted against the cube of the constant current value. There was close agreement between the slopes determined for each of the 4 constant current levels tested.

Table 4. Summary of thermal conductivity values at 60 °C. Uncertainty reflects the standard error of the mean.

Bio-oil Fraction	**k (W m^{-1} K^{-1})**
SF1	0.362 ± 0.011
SF2	0.226 ± 0.002
SF3	0.336 ± 0.007
SF4	0.298 ± 0.005
SF5	0.847 ± 0.015
SF6	0.444 ± 0.008
Whole	0.372 ± 0.003

Predicting the thermal conductivity of a pure liquid substance has been the focus of much research over the last decades, and a number of theoretical models have been

developed, most of which are based on group contribution theory [30]. Thus, current attempts at predicting the thermal conductivity of a fluid mixture as complex as bio-oil will lead to highly inaccurate results. For example, SF5 was a clear outlier with a mean of 0.847 W m^{-1} K^{-1}. Given the high moisture content, it was expected that this fraction would have a thermal conductivity more similar to that of water (0.654 W m^{-1} K^{-1}) [31], but this was not the case. The data gathered from the THW tests and the linear fit correlation of the experimental data for each bio-oil sample can be found in Appendix C.

Dynamic Viscosity

Dynamic viscosity was measured at 60 °C for all of the bio-oil fractions. A summary of this data is shown in Table 5. All of the samples were evaluated at an elevated temperature in an effort to provide meaningful values for all of the fractions, and to report data at a common temperature so that comparisons can be made between the fractions. Given that SF1 and SF2 were semi-solid at ambient conditions, the lowest reasonable temperature to evaluate the bio-oil was determined to be 60 °C. Calibration tests were conducted using manufacturer-recommended silicone oils prior to evaluation of the bio-oil.

SF2 was the most viscous sample by a substantial margin. This was likely due to the high molecular weight and low moisture of this specific fraction as demonstrated in Table 2. It was hypothesized that the liquid products collected in SF2 were predominantly aerosols entrained in the vapor stream exiting the fluidized bed reactor. Thus, these molecules were large enough to remain in the liquid phase even at 500 °C.

Interestingly, the viscosity of the whole bio-oil was substantially lower than expected based on the high initial viscosity of SF1 and SF2, which account for 46.6 wt% of the whole bio-oil. The weighted average determination of viscosity for the whole bio-oil suggested that the whole bio-oil viscosity would be approximately 500 cP. Clearly, mixture viscosity cannot be determined in this manner, but it does illustrate the substantial effect that dilution has on the viscosity of the heavy bio-oil products. Conversely, if bio-oil forms an emulsion, the viscosity of the fluid is likely to be greater than that of either the individual continuous or dispersed phases. This phenomenon is due to the non-Newtonian behavior of emulsions, and it is correlated mainly with the volume fraction of the dispersed phase [32]. Given that the viscosity of whole oil was within the range of values measured for the constituent fractions, it was assumed that an emulsion was not an issue.

Table 5. Summary of dynamic viscosity values at 60 °C. Uncertainty reflects the standard error of the mean.

Bio-oil Fraction	**μ (cP)**
SF1	267.9± 0.4
SF2	1607 ± 3
SF3	4.65 ± 0.01
SF4	6.66 ± 0.01
SF5	0.98 ± 0.01
SF6	1.51 ± 0.01
Whole	21.4 ± 0.90

Surface Tension

The mean value and the standard error uncertainty for the samples are shown in Table 6. Surface tension was characterized for all of the low-viscosity oils at 60 °C and ambient pressure. Due to the high initial viscosity of SF1 and SF2, it was not possible to precisely measure the surface tension of these samples. Even when the fluid temperature was raised to 60 °C, no meaningful results could be obtained. It was assumed that the surface tension of these fluids was negligible, and that in most applications viscosity would be the primary driver for their fluid behavior. Support for this assumption can be seen in the general trend observed from plotting surface tension against dynamic viscosity as shown in Figure 9. Considering this trend and the magnitude of the viscosity values for SF1 and SF2 it stands to reason that the surface tension would effectively approach zero.

Table 6. Summary of surface tension values at 60 °C and ambient pressure. Uncertainty reflects the standard error of the mean.

Bio-oil Fraction	**γ (dyne cm^{-1})**
SF1	N/A
SF2	N/A
SF3	35.0 ± 0.4
SF4	32.7 ± 0.2
SF5	37.0 ± 1.1
SF6	33.9 ± 0.2
Whole	31.3 ± 1.2

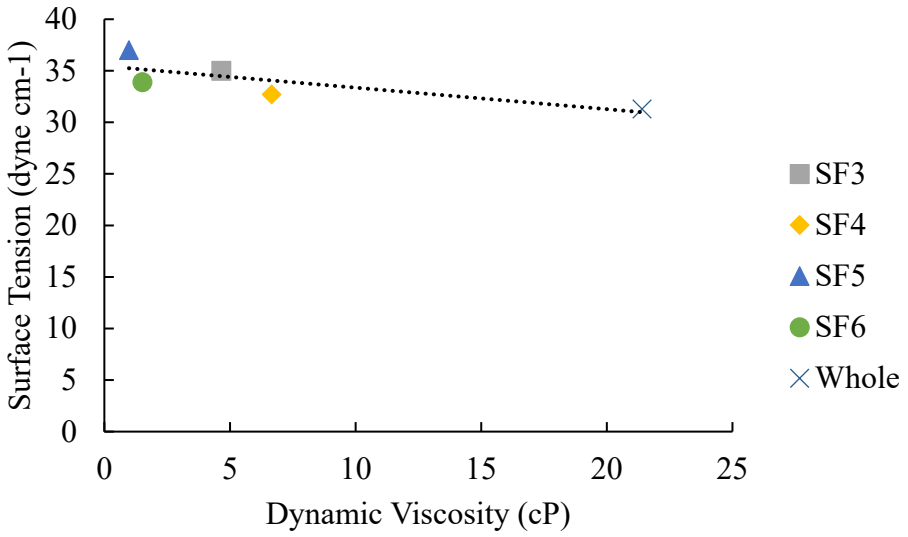

Figure 9. Comparison of surface tension and dynamic viscosity values for all but SF1 and SF2. A general trend of decreasing surface tension with increasing viscosity can be observed.

Enthalpy of Vaporization

The total enthalpy of vaporization for each bio-oil stage fraction was calculated from the quantification of volatile compounds. A summary of these results is reported in Table 7. Stage fractions high in moisture content, specifically SF5 and SF6, had the highest enthalpies of vaporization. This is due to the large enthalpy of vaporization of water in comparison to other quantified compounds in these fractions. Bio-oils SF1 and SF2 had enthalpies of vaporization significantly lower than the other stage fractions. This is attributed to a combination of low moisture content and low total quantification of identifiable compounds which can be seen in Appendix D. SF1 and SF2 also contain a large percentage of high molecular weight compounds that are not volatile during GC analysis and do not contribute

to the overall enthalpy of vaporization calculation. A more detailed analysis of the bio-oil fractions is discussed later.

Table 7. Summary of enthalpy of vaporization values calculated for each stage fraction. Uncertainty reflects the standard error of the mean.

Bio-oil Fraction	**ΔH_{vap} (kJ kg^{-1})**
SF1	233.6 $\pm$ 13.6
SF2	160.2 $\pm$ 11.7
SF3	703.6 $\pm$ 6.9
SF4	591.9 $\pm$ 14.9
SF5	1691.1 $\pm$ 48.3
SF6	1183.3 $\pm$ 28.9
Whole	871.7 $\pm$ 26.9

A summary of the quantified compounds and their respective calculated enthalpies of vaporization for the whole bio-oil fraction is shown in Table 8. Water accounts for 86% of the total enthalpy of vaporization for the whole bio-oil. Identifiable compounds from GC, IC, and HPLC account for 12% of the calculated enthalpy of vaporization with the remainder attributed to GC unidentified compounds. While the boiling points and enthalpies of vaporization for the unidentified compounds could not be determined directly, the enthalpy of vaporization for this portion was assumed to be equal to the average of the enthalpy of vaporization for the GC identified compounds. Approximately 59 wt% of the whole bio-oil was quantified using GC, IC, and HPLC analyses, with the remaining concentration denoted as non-volatile. Complete quantification and calculated enthalpies of vaporization for all bio-oil stage fractions can be found in the Appendix D.

Table 8: Summary of compound concentrations and enthalpy of vaporization values calculated for the whole bio-oil fraction. Uncertainty reflects the standard error of the mean.

Whole Bio-oil Components	**Concentration (wt%)**	**ΔH_{vap} (kJ)***
GC Identified Detectables	13.23 ± 0.04	66.47 ± 0.27
GC Unidentified Detectables	4.07 ± 0.26	17.13 ± 1.09
IC Detectables	3.18 ± 0.04	14.71 ± 0.22
HPLC Detectables	5.05 ± 0.01	21.81 ± 0.02
Water	33.27 ± 1.17	751.55 ± 26.36
Non-volatiles†	41.21 ± 1.34	-
Total	**100**	**871.67 ± 26.93**

***** per kg of whole bio-oil

† determined by difference

The non-volatile fraction of the bio-oil was calculated from a balance of the characterized volatile fraction (GC-identified, GC-unidentified, HPLC and IC detectable). This non-volatile fraction contains higher molecular weight compounds consisting of non-volatile sugars and lignin-derived oligomers commonly referred to as pyrolytic lignin. As gas chromatography analysis can only detect up to 40 wt% of bio-oil [33], the remaining fraction without known chemical data is often referred to as non-volatile and reported as pyrolytic lignin in literature [34]. Elder et al. was able to quantify phenolic monomers via gas chromatography but concluded that about 75% of the phenolic fraction in bio-oil is non-volatile [35]. As the characterized bio-oil fraction was conducted up to 300 °C using gas chromatography, the remaining fraction is denoted as non-volatile with an assumed enthalpy of vaporization of zero. Despite this portion of the mixture being non-volatile with zero

enthalpy of vaporization at these conditions, the values reported in Table 7 are on a whole mixture basis. Alternatively, the enthalpy of vaporization could be normalized for volatile-content, which would allow for ready comparison between bio-oil fractions. However, from a process design standpoint, it is more desirable to determine the enthalpy of vaporization for the whole fluid mixture as is reported here.

As seen in Table 8, the non-volatile fraction accounts for a significant amount of the whole bio-oil at approximately 41 wt%. The mechanism of the formation of these non-volatile species is continually debated in literature [36, 37]. One theory suggests that primary pyrolysis vapors, such as monomeric compounds, recombine in the vapor phase during condensation to produce phenolic oligomers [38, 39]. A second theory suggests that these oligomers are thermally ejected from the biomass as aerosols [40, 41]. More recently, Bayerbach et al. concluded that the formation of pyrolytic lignin is a combination of both thermal ejection and recombination reactions [34]. While the actual transport phase of the non-volatile fraction is beyond the scope of this paper, its enthalpy of vaporization was accounted for and assumed to be zero, as mentioned previously.

Conclusions

Economical and accessible methods to determine the specific heat, thermal conductivity, viscosity, surface tension, and enthalpy of vaporization of bio-oils have been demonstrated on whole and fractionated bio-oil from fast pyrolysis. Fractionation of bio-oil into subgroups of compounds according to dewpoint, allows for a closer examination of the driving factors behind the thermo-physical properties of bio-oil. For example, water appears

to be a significant contributing factor to most thermal properties with the exception of thermal conductivity. Similarly, the physical properties of the heaviest fractions (SF1 and SF2) were driven by their high percentage of non-volatile compounds (65.6 and 76.4 wt%, respectively). Robust analytical methods and availability of engineering data for bio-oils will help to de-risk the design and implementation of new technologies, and therefore encourage development of the biorenewables industry.

Acknowledgements

The authors would like to thank Kyle Nussdorfer, Cody Christianson, and Kelley Okoren for their assistance in setting up the tests and conducting experiments, and Joseph Polin for producing the bio-oil analyzed in this study. The authors would also like to express much gratitude to Patrick Johnston for his insight during discussion on bio-oil quantification. Dr. Steven Hoff's generous donation of the data logger used extensively in this study was greatly appreciated.

Funding for this research was provided by the Gary and Donna Hoover Endowment in Mechanical Engineering at Iowa State University and the U.S. Department of Energy under contract #EE0005974.

References

1. Venderbosch, R.H. and W. Prins, *Fast pyrolysis technology development.* Biofuels, Bioproducts and Biorefining, 2010. **4**(2): p. 178-208.

2. Henrich, E., et al., *Fast pyrolysis of lignocellulosics in a twin screw mixer reactor.* Fuel Processing Technology, 2016. **143**: p. 151-161.

3. Bridgwater, A.V., *Review of fast pyrolysis of biomass and product upgrading.* Biomass and Bioenergy, 2012. **38**: p. 68-94.

4. Oasmaa, A., et al., *Norms, Standards, and Legislation for Fast Pyrolysis Bio-oils from Lignocellulosic Biomass.* Energy & Fuels, 2015. **29**(4): p. 2471-2484.

5. Elliott, D.C., *Biofuel from fast pyrolysis and catalytic hydrodeoxygenation.* Current Opinion in Chemical Engineering, 2015. **9**: p. 59-65.

6. Boucher, M.E., A. Chaala, and C. Roy, *Bio-oils obtained by vacuum pyrolysis of softwood bark as a liquid fuel for gas turbines. Part I: Properties of bio-oil and its blends with methanol and a pyrolytic aqueous phase.* Biomass and Bioenergy, 2000. **19**(5): p. 337-350.

7. Oasmaa, A. and S. Czernik, *Fuel Oil Quality of Biomass Pyrolysis OilsState of the Art for the End Users.* Energy & Fuels, 1999. **13**(4): p. 914-921.

8. Oasmaa, A., E. Kuoppala, and Y. Solantausta, *Fast pyrolysis of forestry residue. 2. Physicochemical composition of product liquid.* Energy & fuels, 2003. **17**(2): p. 433-443.

9. Lu, Q., W.-Z. Li, and X.-F. Zhu, *Overview of fuel properties of biomass fast pyrolysis oils.* Energy Conversion and Management, 2009. **50**(5): p. 1376-1383.

10. Oasmaa, A. and C. Peacocke, *A guide to physical property characterisation of biomass-derived fast pyrolysis liquids*. 2001: Technical Research Centre of Finland Espoo.

11. He, R., et al., *Effects of high-pressure homogenization on physicochemical properties and storage stability of switchgrass bio-oil.* Fuel Processing Technology, 2009. **90**(3): p. 415-421.

12. Oasmaa, A., et al., *Fast Pyrolysis of Forestry Residue and Pine. 4. Improvement of the Product Quality by Solvent Addition.* Energy & Fuels, 2004. **18**(5): p. 1578-1583.

13. Mercader, F.d.M., et al., *Pyrolysis oil upgrading by high pressure thermal treatment.* Fuel, 2010. **89**(10): p. 2829-2837.

14. Zhang, Q., et al., *Review of biomass pyrolysis oil properties and upgrading research.* Energy conversion and management, 2007. **48**(1): p. 87-92.

15. He, R., et al., *Influence of pyrolysis condition on switchgrass bio-oil yield and physicochemical properties.* Bioresource Technology, 2009. **100**(21): p. 5305-5311.

16. Thangalazhy-Gopakumar, S., et al., *Physiochemical properties of bio-oil produced at various temperatures from pine wood using an auger reactor.* Bioresource Technology, 2010. **101**(21): p. 8389-8395.

17. Pollard, A.S., M.R. Rover, and R.C. Brown, *Characterization of bio-oil recovered as stage fractions with unique chemical and physical properties.* Journal of Analytical and Applied Pyrolysis, 2012. **93**(0): p. 129-138.

18. Rover, M.R., et al., *The effect of pyrolysis temperature on recovery of bio-oil as distinctive stage fractions.* Journal of Analytical and Applied Pyrolysis, 2014. **105**(0): p. 262-268.

19. Mohan, D., C.U. Pittman, and P.H. Steele, *Pyrolysis of wood/biomass for bio-oil: a critical review.* Energy & fuels, 2006. **20**(3): p. 848-889.

20. Stalhane, B. and S. Pyk, *New method for determining the coefficients of thermal conductivity.* Tek. Tidskr, 1931. **61**(28): p. 389-393.

21. Pittman, J.F.T., *Fluid thermal conductivity determination by the transient, line source method*. 1968, University of London.

22. Alvarado, S., et al., *A hot-wire method based thermal conductivity measurement apparatus for teaching purposes.* European Journal of Physics, 2012. **33**(4): p. 897.

23. Kwon, S.Y. and S. Lee, *Precise measurement of thermal conductivity of liquid over a wide temperature range using a transient hot-wire technique by uncertainty analysis.* Thermochimica Acta, 2012. **542**: p. 18-23.

24. Komini Babu, S., et al., *Measurement of thermal conductivity of fluid using single and dual wire transient techniques.* Measurement, 2013. **46**(8): p. 2746-2752.

25. Chemistry, R.S.o. *ChemSpider*. 2015 [cited 2016; Available from: http://www.chemspider.com/.

26. Choi, Y.S., et al., *Detailed characterization of red oak-derived pyrolysis oil: Integrated use of GC, HPLC, IC, GPC and Karl-Fischer.* Journal of Analytical and Applied Pyrolysis, 2014. **110**(0): p. 147-154.

27. Beach, C.A., et al., *Quantitative carbon detector for enhanced detection of molecules in foods, pharmaceuticals, cosmetics, flavors, and fuels.* Analyst, 2016. **141**(5): p. 1627-1632.

28. Marsh, K.N. and K. Marsh, *Recommended reference materials for the realization of physicochemical properties*. 1987: Blackwell Scientific Publications Oxford, UK.

29. Toolbox, T.E. *Methanol - Thermophysical Properties*. 2016 26 May 2016].

30. Pandey, J., et al., *Estimation of thermal conductivity of binary liquid mixtures employing new approach.* Indian Journal of Chemical Technology, 2007. **14**(6): p. 638.

31. Sengers, J. and J.T.R. Watson, *Improved international formulations for the viscosity and thermal conductivity of water substance*. 1986: American Chemical Society and the American Institute of Physics for the National Bureau of Standards.

32. Farah, M.A., et al., *Viscosity of water-in-oil emulsions: Variation with temperature and water volume fraction.* Journal of Petroleum Science and Engineering, 2005. **48**(3–4): p. 169-184.

33. Scholze, B. and D. Meier, *Characterization of the water-insoluble fraction from pyrolysis oil (pyrolytic lignin). Part I. PY–GC/MS, FTIR, and functional groups.* Journal of Analytical and Applied Pyrolysis, 2001. **60**(1): p. 41-54.

34. Bayerbach, R. and D. Meier, *Characterization of the water-insoluble fraction from fast pyrolysis liquids (pyrolytic lignin). Part IV: Structure elucidation of oligomeric molecules.* Journal of Analytical and Applied Pyrolysis, 2009. **85**(1): p. 98-107.

35. Elder, T. and E. Soltes, *Pyrolysis of lignocellulosic materials. Phenolic constituents of a wood pyrolytic oil.* Wood and Fiber Science, 2007. **12**(4): p. 217-226.

36. Garcia-Perez, M., et al., *Fast pyrolysis of oil mallee woody biomass: effect of temperature on the yield and quality of pyrolysis products.* Industrial & engineering chemistry research, 2008. **47**(6): p. 1846-1854.

37. Daugaard, D.E., *The transport phase of pyrolytic oil exiting a fast fluidized bed reactor*, in *Mechanical Engineering*. 2003, Iowa State University.

38. Evans, R.J. and T.A. Milne, *Molecular characterization of the pyrolysis of biomass.* Energy & Fuels, 1987. **1**(2): p. 123-137.

39. Patwardhan, P.R., R.C. Brown, and B.H. Shanks, *Understanding the fast pyrolysis of lignin.* ChemSusChem, 2011. **4**(11): p. 1629-1636.

40. Piskorz, J., P. Majerski, and D. Radlein. *Pyrolysis of Biomass–Aerosol Generation: Properties, Applications, and Significance for Process Engineers*. in *Biomass Conference of the Americas, 4th. Biomass: A Growth Opportunity in Green Energy and Value-Added Products, Elsevier Science, Oxford, UK, Oakland California*. 1999.

41. Lede, J., et al., *The Nature and Properties of Intermediate and Unvaporized Biomass Pyrolysis Materials*, in *Developments in Thermochemical Biomass Conversion: Volume 1 / Volume 2*, A.V. Bridgwater and D.G.B. Boocock, Editors. 1997, Springer Netherlands: Dordrecht. p. 27-42.

CHAPTER 7

CONCLUSIONS AND FUTURE WORK

Conclusions

Solvent liquefaction (SL) is a promising technology to convert biomass to liquids suitable for use as fuels and chemicals. However, there are a number of barriers to its commercial development. The overall goal of this dissertation was to address these technical barriers as they pertained to the development of the SL process development unit (PDU) discussed in *Chapter 2*.

The SL PDU was designed to process 1 kg hr^{-1} of dry southern yellow pine in a hydrocarbon solvent. The pine was converted to liquids with an average yield of 51.2 wt%. In-situ hydrogenation of the biomass-derived products, by a hydrogen donor solvent (HDS), reduced the oxygen content to 23.2 wt% in the whole oil. The low oxygen content of the bio-oil and presence of a hydrocarbon solvent resulted in a thermally stable heavy oil product. Short-duration exposure to elevated temperatures up to 300 °C resulted in less than 5 wt% change in the molecular weight of the heavy oil; a significant improvement over fast pyrolysis bio-oils. In addition to exploring the reaction performance, the SL PDU demonstrated three unit operations critical to the large-scale success of this SL technology. Continuous removal of solid residue was demonstrated to be 99.8% effective. Recovery of 97 wt% of the acetone used to aid solids filtration was also demonstrated, resulting in a 3% loss to the heavy oil. Finally, thermal separation of the medium and heavy oil was demonstrated using a packed distillation column. Due to the improved thermal stability of the oil, a

medium oil cut, which accounted for approximately 93 wt% of the incoming solvent, was consistently recovered. These promising results indicate the ability of SL to produce high yields of high quality bio-oil at a commercially-relevant scale.

Benchtop experiments conducted for the development of the SL PDU indicated feedstock moisture had a profound effect on liquid yields and quality. As discussed in *Chapter 3*, liquid yields decreased by as much as 25, 21, and 35 wt% when moisture was increased from 1 to 50 wt% for pine, cellulose, and lignin, respectively. A corresponding increase in solid residue was also observed. Detailed analysis of the solid residue indicated acid-catalyzed polymerization of the monomeric products was the likely mechanism. This was hypothesized to be due to the ionic dissociation of water at reaction conditions. The reduction in liquid yield and corresponding reduction in monomer yield indicated that hydrocarbon-based SL of biomass was significantly influenced by moisture. Therefore, this SL technology is not recommended for use with high-moisture feedstocks.

Chapter 4 explored the development of a SL process to convert technical lignin to liquids with a high selectivity for phenolic monomers (PM). A set of bench-scale experiments were used to construct a statistical model based on response surface methodology. The model was then used to evaluate the influence of hydrogen donor solvent blend ratio, reaction temperature, solids loading, and residence time. The solvent system was designed to use o-cresol as a model phenolic solvent. Maximum liquid yield (58.6 wt%) occurred at temperatures as low as 260 °C when the solvent was composed of greater than 70 wt% o-cresol. Furthermore, approximately 40 wt% of the liquid product was distillable due to a high concentration of lignin-derived PM. These results demonstrated the technical

feasibility of a process wherein lignin is converted to high yields of PM. The excess production of PM suggests that these molecules could be used as a recycle solvent to sustain a continuous process with limited solvent inputs.

In order for SL to utilize an internal recycle solvent, product streams targeted for recycle must demonstrate sufficient thermal stability for conventional thermal separations to be employed. *Chapter 5* examined the effect of rapid thermal processing on bio-oils from fast pyrolysis. Bio-oil acidity, as measured by its total acid number (TAN), was determined to be the strongest indicator of thermal stability. Increased acidity was found to catalyze polymerization of biomass-derived products, which resulted in an increase in molecular weight. These trends were exacerbated by both elevated temperature and increased reaction time. This work was then extended to the products of the SL PDU prior to implementation of the solvent fractionation system.

Design work prior to construction of the SL PDU pointed to a lack of engineering data for the bio-oils produced from thermochemical conversion of biomass. *Chapter 6* discussed the development of alternative methods for determining many of the thermophysical properties of bio-oils necessary for effective design of a processing plant. This work focused on utilizing readily available laboratory equipment so as to improve the accessibility and reduce the expense of gathering these types of data.

Overall this work demonstrated from the potential of SL to convert biomass to bio-oil. This technology is capable of producing high yields of thermally stable bio-oil with low oxygen and moisture content. The improvements and findings presented in this dissertation

are intended to reduce the risk of developing similar SL processes, with the ultimate goal of enabling commercial-scale production of advanced biorenewable products from SL.

Future Work

This work was intended to improve the development of commercially-viable SL technologies. A number of opportunities for improvement were discovered.

The most critical area for further investigation is product separation. Separation of solid residue was demonstrated in *Chapter 2* by use of barrier filters. This resulted in high recovery of solid residue, but at the expense of liquid yield which was subsequently lost to the solid stream. Continuous centrifugation or similar technologies would be more effective than barrier filtration at larger scales, and therefore studies into these alternative means of solids recovery are recommended. Similarly, investigations into product purification and separation are needed to better predict process economics.

The separation of water from bio-oil product streams also deserves further study. Certain SL systems, such as the hydrocarbon-based system discussed in *Chapter 3*, are significantly impacted by moisture. Some systems, however, may not be as adversely affected. Regardless of its influence on biomass conversion, it is generally preferred to remove water to improve the overall quality and improve the value of product streams. For this reason, the techno-economic impact of drying feedstock versus recovering water from a product should be evaluated. For example, the cost of implementing a continuous dryer system would need to be evaluated against the cost and complexity of stripping water from a

stream of solvent and light oxygenates, or against the cost of sending an aqueous stream to waste-water treatment.

If effective separations are achieved, an evaluation on long-term recycle solvent operation is essential. For example, development of the process discussed in *Chapter 4* is entirely contingent upon the phenolic monomer (PM) recycle solvent maintaining a stable composition. To achieve this goal a continuous pilot plant, similar to that described in *Chapter 2*, would need to operate for an extended period of time during which the recycle solvent would need to be monitored closely to determine whether or not the composition was changing due to a significant shift in the selectivity of producing specific PM from lignin. For instance, results from *Chapter 4* suggested that phenol would likely be the PM with the highest yield from lignin. Furthermore, a long-term study would also provide better insight into the effective production rates of each of the product streams.

Additionally, other sources of lignin should be evaluated using the process described in *Chapter 4*. It is well known that both the kind of biomass and extraction method have significant impacts on lignin structures. As additional methods for biomass extraction techniques are adopted for the cellulosic ethanol industry, these new forms of technical lignin should be evaluated. Similarly, the effect of residual carbohydrate content in these lignin streams on SL product composition should be evaluated. This is a potentially significant variable between different extraction methods.

Experimentation on the SL PDU was frequently hampered by process upsets due to pressure loss in the extruder feeder (EXT-1). Alternative feeder mechanisms have been identified, but additional testing and evaluation of these are necessary. Furthermore, ways to

increase biomass throughput for a given reactor size should be explored. Whole biomass, such as grass and wood, are traditionally very porous and absorb a significant amount of solvent. Therefore, when biomass and solvent are mixed the material behaves more like a wet solid than a liquid. A number of possible remedies exist to improve the consistency of the slurry. One option is to implement a pretreatment process that densifies biomass prior to making a slurry for pumping. This could result in a staged solvent liquefaction process, or could be as simple as utilizing only extracted biomass streams, such as lignin or cellulose, as a feedstock. Another option is to implement a solvent recycle loop with which to flood biomass with an excess of solvent simply for the purpose of pumping. Excess solvent could then be extracted from the process, after reaching final pressure, and recycled to a slurry tank.

APPENDIX A

PHYSICAL BEHAVIOR OF WATER DURING SOLVENT LIQUEFACTION OF BIOMASS IN A HYDROCARBON-BASED SOLVENT

It was important to understand the behavior of water in the reactor because interaction between water and other volatile compounds in the reactor was expected to skew the boiling point curve of water from the theoretical curve calculated in the previous section. A series of tests were conducted to elucidate the actual boiling point of water during an experiment, and to verify that water vaporized from the reactor as anticipated.

Vaporizing 25 g of water (50 wt% moisture) was calculated to require 55.8 kJ. Assuming water would vaporize over a span of approximately 5 min, this would result in 185.8 W of power from the 1000 W heater. The boiling point correspondingly was determined by stagnation of the temperature profile upon heating the reactor and its contents. An example of the observed phenomenon is shown in Figure 1. The effective boiling point of water was determined to be 220, 250, and 265 °C for reactions at 15, 29, and 42 bar, respectively. Further validation of the predicted behavior was achieved by recovery of at least 95 wt% of the initial moisture in Condenser 1. No thermal stagnation or water collection in Condenser 1 was observed for experiments at 70 bar.

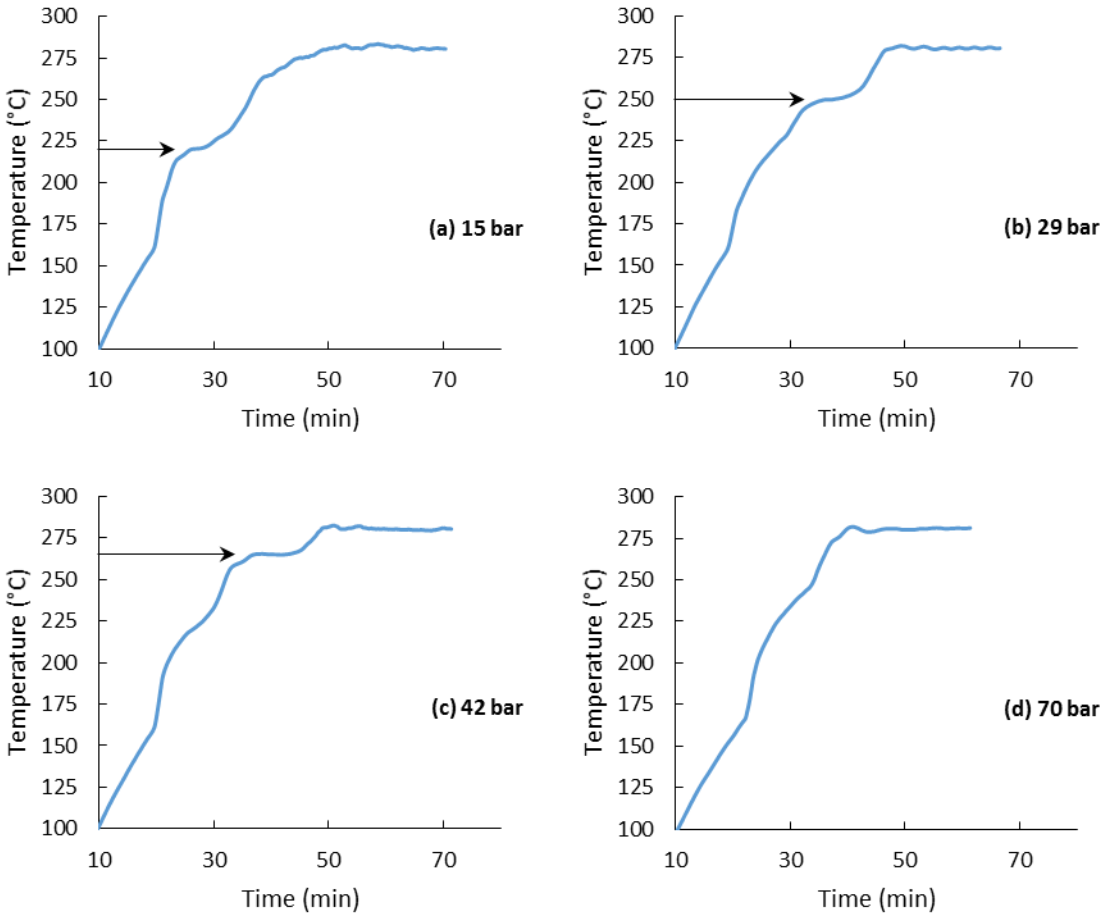

Figure 1. Sample temperature profiles for 50 wt% moisture at (a) 15 bar, (b) 29 bar, (c) 42 bar, and (d) 70 bar. Arrows indicate isothermal regions during which water was vaporized.

APPENDIX B

EFFECT OF MOISTURE ON SOLVENT LIQUEFACTION OF LOBLOLLY PINE

The impact of drying on the liquefaction performance of pine was a principal concern that needed to be addressed. Very little research has evaluated this consideration for any biomass sources. This is most likely due to the fact that, as previously discussed, most processes require a well-dried feedstock regardless of any adverse effects the drying process may have. However, there is cause for concern over the effects of drying a feed. Fully drying sub-bituminous coal, for instance, has been suggested to allow for partial oxidation and molecular rearrangement resulting in a more recalcitrant feedstock [1]. Some investigations into high-temperature drying found that high levels of biomass moisture can cause biomass degradation due to reactive drying at temperatures of 150-200 °C [2, 3]. Up to 120 °C, however, drying has been shown to have a negligible effect on biomass, with a loss of moisture and particle shrinkage to be the extent of the impact [3].

A series of tests were conducted to verify that the process of drying biomass does not significantly alter the biomass substrate in a manner that influences its conversion during SL. Three portions of as-received feedstock (55 wt% moisture) were randomly selected and assigned to various degrees of drying. One was dried to less than 1 wt% final moisture while the other two were partially dried to final moisture contents of 25 wt% and 40 wt%. These feedstocks were liquefied in tetralin at 280 °C temperature, and 29-70 bar pressure. The effects of drying on SL product distribution are shown in Figure 1. The linear trend of the data demonstrates that the act of drying the loblolly pine did not appear to have a significant

effect on the SL process. Furthermore, wetting fully-dried biomass with deionized water appears to be a valid procedure for simulating biomass moisture.

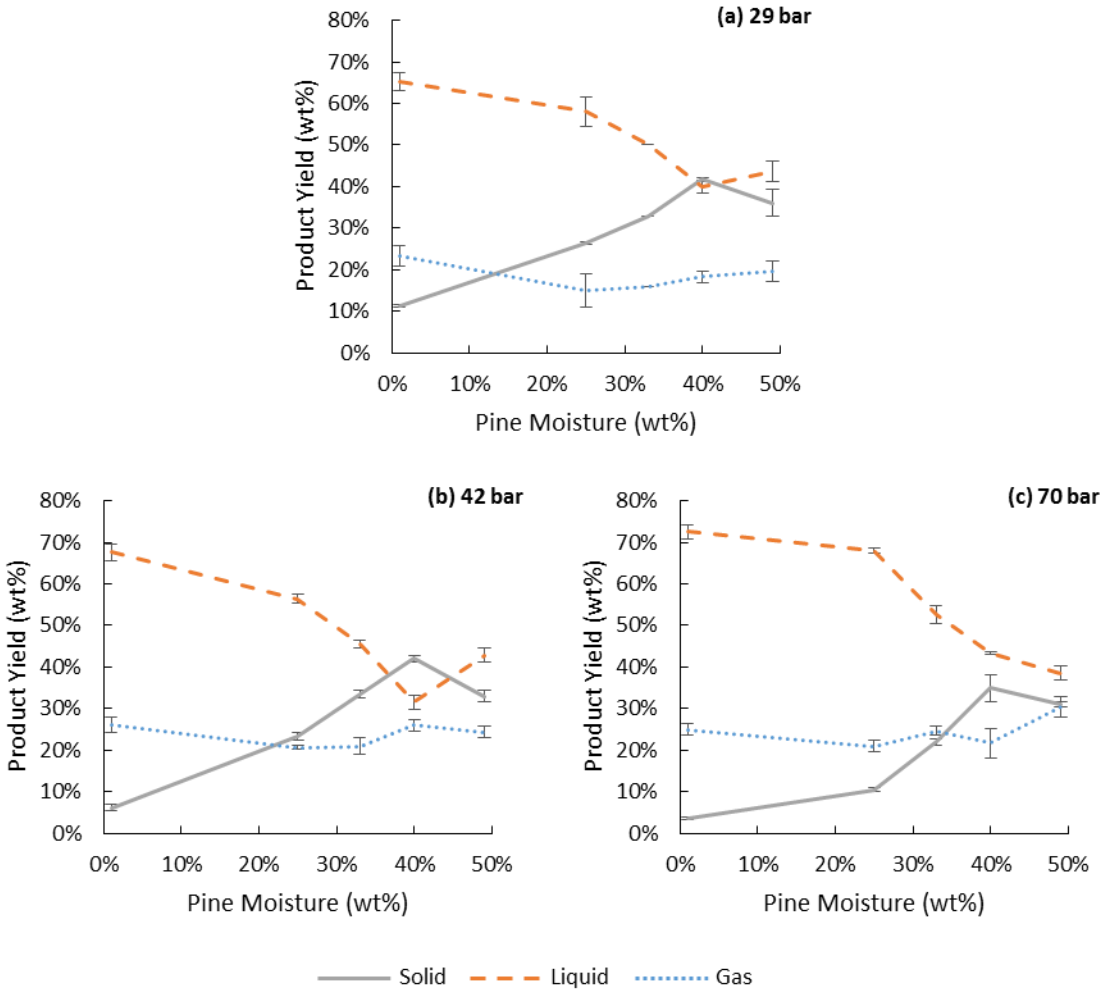

Figure 1. Product mass yields from the liquefaction of loblolly pine in tetralin at 280 °C as a function of pine moisture. Samples at 1, 33, and 50 wt% moisture were fully dried and wetted with DI water while samples at 25 and 40 wt% moisture were partially dried from the as-received moisture content of 55 wt%. Error bars represent the standard error of the mean for a minimum of two experiments.

Figure 1 demonstrates the significant impact that moisture has on the SL of pine in tetralin at 280 °C. Solid yield increased by as much as 25 wt% when comparing the yield at 1

and 50 wt% moisture. At each pressure, an increase in moisture resulted in an increase in solid yield, a corresponding decrease in liquid yield, and relatively constant gas production.

Detailed product characterization was not possible primarily because of low concentrations of many solubilized and liquid species in the heavy oil. Subsequent trials with cellulose and lignin were conducted to clarify the role of moisture on the liquefaction of biomass constituents.

References

1. Derbyshire, F. and P. Stansberry, *Comments on the reactivity of low-rank coals in liquefaction.* Fuel, 1987. **66**(12): p. 1741-1742.

2. Borrega, M. and P. Kärenlampi, *Effect of relative humidity on thermal degradation of Norway spruce (Picea abies) wood.* Journal of Wood Science, 2008. **54**(4): p. 323-328.

3. Shankar Tumuluru, J., et al., *REVIEW: A review on biomass torrefaction process and product properties for energy applications.* Industrial Biotechnology, 2011. **7**(5): p. 384-401.

APPENDIX C

THERMAL CONDUCTIVITY RESULTS

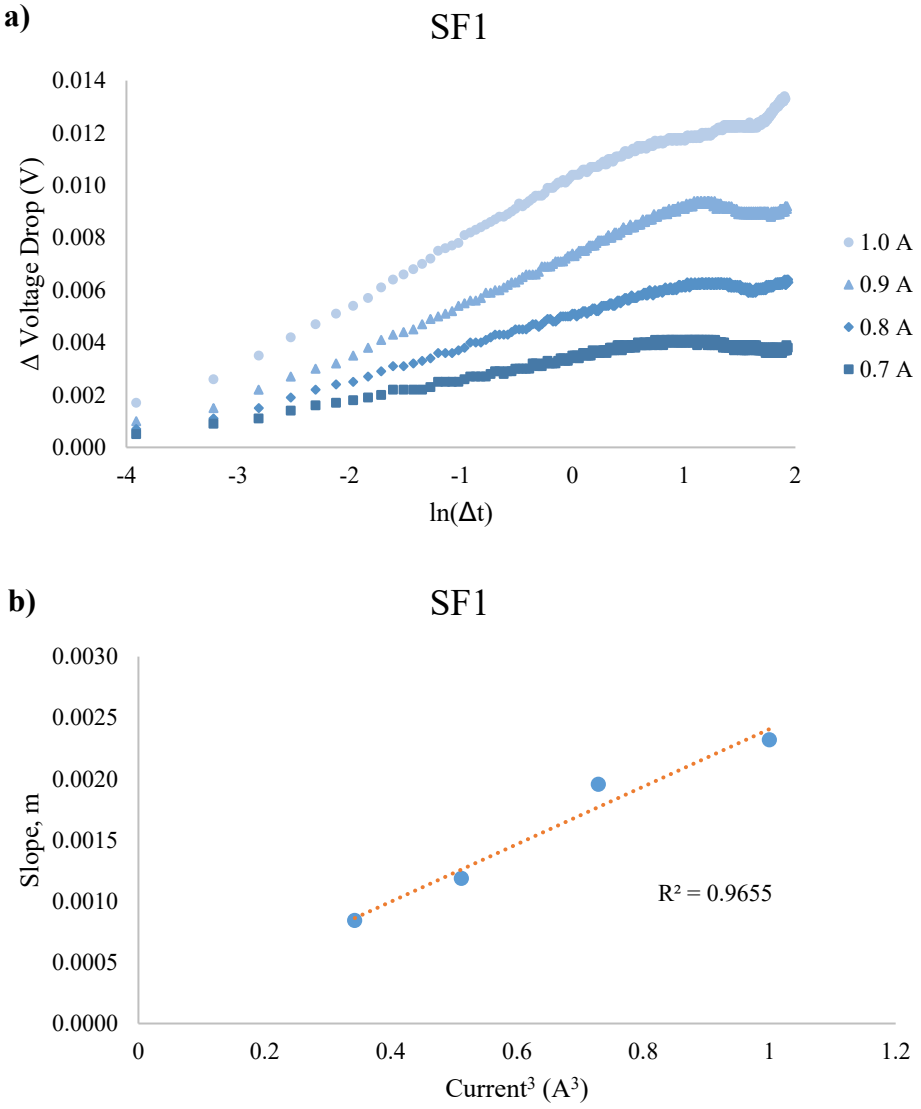

Figure 1. a) Plot of the change in voltage drop across the THW at each constant current level for SF1 experiments. The abscissa is plotted as the natural log of time elapsed in seconds. b) Plot comparing the slope values obtained from a linear fit of the experimental data, plotted against the cube of the constant current value. There was close agreement between the slopes determined for each of the 4 constant current levels tested.

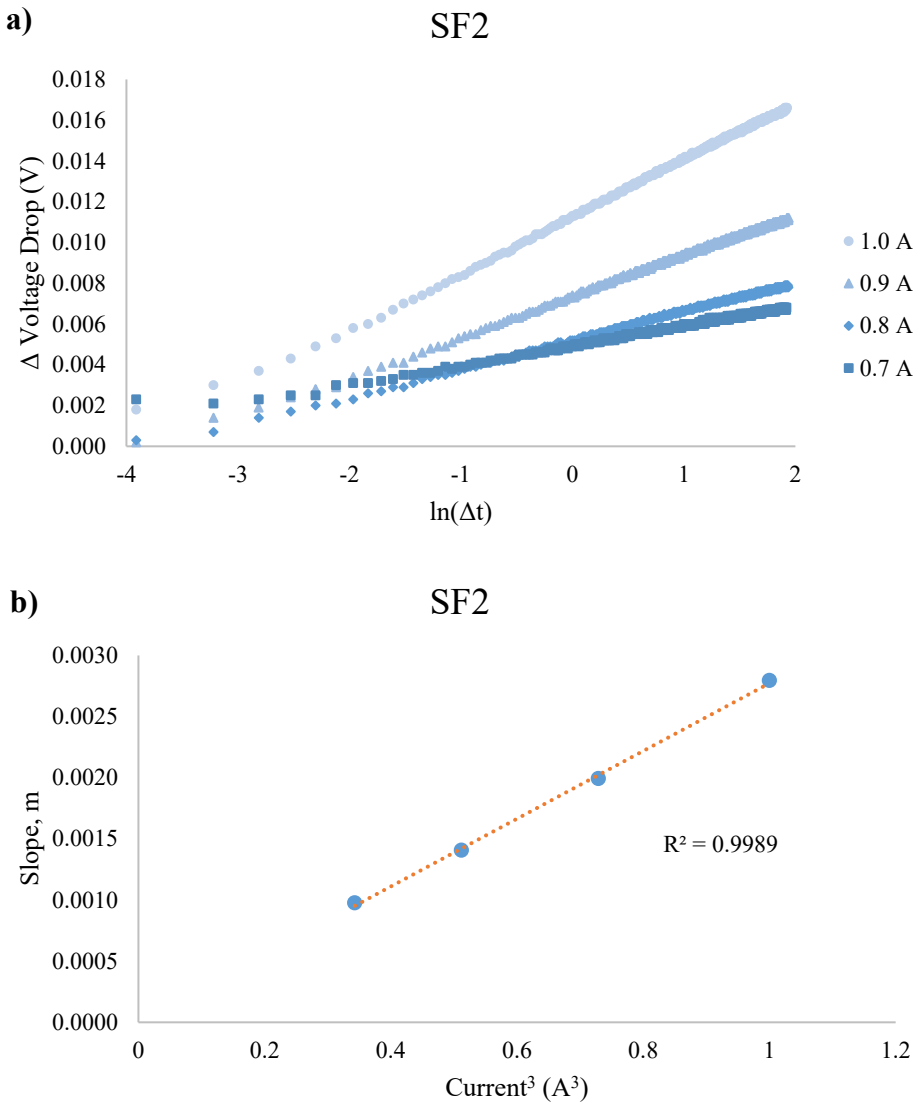

Figure 2. a) Plot of the change in voltage drop across the THW at each constant current level for SF2 experiments. The abscissa is plotted as the natural log of time elapsed in seconds. b) Plot comparing the slope values obtained from a linear fit of the experimental data, plotted against the cube of the constant current value. There was close agreement between the slopes determined for each of the 4 constant current levels tested.

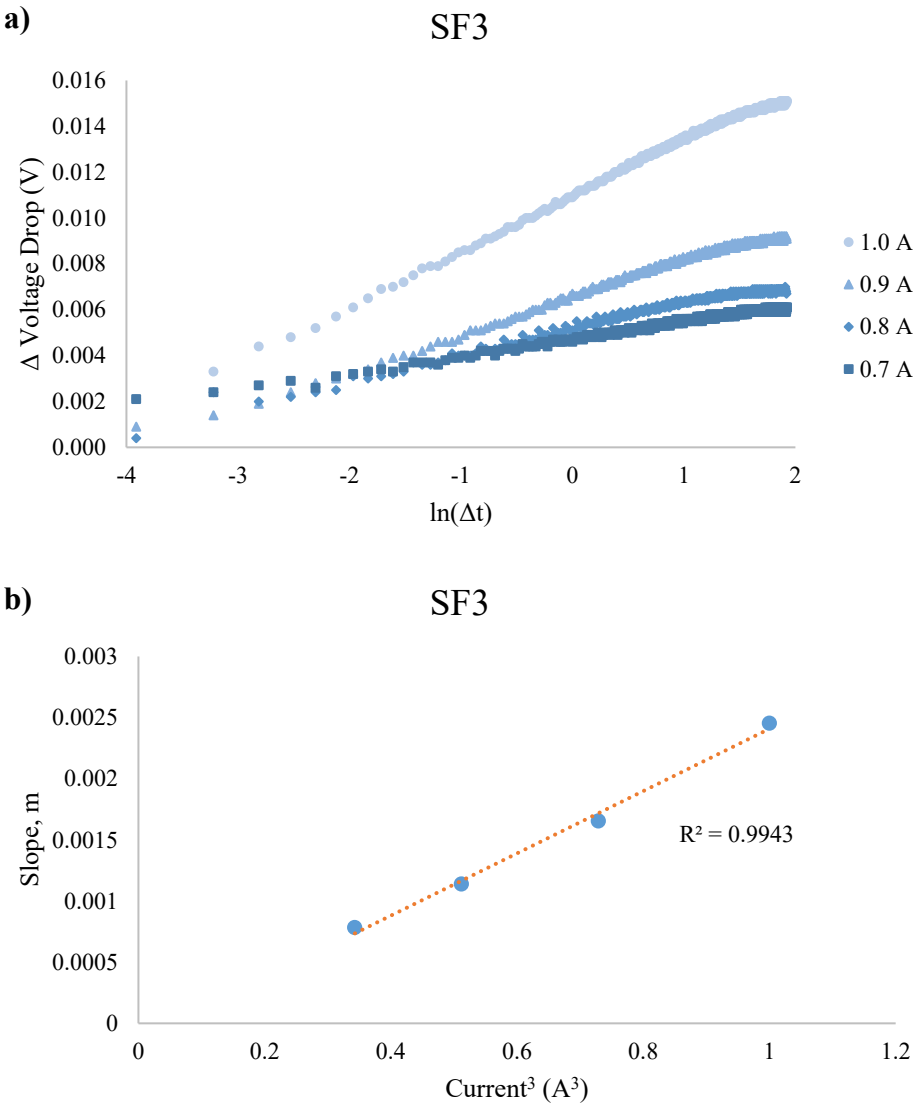

Figure 3. a) Plot of the change in voltage drop across the THW at each constant current level for SF3 experiments. The abscissa is plotted as the natural log of time elapsed in seconds. b) Plot comparing the slope values obtained from a linear fit of the experimental data, plotted against the cube of the constant current value. There was close agreement between the slopes determined for each of the 4 constant current levels tested.

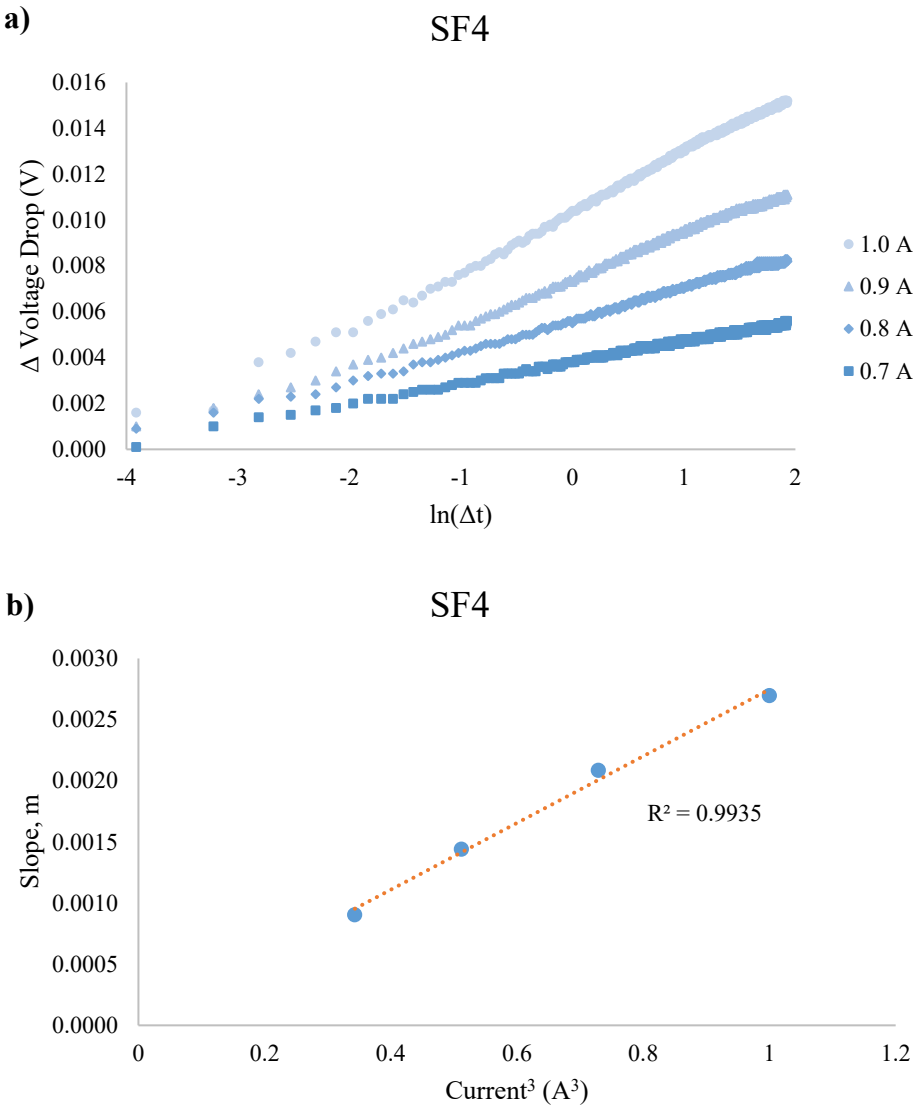

Figure 4. a) Plot of the change in voltage drop across the THW at each constant current level for SF4 experiments. The abscissa is plotted as the natural log of time elapsed in seconds. b) Plot comparing the slope values obtained from a linear fit of the experimental data, plotted against the cube of the constant current value. There was close agreement between the slopes determined for each of the 4 constant current levels tested.

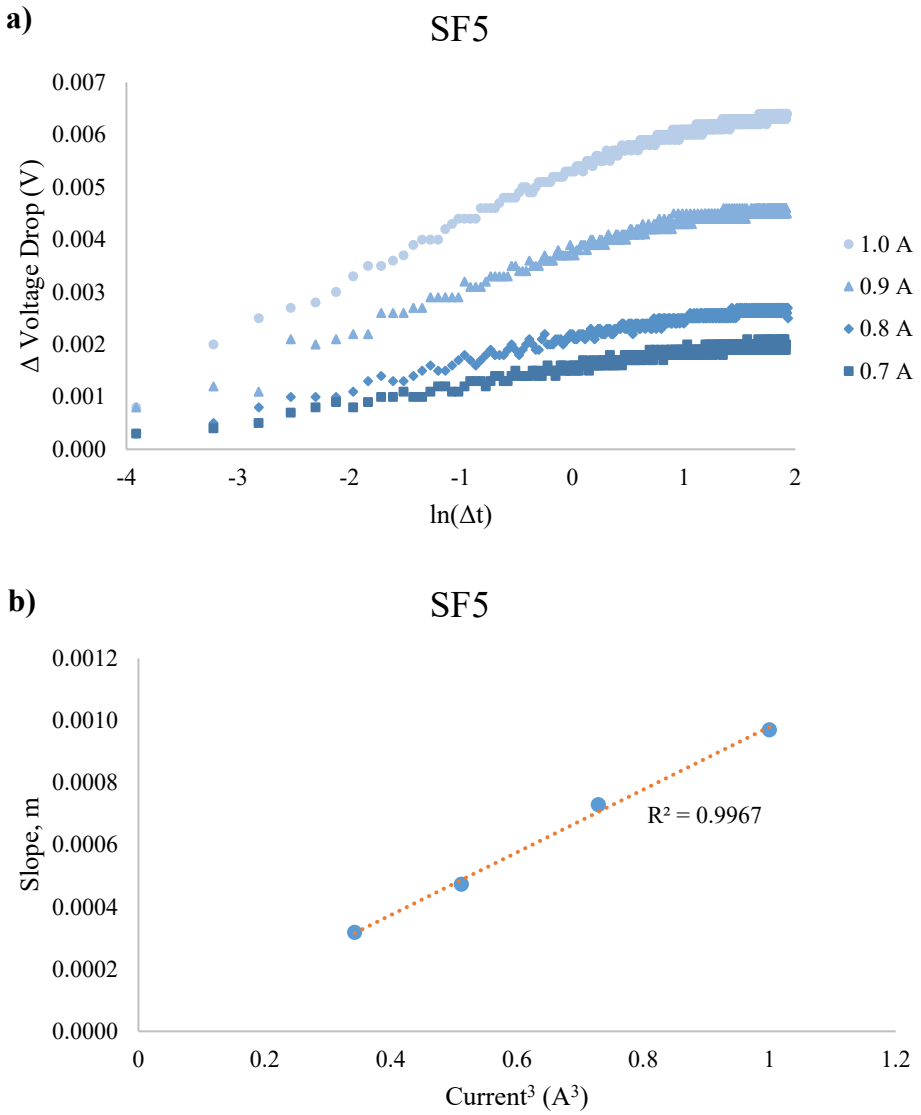

Figure 5. a) Plot of the change in voltage drop across the THW at each constant current level for SF5 experiments. The abscissa is plotted as the natural log of time elapsed in seconds. b) Plot comparing the slope values obtained from a linear fit of the experimental data, plotted against the cube of the constant current value. There was close agreement between the slopes determined for each of the 4 constant current levels tested.

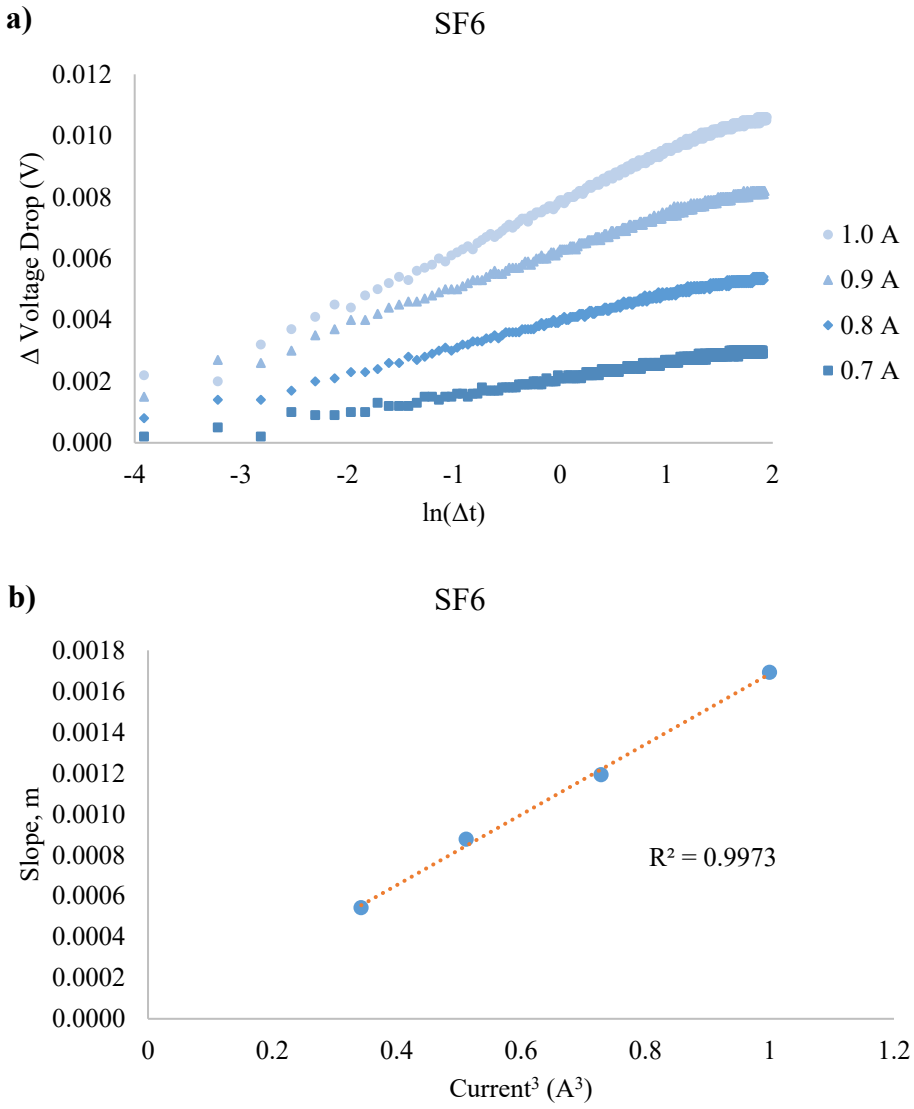

Figure 6. a) Plot of the change in voltage drop across the THW at each constant current level for SF6 experiments. The abscissa is plotted as the natural log of time elapsed in seconds. b) Plot comparing the slope values obtained from a linear fit of the experimental data, plotted against the cube of the constant current value. There was close agreement between the slopes determined for each of the 4 constant current levels tested.

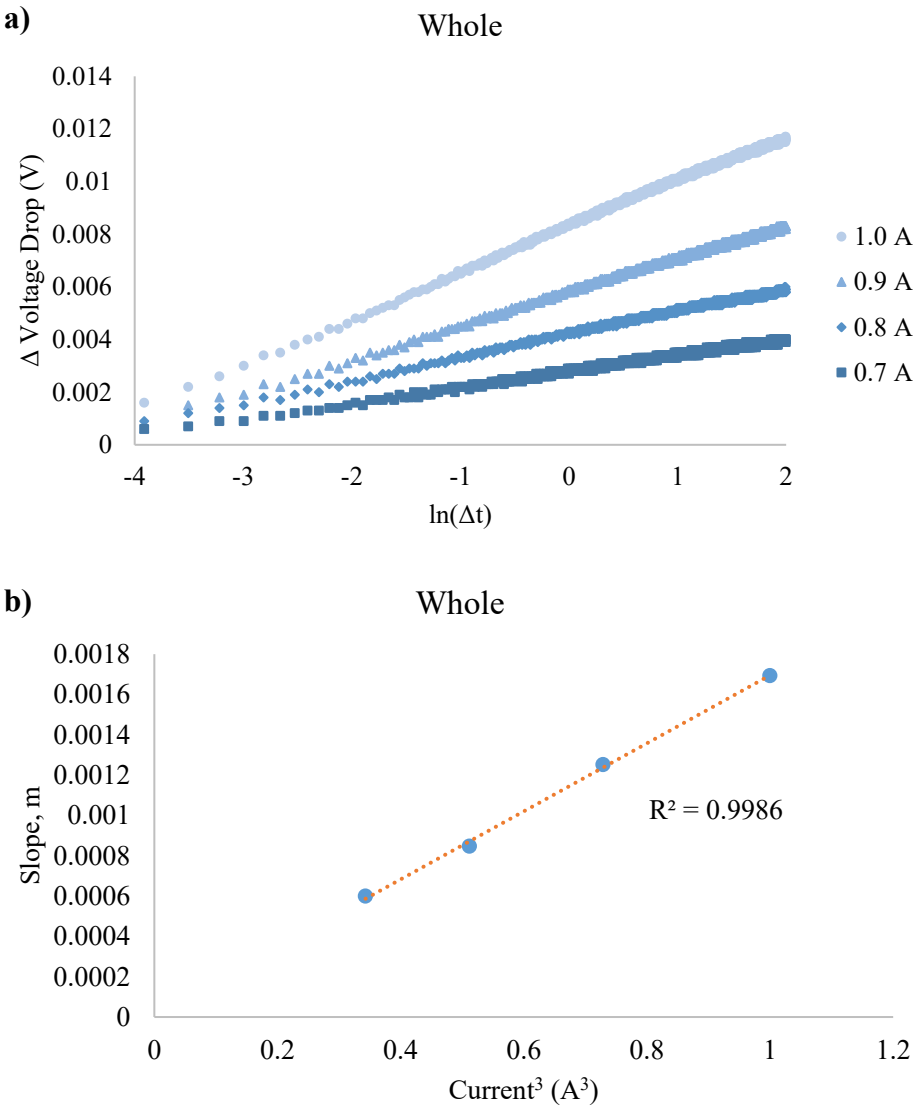

Figure 7. a) Plot of the change in voltage drop across the THW at each constant current level for Whole bio-oil experiments. The abscissa is plotted as the natural log of time elapsed in seconds. b) Plot comparing the slope values obtained from a linear fit of the experimental data, plotted against the cube of the constant current value. There was close agreement between the slopes determined for each of the 4 constant current levels tested.

APPENDIX D

ENTHALPY OF VAPORIZATION RESULTS

Table 1: Standard enthalpies of vaporization for characterized bio-oil components

Bio-oil Components	**ΔH_{vap} (kJ/mol)**	**ΔH_{vap} (kJ/kg)**
GC Identified Detectables	**-**	**-**
Acetaldehyde	25.8	585.7
Formaldehyde	22.3	742.6
Glycolaldehyde	43.0	716.0
Acetol	44.6	602.1
2,5-dimethoxytetrahydrofuran (cis)	36.7	277.7
Propanal	28.3	487.3
2,5-dimethoxytetrahydrofuran (trans)	36.7	277.7
Furfural	43.0	447.5
2-Furanmethanol	64.4	656.5
Acetoxyacetone	39.1	336.7
2-Methyl-2-cyclopenten-1-one	39.4	409.9
2-Hydroxy-2-cyclopenten-1-one	57.6	587.2
5-Methylfurfural	42.3	384.2
3-Methyl-2-cyclopenten-1-one	39.4	409.9
2(5H)-furanone	44.0	523.4
Methylcyclopentenolone	56.0	499.4
3-Methyl-2(5H)-furanone	45.9	467.9
Phenol	43.5	462.2
2-Methoxyphenol	45.9	369.8

O-cresol	44.5	411.5
P-cresol	45.6	421.7
4-Methyl-5H-furan-2-one	45.9	467.9
2-Methoxy-4-methylphenol	47.5	343.8
2,4-Dimethylphenol	46.5	380.6
2,3-Dimethylphenol	47.2	386.4
3-Ethylphenol	46.6	381.5
3,4-Dimethylphenol	48.2	394.6
4-Ethyl-2-methoxyphenol	50.3	330.5
1,4;3,6-Dianhydro-α-d-glucopyranose	58.3	404.4
2-Methoxy-4-vinylphenol	50.2	334.3
Eugenol	51.2	311.8
2-Methoxy-4-propylphenol	52.2	314.0
5-Hydroxymethylfurfural	56.1	444.8
2,6-Dimethoxyphenol	52.3	339.3
Isoeugenol	52.5	319.7
4-Methyl-2,6-dimethoxyphenol	52.7	313.3
1,4-Benzenediol	54.6	495.9
Vanillin	54.2	356.2
2,5-Dimethoxybenzylalcohol	57.7	343.1
4-Hydroxy-3-methoxyacetophenone	55.9	336.4
4-Allyl-2,6-dimethoxyphenol	56.3	289.9
4-Hydroxy-3,5-dimethoxybenzaldehyde	58.6	321.7
GC Unidentified Detectables[†]	**-**	**421.1**
IC Detectables	**-**	**-**

Acetic acid	23.7	394.7
Propanoic acid	40.1	541.3
Glycolic acid	58.5	769.2
Formic acid	22.7	493.2
HPLC Detectables	**-**	**-**
Cellobiosan	108.3	334.0
Xylose	77.2	514.2
Galactose	76.6	425.2
Mannose	76.6	425.2
Levoglucosan	73.1	450.8
Water	**40.7**	**2259.2**
Non-volatiles	**-**	**-**

† calculated by average of GC identifiable compounds

Table 2: Summary of compound concentrations and enthalpy of vaporization values calculated for the SF1 bio-oil fraction. Uncertainty reflects the standard error of the mean.

SF1 Bio-oil Components	**Concentration (wt%)**	**ΔH_{vap} (kJ)***
GC Identified Detectables	**14.26 ± 0.06**	**60.30 ± 0.18**
Acetaldehyde	0.01 ± 0.01	0.01 ± 0.01
Formaldehyde	0.05 ± 0.01	0.40 ± 0.02
Glycolaldehyde	0.50 ± 0.01	3.60 ± 0.09
Acetol	0.64 ± 0.01	3.87 ± 0.02
2,5-dimethoxytetrahydrofuran (cis)	0.25 ± 0.03	0.71 ± 0.09
Propanal	0.09 ± 0.01	0.45 ± 0.01
2,5-dimethoxytetrahydrofuran (trans)	0.04 ± 0.01	0.12 ± 0.01
Furfural	0.30 ± 0.01	1.36 ± 0.03
2-Furanmethanol	0.12 ± 0.01	0.77 ± 0.02
Acetoxyacetone	0.09 ± 0.01	0.29 ± 0.01
2-Methyl-2-cyclopenten-1-one	0.09 ± 0.01	0.35 ± 0.01
2-Hydroxy-2-cyclopenten-1-one	0.81 ± 0.01	4.73 ± 0.06
5-Methylfurfural	0.17 ± 0.01	0.63 ± 0.02
3-Methyl-2-cyclopenten-1-one	0.13 ± 0.01	0.53 ± 0.01
2(5H)-furanone	0.69 ± 0.01	3.62 ± 0.03
Methylcyclopentenolone	0.66 ± 0.01	3.31 ± 0.02
3-Methyl-2(5H)-furanone	0.23 ± 0.01	1.08 ± 0.02
Phenol	0.20 ± 0.01	0.92 ± 0.01
2-Methoxyphenol	0.50 ± 0.01	1.85 ± 0.04
O-cresol	0.13 ± 0.01	0.54 ± 0.01
P-cresol	0.30 ± 0.02	1.25 ± 0.10
4-Methyl-5H-furan-2-one	0.48 ± 0.02	2.23 ± 0.10

2-Methoxy-4-methylphenol	0.92 ± 0.01	3.16 ± 0.01
2,4-Dimethylphenol	0.29 ± 0.01	1.09 ± 0.01
2,3-Dimethylphenol	0.05 ± 0.01	0.17 ± 0.01
3-Ethylphenol	0.08 ± 0.01	0.32 ± 0.01
3,4-Dimethylphenol	0.03 ± 0.01	0.11 ± 0.01
4-Ethyl-2-methoxyphenol	0.24 ± 0.01	0.79 ± 0.01
1,4;3,6-Dianhydro-α-d-glucopyranose	0.27 ± 0.01	1.08 ± 0.01
2-Methoxy-4-vinylphenol	1.61 ± 0.01	5.38 ± 0.03
Eugenol	0.36 ± 0.01	1.13 ± 0.01
2-Methoxy-4-propylphenol	0.08 ± 0.01	0.24 ± 0.01
5-Hydroxymethylfurfural	0.75 ± 0.01	3.34 ± 0.01
2,6-Dimethoxyphenol	0.20 ± 0.01	0.69 ± 0.01
Isoeugenol	1.21 ± 0.01	3.86 ± 0.02
4-Methyl-2,6-dimethoxyphenol	0.08 ± 0.01	0.24 ± 0.01
1,4-Benzenediol	0.31 ± 0.01	1.56 ± 0.01
Vanillin	0.59 ± 0.01	2.09 ± 0.01
2,5-Dimethoxybenzylalcohol	0.25 ± 0.01	0.87 ± 0.01
4-Hydroxy-3-methoxyacetophenone	0.33 ± 0.01	1.10 ± 0.01
4-Allyl-2,6-dimethoxyphenol	0.14 ± 0.01	0.42 ± 0.01
4-Hydroxy-3,5-dimethoxybenzaldehyde	0.01 ± 0.01	0.02 ± 0.01
GC Unidentified Detectables	**3.61 ± 0.12**	**15.21 ± 0.51**
IC Detectables	**2.19 ± 0.01**	**12.67 ± 0.01**
Acetic acid	0.70 ± 0.01	2.75 ± 0.03
Propanoic acid	0.12 ± 0.01	0.66 ± 0.01
Glycolic acid	0.91 ± 0.01	6.97 ± 0.03

Formic acid	0.46 ± 0.01	2.29 ± 0.01
HPLC Detectables	**9.81 ± 0.01**	**43.14 ± 0.19**
Cellobiosan	1.12 ± 0.01	3.74 ± 0.01
Xylose	0.73 ± 0.02	3.75 ± 0.09
Galactose	0.57 ± 0.01	2.42 ± 0.05
Mannose	0.29 ± 0.02	1.24 ± 0.10
Levoglucosan	7.10 ± 0.03	31.99 ± 0.14
Water	**4.53 ± 0.28**	**102.24 ± 12.72**
Non-volatiles[†]	**65.60 ± 0.80**	**-**
Total	**100**	**233.56 ± 13.60**

* per kg of whole bio-oil

[†] determined by difference

Table 3: Summary of compound concentrations and enthalpy of vaporization values calculated for the SF2 bio-oil fraction. Uncertainty reflects the standard error of the mean.

SF2 Bio-oil Components	**Concentration (wt%)**	**ΔH_{vap} (kJ)***
GC Identified Detectables	**8.31 ± 0.01**	**33.84 ± 0.01**
Acetaldehyde	0.01 ± 0.01	0.01 ± 0.01
Formaldehyde	0.01 ± 0.01	0.01 ± 0.01
Glycolaldehyde	0.01 ± 0.01	0.01 ± 0.01
Acetol	0.39 ± 0.01	2.38 ± 0.06
2,5-dimethoxytetrahydrofuran (cis)	0.09 ± 0.01	0.24 ± 0.01
Propanal	0.06 ± 0.01	0.28 ± 0.01
2,5-dimethoxytetrahydrofuran (trans)	0.05 ± 0.01	0.15 ± 0.01
Furfural	0.21 ± 0.01	0.92 ± 0.02
2-Furanmethanol	0.07 ± 0.01	0.44 ± 0.01
Acetoxyacetone	0.05 ± 0.01	0.17 ± 0.01
2-Methyl-2-cyclopenten-1-one	0.06 ± 0.01	0.23 ± 0.01
2-Hydroxy-2-cyclopenten-1-one	0.44 ± 0.01	2.56 ± 0.01
5-Methylfurfural	0.07 ± 0.01	0.29 ± 0.01
3-Methyl-2-cyclopenten-1-one	0.08 ± 0.01	0.31 ± 0.01
2(5H)-furanone	0.34 ± 0.01	1.80 ± 0.02
Methylcyclopentenolone	0.35 ± 0.01	1.74 ± 0.02
3-Methyl-2(5H)-furanone	0.14 ± 0.01	0.64 ± 0.01
Phenol	0.10 ± 0.01	0.45 ± 0.01
2-Methoxyphenol	0.28 ± 0.01	1.05 ± 0.01
O-cresol	0.07 ± 0.01	0.27 ± 0.01
P-cresol	0.17 ± 0.01	0.72 ± 0.01
4-Methyl-5H-furan-2-one	0.25 ± 0.01	1.18 ± 0.02

2-Methoxy-4-methylphenol	0.52 ± 0.01	1.78 ± 0.03
2,4-Dimethylphenol	0.15 ± 0.01	0.57 ± 0.02
2,3-Dimethylphenol	0.02 ± 0.01	0.09 ± 0.01
3-Ethylphenol	0.04 ± 0.01	0.16 ± 0.01
3,4-Dimethylphenol	0.02 ± 0.01	0.08 ± 0.03
4-Ethyl-2-methoxyphenol	0.13 ± 0.01	0.44 ± 0.01
1,4;3,6-Dianhydro-α-d-glucopyranose	0.18 ± 0.01	0.73 ± 0.02
2-Methoxy-4-vinylphenol	0.91 ± 0.01	3.05 ± 0.01
Eugenol	0.22 ± 0.01	0.68 ± 0.01
2-Methoxy-4-propylphenol	0.05 ± 0.01	0.15 ± 0.01
5-Hydroxymethylfurfural	0.58 ± 0.01	2.56 ± 0.01
2,6-Dimethoxyphenol	0.11 ± 0.01	0.39 ± 0.02
Isoeugenol	0.76 ± 0.01	2.42 ± 0.01
4-Methyl-2,6-dimethoxyphenol	0.07 ± 0.01	0.22 ± 0.01
1,4-Benzenediol	0.20 ± 0.01	0.97 ± 0.01
Vanillin	0.45 ± 0.01	1.59 ± 0.03
2,5-Dimethoxybenzylalcohol	0.23 ± 0.01	0.79 ± 0.01
4-Hydroxy-3-methoxyacetophenone	0.28 ± 0.01	0.95 ± 0.01
4-Allyl-2,6-dimethoxyphenol	0.14 ± 0.01	0.40 ± 0.01
4-Hydroxy-3,5-dimethoxybenzaldehyde	0.01 ± 0.01	0.01 ± 0.01
GC Unidentified Detectables	**2.00 ± 0.09**	**8.44 ± 0.36**
IC Detectables	**0.98 ± 0.01**	**5.62 ± 0.01**
Acetic acid	0.32 ± 0.01	1.26 ± 0.01
Propanoic acid	0.06 ± 0.01	0.35 ± 0.01
Glycolic acid	0.39 ± 0.01	2.97 ± 0.01

Formic acid	0.21 ± 0.01	1.04 ± 0.01
HPLC Detectables	**8.98 ± 0.14**	**38.23 ± 0.61**
Cellobiosan	2.23 ± 0.01	7.46 ± 0.02
Xylose	0.68 ± 0.01	3.52 ± 0.03
Galactose	0.19 ± 0.02	0.82 ± 0.10
Mannose	0.13 ± 0.02	0.54 ± 0.07
Levoglucosan	5.75 ± 0.14	25.90 ± 0.63
Water	**3.28 ± 0.30**	**74.11 ± 11.91**
Non-volatiles†	**76.44 ± 0.48**	**-**
Total	**100**	**160.23 ± 11.66**

* per kg of whole bio-oil

† determined by difference

Table 4: Summary of compound concentrations and enthalpy of vaporization values calculated for the SF3 bio-oil fraction. Uncertainty reflects the standard error of the mean.

SF3 Bio-oil Components	**Concentration (wt%)**	**ΔH_{vap} (kJ)***
GC Identified Detectables	**38.78 ± 0.94**	**206.62 ± 5.11**
Acetaldehyde	0.06 ± 0.01	0.35 ± 0.02
Formaldehyde	2.95 ± 0.04	21.89 ± 0.32
Glycolaldehyde	10.23 ± 0.38	73.23 ± 2.70
Acetol	2.73 ± 0.05	16.42 ± 0.30
2,5-dimethoxytetrahydrofuran (cis)	1.45 ± 0.04	4.03 ± 0.10
Propanal	0.21 ± 0.08	1.00 ± 0.40
2,5-dimethoxytetrahydrofuran (trans)	2.12 ± 0.07	5.89 ± 0.18
Furfural	1.05 ± 0.04	4.71 ± 0.18
2-Furanmethanol	0.39 ± 0.01	2.56 ± 0.02
Acetoxyacetone	0.38 ± 0.01	1.27 ± 0.01
2-Methyl-2-cyclopenten-1-one	0.30 ± 0.01	1.23 ± 0.01
2-Hydroxy-2-cyclopenten-1-one	2.83 ± 0.06	16.61 ± 0.38
5-Methylfurfural	0.44 ± 0.14	1.69 ± 0.55
3-Methyl-2-cyclopenten-1-one	0.34 ± 0.02	1.41 ± 0.08
2(5H)-furanone	1.90 ± 0.06	9.92 ± 0.29
Methylcyclopentenolone	1.58 ± 0.01	7.88 ± 0.03
3-Methyl-2(5H)-furanone	0.11 ± 0.01	0.49 ± 0.02
Phenol	0.62 ± 0.02	2.88 ± 0.07
2-Methoxyphenol	1.36 ± 0.02	5.01 ± 0.09
O-cresol	0.36 ± 0.01	1.48 ± 0.02
P-cresol	0.66 ± 0.01	2.80 ± 0.03
4-Methyl-5H-furan-2-one	0.60 ± 0.01	2.82 ± 0.03

2-Methoxy-4-methylphenol	1.84 ± 0.02	6.32 ± 0.06
2,4-Dimethylphenol	0.35 ± 0.01	1.32 ± 0.01
2,3-Dimethylphenol	0.07 ± 0.01	0.26 ± 0.01
3-Ethylphenol	0.10 ± 0.01	0.37 ± 0.01
3,4-Dimethylphenol	0.05 ± 0.01	0.18 ± 0.03
4-Ethyl-2-methoxyphenol	0.40 ± 0.01	1.32 ± 0.01
1,4;3,6-Dianhydro-α-d-glucopyranose	0.15 ± 0.01	0.60 ± 0.01
2-Methoxy-4-vinylphenol	1.41 ± 0.02	4.70 ± 0.07
Eugenol	0.46 ± 0.01	1.42 ± 0.01
2-Methoxy-4-propylphenol	0.11 ± 0.01	0.34 ± 0.01
5-Hydroxymethylfurfural	0.12 ± 0.01	0.53 ± 0.01
2,6-Dimethoxyphenol	0.06 ± 0.01	0.19 ± 0.01
Isoeugenol	0.69 ± 0.01	2.20 ± 0.03
4-Methyl-2,6-dimethoxyphenol	0.01 ± 0.01	0.02 ± 0.01
1,4-Benzenediol	0.07 ± 0.01	0.34 ± 0.01
Vanillin	0.17 ± 0.01	0.59 ± 0.01
2,5-Dimethoxybenzylalcohol	0.04 ± 0.01	0.13 ± 0.01
4-Hydroxy-3-methoxyacetophenone	0.05 ± 0.01	0.16 ± 0.01
4-Allyl-2,6-dimethoxyphenol	0.02 ± 0.01	0.06 ± 0.01
4-Hydroxy-3,5-dimethoxybenzaldehyde	0.01 ± 0.01	0.01 ± 0.01
GC Unidentified Detectables	**10.93 ± 0.13**	**46.04 ± 0.53**
IC Detectables	**5.47 ± 0.02**	**25.44 ± 0.14**
Acetic acid	3.48 ± 0.01	13.72 ± 0.01
Propanoic acid	0.39 ± 0.01	2.12 ± 0.04
Glycolic acid	0.62 ± 0.02	4.76 ± 0.13

Formic acid	0.98 ± 0.01	4.84 ± 0.02
HPLC Detectables	**1.98 ± 0.03**	**8.58 ± 0.14**
Cellobiosan	0.02 ± 0.01	0.06 ± 0.03
Xylose	0.01 ± 0.01	0.07 ± 0.07
Galactose	0.01 ± 0.01	0.01 ± 0.01
Mannose	1.24 ± 0.02	5.27 ± 0.09
Levoglucosan	0.70 ± 0.07	3.17 ± 0.33
Water	**18.45 ± 0.28**	**416.87 ± 12.83**
Non-volatiles[†]	**24.39 ± 0.54**	**-**
Total	**100**	**703.56 ± 6.91**

* per kg of whole bio-oil

[†] determined by difference

Table 5: Summary of compound concentrations and enthalpy of vaporization values calculated for the SF4 bio-oil fraction. Uncertainty reflects the standard error of the mean.

SF4 Bio-oil Components	**Concentration (wt%)**	**ΔH_{vap} (kJ)***
GC Identified Detectables	**31.54 ± 0.56**	**152.32 ± 3.24**
Acetaldehyde	0.07 ± 0.01	0.43 ± 0.01
Formaldehyde	1.53 ± 0.03	11.38 ± 0.22
Glycolaldehyde	5.14 ± 0.30	36.83 ± 2.15
Acetol	2.24 ± 0.07	13.47 ± 0.42
2,5-dimethoxytetrahydrofuran (cis)	0.94 ± 0.03	2.60 ± 0.08
Propanal	0.19 ± 0.01	0.91 ± 0.03
2,5-dimethoxytetrahydrofuran (trans)	1.25 ± 0.05	3.46 ± 0.14
Furfural	0.83 ± 0.01	3.71 ± 0.04
2-Furanmethanol	0.29 ± 0.01	1.93 ± 0.03
Acetoxyacetone	0.29 ± 0.01	0.97 ± 0.01
2-Methyl-2-cyclopenten-1-one	0.27 ± 0.01	1.09 ± 0.01
2-Hydroxy-2-cyclopenten-1-one	1.59 ± 0.01	9.36 ± 0.02
5-Methylfurfural	0.28 ± 0.01	1.09 ± 0.03
3-Methyl-2-cyclopenten-1-one	0.29 ± 0.01	1.17 ± 0.01
2(5H)-furanone	1.46 ± 0.03	7.63 ± 0.18
Methylcyclopentenolone	1.56 ± 0.01	7.79 ± 0.01
3-Methyl-2(5H)-furanone	0.04 ± 0.01	0.19 ± 0.01
Phenol	0.53 ± 0.01	2.44 ± 0.01
2-Methoxyphenol	1.22 ± 0.01	4.51 ± 0.01
O-cresol	0.34 ± 0.01	1.40 ± 0.01
P-cresol	0.68 ± 0.01	2.86 ± 0.01
4-Methyl-5H-furan-2-one	0.71 ± 0.01	3.33 ± 0.01

2-Methoxy-4-methylphenol	2.04 ± 0.01	7.03 ± 0.02
2,4-Dimethylphenol	0.40 ± 0.01	1.51 ± 0.01
2,3-Dimethylphenol	0.09 ± 0.01	0.34 ± 0.01
3-Ethylphenol	0.12 ± 0.01	0.47 ± 0.01
3,4-Dimethylphenol	0.07 ± 0.01	0.26 ± 0.01
4-Ethyl-2-methoxyphenol	0.52 ± 0.01	1.71 ± 0.01
1,4;3,6-Dianhydro-α-d-glucopyranose	0.28 ± 0.01	1.12 ± 0.01
2-Methoxy-4-vinylphenol	2.27 ± 0.01	7.59 ± 0.03
Eugenol	0.73 ± 0.01	2.28 ± 0.01
2-Methoxy-4-propylphenol	0.17 ± 0.01	0.52 ± 0.01
5-Hydroxymethylfurfural	0.33 ± 0.01	1.45 ± 0.02
2,6-Dimethoxyphenol	0.09 ± 0.01	0.32 ± 0.03
Isoeugenol	1.58 ± 0.02	5.04 ± 0.05
4-Methyl-2,6-dimethoxyphenol	0.08 ± 0.02	0.25 ± 0.07
1,4-Benzenediol	0.19 ± 0.01	0.92 ± 0.07
Vanillin	0.48 ± 0.03	1.72 ± 0.12
2,5-Dimethoxybenzylalcohol	0.13 ± 0.01	0.45 ± 0.01
4-Hydroxy-3-methoxyacetophenone	0.16 ± 0.01	0.53 ± 0.01
4-Allyl-2,6-dimethoxyphenol	0.09 ± 0.01	0.27 ± 0.01
4-Hydroxy-3,5-dimethoxybenzaldehyde	0.01 ± 0.01	0.01 ± 0.01
GC Unidentified Detectables	**11.52 ± 1.61**	**48.50 ± 6.77**
IC Detectables	**4.47 ± 0.01**	**22.03 ± 0.13**
Acetic acid	2.41 ± 0.01	9.50 ± 0.02
Propanoic acid	0.32 ± 0.01	1.76 ± 0.06
Glycolic acid	0.80 ± 0.03	6.18 ± 0.26

Formic acid	0.93 ± 0.01	4.59 ± 0.05
HPLC Detectables	**1.60 ± 0.05**	**7.07 ± 0.22**
Cellobiosan	0.03 ± 0.01	0.11 ± 0.03
Xylose	0.09 ± 0.01	0.44 ± 0.02
Galactose	0.01 ± 0.01	0.01 ± 0.01
Mannose	0.71 ± 0.01	3.02 ± 0.01
Levoglucosan	0.78 ± 0.04	3.51 ± 0.20
Water	**16.02 ± 0.36**	**362.03 ± 18.10**
Non-volatiles[†]	**34.85 ± 0.19**	**-**
Total	**100**	**591.95 ± 14.93**

* per kg of whole bio-oil

[†] determined by difference

Table 6: Summary of compound concentrations and enthalpy of vaporization values calculated for the SF5 bio-oil fraction. Uncertainty reflects the standard error of the mean.

SF5 Bio-oil Components	**Concentration (wt%)**	**ΔH_{vap} (kJ)***
GC Identified Detectables	**9.04 ± 0.05**	**52.61 ± 0.41**
Acetaldehyde	0.50 ± 0.02	2.91 ± 0.10
Formaldehyde	2.19 ± 0.03	16.24 ± 0.23
Glycolaldehyde	0.72 ± 0.01	5.13 ± 0.03
Acetol	2.63 ± 0.01	15.84 ± 0.07
2,5-dimethoxytetrahydrofuran (cis)	0.20 ± 0.01	0.54 ± 0.02
Propanal	0.02 ± 0.01	0.10 ± 0.01
2,5-dimethoxytetrahydrofuran (trans)	1.22 ± 0.01	0.61 ± 0.04
Furfural	0.83 ± 0.01	3.71 ± 0.03
2-Furanmethanol	0.04 ± 0.01	0.24 ± 0.01
Acetoxyacetone	0.11 ± 0.01	0.38 ± 0.01
2-Methyl-2-cyclopenten-1-one	0.15 ± 0.01	0.60 ± 0.01
2-Hydroxy-2-cyclopenten-1-one	1.15 ± 0.01	0.87 ± 0.01
5-Methylfurfural	0.12 ± 0.01	0.48 ± 0.01
3-Methyl-2-cyclopenten-1-one	0.06 ± 0.01	0.24 ± 0.01
2(5H)-furanone	0.22 ± 0.01	1.16 ± 0.01
Methylcyclopentenolone	0.11 ± 0.01	0.53 ± 0.01
3-Methyl-2(5H)-furanone	0.06 ± 0.01	0.27 ± 0.01
Phenol	0.07 ± 0.01	0.30 ± 0.01
2-Methoxyphenol	0.22 ± 0.01	0.82 ± 0.01
O-cresol	0.04 ± 0.01	0.15 ± 0.01
P-cresol	0.05 ± 0.01	0.22 ± 0.01
4-Methyl-5H-furan-2-one	0.04 ± 0.01	0.19 ± 0.01

2-Methoxy-4-methylphenol	0.18 ± 0.01	0.63 ± 0.01
2,4-Dimethylphenol	0.02 ± 0.01	0.09 ± 0.01
2,3-Dimethylphenol	0.01 ± 0.01	0.01 ± 0.01
3-Ethylphenol	0.01 ± 0.01	0.03 ± 0.01
3,4-Dimethylphenol	0.01 ± 0.01	0.01 ± 0.01
4-Ethyl-2-methoxyphenol	0.03 ± 0.01	0.10 ± 0.01
1,4;3,6-Dianhydro-α-d-glucopyranose	0.01 ± 0.01	0.01 ± 0.01
2-Methoxy-4-vinylphenol	0.03 ± 0.01	0.09 ± 0.01
Eugenol	0.03 ± 0.01	0.09 ± 0.01
2-Methoxy-4-propylphenol	0.01 ± 0.01	0.02 ± 0.01
5-Hydroxymethylfurfural	0.01 ± 0.01	0.01 ± 0.01
2,6-Dimethoxyphenol	0.01 ± 0.01	0.01 ± 0.01
Isoeugenol	0.01 ± 0.01	0.02 ± 0.01
4-Methyl-2,6-dimethoxyphenol	0.01 ± 0.01	0.01 ± 0.01
1,4-Benzenediol	0.01 ± 0.01	0.01 ± 0.01
Vanillin	0.01 ± 0.01	0.01 ± 0.01
2,5-Dimethoxybenzylalcohol	0.01 ± 0.01	0.01 ± 0.01
4-Hydroxy-3-methoxyacetophenone	0.01 ± 0.01	0.01 ± 0.01
4-Allyl-2,6-dimethoxyphenol	0.01 ± 0.01	0.01 ± 0.01
4-Hydroxy-3,5-dimethoxybenzaldehyde	0.01 ± 0.01	0.01 ± 0.01
GC Unidentified Detectables	**3.77 ± 0.72**	**15.87 ± 3.01**
IC Detectables	**4.21 ± 0.11**	**17.77 ± 0.57**
Acetic acid	3.32 ± 0.04	13.09 ± 0.14
Propanoic acid	0.36 ± 0.02	1.97 ± 0.13
Glycolic acid	0.04 ± 0.02	0.31 ± 0.15

Formic acid	0.49 ± 0.03	2.40 ± 0.14
HPLC Detectables	**1.12 ± 0.05**	**4.85 ± 0.22**
Cellobiosan	0.01 ± 0.01	0.01 ± 0.01
Xylose	0.01 ± 0.01	0.01 ± 0.01
Galactose	0.01 ± 0.01	0.01 ± 0.01
Mannose	0.77 ± 0.04	3.26 ± 0.15
Levoglucosan	0.35 ± 0.03	1.59 ± 0.15
Water	**70.82 ± 0.91**	**1600.03 ± 45.91**
Non-volatiles[†]	**11.04 ± 2.66**	**-**
Total	**100**	**1691.13 ± 48.26**

* per kg of whole bio-oil

[†] determined by difference

Table 7: Summary of compound concentrations and enthalpy of vaporization values calculated for the SF6 bio-oil fraction. Uncertainty reflects the standard error of the mean.

SF6 Bio-oil Components	**Concentration (wt%)**	**ΔH_{vap} (kJ)***
GC Identified Detectables	**26.04 ± 0.36**	**146.24 ± 2.80**
Acetaldehyde	0.48 ± 0.02	2.79 ± 0.09
Formaldehyde	6.62 ± 0.26	49.18 ± 1.90
Glycolaldehyde	2.31 ± 0.14	16.51 ± 1.01
Acetol	4.47 ± 0.02	26.91 ± 0.14
2,5-dimethoxytetrahydrofuran (cis)	0.40 ± 0.02	1.10 ± 0.04
Propanal	0.06 ± 0.01	0.30 ± 0.04
2,5-dimethoxytetrahydrofuran (trans)	0.65 ± 0.01	1.79 ± 0.01
Furfural	2.35 ± 0.01	10.53 ± 0.03
2-Furanmethanol	0.05 ± 0.01	0.30 ± 0.01
Acetoxyacetone	0.45 ± 0.01	1.51 ± 0.01
2-Methyl-2-cyclopenten-1-one	0.53 ± 0.01	2.19 ± 0.01
2-Hydroxy-2-cyclopenten-1-one	0.91 ± 0.01	5.34 ± 0.04
5-Methylfurfural	0.66 ± 0.01	2.54 ± 0.01
3-Methyl-2-cyclopenten-1-one	0.26 ± 0.01	1.08 ± 0.01
2(5H)-furanone	0.86 ± 0.01	4.48 ± 0.02
Methylcyclopentenolone	0.72 ± 0.01	3.57 ± 0.01
3-Methyl-2(5H)-furanone	0.04 ± 0.01	0.17 ± 0.01
Phenol	0.31 ± 0.01	1.45 ± 0.01
2-Methoxyphenol	1.11 ± 0.01	4.12 ± 0.01
O-cresol	0.22 ± 0.01	0.92 ± 0.01
P-cresol	0.32 ± 0.01	1.36 ± 0.01
4-Methyl-5H-furan-2-one	0.23 ± 0.01	1.09 ± 0.01

2-Methoxy-4-methylphenol	1.08 ± 0.01	3.72 ± 0.01
2,4-Dimethylphenol	0.16 ± 0.01	0.60 ± 0.01
2,3-Dimethylphenol	0.01 ± 0.01	0.05 ± 0.01
3-Ethylphenol	0.04 ± 0.01	0.14 ± 0.01
3,4-Dimethylphenol	0.01 ± 0.01	0.05 ± 0.01
4-Ethyl-2-methoxyphenol	0.20 ± 0.01	0.65 ± 0.01
1,4;3,6-Dianhydro-α-d-glucopyranose	0.03 ± 0.01	0.12 ± 0.01
2-Methoxy-4-vinylphenol	0.22 ± 0.01	0.74 ± 0.01
Eugenol	0.14 ± 0.01	0.45 ± 0.01
2-Methoxy-4-propylphenol	0.05 ± 0.01	0.14 ± 0.01
5-Hydroxymethylfurfural	0.01 ± 0.01	0.05 ± 0.01
2,6-Dimethoxyphenol	0.01 ± 0.01	0.02 ± 0.01
Isoeugenol	0.05 ± 0.01	0.17 ± 0.01
4-Methyl-2,6-dimethoxyphenol	0.01 ± 0.01	0.02 ± 0.01
1,4-Benzenediol	0.01 ± 0.01	0.04 ± 0.01
Vanillin	0.01 ± 0.01	0.04 ± 0.01
2,5-Dimethoxybenzylalcohol	0.01 ± 0.01	0.01 ± 0.01
4-Hydroxy-3-methoxyacetophenone	0.01 ± 0.01	0.01 ± 0.01
4-Allyl-2,6-dimethoxyphenol	0.01 ± 0.01	0.01 ± 0.01
4-Hydroxy-3,5-dimethoxybenzaldehyde	0.01 ± 0.01	0.01 ± 0.01
GC Unidentified Detectables	**6.83 ± 0.44**	**28.87 ± 1.87**
IC Detectables	**7.31 ± 0.03**	**31.07 ± 0.11**
Acetic acid	5.56 ± 0.02	21.95 ± 0.06
Propanoic acid	0.69 ± 0.01	3.73 ± 0.06
Glycolic acid	0.06 ± 0.01	0.49 ± 0.03

Formic acid	0.99 ± 0.01	4.89 ± 0.02
HPLC Detectables	**2.07 ± 0.01**	**9.00 ± 0.03**
Cellobiosan	0.01 ± 0.01	0.01 ± 0.01
Xylose	0.01 ± 0.01	0.01 ± 0.01
Galactose	0.01 ± 0.01	0.01 ± 0.01
Mannose	1.31 ± 0.03	5.56 ± 0.14
Levoglucosan	0.76 ± 0.03	3.44 ± 0.11
Water	**42.85 ± 0.50**	**968.18 ± 27.82**
Non-volatiles[†]	**14.89 ± 1.18**	**-**
Total	**100**	**1183.27 ± 28.89**

* per kg of whole bio-oil

[†] determined by difference

Table 8: Summary of compound concentrations and enthalpy of vaporization values calculated for the whole bio-oil fraction. Uncertainty reflects the standard error of the mean.

Whole Bio-oil Components	**Concentration (wt%)**	**ΔH_{vap} (kJ)***
GC Identified Detectables	**13.23 ± 0.04**	**66.47 ± 0.27**
Acetaldehyde	0.22 ± 0.01	1.32 ± 0.05
Formaldehyde	1.45 ± 0.01	10.75 ± 0.04
Glycolaldehyde	1.32 ± 0.02	9.43 ± 0.12
Acetol	1.73 ± 0.01	10.40 ± 0.05
2,5-dimethoxytetrahydrofuran (cis)	0.29 ± 0.01	0.80 ± 0.03
Propanal	0.06 ± 0.01	0.31 ± 0.03
2,5-dimethoxytetrahydrofuran (trans)	0.32 ± 0.01	0.88 ± 0.01
Furfural	0.65 ± 0.01	2.92 ± 0.01
2-Furanmethanol	0.09 ± 0.01	0.59 ± 0.01
Acetoxyacetone	0.13 ± 0.01	0.44 ± 0.01
2-Methyl-2-cyclopenten-1-one	0.14 ± 0.01	0.59 ± 0.01
2-Hydroxy-2-cyclopenten-1-one	0.61 ± 0.01	3.57 ± 0.02
5-Methylfurfural	0.17 ± 0.01	0.66 ± 0.04
3-Methyl-2-cyclopenten-1-one	0.11 ± 0.01	0.46 ± 0.01
2(5H)-furanone	0.52 ± 0.01	2.71 ± 0.01
Methylcyclopentenolone	0.44 ± 0.01	2.21 ± 0.01
3-Methyl-2(5H)-furanone	0.11 ± 0.01	0.53 ± 0.01
Phenol	0.16 ± 0.01	0.74 ± 0.01
2-Methoxyphenol	0.44 ± 0.01	1.62 ± 0.01
O-cresol	0.10 ± 0.01	0.41 ± 0.01
P-cresol	0.20 ± 0.01	0.85 ± 0.02
4-Methyl-5H-furan-2-one	0.24 ± 0.01	1.14 ± 0.03

2-Methoxy-4-methylphenol	0.61 ± 0.01	2.11 ± 0.01
2,4-Dimethylphenol	0.15 ± 0.01	0.55 ± 0.01
2,3-Dimethylphenol	0.02 ± 0.01	0.08 ± 0.01
3-Ethylphenol	0.04 ± 0.01	0.16 ± 0.01
3,4-Dimethylphenol	0.02 ± 0.01	0.06 ± 0.01
4-Ethyl-2-methoxyphenol	0.14 ± 0.01	0.47 ± 0.01
1,4;3,6-Dianhydro-α-d-glucopyranose	0.12 ± 0.01	0.48 ± 0.01
2-Methoxy-4-vinylphenol	0.72 ± 0.01	2.41 ± 0.01
Eugenol	0.19 ± 0.01	0.61 ± 0.01
2-Methoxy-4-propylphenol	0.04 ± 0.01	0.14 ± 0.01
5-Hydroxymethylfurfural	0.32 ± 0.01	1.40 ± 0.01
2,6-Dimethoxyphenol	0.08 ± 0.01	0.26 ± 0.01
Isoeugenol	0.52 ± 0.01	1.67 ± 0.01
4-Methyl-2,6-dimethoxyphenol	0.04 ± 0.01	0.11 ± 0.01
1,4-Benzenediol	0.12 ± 0.01	0.60 ± 0.01
Vanillin	0.26 ± 0.01	0.91 ± 0.01
2,5-Dimethoxybenzylalcohol	0.12 ± 0.01	0.40 ± 0.01
4-Hydroxy-3-methoxyacetophenone	0.15 ± 0.01	0.49 ± 0.01
4-Allyl-2,6-dimethoxyphenol	0.07 ± 0.01	0.20 ± 0.01
4-Hydroxy-3,5-dimethoxybenzaldehyde	0.01 ± 0.01	0.01 ± 0.01
GC Unidentified Detectables	**4.07 ± 0.26**	**17.13 ± 1.09**
IC Detectables	**3.18 ± 0.04**	**14.71 ± 0.22**
Acetic acid	2.10 ± 0.01	8.28 ± 0.05
Propanoic acid	0.25 ± 0.01	1.37 ± 0.05
Glycolic acid	0.35 ± 0.01	2.72 ± 0.07

Formic acid	0.47 ± 0.01	2.34 ± 0.05
HPLC Detectables	**5.05 ± 0.01**	**21.81 ± 0.02**
Cellobiosan	0.84 ± 0.01	2.81 ± 0.01
Xylose	0.33 ± 0.01	1.69 ± 0.01
Galactose	0.16 ± 0.01	0.67 ± 0.02
Mannose	0.56 ± 0.03	2.37 ± 0.11
Levoglucosan	3.16 ± 0.03	14.26 ± 0.12
Water	**33.27 ± 1.17**	**751.55 ± 26.36**
Non-volatiles†	**41.21 ± 1.34**	**-**
Total	**100**	**871.67 ± 26.93**

* per kg of whole bio-oil

† determined by difference